Use Authorization

In presenting this dissertation in partial fulfillment of the requirements for an advanced degree at Idaho State University, I agree that the Library shall make it freely available for inspection. I further state that permission to download and/or print my dissertation for scholarly purposes may be granted by the Dean of the Graduate School, Dean of my academic division, or by the University Librarian. It is understood that any copying or publication of this dissertation for financial gain shall not be allowed without my written permission.

Signature _____

Date _____

DEVELOPMENT OF A PLUTONIUM-DTPA BIOKINETIC MODEL WITH SUGGESTED MODIFICATION TO THE PLUTONIUM SYSTEMIC MODEL

by

Kevin Konzen

A dissertation

submitted in partial fulfillment

of the requirements for the degree of

Doctor of Philosophy in Applied Physics

Idaho State University

October 2014

To the Graduate Faculty:

The members of the committee appointed to examine the dissertation of Kevin Konzen find it satisfactory and recommend that it be accepted.

_____
Dr. Richard Brey,
Major Advisor

_____
Dr. Scott Miller,
Co-Advisor

_____
Dr. Thomas Gesell,
Committee Member

_____
Dr. Jason Harris,
Committee Member

_____
Dr. DeWayne Derryberry,
Graduate Faculty Representative

ACKNOWLEDGEMENTS

I would like to thank the following individuals for their support in this research. This project would not have started without the encouragement from my advisor, Dr. Richard Brey, in pursuing a doctorate in this field, and for extending an invitation to participate with his internal dosimetry research group. Dr. Brey dedicated his time to meet frequently with the research group where we had several interesting discussions and debates on the subject. His mentoring was invaluable to this research. I would like to thank Dr. Scott Miller for accepting the invitation to serve on the committee as my co-advisor and for the valuable discussions we had on physiology and its basis for the systemic model. I wanted to thank Dr. DeWayne Derryberry for providing consultation in the regression and statistics used in this research. I extend a special thanks to Dr. Thomas Gesell and Dr. Jason Harris for serving on the committee and supporting me in this research.

I also want to thank the important people in my life that has also led me on this path of achievement. First of all, my wife and partner, who has supported me and sacrificed the normalcy of our life while I completed this research, always with encouragement. My father, who had inspired determination and perseverance as necessary life skills, and one who has set the bar for high standards and achievement, continues to provide support and encouragement.

And finally, I would like to thank the students of Dr. Brey's internal dosimetry research group for their support and encouragement.

TABLE OF CONTENTS

List of Figures

List of Tables

List of Abbreviations

AI	alveolar interstitium
Am	americium
AMAD	activity median aerodynamic diameter
AOV	analysis of variance
bb	bronchioles
BB	bronchi
Bq	Becquerel
Ca	calcium
Ca-DTPA	calcium diethylenetriaminepentaacetic acid in a salt complex
$CaHPO_4$	calcium hydroxyapatite
CEqD	committed equivalent dose
CIS	colloid and intermediate state
Cl	chlorine
Cm	curium
CONRAD	Coordinated Network for Radiation Dosimetry
CortMarrow	cortical marrow
CortSurf	cortical surface
CortVol	cortical volume
$D_{T,R}$	absorbed dose
df	degrees of freedom
DHHS	U. S. Department of Health and Human Services
DMT	divalent metal transporter
DOE	U.S. Department of Energy
DTPA	diethylenetriaminepentaacetic acid
E	committed effective dose
EDTA	ethylenediaminetetraacetic acid
ET	extrathoracic
FDA	U.S. Food and Drug Administration
Fe	iron
GI	gastrointestinal
HCO_3	bicarbonate
ICRP	International Commission on Radiological Protection
IRF	intake retention fraction
K	potassium
kBq	kilobecquerel
kDa	kilodalton
keV	kiloelectronvolt
kg	kilogram
λ	decay constant
LLI	lower large intestine
ln	natural log
LN	lymph nodes
MeV	megaelectronvolt

mg	milligram
Mg	magnesium
min	minute
mL	milliliter
mmol	millimole
Na	sodium
NCRP	National Council on Radiation Protection and Measurements
nm	nanometer
PABS	particles, aggregates and bound state
pCi	picocurie
PO_4	phosphate
PTH	parathyroid hormone
Pu	plutonium
Pu-DTPA	plutonium diethylenetriaminepentaacetic acid
Pu-Tf	plutonium-transferrin
RE	reticuloendothelial
seq	sequestered
SI	small intestine
SF	scattering factor
SO_4	sulfate
ST	stomach
ST0	rapid turnover soft tissues (e.g., extracellular fluids)
ST1	intermediate soft tissues
ST2	tenaciously retained soft tissues
Tf	transferrin
TfR	transferrin receptor
Th	thorium
TrabMarrow	trabecular marrow
TrabSurf	trabecular surface
TrabVol	trabecular volume
μCi	microcurie
UK	United Kingdom
ULI	upper large intestine
μm	micron
μmol	micromole
U.S.	United States
USTUR	United States Tranuranium and Uranium Registries
w_R	radiation weighting factor
w_T	tissue weighting factor
χ^2	chi-square
χ_0^2	chi-squared statistic
Zn-DTPA	zinc diethylenetriaminepentaacetic acid in a salt complex

Abstract

The biokinetic model provides a mathematical means of predicting the distribution, retention and clearance of contaminants within the human body that may be used in deriving organ, tissue and whole body dose. The International Commission on Radiological Protection (ICRP) has recommended a systemic model for the assessment of plutonium intakes. The latest revision provided in publication 67 is the current model used by contractors regulated by the U.S. Department of Energy for assessing internal contamination. The ICRP 67 biokinetic model is based on unperturbed contaminant retention and clearance; however, individuals with significant intakes are likely to receive medical treatment to accelerate the contaminant clearance. This research attempted to understand the physiological and cellular processes that would explain plutonium metabolism and the influence of chelation treatment. This effort led to the development of a plutonium-DTPA biokinetic model that could be used to supplement the existing ICRP 67 model that would support intakes due to wounds and inhalation. In addition, several investigators have recommended changes to the ICRP 67 model based on the findings of recent human injection studies and the examination of occupational exposures. This research also studied a possible alternative of the ICRP 67 model that while maintaining its basic structure, would continue to support efficient coupling with intake models. The development of the plutonium-DTPA biokinetic model originated from a review of a wound case, and its use was validated against the excretion and tissue data made available by the United States Transuranium and Uranium Registry. These results confirmed that the plutonium-DTPA biokinetic model improved predictions when coupled to the systemic model, with improvements due to a proposed modification of the

ICRP 67 model. Furthermore, the proposed modification to the ICRP 67 model was based on incorporating physiological processes of the skeleton and liver that seemed to enhance the original model when it was employed with verified human data. This research led to the development of a plutonium-DTPA biokinetic model and included a modification of the plutonium systemic model that incorporated physiologically based improvements while maintaining efficient coupling with intake biokinetic models.

Chapter 1: Introduction

Radionuclides can enter the body through various means, including inhalation, ingestion, absorption and injection (e.g., wound). Biokinetic models are used to describe the subject's radionuclide retention, distribution and clearance following an intake of radioactive material for assessing internal contamination. These models are relied on for determining the initial intake, assignment of individual dose, and determining the need if any for medical intervention. Medical intervention might include tissue excision of a wound involving radioactive material that is normally followed by the administration of a chelating agent for removing contaminants that had been absorbed. The recommended biokinetic models assume normal physiological processes for radionuclide clearance with expected urine and fecal excretion over incremental time periods. Medical intervention can reduce the initial intake quantity and enhance its excretion, thus rendering these models inaccurate. Several investigators have suggested revised biokinetic models for chelation following a transuranic radionuclide intake with some success (Breustedt et al. 2009, James et al. 2007).

The physiological understanding of the skeleton, liver and tissue macrophage behavior has improved over the years prompting a review of the current recommended biokinetic models. There exists some uncertainty on the efficacy of organ and tissue chelation involving the liver and skeleton. Chelation administration operates under the premise that it is effective while the radionuclide exists in the blood and extracellular compartments prior to organ and tissue incorporation where a late chelation treatment would be futile. However, several studies indicate that late chelation treatment has

resulted in an enhanced excretion of the contaminant when compared to no treatment (James et al. 2007, IAEA 1978). Understanding of the skeleton, liver and tissue macrophage behavior should help to explain the chelation biochemistry that can support experimental observation and the benefit of late chelation treatment.

1.1 Biokinetic Models

The comprehension of biokinetic models is essential for assessing radiological intakes. The U.S. Department of Energy currently employs the following models: ICRP publication 66 (ICRP 66), *Human respiratory tract model for radiological protection* (1994), for the lung model; ICRP publication 67 (ICRP 67), *Age dependent doses to members of the public from intake of radionuclides: Part 2 ingestion dose coefficients* (1993), for the systemic model; NCRP Report No. 156 (NCRP 156), *Development of a biokinetic model for radionuclide-contaminated wounds and procedures for their assessment, dosimetry and treatme*nt (2007), for the wound model; and ICRP publication 30 (ICRP 30), *Limits on intakes of radionuclides by workers* (1979) for the gastrointestinal (GI) tract model. These biokinetic models were derived from human and animal studies and experiments, and are revised as necessary upon acquiring new information. For example, Leggett et al. (2005) recommended an improved biokinetic model for plutonium (referred to as the Leggett 2005 model in this work) due to recently acquired information since the ICRP 67 publication, which included epidemiological information obtained from a Mayak Production Association worker study and human injection studies conducted in the United Kingdom.

Each of these biokinetic models represent a mathematical compartment simulation where specified transfer rates and initial deposition leads to a differential expression for deriving organ, tissue and whole body dose. These models can also be used to estimate excretion activity for incremental time periods based on a known intake. The complexity of biokinetic models usually increases with the advancement of mathematical capabilities and biokinetic knowledge; even though the goal is to provide a parsimonious model that can accurately describe the pertinent kinetics important to dosimetry.

1.2 Chelation Influence

Chelation with diethylenetriaminepentaacetic acid (DTPA) in a calcium or zinc salt complex has been approved by the U.S. Food and Drug Administration (FDA) for treating transuranic intakes (NCRP 2007). Several studies have shown that DTPA is effective at chelating and removing plutonium from the body when the radionuclide exists in the blood and extracellular fluids of soft tissues, or is loosely bound on skeletal surfaces (Breustedt et al. 2009, Durbin et al. 1998, Fritsch et al. 2010). Furthermore, studies have indicated that liver and skeleton decorporation is evident in animal experiments and human cases (Bhattacharyya et al. 1978, Cohen et al. 1974, Fritsch et al. 2010, Gremy et al. 2010, James et al. 2007, Phan et al. 2004, Roedler et al. 1989).

Breustedt et al. (2009) proposed a compartment model for the Pu-DTPA complex following chelation that was the result of the Coordinated Network for Radiation Dosimetry (CONRAD) project research. CONRAD is a European committee where a task group was chartered with studying biokinetic models and developing a decorporation

therapy model with a focus on the Pu-DTPA complex (Breustedt et al. 2009). The CONRAD model is illustrated in Figure 1.

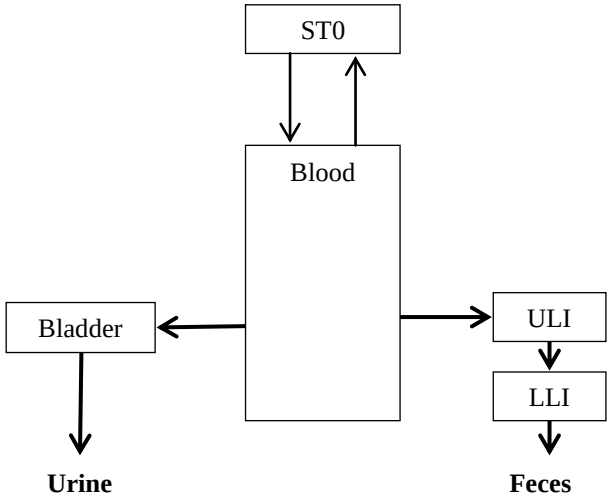

Figure 1: CONRAD proposed compartment structure for DTPA (Breustedt et al. 2009).

The CONRAD task group studied Case 123 in the IDEAS database (Hurtgen et al. 2006) for optimizing the fit of chelation being applied to the model since this case had early excretion data prior to DTPA administration (Breustedt et al. 2010). Case 123 had a wound from broken glass with a pH 1 solution of hexavalent ^{239}Pu.[1] Surface decontamination reduced the contamination from 2.22 MBq to 555 kBq, and tissue excision reduced it further to about 74 kBq.

The CONRAD task group had adapted the Stather et al. (1983) DTPA compartment model, which included the blood and extracellular fluid compartments; to the Leggett 2005 model and the ICRP 30 GI tract model (Breustedt et al. 2009). A second-order kinetics mechanism was introduced to the series of first-order differential

[1] Information was provided in IDEAS database with a reference to Jeanmaire 1964 Case 1. IDEAS database was available online at: http://www.sckcen.be/ideas/ ; accessed on January 31, 2013.

equations to describe the formation of the Pu-DTPA complex in the model (Breustedt et al. 2009, 2010). The CONRAD task group had considered the Pu-DTPA complex only in the blood and extracellular fluids (Breustedt et al. 2009). The CONRAD task group recommended the initial parameters specified in Table 1, which were based on DTPA kinetics with the assumption that the Pu-DTPA complex would have similar characteristics (Breustedt et al. 2009).

Table 1: CONRAD task group recommended transfer rates (Breustedt et al. 2009).

Transfer Compartments	Transfer Rate (d^{-1})
Blood to interstitium	145 ± 11
Interstitium to blood	64 ± 4
Interstitium to lymph	0.0123 ± 0.012
Lymph to blood	0.405 ± 0.036
Blood to urinary bladder	45.7 ± 0.8

The CONRAD task group indicated that there was an increase in fecal excretion; however, no parameters were suggested for the model (Breustedt et al. 2009). The urine excretion results were plotted in relation to the CONRAD proposed model prediction in Figure 2.

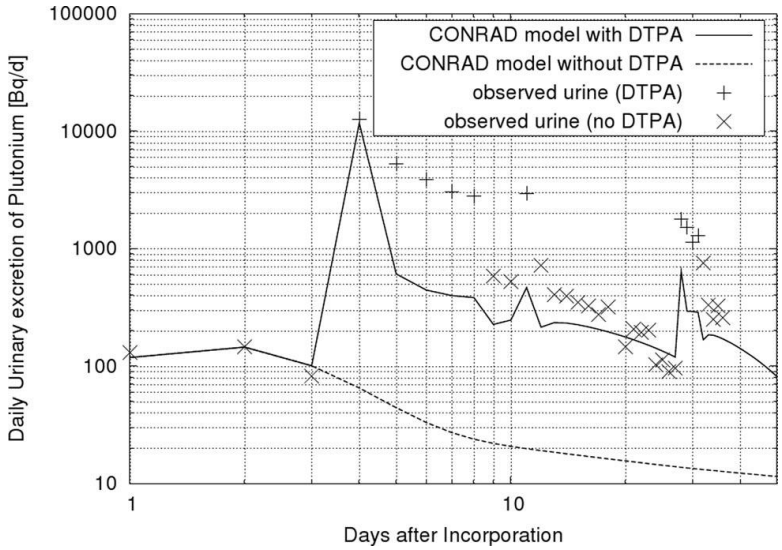

Figure 2: IDEAS Case 123 urine excretion results compared to the CONRAD model. Reprinted with permission from Lippincott Williams and Wilkins/Wolters Kluwer Health: Health Physics Journal (Breustedt 2010).

Figure 2 illustrated that the CONRAD model was able to predict the initial urine enhancement on the 4th day due to chelation; however, it compared poorly to subsequent samples. It is believed by this author that the inaccuracy in fitting the excretion data at times after the 4th day was primarily due to restricting the DTPA influence to only the blood and extracellular fluid compartments in the compartment model, and also due to the rapid clearance of these compartments.

James et al. (2007) proposed revising the transfer rates in the ICRP 66 and ICRP 67 biokinetic models after considering the excretion data from the United States Transuranium and Uranium Registries (USTUR) Case 0269 which was due to plutonium inhalation. The ICRP default assumptions were revised to a 2-μm Activity Median Aerodynamic Diameter (AMAD) particle size, with revised ICRP 66 particle transformation fractions that included a bound fraction of 8%. The model prediction compared to USTUR Case 0269 urine excretion data was illustrated in Figure 3.

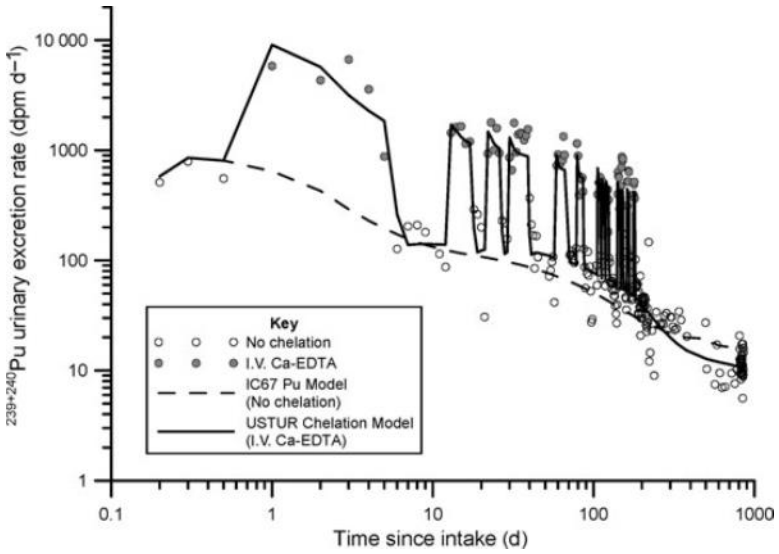

Figure 3: USTUR Case 0269 urine excretion results compared to revised ICRP 66 and ICRP 67 biokinetic models. Reprinted with permission from Oxford Journals: Radiation Protection Dosimetry (James et al. 2007).

Figure 3 illustrated that the revised ICRP 66 and ICRP 67 biokinetic model proposed by James et al. (2007) compared favorably to the measured urine excretion results. James et al. (2007) had considered the idea that chelation would enhance the transfer rates from all of the soft tissues, skeleton, kidneys, testes, and liver compartments to the blood or excretion compartments, including enhancement of the transfer rates from the blood compartment to the urinary pathway and bladder compartments. However no specific recommendations were provided for the revised biokinetic model transfer rates, with James et al. (2007) stating that this was a 'work in progress'. Unfortunately, Dr. James had passed away prior to completion of the work in this area.

1.3 ICRP 67 Plutonium Systemic Model

The ICRP 67 plutonium systemic model was mostly adopted by Leggett (1992) with the addition of a second liver compartment and is the current recommended standard for dosimetry purposes (ICRP 1993). The ICRP 67 plutonium biokinetic model is likely

to be updated based on new acquired knowledge since its publication (Leggett et al. 2005). Improvements have been suggested for eliminating the intermediate soft tissues (ST1) to bladder pathway and enhanced prediction for multiple bioassay types due to expanded human experiment data. Figure 4 illustrates a few inadequacies with the current model with respect to fecal and blood bioassays.

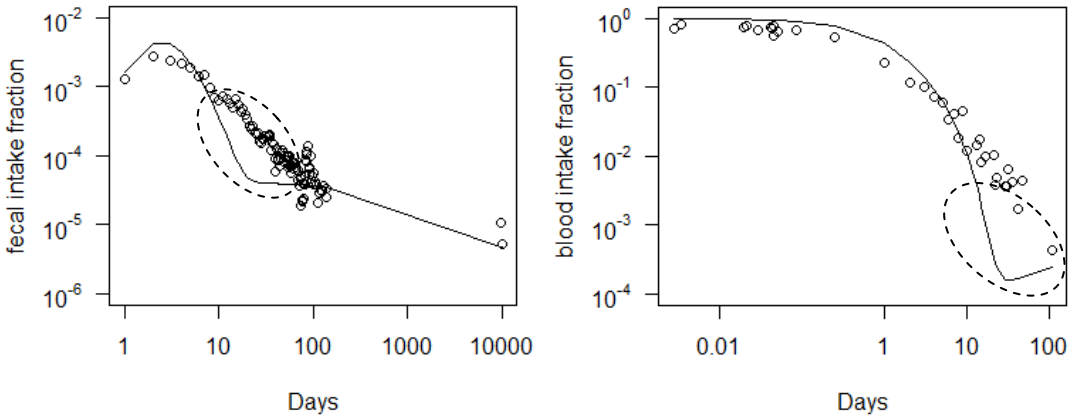

Figure 4: ICRP model prediction of fractional intake due to intravenous injection compared to mean fecal and blood plutonium bioassay where noted inconsistencies existed (denoted by dashed oval area).

Figure 4 illustrates how the ICRP 67 model under predicts the blood and fecal bioassays for intermediate periods from 10 to 100 days for fecal and blood bioassays. The Leggett 2005 model changes the basic structure of the ICRP 67 systemic model by including a second blood compartment and a third liver compartment. For injection cases, the ICRP 67 model assumes the entire quantity is initially assigned to the blood compartment; whereas, the Leggett 2005 model requires that the injection quantity be divided between the first blood and extracellular fluid compartments. This becomes unclear when the model is coupled with other intake models (e.g., NCRP 156 wound model, ICRP 66 lung model and ICRP 30 GI tract model) that rely on input into the blood

compartment. Although the Leggett 2005 model includes added complexity it showed substantial improvement compared to predictions provided by the ICRP 67 model.

1.4 Research Objectives

The primary research focus, in the present effort, was to develop a Pu-DTPA biokinetic model that could be used to supplement the standard ICRP recommended models for cases involving the administration of DTPA for treatment of incorporated plutonium originating from wounds and inhalation intakes. The Pu-DTPA biokinetic model was developed to estimate the initial intake quantity from inspection of bioassay samples influenced by chelation; to estimate the potential dose saved with various DTPA treatments; and to recommend an optimum chelation treatment program.

The Pu-DTPA model was developed using IDEAS Case 123 with validation performed with autopsy results from USTUR Case 0269. Additionally, this research reviewed the physiological processes of the skeleton and liver with an evaluation of the ICRP 67 biokinetic model for possible improvement.

1.5 Hypothesis

The purpose of this study is to compare performance results of various compartment model predictions to measurement data. Two general types of tests were performed:

1- Goodness-of-fit

Each model will be fitted to the data and the fit assessed using a chi-square test statistic. A model fits this data when chi-square is small and the associated p-value is

large. A model fails to fit the data when the chi-square test statistic is large, and the p-value is small. On an absolute scale, p-values less than 0.01 indicate a very poor fit to the data, while p-values greater than 0.10 represent a good fit to the data. It is also possible to rank the fit of the models by comparing their p-values. The model with the largest p-value best fits the data.

2 – Internal consistency

For each model, predictions of intake were made for different bioassay types. An Analysis of Variance (AOV) F-test was used to assess the internal consistency of these measures, as they should all, in ideal circumstances, produce the same mean intake level. The understanding of p-values (in this case from an AOV F-test) can be understood as before. On an absolute scale, p-values less than 0.01 indicates a lack of internal consistency, while p-values greater than 0.10 represent internal consistency. Again, it is also possible to rank the internal consistency of each model by comparing their p-values. The model with the largest p-value has the greatest internal consistency.

Chapter 2: Literature Review

2.1 Plutonium

Plutonium and uranium were originally produced by the Manhattan project for military purposes during World War II (DOE 1997). Biological studies with rats began shortly after the first separation of plutonium in 1944 due to its recognized danger (Durbin 1971). The first experiment results reinforced the hypothesis that it was a non-trivial toxic material by demonstrating that it would stay in the lungs, and systemic absorption would lead to bone deposition. It became clear that avoiding the inhalation or ingestion of plutonium would rapidly become a priority (Durbin 1971). Plutonium production continued during the cold war era in order to amass a nuclear stockpile to be used as a deterrent, which involved a vast network of facilities across the country (DOE 1997). After the cold war, there has been a concerted effort to dismantle and cleanup these facilities, which have resulted in internal contamination exposures due to inhalations, ingestions and wounds. Unexpected acute occupational exposures have warranted medical intervention for mitigating the dose consequences. One of the primary intervention methods for mitigating plutonium uptakes is the administration of a chelating agent to aid in the binding and elimination of plutonium from the body.

2.1.1 Plutonium Biochemistry

Plutonium is an actinide that has a tendency to hydrolyze and form complex ions under physiological conditions (Durbin 1975, ICRP 1972, Taylor 1998). Plutonium has multiple valance states but is stable as Pu(IV) in a physiological pH (Durbin 1975, ICRP 1972). Durbin (1975) had indicated that Pu(IV) in biological fluids does not exist as an

ion but exists as either a complex that is monomeric and soluble, or as a hydrolysis product that is likely polymeric, colloidal and insoluble. Pu(IV) has a strong tendency to hydrolyze upon entering the body fluids, resulting in a polymeric form; however, most is bound to serum proteins, primarily transferrin (Tf), with some bound to albumin (Durbin 1975, Taylor 1998). Plutonium binds with the transferrin protein since it has a similar charge to radius ratio as Fe(III), where the Pu-Tf accounts for 70 to 90% of the plutonium in plasma (ICRP 1972, Jensen et al. 2012). Plutonium can complex with nonprotein ligands, polycarboxylates such as citrate and lactate, and the carboxyl groups of bone sialoprotein (Chipperfield and Taylor 1970, DHHS 2010). Actinide's hydrolytic behavior is determined by its valence state and its ionic radius, with smaller ionic radii having an increasing tendency to hydrolyze (ICRP 1972). This hydrolytic interaction accounts for the Pu(IV) low absorption properties in the gastrointestinal tract and wounds (ICRP 1972). Absorption in the lungs is dictated by the particle size, density and solubility, where plutonium oxide has an initial blood absorption of 0.1% coupled with significant long-term lymph node retention, while plutonium nitrate has an initial absorption of 10% with little long-term lymph node retention (ICRP 1972). Systemic plutonium is deposited primarily in the liver and skeleton, with the liver favoring deposition of polymeric plutonium, and the skeleton favoring deposition of monomeric plutonium (ICRP 1972). Polymeric forms of plutonium, including particles and colloids, are treated as toxins and are removed by the liver (Hall et al. 1978, Leggett 1985).

Chemical form influences the rate of absorption from wounds, with Pu(IV) citrate complexes having a faster absorption rate than Pu(IV) nitrate forms for intramuscular injections, and PuO_2 having a slower absorption rate (ICRP 1972). It has been

demonstrated that Pu(IV) complexes injected to simulate wounds were translocated to tissues in a monomeric form with low liver deposition; however, over time the liver deposition increased, indicating that late polymeric complexes were being formed (ICRP 1972). Deposition on skeletal surfaces would increase the risk for bone sarcomas; however, deposition in the bone marrow, liver and spleen would increase the risk for leukemia or hepatic tumors (ICRP 1972). Skeletal deposition of high Pu(IV) concentrations associated with radiation damage would be expected to have an increased retention rate due to a decrease in the bone remodeling rate (ICRP 1972). Osteoclast activity is inhibited at high plutonium concentrations of 2.8 $\mu Ci\ kg^{-1}$; however, osteoclast activity is unperturbed at plutonium concentrations of 0.3 $\mu Ci\ kg^{-1}$ (ICRP 1972).

Diferric Tf transports iron to storage sites in the liver, spleen, intestinal lining, and to the bone marrow to support erythropoiesis, in which two-thirds of the bodies iron content is stored in the hemoglobin (Forejtnikova et al. 2010, Gropper et al 2009, Jensen et al. 2012). The Tf receptor (TfR), which is a transmembrane protein integrated with receptor cell membranes, forms a complex with diferric Tf incorporating it through clathrin-mediated endocytosis (Gropper et al. 2009, Jensen et al. 2012, Mayle et al. 2012). Transferrin receptors for diferric Tf is associated with the liver, intestine and erythrocyte formation (Cheng et al. 2004, Gropper et al. 2009, Kawabata et al. 2001). The Pu-Tf complex is not known for its cellular incorporation ability; however, a recent study had determined that when the Pu(IV) and Fe(III) ions are bound within the C and N lobe of the transferrin protein, respectively (Pu_CFe_NTf) cellular incorporation was possible (Jensen et al. 2012). When considering normal transferrin iron loadings (i.e., 37% Apo-Tf, 45%Fe_NTf, 8% Fe_CTf and 11% Fe_2Tf), Pu(IV) interaction with Tf will have an

opportunity of being in the correct arrangement for cellular uptake (Jensen et al. 2012). The mechanism for Fe(III) incorporation includes Tf-TfR complex-mediated endocytosis followed by lowering the pH to 5.5 by proton ATPase import into the endosome, causing the Fe(III) ions to be released from the Tf protein (Gropper et al. 2009). Once released, the Fe(III) is reduced to Fe(II) and is transported into the cytosol by the divalent metal transporter 1 (DMT1) protein, while the endosome returns to the cell membrane, releasing the Tf back into circulation (Gropper et al. 2009). It is unclear if Pu(IV) can be reduced and transported into the hemoglobin cytosol using this same process, which requires further study (Jensen et al. 2012).

The fate of the plutonium ion remains unclear. Pu(IV) may bind to the cell membrane and never becomes incorporated into cells (Taylor 1998). But, it is alternatively plausible that the Pu(IV) stays within the endosome and returns to the surface with the Tf-TfR for release back into circulation. Figure 5 illustrates ^{238}Pu whole-blood retention in nonhuman primates for the first 2 weeks following intramuscular injection of a plutonium citrate solution (Durbin and Jeung 1990, Konzen et al. 2014 in press).

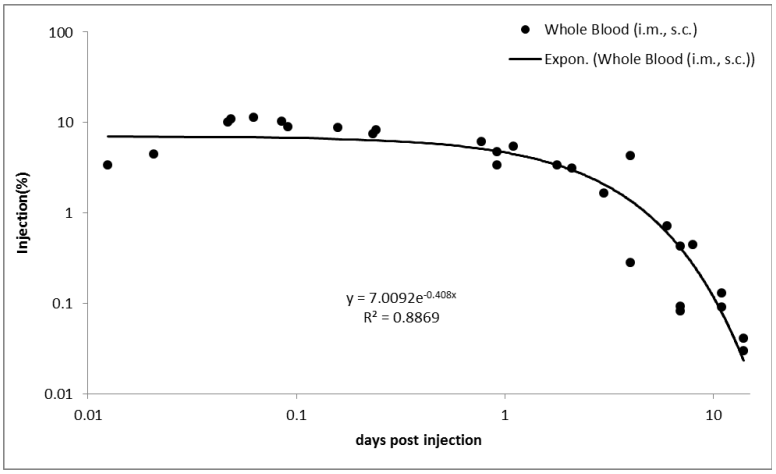

Figure 5: ^{238}Pu retention in whole blood following i.m. or s.c. injection in primates showing an exponential decay (Konzen et al. 2014 in press).

Figure 5 illustrates the short-term retention of ^{238}Pu in whole-blood sampled from nonhuman primates (Konzen et al. 2014 in press). These results indicated an exponential decrease in whole-blood retention, which is contrary to heme cell retention of plutonium if the possibility existed, since hemoglobin has a 4-month life-span and plutonium incorporation would increase towards an equilibrium value if cellular incorporation was occurring. These results also indicate the plutonium does not stay attached to the cell membrane and dissociates from whole-blood cells.

2.1.2 Pu(IV) distribution

Upon initial absorption, Pu(IV) rapidly associates with iron transporting and storage proteins (i.e., transferrin and ferritin), with components of bone and forms insoluble deposits within cells (Grube et al. 1978, O'Boyle et al. 1997). The liver hepatocytes account for 97% of the iron stored in the liver and is the major site for monomeric plutonium deposition (Grube et al. 1978). Schubert et al. (1961) found that the liver had twice as much activity compared to the skeleton for the polymeric form, with the spleen retention accounting for 0.1% and 1.3% of monomeric and polymeric

forms, respectively. Experimental evidence indicates that the chemical form of plutonium while injected intravenously into the body will influence its distribution in the blood, soft tissues and skeleton (Richardson 2010); the monomeric form of plutonium is the primary interest for occupational exposures. Monomeric plutonium is rapidly bound by the transferrin protein and transported to iron utilization sites, where it dissociates from transferrin at the surfaces of developing red cells and targets either the nearest bone surface, recombines with Tf, or enters blood circulation and targets a remote bone surface (Leggett 1985, Durbin et al. 1972). It also has been speculated that the small deposition of plutonium bound to periosteal surfaces are due to the centrifugal blood flow from the bone cavity, carrying some of the plutonium dissociated in the blood marrow that was not deposited locally (Leggett 1985).

Monomeric plutonium deposits preferentially at bone surfaces, with little initial distribution to the marrow; whereas, highly polymeric plutonium deposits preferentially in the marrow (DHHS 2010), which is likely due to being engulfed by tissue macrophages. Rabbit studies have discovered that monomeric plutonium was absent from the bone marrow a few days after injection; while most of the polymeric plutonium was found in the bone marrow (Leggett 1985, Rosenthal et al. 1972). Studies have indicated that plutonium concentrations in endosteal surfaces of dogs are greater in resorbing surfaces than in resting surfaces (Leggett 1985, Polig et al. 1998), while americium that is less readily hydrolyzed and less stable when bound to transferrin, is uniformly distributed on all bone surfaces (Durbin 1975). This may be explained since plutonium appears to be released from the transferrin protein at erythropoeitic sites of the bone marrow, which are also located near bone remodeling sites. The trabecular uptake

exceeded the cortical uptake by 10, with subsequent transfer of trabecular activity to the cortical bone with time that was experienced in a beagle dog study (Polig et al. 1998). Polig et al. (1998) had indicated that plutonium deposits are three times greater at bone forming sites, whereas americium deposits are uniformly deposited between bone forming and resting sites.

Osteoclast resorption of the matrix and mineral appears to be the only mechanism for skeletal removal of actinides (Durbin and Schmidt 1985). The initial surface deposit is partly buried by apposition of new bone, while some is resorbed with polymeric forms being engulfed by macrophages and monomeric forms recirculated (Durbin and Schmidt 1985, Leggett 1985). The biokinetic model assumes that 60% of the skeletal deposition is on trabecular surfaces with 40% on cortical surfaces, where unbound plutonium can attach to bone surfaces by binding with exposed mineral, collagen and glycoproteins (Leggett 1985).

In summary, monomeric plutonium complexes with serum proteins, primarily transferrin, and targets iron storage sites of the liver. It also deposits preferentially on trabecular bone surfaces due to their vicinity to erythropoeitic sites. Tissue macrophages will phagocytize resorbed polymeric plutonium, releasing monomeric plutonium which either deposits on bone surfaces, or enters circulation, complexing with a transferrin protein, thus repeating the process. Discussion of the different organ kinetics is provided in the following sections.

2.2 Physiology

2.2.1 Skeleton

The skeleton includes a dynamic and complex network of bone lining cells (i.e., osteoprogenitor and osteoblast cells), with osteocytes integrated throughout the skeletal matrix, that is able to continually monitor and rebuild itself in response to the various stresses demanded of it (Barrett et al. 2012, Bilezikian et al. 2008, Hall 2011). The skeleton is a metabolically active organ that continuously remodels to maintain its structural integrity and serves as the primary storage site for calcium and phosphorus (Raisz 1999). Bone consists of 50 to 70% mineral (i.e., hydroxyapatite, small amounts of carbonate, magnesium, acid phosphate and missing hydroxyl groups), 20 to 40% organic matrix (e.g., collagen), 5 to 10% water and <3% lipids (Clarke 2008). Osteogenic cells originate from mesenchymal stem cells which differentiate into different lineages, where osteodifferentiation leads to the osteoblast (Bilezikian et al. 2008). Osteoblasts differentiate into osteocytes when incorporated in the bone matrix, quiescence into bone lining cells, or undergo apoptosis during and upon completion of the bone mineralization process (Bilezikian et al. 2008, Hall 2011). The bone lining cells are connected to each other by gap junctions, creating a paracellular pathway that can allow small ions to pass, where the bone lining cells create a membrane (i.e., periosteum for external bone and endosteum for the interior bone matrix) that provides a separation between the bone fluid and the extracellular fluids (Barrett et al. 2012, Talmage and Talmage 2007, Teti and Zallone 2009). Extracellular fluids provide nutrients and minerals by diffusion across the skeletal membrane to the bone cells and skeletal structure while removing spent waste

products (Barrett et al. 2012). Figure 6 presents a conceptual understanding of the osteogenic cellular matrix.

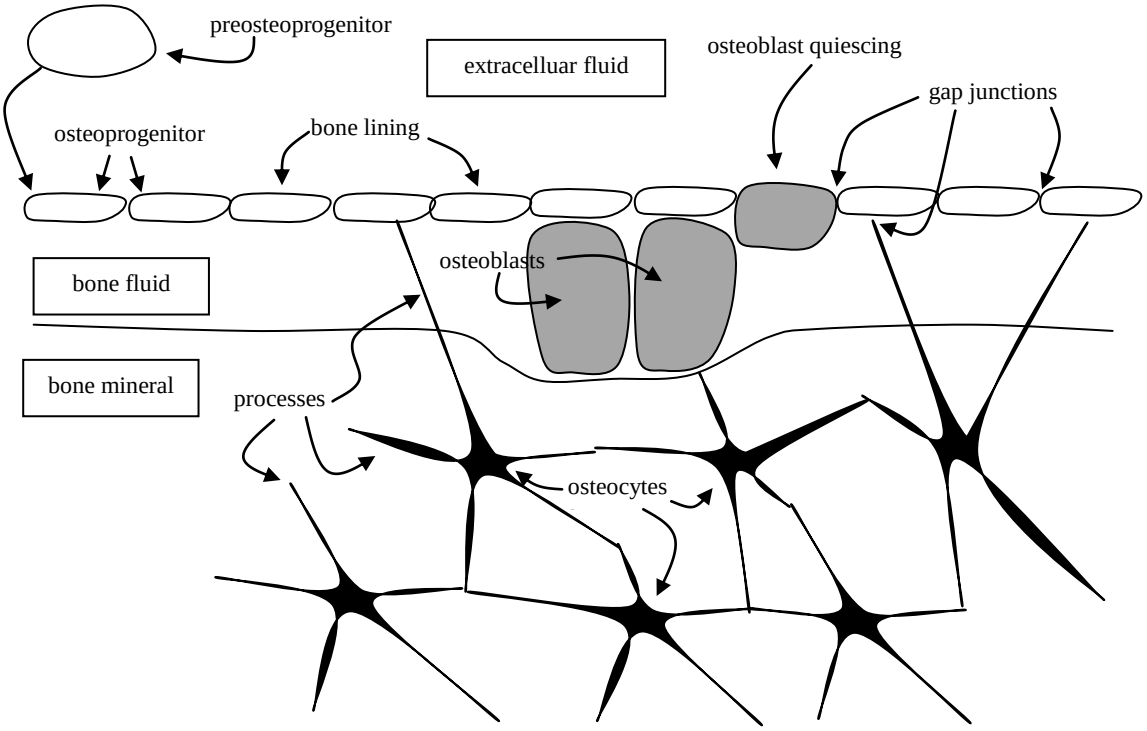

Figure 6: Osteogenic cell matrix. The preosteoprogenitor differentiates into the osteoprogenitor cell that maintains the bone lining, assisted by the osteoblasts. Osteoprogenitors differentiate into osteoblasts during the bone remodeling process. Osteoblasts differentiate into osteocytes when incorporated into the bone matrix or quiescent into a bone-lining cell. The osteocyte processes communicate with the bone lining cells and with each other via gap junctions to maintain the osteocytic membrane system. Gap junctions are present in bone lining cells that maintain the endosteal membrane, creating a separation between the extracellular fluid and bone fluid.

Osteocytes reside within the lacunae of the bone calcified matrix with processes that also connect via gap junctions with other osteocytes and the bone lining cells through the canaliculi, creating an osteocytic membrane system that also separates extracellular fluid from the bone fluid (Bilezikian et al. 2008, Fawcett 1997, Hall 2011, Talmage and Talmage 2007, Teti and Zallone 2009). There are approximately 10,000 osteocyte cells per mm^3 making up approximately 90 – 95% of all bone cells in the human skeleton that includes approximately 50 processes per cell, where no part of the bone matrix is more

than a few microns from a lacunae containing an osteocyte (Bilezikian et al. 2008). When an osteocyte process is broken due to fractures in the bone matrix that results in osteocyte apoptosis, a signal is sent from this network to the bone lining cells that initiates the bone remodeling process (Bilezikian et al. 2008, Ross and Pawlina 2011, Sims and Gooi 2008).

Skeleton structure

The skeleton consists of cortical (compact) bone and trabecular (spongy) bone that make up 80% and 20% of the human skeleton, respectively (Barrett et al. 2012). Cortical bone makes up the outer layer of most bones, consisting of osteons where collagen is arranged in concentric layers (lamellae) with incorporated Haversian and Volkman canals containing blood vessels, where nutrients are provided by ramification through the canaliculi (Barrett et al. 2012, Ross and Pawlina 2011). Trabecular bone makes up the bone interior that is arranged as trabeculae with numerous interconnecting marrow spaces and nutrients are provided through diffusion (Bartlett et al. 2012, Ross and Pawlina 2011). Marrow can consist of red or yellow marrow, where the red marrow is the site for erythrocyte formation (i.e., typically associated with the vertebrae, iliac crest, ribs, sternum, scapula, and proximal humerus) and the yellow marrow consists of fat cells (Durbin and Schmidt 1985, Ross and Pawlina 2011). Red marrow involving erythrocyte formation is associated with trabecular bone, where monomeric plutonium is released from the Pu-Tf complex and is either locally deposited in active sites, which is assumed to be based on the mineralization rate of forming bone following resorption, with some entering circulation.

Bone remodeling

Bone remodeling occurs via osteoblasts and osteoclasts, responsible for bone formation and resorption, respectively (Ganong 2003). Osteoclasts are multinucleate cells that bind to bone surfaces through integrins, where the ruffled border creates a seal with the bone mineral surface (Ganong 2003, Hall 2011). Protons, hydrochloric acid and proteases are transported into this area to lower the pH to 4-5 for dissolving the bone mineral (i.e., hydroxyapatite), collagen and bone matrix proteins (Matsuo and Irie 2008, Ross and Pawlina 2011). Bone remodeling takes approximately 100 days, where the first three weeks involve resorption, followed by rebuilding the collagen framework and mineralization (Ganong 2003, Hall 2011). About 5% of the skeleton is undergoing the resorption process at any time, with renewal rates of cortical and trabecular bone of 4% and 20% per year, respectively, where calcium turnover for an adult is 18% per year (Barrett et al. 2012). Calcium turnover is stimulated by bone stress, such as physical stress from exercise or load carrying, which stimulates osteoblastic deposition and calcification of bone (Hall 2011). Bone fractures also stimulate osteoblast formation from osteoprogenitor cells, resulting in the formation of an osteoblastic bulge (i.e., callus) consisting of an organic bone matrix followed shortly by calcium salt deposition (Hall 2011).

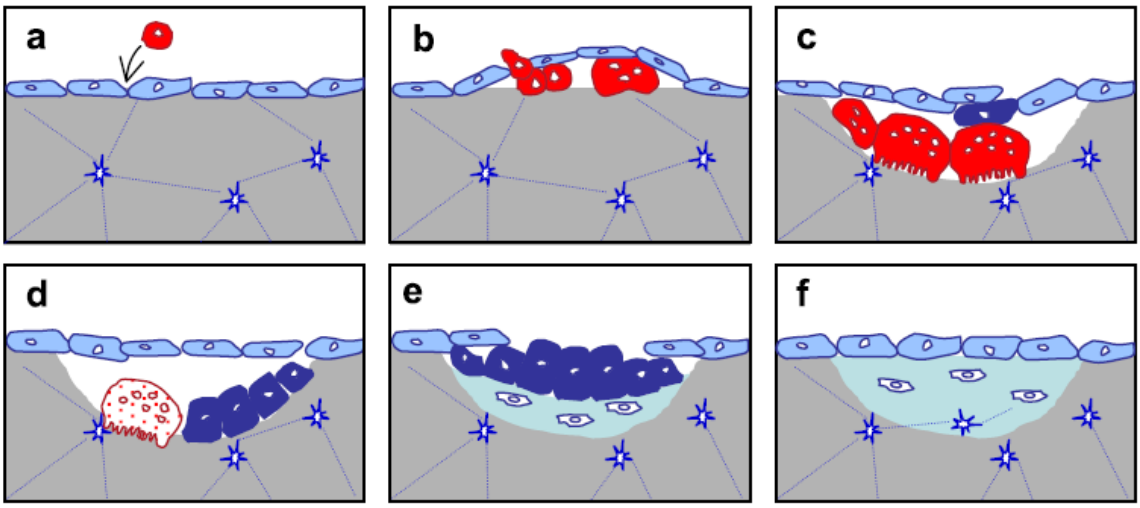

Figure 7: Bone remodeling. Reprinted with permission from Elsevier (Matsuo and Irie 2008).

Figure Note: Bone remodeling begins upon signal initiation by transporting monocytes across the bone lining cell membrane (a) and differentiating into an osteoclast (b) that initiates the resorption process. Upon completion, the osteoclast in contact with the bone lining cell membrane induces osteoblast differentiation (c). Upon completion of resorption, the osteoclast experiences apoptosis while the osteoblasts begin bone formation (d). Incorporated osteoblasts begin to differentiate into osteocytes (e) while maintaining the bone lining cell membrane. Upon completion of bone remodeling, the osteoblasts differentiate into bone lining cells (f) thus entering into quiescence.

Figure 7 illustrates that the monocytes pass through the bone lining cell membrane before differentiating into osteoclasts to begin the resorption process (Matsuo and Irie 2008). The osteoclasts are derived from hematopoietic stem cells with similar characteristics as macrophages that rely on osteoprogenitor and osteoblast interaction for osteoclast differentiation and for initiating and terminating the resorption process (Matsuo and Irie 2008). Osteoclasts and osteoblasts can make direct contact for membrane-bound proteins and receptor interaction, as well as form gap junctions for small ion passage (Matsuo and Irie 2008). The osteoclasts remain covered by the bone lining cell membrane, where the membrane integrity is maintained for the complete remodeling process (Matsuo and Irie 2008). The osteoclast lysosomes catabolize the minerals, releasing calcium ions and soluble inorganic phosphates to the interstitial fluids

(Barrett et al. 2012, Ross and Pawlina 2011). Osteoblasts should be able to incorporate the calcium and phosphate ions released during resorption through diffusion and by the osteoblast-osteoclast gap junctions providing support for calcium homeostasis and for rebuilding of the resorption site.

Bone formation

During bone formation, osteoblasts are responsible for producing collagen monomers which produce collagen fibers, resulting in the formation of the osteoid in which calcium salts readily precipitate and ultimately form a hydroxyapatite crystal over several weeks or months, while a few percent are maintained in an amorphous form (Hall 2011). Boonrungsiman et al. (2012) was able to identify calcium-phosphate within osteoblast intracellular vesicles that was transported to the extracellular matrix for deposit and mineralization on collagen fibers of mouse osteoblast cultures that was studied *in vitro*. The mineralization process involves matrix proteins, which include calcium-binding proteins such as osteocalcin and osteonectin; multiadhesive glycoproteins such as bone sialoproteins, osteopontin and thrombospondin, various proteoglycans and alkaline phosphatase (Ross and Pawlina 2011). During the osteoid formation, some of the osteoblasts become entrapped and quiescent, forming an osteocyte (Hall 2011). Osteoblasts remaining on the surface will flatten and continue to function as bone-lining membrane (Fawcett 1997).

Luciani et al. (2006) hypothesized that bone tumors are primarily associated with the osteoblastic cell line. This helps explain the relatively higher toxicity of plutonium by relating it to the radiation dose received at bone formation sites of trabecular bone.

This appears to be consistent with observations that bone remodeling sites involve osteoprogenitor cells differentiating into osteoblasts that support bone remodeling, with osteoblasts differentiating into either osteocytes or quiescing into surface lining cells, thus the increased cellular differentiating activity supports Luciani et al.'s (2006) hypothesis. It also explains the hypothesis of plutonium having a higher toxicity than americium, since plutonium is at a higher concentration at bone remodeling sites because of its higher affinity for complexing with the transferrin protein and its propensity of being released in active bone marrow in the vicinity of active bone remodeling sites.

Skeleton metal dynamics

Metals are taken up in regions of the skeleton with the highest turnover rate, whereas retention is highest in regions with the lowest turnover rates, thus characterizing bone as a metal reservoir (Bilezikian et al. 2008) with an affinity for radionuclides such as uranium, strontium, cesium and plutonium (Moore et al. 2005). Metal deposition on bone surfaces is due to exchanges with other elements. Once deposited such materials typically experience a rapid exchange and are resorbed into circulation (Bilezikian et al. 2008). Membrane intercellular transport was observed for lanthanum which was observed to be present in the channels between the bone lining cells and also mixed in the bone fluid of a rat's tibia after injections that occurred shortly before sacrifice (Talmage and Talmage 2007, Teti and Zallone 2009). The tight junctions that exist in epithelial membranes have similar characteristics as the bone lining cells, thus metals that pass the epithelial membrane in an ionic or monomeric form would be capable of passing the bone lining cells and entering the bone fluid. Additional evidence exists that supports this understanding. It has been shown that these channels allow the rapid response important

to maintain calcium homeostasis in extracellular fluids during parathyroid hormone (PTH) or calcitonin infusions; where the active transport of Ca^{2+} was insufficient to maintain calcium homeostasis alone (Talmage and Talmage 2007, Teti and Zallone 2009). The distribution of transuranic radionuclides within the bone matrix is primarily on the bone surfaces, whereas, the distribution of calcium-like radionuclides, such as strontium and uranium, is within the bone volume (Richardson 2010).

Radionuclides that target the bone volume would experience a different path. For example lead readily displaces Ca^{2+} by cation exchange processes in the hydroxyapatite crystal (Pounds et al. 1991). Lead ions cross osteoblast cell membranes with half-times of approximately 1-min using the Ca^{2+} receptor system (Pounds et al. 1991). It is suggested that calcium-like elements incorporated in the osteoblast would be able to enter the calcium vesicles supporting bone mineralization as described by Boonrungsiman (2012), thus describing the bone volume pathway.

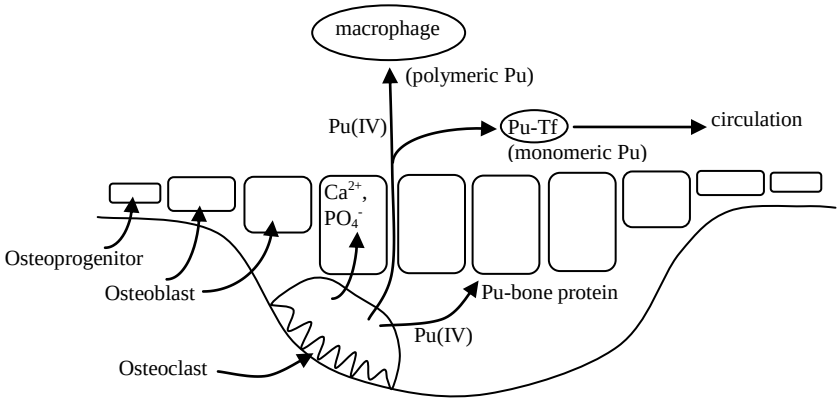

Figure 8: Resorption process of osteoclast.

Resorbed plutonium ions are not expected to diffuse across the osteoblast membrane due to the specificity of ion channels for Ca^{2+} and PO_4^- (Barrett et al. 2012). Figure 8 illustrates that plutonium ions bond with bone glycoproteins that may bind to the

osteoblast cell membrane, rebind to the bone surface during mineralization, cross the bone lining membrane to be engulfed by tissue macrophages or bond with transferrin, based on whether the plutonium ion was in a polymeric or monomeric form (Durbin and Schmidt 1985, Leggett 1985). It is likely that plutonium would exist as a polymeric complex upon resorption, possibly with a small percentage being of a monomeric form, which would indicate that most of the resorbed plutonium would be phagocytized by the tissue macrophages near the bone lining upon resorption (Richardson 2010).

The bone matrix consists of collagen fiber, accounting for 90% of the organic material, that has been mineralized, primarily in a hexagonal crystalline structure known as hydroxyapatite [$Ca_{10}(PO_4)_6(OH)_2$], which is known for its strong plutonium adsorption properties (Fawcett 1997, Moore et al. 2005, Thomson et al. 2003). Americium and plutonium are localized in bone where the surfaces indicate the presence of mucosubstances (e.g., bone proteins, glycoproteins) where it was clear that the mode of uptake differed from alkaline earths and from each other (Chipperfield and Taylor 1970). Bone sialoprotein; a highly acidic glycoprotein, had a much higher affinity for plutonium than for transferrin *in vitro* when pH is between 4 to 8 that is attributed to the ionized carboxyl groups of the bone sialoprotein (Chipperfield and Taylor 1970). Chipperfield and Taylor (1972) used a gel filtration technique to study the binding characteristics of several actinides to five types of bone glycoproteins. Table 2 summarizes these results.

Table 2: *In vitro* binding of actinides to bovine cortical bone proteins (Chipperfield and Taylor 1972)

Protein	Pu(IV)	Am(III)	Cm(III)
Bone sialoprotein	54.7 ± 9.3	10.4 ± 2.9	12.2 ± 1.1
Bone chondroitin sulfate-protein complex	49.2 ± 3.0	14.9 ± 6.6	10.1 ± 1.6
Cerylpyridinium chloride-soluble glycoprotein	36.6 ± 5.1	4.6 ± 2.9	8.7 ± 1.2
Glycoprotein I	30.0 ± 12.4	2.8 ± 0.9	37.5 ± 12.6
Glycoprotein II	50.3 ± 9.4	5.1 ± 2.0	8.2 ± 1.3
Soluble collagen	23.3 ± .3	0.6 ± 0.2	0.9 ± 0.3
Human serum albumin	1.2 ± 0.8	0.1 ± 0.1	
Human transferrin	18.9 ± 6.9	0.2 ± 0.0	0.0

Note: results are percent recovery of actinide protein complex.

Chipperfield and Taylor (1972) indicated that Pu(IV) had a high affinity for bone glycoproteins with 30 to 55% recovery of the actinide protein complex during *in vitro* experiments. There was a 23% recovery of the Pu(IV) collagen complex; however, Chipperfield and Taylor (1972) suggested that collagen binding *in vivo* may not actually occur due to the presence and competition with the bone glycoproteins. This can be extended to DTPA effectiveness at forming complexes with Pu(IV) that is influenced by the competition with endogenous ligands. Differences in ^{239}Pu toxicity compared to ^{241}Am have been identified several times. The differences seem to be related to the variation in radionuclide distributions on forming and resting bone surfaces (Lloyd et al. 1984, Mays et al. 1987, Polig et al. 1998), and as illustrated here by their different affinities for bone proteins. Chipperfield and Taylor (1972) investigated the effect of preventing actinide binding to bone mineral in the presence of different chemicals. Their results are summarized in Table 3.

Table 3: *In vitro* inhibition of actinide binding to bone mineral in the presence of chelating agents (Chipperfield and Taylor 1972).

Substance	Pu(IV)		Am(III)		Cm(III)	
	Metal	Glycoprotein	Metal	Glycoprotein	Metal	Glycoprotein
None, control	1.5 ± 0.3	-	0.6 ± 0.1	-	1.1 ± 0.0	-
Citrate	27.3 ± 4.3	-	0.5 ± 0.2	-	1.1 ± 0.8	-
EDTA	8.8 ± 1.4	-	30.7 ± 2.4	-	39.3 ± 2.0	-
DTPA	86.1 ± 4.0	-	100.9 ± 1.3	-	99.0 ± 2.3	-
Bone Sialoprotein	30.5 ± 1.6	100.7 ± 6.5	9.5 ± 1.1	96.1 ± 11.9	10.7 ± 0.7	101.0 ± 2.5
Bone Chondroitin sulfate-protein complex	11.6 ± 1.9	100.2 ± 11.7	5.9 ± 2.8	98.0 ± 17.9	4.8 ± 1.6	99.5 ± 7.0
Transferrin	1.8 ± 0.9	99.5 ± 8.2	0.5 ± 0.2	107.6 ± 4.3	10.8 ± 0.1	96.2 ± 2.0

Note: results are percent recovery of actinide protein complex.

Table 3 displays the non-bound actinide recovery from bone mineral in the presence of different chemicals, or in the presence of the chemicals while also in the presence of glycoproteins. Table 3 illustrated that DTPA is effective at preventing Pu(IV), Am(III) and Cm(III) from binding to bone mineral. The author notes that DTPA is more effective than EDTA and citrate complexes in preventing actinide binding in bone material (Chipperfield and Taylor 1972). Transferrin by itself did not prevent bone mineral binding; whereas, bone sialoprotein and bone chondroitin sulfate-protein complex had some success (Chipperfield and Taylor 1972). When these proteins were present with glycoproteins; bone mineral binding was essentially prevented (Chipperfield and Taylor 1972). Chipperfield and Taylor (1972) illustrated the high affinity of plutonium to bone proteins in relation to transferrin that was illustrated in Table 2, and how DTPA and glycoproteins were successful in preventing plutonium from being bound to bone mineral that was illustrated in Table 3. This seems to explain the prevention of skeleton incorporation during the initial phases of plutonium deposition after complexing

with DTPA; however, it does not support skeleton decorporation after plutonium has been integrated into the skeleton matrix.

Calcium homeostasis

The skeleton plays a significant role in maintaining calcium and phosphate homeostasis in response to the endocrine system (Barrett et al. 2012). Calcium homeostasis is regulated by the parathyroid hormone (PTH) and calcitonin, which are secreted by the parathyroid and thyroid glands, respectively (Ross and Pawlina 2011). PTH raises the blood calcium concentration while calcitonin acts to lower the blood calcium concentration (Ross and Pawlina 2011). A network of osteocytes and surface lining osteoblasts, known collectively as the osteocytic membrane system, separates the extracellular fluid from the bone, with bone fluid existing between the membrane and the bone (Hall 2011). The osteocytic membrane system responds to PTH through receptor proteins to regulate the calcium ion concentration in extracellular fluids (Hall 2011). This is accomplished by exchanging with amorphous calcium phosphate compounds located near the cells (Hall 2011). PTH enhances absorption of calcium from the intestines through the formation of 1,25-dihydroxycholecalciferol from vitamin D in the kidneys, and enhances phosphate excretion in the urine (Barrett et al. 2012, Hall 2011). Extended periods of excess PTH stimulate the osteoclastic system which may continue to grow for months (Hall 2011). Osteoclasts do not have receptors for PTH, where resorption is governed by osteoclast interaction with the osteoprogenitor and osteoblast cells (Barrett et al. 2012, Pounds et al. 1991). Calcitonin, on the other hand, interacts directly with osteoclasts, inhibiting bone resorption while increasing calcium and phosphate excretion in the urine (Barrett et al. 2012, Pounds et al. 1991).

Hall (2011) indicated that there exists exchangeable calcium in bones to maintain equilibrium with the calcium ion concentration in extracellular fluids, for example, if calcium ions increase such as by an injection of calcium salts, equilibrium will be achieved in 30 to 60 minutes, and the reverse is also experienced. There are two types of exchangeable calcium in the bone, one that is readily exchangeable and the other is slowly exchangeable (Ganong 2003). The latter is related to bone resorption that accounts for the calcium exchange of 7.5 mmol per day, while readily exchangeable calcium accounts for the exchange of 500 mmol per day (Ganong 2003). The bone matrix contains significant concentrations of citrate and carbonate ions in the fluid surrounding each hydroxyapatite crystal and is believed to facilitate ion exchange between the crystal and body fluid (Fawcett 1997). A small portion of exchangeable calcium is available in tissue cells, such as the liver; however, most of the exchangeable calcium is in the bone in the form of $CaHPO_4$, which accounts for 0.4 to 1% of the total bone calcium (Hall 2011). Boonrungsiman et al. (2012) observed the vesicle transport of calcium by the osteoblast for bone mineralization. It has been hypothesized that the osteoblast calcium intracellular content could be the source of readily exchangeable calcium accounting for the homeostatic concentration changes observed. Calcium and phosphate homeostasis are interrelated and understanding their response can be extended to metal biochemistry.

2.2.2 Liver

The primary function of the liver is to filter blood from the gastrointestinal tract via the portal vein (1350 mL min^{-1}) and circulating blood (300 mL min^{-1}) from the hepatic artery (Barrett et al. 2012, McCorry 2009, Ross and Pawlina 2011). The liver

provides most of the plasma proteins, including albumin, lipoproteins, and glycoproteins (Ross and Pawlina 2011). The liver also stores and metabolizes iron, and is integral to maintaining iron homeostasis. A decrease in circulating iron causes the liver ferritin to release iron into the blood stream (McCorry 2009, Ross and Pawlina 2011).

Blood is filtered through sinusoids between hepatic cells draining to the hepatic veins (Barrett et al. 2012). The hepatic sinuses normally store 450 mL of blood that can be used to make up the blood volume (McCorry 2009). The liver's Kupffer cells and hepatocytes detoxify the body. The metabolites produced are secreted in the bile that is stored in the gall bladder and eventually eliminated through the duodenum of the small intestine (Barrett et al. 2012). Some of the bile salts are reabsorbed in the intestine and excreted again, a process known as enterohepatic circulation (Barrett et al. 2012). A small quantity of these bile salts enters circulation and are excreted in the urine (Barrett et al. 2012). Bilirubin is the product of hemoglobin that has been catabolized once it has served its useful life (Barrett et al. 2012). Most of the bilirubin is bound to albumin and transported into the hepatocyte where it is conjugated to glucuronic acid and secreted into bile; however, a small portion escapes into the blood and this too is excreted in urine (Barrett et al. 2012). The liver consists primarily of hepatocytes and Kupffer cells, contributing to fecal excretion by the liver-biliary pathway, and is centrally important to maintaining iron homeostasis.

Kupffer Cells

Kupffer cells are derived from monocytes making up the mononuclear phagocytotic system or tissue macrophage system, previously called the

reticuloendothelial system (Barrett et al. 2012, Ross and Pawlina 2011). The Kupffer cells form part of the lining of the sinusoid, neighboring endothelial cells; however, junctions are not formed with the endothelial cells (Ross and Pawlina 2011). There is some evidence that suggests Kupffer cells participate in catabolizing senescent red blood cells that make it to the liver from the spleen, which is evident due to red cell fragments and ferritin iron observed within its cytoplasm (Ross and Pawlina 2011). Kupffer cells catabolize polymeric compounds, such as oxides and colloids, with animal studies indicating that 80% is released into circulation within 10 days (Hershko 1975). Beagle dog studies demonstrated that nearly all of the phagocytized plutonium in particulate form was transferred to the blood stream, which was evident by the gradual accumulation of skeletal plutonium and gradual decrease of the plutonium in phagocytic cells (Leggett 1985). Intracellular storage of iron is due to the ferritin protein, and iron is released from Kupffer cells through the transmembrane protein ferroportin (Barrett et al. 2012).

Hepatocytes

Hepatocytes are polygonal cells measuring 20 to 30 microns per side, making up approximately 80% of the liver cell population, with an average lifespan of 5 months (Ross and Pawlina 2011). Hepatocytes store iron as ferritin within its cytoplasm (Ross and Pawlina 2011). Synthesized proteins and lipoproteins from the hepatocytes enter circulation by the perisinusoidal space (Ross and Pawlina 2011). The hepatic lymph originates within the perisinusoidal space and drains to the periportal connective tissue in the periportal space (Ross and Pawlina 2011). The lymph fluid enters lymphatic capillaries, flowing in the same direction as the bile, where 80% drains into the thoracic duct (Ross and Pawlina 2011).

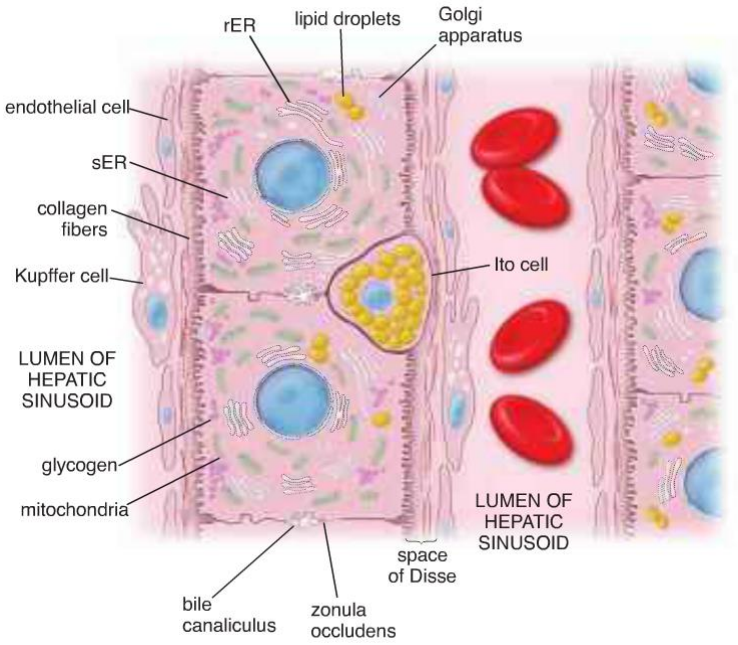

Figure 9: Cell diagram illustrates a one-cell thick plate of hepatocytes that is separated from the hepatic sinusoidal lumen by the endothelial and Kupffer cells. The space of Disse is the interstitial space between the endothelial cellular membrane and the hepatocytes. The Ito cell is important for storing vitamin A and responsible for producing collagen fibers found in the space of Disse. The bile canaliculus runs the perimeter of the hepatocyte that is used for bile excretion leading to the gall bladder. Reprinted with permission from Wolters Kluwer Health/LWW (Ross and Pawlina 2011).

Figure 9 illustrates the liver cellular matrix, where the hepatocytes make up 78% of the liver volume (Wisse et al. 1996). Kupffer cells and endothelial cells comprise 2.1% and 2.8% of the liver volume, respectively (Wisse et al. 1996). The hepatocytes border the perisinusoidal space (i.e., space of Disse), bile canaliculus between neighboring cells including the hepatic stellate cells (Ito cells), with endothelial and Kupffer cells forming a discontinuous endothelial cellular membrane between the hepatocyte and the hepatic sinusoids (Ross and Pawlina 2011). Kupffer cells are derived from the monocyte family all of which have a high phagocytotic capacity engulfing old and foreign cells, parasites, bacteria, viruses and particulate substances (Ross and Pawlina 2011, Wisse et al. 1996). The space of Disse consists of sparse collagen fibers, microvilli projecting from the hepatocytes, endothelial fenestrae, Ito cells, and white

blood cells that assist in the endothelial membrane function (Ross and Pawlina 2011, Wisse et al. 1996). The Ito cell produces the collagen fibers in the perisinusoidal space (i.e., space of Disse), which may also differentiate into myofibroblasts resulting in liver fibrosis (Ross and Pawlina 2011). Plutonium bound to transferrin that is transported to the liver, may be released at the hepatocyte cell membrane or possibly inside where it has been shown that the Pu(IV) may be transferred to the ferritin protein at physiological pH (Leggett 1985). The ferritin complex is more stable than the transferrin complex (Leggett 1985). Plutonium found in the biliary pathway is associated with its release from the hepatocytes. It is unlikely to originate from Kupffer cells due to the vicinity of the bile canaliculus. This observation is important to understanding DTPA influence.

Biliary Pathway

The human liver secretes about one liter of bile a day (Ross and Pawlina 2011). The bile emulsifies fat and is used by the liver for the excretion of cholesterol, bilirubin, iron and copper (Ross and Pawlina 2011). The biliary pathway originates in the hepatocyte, which secretes to the bile canaliculus, making its way to the gall bladder for secretion into the duodenum of the small intestine (Ross and Pawlina 2011). The gall bladder can store about 50 milliliters and is able to concentrate incoming bile by 10 fold (Ross and Pawlina 2011). The bile duct joins with the pancreatic duct prior to the duodenum entry (Ross and Pawlina 2011). Bile salts make up approximately 50% of the bile excretion, where many of the bile salts (about 90%) and electrolytes are reabsorbed by the gut and transported in the portal vein back to the liver where it is reabsorbed by the hepatocytes, only to be secreted back into the bile, thus describing enterohepatic circulation (McCorry 2009, Ross and Pawlina 2011). Electrolytes that are reabsorbed in

the enterohepatic circulation include Na^{+}, K^{+}, Ca^{2+}, Mg^{2+}, Cl^{-} and HCO_3^{-} (McCorry 2009, Ross and Pawlina 2011). The biliary pathway contributes to the GI tract excretion of plutonium, which is based on excretion of the hepatocytes to the adjacent bile canaliculus. It may be possible that plutonium DTPA complexes may participate in enterohepatic circulation and may increase urinary excretion a small percentage, which would require further study.

Iron Homeostasis

Most of the body's 3 to 5 grams of iron is stored in the hemoglobin (about 70%), with ferritin containing approximately 27%, and 3% in myoglobin (Barrett et al. 2012, Metzler 2001). Iron is essential due to its ability to bind to oxygen and is needed for erythropoiesis, where it is stored in the heme cell during hemoglobin production (Domenico et al. 2011). Iron entering circulation is primarily recycled from senescent erythrocytes from macrophages (20 mg day^{-1}), with intestinal absorption making up about 1 to 2 mg per day, and delivered by the transferrin protein to cell-surface transferrin receptors (Domenico et al. 2011, Palaneeswari 2013). Transferrin is a bilobed glycoprotein of 80 kilodaltons (kDa) that can bind up to 2 ferric ions [Fe(III)] where it is typically 35% saturated in plasma (Barrett et al. 2012, Cheng et al. 2004). Transferrin binding with iron prevents iron from creating hydroxyl radicals that are known to be toxic (McCorry 2009). Iron toxicity can occur when transferrin is 100% saturated with iron that would allow free iron to circulate unimpeded, creating hydroxyl radicals (McCorry 2009). Iron is imported into cells through transferrin receptor-mediated endocytosis, where the pH is lowered in the resultant endosome that causes a release of Fe(III) from the transferrin protein and a reduction to Fe(II), where the divalent metal transporter 1

(DMT1) protein transports the Fe(II) into the intracellular fluids (McCorry 2009). The endosome returns to the cell membrane releasing the transferrin protein into circulation (McCorry 2009). Diferric transferrin receptors are predominant in the liver, intestine and in erythropoiesis (Cheng et al. 2004, Forejtnikova et al. 2010, Gropper et al. 2009, Kawabata et al. 2001, McCorry 2009).

Iron is exported out of cells by ferroportin, which is a transmembrane protein that exports Fe(II) out of iron storage cells (Barrett et al. 2012, Palaneeswari et al. 2013). Ferroportin is also a cell-surface receptor for hepcidin (Sohn et al. 2011). Ferroportin exists in macrophages (primarily in the liver, spleen and bone marrow), hepatocytes and duodenal enterocytes (Sohn et al. 2011). Ferroportin regulation is crucial for maintaining iron homeostasis, where an iron deficiency up-regulates ferroportin, while an iron overload condition down-regulates ferroportin (Palaneeswari et al. 2013, Sohn et al. 2011). The liver (hepatocyte) synthesizes hepcidin, which is a peptide hormone that can bind with ferroportin to prevent iron exportation (Ghoti et al. 2011). Once ferroportin binds with hepcidin, it is internalized and degraded (Domenico et al. 2011). Hepcidin is a negative regulator of iron, where high hepcidin levels decrease iron uptake into the blood plasma, and low hepcidin levels increases iron uptake (Domenico et al. 2011). During an iron overload condition, iron is removed from plasma and stored in parenchymal tissues, such as hepatocytes and islet cells of the pancreas (Domenico et al. 2011). Hepcidin production is increased when the body is experiencing iron overload, and decreased when the body's need for iron increases, which can be determined by transferrin saturation (Forejtnikova et al. 2010, Ghoti et al. 2011). Iron regulation by hepcidin may help to explain iron chelation due to Ca-DTPA administration, where an iron deficiency in

circulation would reduce the hepcidin level, causing an upregulation of the ferroportin transmembrane proteins and increasing the transfer of iron from storage sites (e.g., hepatocytes, Kupffer cells and tissue macrophages) into the circulatory system. Cellular depletion of monomeric plutonium may also occur based on this mechanism, where chelation may increase circulatory plutonium levels that would be available for chelation. Understanding iron homeostasis and the effects of iron chelation on plutonium recovery can lead to alternative treatment strategies for plutonium and is suggested for future research.

2.2.3 Circulation

Blood Plasma

The average adult male has 5.3 liters and adult female has 3.9 liters of total blood volume that circulates throughout the body at 6.5 and 5.9 liters per minute, respectively, delivering nutrients, hormones and oxygen to cells while removing waste and carbon dioxide (ICRP 2002a, Ross and Pawlina 2011). Blood is made up of approximately 45% cells (i.e., erythrocytes, leukocytes and thrombocytes) and 55% plasma (Ross and Pawlina 2011). The erythrocytes (i.e., red blood cells) make up approximately 99% of the blood volume while thrombocytes (i.e., platelets) and leukocytes (i.e., lymphocytes, monocytes, and granulocytes) make up approximately 1% and 0.1% of the blood volume, respectively. Plasma consists of approximately 90% water, which acts as a solvent for transporting proteins, dissolved gases, electrolytes, nutrients, hormones, enzymes and waste materials (McCorry 2009, Ross and Pawlina 2011). Albumin accounts for approximately half of the plasma proteins, the remainder includes globulins (e.g.,

antibodies, transferrin) and fibrinogen making up approximate 8% of the plasma content, while solutes make up the remainder (McCorry 2009, Ross and Pawlina 2011). Electrolytes in the plasma include Na^+, K^+, Ca^{2+}, Mg^{2+}, Cl^-, HCO_3^-, PO_4^{3-}, and SO_4^{2-} (McCorry 2009, Ross and Pawlina 2011). Serum is related to and very similar to blood plasma with the exception of clotting factors and both terms can be used interchangeably (Ross and Pawlina 2011). Interstitial fluid surrounds tissue cells with electrolytes, which is derived from blood plasma (Ross and Pawlina 2011). An epithelial lining separates interstitial fluid from blood plasma (Ross and Pawlina 2011). The physiological pH of blood and plasma is maintained at about 7.4 (McCorry 2009). The blood plasma contains about 50 to 80 mg of citrate in its 3-liter volume that would normally be available for complexing with plutonium ions in circulation (Newton et al. 1998), however, the transferrin protein has a higher affinity for plutonium in circulation (Durbin 1975, Taylor 1998) than citrate, which implies that citrate and transferrin would serve as competing but unequally plausible sites for plutonium binding.

Lymphatic Circulation

The largest lymphatic vessel is the thoracic duct, which drains the thymus, spleen and thoracic lymph nodes (Ross and Pawlina 2011). Initial lymphatic vessels are found in areas of the intestine and skeletal muscle, where tissue fluid enters through loose endothelial cell junctions, lacking smooth muscle and valves the lymph is massaged by muscle contractions of the associated organs, tissues, arterioles and venules (Barrett et al. 2012). Lymph fluid drains into collecting lymph vessels that contain valves and smooth muscle that propels the fluid principally through peristaltic contraction, which is aided by skeletal muscle movement, thoracic pressure and blood flow at the terminal ends (Barrett

et al. 2012). The normal lymph flow is 2 to 4 liters every 24 hours, with fluid entering the lymph system through loose junctions of the endothelial cells (Barrett et al. 2012). Lymphocytes located in the subepithelial tissue of the alimentary canal and respiratory passages intercept antigens and travel to the regional lymph nodes (Ross and Pawlina 2011). Lymph nodes filter the lymph before returning it to the blood vascular system (Ross and Pawlina 2011). Plutonium in an insoluble or polymeric form that has been phagocytized by tissue macrophages is capable of being transported to regional lymph nodes, or may become bound in tissue when the particle is too large or has been engulfed into a larger macrophage due to irradiation damage of former macrophages (Jee 1972, Sanders 1970).

2.2.4 Soft Tissues

Soft tissues are a generic categorization of body organs and tissues that are not otherwise specifically identified in the ICRP 67 systemic model, which includes massive soft tissues, such as muscle, skin and fat (Leggett 1992). Some organs have been specifically identified in the compartment model due to their dosimetry significance, which includes the liver, kidneys, bladder, testes and ovaries. ICRP publication 60 (1991) also specifically identifies additional tissues of interest which are treated as remainder organs and reported in dosimetry results when they are target organs of significance. ICRP (1994) describes three categorial compartments that make up the soft tissues, with ST0 representing extracellular fluids that rapidly exchanges with the blood compartment, ST1 representing intermediate retention soft tissues, and ST2 representing tenaciously retained soft tissues. Soluble plutonium may be taken up by soft tissues in a fashion similar to iron uptake, but there is evidence that within a few months, most of the

plutonium is lost to soft tissues and incorporated within the skeleton and liver (Leggett 1985). Soft tissues also consist of lymphatic circulation, interstitial fluid, and organized tissue cells that are specific to the organ (Ross and Pawlina 2011). Organs generally can be described as sets of epithelial cells that make up a cellular membrane enclosing functional cells that are joined by cell-to-cell junctions that allows communication of various materials among cells but effectively separates extracellular fluids from the internal organ space existing within a barrier (Ross and Pawlina 2011). Soluble plutonium may be incorporated into soft tissues through protein exchange or protein receptors that mediate the transport into the cells. Monomeric plutonium may be able to pass the tight junctions of the cellular membrane due its small size in a manner similar to its transport across the pulmonary epithelium.

2.2.5 Kidneys

The kidney consists of renal tubes and a glomerulus that is a unit nephron (Barrett et al. 2012). The kidneys receive 25% of the cardiac output, approximately 1.2 to 1.3 liters of blood per minute (Barrett et al. 2012). The human kidney contains approximately one million nephrons (Barrett et al. 2012). The kidney filters the blood plasma, removing metabolic waste (i.e., urea, ammonium, and foreign chemicals), while reabsorbing glucose and amino acids, and regulating calcium and phosphate uptake (Barrett et al. 2012). Glomerular filtrate (i.e., glomerulus capillary filtration) continues down the renal tubes where water and solutes are reabsorbed (Barrett et al. 2012). The glomerular basement membrane lines the glomerular capillary that acts as a filtration barrier where proteins (e.g., albumin and transferrin) and particles larger than 70 kDa (3.6 nm radius) are not able to pass (Ross and Pawlina 2011), which explains why plutonium

has a low urinary excretion rate when it is complexed with the transferrin protein (Durbin 2008, Leggett 1985).

2.2.6 Monocyte-Macrophage System

Monocytes are formed from hemopoiesis in the bone marrow and enter circulation with a 72 hour life span (Barrett et al. 2012, Ross and Pawlina 2011). Monocytes that enter tissues differentiate into tissue macrophages with a typical 3-month life-span (Barrett et al. 2012). Tissue macrophages are readily found in the liver (Kupffer cells), spleen, lungs, bone marrow, connective tissue, lymph nodes and thymus (Barrett et al. 2012, Ross and Pawlina 2011). Some monocytes differentiate into multinucleated giant cells, such as the osteoclast, and Langhans giant cells when encountering large foreign bodies (Barrett et al. 2012, Ross and Pawlina 2011). The mononuclear phagocytotic system includes macrophages derived from monocytes that also function as antigen presenting cells (Ross and Pawlina 2011). Macrophages are able to phagocytize polymeric material by engulfing the debris in an endosome and digesting it with enzymes provided by a lysosome (Barrett et al. 2012). Senescent erythrocytes (i.e., aged red blood cells of around 4 months old) are digested by macrophages existing in the spleen, bone marrow and liver (Ross and Pawlina 2012). The heme and globin dissociate from the erythrocyte, where the heme iron is released and stored in the spleen as hemosiderin or ferritin for reuse in hemoglobin synthesis (Ross and Pawlina 2011). The globin is hydrolyzed to amino acids and reused, while the heme moiety is degraded into bilirubin and transported to the liver, being bound to albumin, and excreted as bile (Ross and Pawlina 2011). Plutonium complexes that have been catabolized within the

macrophage's lysosome can also be released back into circulation in a monomeric form, similar to iron, which is presumed to be by the ferroportin transmembrane protein.

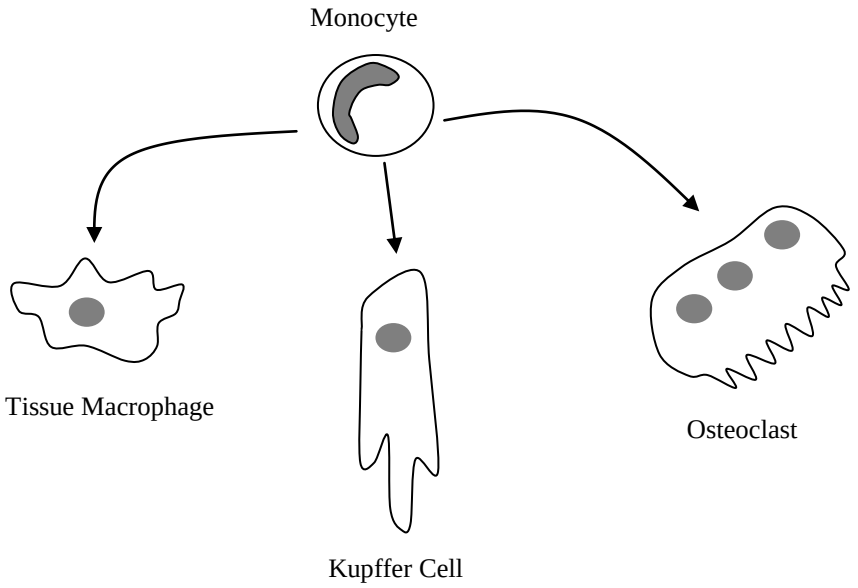

Figure 10: Monocyte differentiation into tissue macrophages, Kupffer cells and osteoclasts.

The monocyte-macrophage system consists of tissue macrophages, Kupffer cells, and osteoclasts (illustrated in Figure 10), which is responsible for the retention of polymeric plutonium, while also being responsible for skeleton resorption.

2.2.7 Cellular Membrane

Cell membranes consist of a lipid bilayer made of phospholipid molecules that are polarized with a hydrophilic head and hydrophobic tail (McCorry 2009). Cellular membranes are integrated with extrinsic proteins lining the cell membrane exterior or interior surface, and transmembrane proteins (McCorry 2009, Ross and Pawlina 2011). The cellular membrane resists entry of water soluble (hydrophilic) molecules into the

cell. A transport mechanism such as an ion channel, or a protein mediated mechanism are necessary if hydrophilic molecules are to enter a cell (McCorry 2009). The cells external surface has a carbohydrate coat that functions to repel negative ions and erythrocytes (McCorry 2009). Lipid soluble substances, such as oxygen, carbon dioxide and fatty acids, are able to pass easily through the membrane (McCorry 2009). Osmosis is where water molecules move towards a higher solute concentration (e.g., water leaving the cell due to extracellular fluids that have a higher solute concentration); mediated transport is performed by a carrier protein with a receptor that is able to transport molecules across the membrane (e.g., receptor-mediated endocytosis); and active transport is performed with proteins that move against the concentration gradient (e.g., ATPase pump that moves 3 Na^+ out of the cell while transporting 2 K^+ into the cell) (McCorry 2009, Ross and Pawlina 2011). The passage of plutonium across the cellular membrane still is not well understood. It is thought to involve carrier proteins, such as transferrin or ferritin. Furthermore, DTPA has been known to remove incorporated plutonium from hepatocytes during experimental observation (Bhattacharyya et al. 1978), even when DTPA was not incorporated in a liposome. Such observations emphasize a general lack of understanding of the interactions of plutonium and cellular membranes.

2.3 DTPA

Description

Diethylenetriaminepentaacetic acid (DTPA) has been used exclusively for human decorporation in the United States since its acceptance by the United States Food and Drug Administration (FDA) in 2004 (NCRP 2007). DTPA is a polydentate ligand that is

able to bind and enclose the contaminant, creating a Werner complex, thus neutralizing it by keeping it from chemically interacting with biological tissues (Crabtree 2005). Ethylenediaminetetraacetic acid (EDTA) was introduced for chelation in the early 1950's in a calcium complex; however, it was soon realized that repeated treatment was renally toxic due to trace metal (e.g., zinc and manganese) depletion (Durbin 2008, IAEA 1978). This led to the design of DTPA that provided better chelation properties; however, the renal toxicity still existed with repeated treatments of Ca-DTPA, which led to the development of Zn-DTPA (Durbin 2008). Zn-DTPA is not as effective initially at removing plutonium; however, repeated use does not lead to renal toxicity by avoiding essential trace metal depletion (Durbin 2008). Several authors have indicated and the IAEA has summarized that Ca-DTPA is more effective at removing plutonium on the first day after intake, but both Ca-DTPA and Zn-DTPA are consistent at removing plutonium after the first day post intake (IAEA 1978, Lloyd et al. 1978).

Multiple treatments of Ca-DTPA had detrimental consequences, in some cases leading to death, due to depletion of endogenous trace metals (Hameln Pharmaceuticals 2004, IAEA 1975). Side effects for Ca-DTPA administration have been observed to include nausea, diarrhea, development of sores and hair loss (Pippard et al. 1986). In a beagle dog study, Ca-DTPA administration was terminated early due to a severe health decline of the animal subjects when given fractionated doses (Lloyd et al. 1976) and another study where fractionated doses led to early death (Taylor et al. 1974). These consequences were related to Ca-DTPA administration that was not evident with Zn-DTPA administration.

Effectiveness

Decorporation effectiveness varies with respect to the type of DTPA administration, route of radionuclide uptake and organ retention. Liver decorporation has been observed almost completely with Ca-DTPA (Cohen et al. 1974, Bhattacharyya et al. 1978, Roedler et al. 1989, Carbaugh et al. 1989). However, there is a lack of clarity on the mechanism of this outcome. Ca-DTPA decorporates plutonium from the liver; however, it is also understood that Ca-DTPA does not pass cellular membranes unless complexed within a liposome (Phan et al. 2004). DTPA is strongly hydrophilic and is known to not enter cells readily, where liver decorporation has been largely attributed to the plutonium existing in the liver extracellular fluid that is in equilibrium with the intracellular plutonium (Grube et al. 1978). Various investigators have indicated that a small percentage of hydrophilic DTPA enters the cells of soft tissues and causes decorporation (Durbin 2008, Fritsch et al. 2010). DTPA has been observed with fast and slow clearance properties following administration (Stather et al. 1983, Breustedt et al. 2009). The majority of DTPA is rapidly cleared from the blood plasma into the urine with a 19-minute half-time (Stather et al. 1983). A small portion (2 to 3%) is excreted with an approximate 7-day half-time that is probably due to lymph circulation and intracellular retention (Breustedt et al. 2009, Fritsch et al. 2010). DTPA effectiveness varies according to the concentration ratio of DTPA to other endogenous ligands, and their behavior, including their affinity for plutonium (Fritsch et al. 2010). It is worth noting that the affinity of biological proteins for americium is much lower than for plutonium, where DTPA appears to have a larger decorporation effect (Chipperfield and Taylor 1972, Fritsch et al. 2010, Taylor 1972).

Grappin et al. (2007) reviewed 1,158 Ca-DTPA treatments in 469 patients inside CEA-COGEMA plants, with administration doses ranging from 0.1 to 1 gram per injection. The majority, 67% of the cases, were administered 0.5 grams (Grappin et al. 2007). Only one adverse reaction was reported. The reaction observed was an immediate allergic skin reaction that rapidly regressed without any long-term consequences (Grappin et al. 2007). Efficacy was measured by the enhanced urinary excretion rate of plutonium. This excretion rate was observed to increase from 25 to 100 times immediately following injection, with a factor of 50 being the typical increase (Grappin et al. 2007). A subsequent treatment was observed to have full efficacy (i.e., maximum observed urine excretion enhancement) for injections separated by 15 to 20 days following the previous injection (Grappin et al. 2007). It was speculated by the investigators that this time was necessary to allow for recycling plutonium to replenish the blood compartment (Grappin et al. 2007). Grappin et al. (2007) proposed daily treatments for 3 to 5 days, followed by 2 to 3 injections per week for 3 weeks, then followed by 1 injection per week for 3 months for wounds with an initial high-level intake.

Chelation is less effective at eliminating polymeric forms of plutonium than when it is in a monomeric form (ICRP 1972). DTPA also does not mobilize PuO_2 in the lungs or thoracic lymph nodes and is not recommended for inhalations unless it is known that it was due to a soluble intake (Catsch 1976). Bhattacharyya et al. (1978) was able to demonstrate a direct relationship between the quantity of monomeric plutonium removed from the liver (assumed to be removed from hepatocytes) of the rat with the activity measured in the bile. Bhattacharyya et al. (1978) reported that approximately 50% of the

liver was decorporated within 24 hours. Considering a single injection treatment, most of the Pu-DTPA was excreted within 4 hours (>90%) with a small percentage exhibiting a prolonged retention in the liver that was consistent with observations from other investigators (Bhattacharyya et al. 1978). Skeletal decorporation has also been observed (Cohen et al. 1974, James et al. 2007), but the mechanism was unclear and it was unclear whether the reduced skeletal activity was due to prevention or actual decorporation of the skeletal matrix.

Schubert et al. (1961) performed a study on mice with monomeric and polymeric forms of plutonium at high activity concentrations (3.3 μCi kg^{-1}) and daily Ca-DTPA treatments starting on the 3rd day following injection. Shubert et al. (1961) indicated from the study that a liver decorporation benefit of 60 to 95% for monomeric plutonium and 10 to 25% for polymeric plutonium was evident after several days of treatment. The skeleton retention in treated mice ranged from 30 to 50% compared to the controls from day 6 to day 21 for the monomeric plutonium injection, which was similar to the polymeric form where the skeleton retention ranged from 20 to 40% over days 6 to day 15 (Schubert et al. 1961). The skeleton decorporation was likely due to prevention instead of skeletal decorporation, where monomeric plutonium was removed from the liver and circulatory system prior to its incorporation; however, polymeric plutonium would be phagocytized within tissue macrophages of the skeleton converting some the plutonium during this time into monomeric plutonium making it available for circulation and chelation.

Taylor et al. (1978) injected young adult beagles with Pu(IV) citrate (~0.1 μCi kg^{-1}) followed by DTPA administration, starting ½ hour after injection and daily thereafter

for up to 14 days. Initial treatments of Ca-DTPA (30 μmol kg^{-1}) and Zn-DTPA (300 μmol kg^{-1}) appeared to have the same affect, with Zn-DTPA requiring 10 times the Ca-DTPA dose for the same effect on the first day. Subsequent daily treatments with multiple treatments of Zn-DTPA (6.8 μmol kg^{-1}) proved to have the same effect as a single treatment of 34 μmol kg^{-1} (Taylor et al. 1978). The initial day 1 urine excretion following Ca-DTPA administered approximately ½ hour post monomeric Pu(IV) injection accounted for 61% of the injected dose, while the fecal excretion accounted for 1%, with urine and fecal excretion accounting for 2.8% and 1.7% on the second day, respectively (Taylor et al. 1978). It appears that many injection studies, such as Taylor et al. (1978) began with the entire dose added to the blood circulation that was available for chelation, where prompt treatment provided the best opportunity for removal; whereas, occupational intakes due to wounds exhibit a slow absorption into the circulatory system, requiring a different treatment strategy.

Rosenthal and Lindenbaum (1967) performed a study by injecting monomeric Pu(IV) into mice (2.6 μCi kg^{-1}), followed by Ca-DTPA administration (500 mg kg^{-1}) starting either 1 hour or 3 days after the Pu(IV) injection, with treatment continued for 12 days. DTPA treatment was less effective in chelating polymeric plutonium due to the larger portion deposited in the liver that was not removed. The same study noted that half of the skeleton burden of either form was removed by DTPA (Rosenthal and Lindenbaum 1967). The Ca-DTPA treatment results indicated that the bone deposition was reduced by one-half and the treatment prevented further bone deposition (Rosenthal and Lindenbaum 1967). This study illustrated that DTPA was not effective at removing plutonium from the liver Kupffer cells, but supports the idea that the skeletal tissue

macrophages would dissolve the polymeric plutonium and introduce monomeric plutonium into circulation which would be available for chelation, that was similar to the Schubert et al. (1961) study.

DTPA oral treatment was studied by Volf et al. (1999). In their experiment, Zn-DTPA was introduced in the drinking water of rats reducing the incidence of osteosarcomas following plutonium injections. A baboon inhalation study indicated that the liver retention on day 90 was 20 and 10 times less than controls for Am and Pu, respectively, with both having a reduced skeleton retention of approximately half that of the controls (Fritsch et al. 2010). DTPA administration has been known to reduce actinide toxicity of the bone and liver and reduce the incidence of bone tumors in animal studies (Durbin 2008, Volf et al. 1999).

Various Treatments

Durbin and Schmidt (1989) and Catsch (1976) supported frequent administrations of Zn-DTPA. They speculated that Zn-DTPA treatments every few hours, were more effective than single-daily treatments. It was thought that this outcome was due to the ability of DTPA to clear from the plasma into urine with a half-time of 19 minutes by glomerular filtration in the kidneys (Stather 1983). Stable complexes of Pu-DTPA have been shown to have a rapid and complete absorption from an injection site followed by its excretion, and DTPA injected at the wound site is recommended for removing plutonium (Catsch 1976, ICRP 1972). A small amount experiences a delayed urinary excretion that may be due to the Pu-DTPA complex binding with plasma proteins, similar to that reported by Babiker (1986) for Cr-EDTA (5 to 19%), and Russell et al. (1983) for

Tc-DTPA (5 to 10%), or alternately it could be retained in intracellular soft-tissue compartments (Breustedt et al. 2009).

DTPA administration by nebulizer or aerosol application following a plutonium inhalation increases absorption of Pu(IV) through the gastrointestinal tract, possibly a thousand fold, but is expected to remain in a Pu-DTPA complex with over 99% being excreted within a few days (Catsch 1976, Hall 1978, IAEA 1976, ICRP 1972). This would give the appearance of increased lung absorption properties due to the added Pu-DTPA complex being absorbed through the small intestine. Stather et al. (1983) had reported that DTPA administration by lung nebulizer and muscle injection is known to have a retention half-time of ~75 minutes in the circulatory system. There appears to be advantages of administering DTPA in the lungs as an aerosol following inhalation of soluble plutonium since DTPA can form a complex with plutonium in lung fluids, and it can cross the pulmonary epithelium to remove plutonium in extracellular fluids (Stather 1983). However, the IAEA (1978) reported that Ca-DTPA administered by inhalation was about 3 times less effective than when administered by injection.

Iron Chelation

The interaction of various chelating agents with Fe(III) and Pu(IV) are similar (Schimmelpfeng 2009). Hershko (1975) experimented with iron chelation by injecting both monomeric and polymeric forms of radioiron into rats. Hershko's (1975) experiment indicated that approximately 90% of the iron was deposited in the liver within one hour after injection with the Kupffer cells containing nearly all of the polymeric iron forms (99-100%) and the parenchymal cells (i.e., hepatocytes) containing nearly all of the

monomeric iron forms (97-100%). In 10 days, one-third of the soluble iron was released from the hepatocytes and distributed to the erythrocytes and residual tissues; while the RE cells had released about 80% of the polymeric iron with the erythrocytes accounting for 56% (Hershko 1975). Half-times describing the blood disappearance were determined to be 16 minutes and less than 2 minutes for monomeric and polymeric forms of radioiron, respectively (Hershko 1975). The Hershko (1975) experiment confirmed that DTPA did not chelate any iron stored in the liver, with the only chelatable iron being that in circulation unattached to the transferrin protein. Calcium-DTPA had been used to chelate iron in the circulatory system in treating iron-overload thalassaemic patients (Flora and Pachauir 2010, Pippard et al. 1986). It was observed that Zn-DTPA was not effective at chelating iron, where Ca-DTPA had a lower stability constant than Fe-DTPA (Flora and Pachauri 2010, Pippard et al. 1986). Iron chelation results in ferroportin up-regulation, releasing iron into the circulatory system from iron storage sites, such as the hepatocytes and Kupffer cells (Anderson et al. 2012, Bridges and Cudkowicz 1984, Domenico et al. 2011).

Summary

According to the animal studies, Ca-DTPA is more effective for initial treatment on the first day compared to Zn-DTPA; however, Zn-DTPA is recommended for protracted and fractionated daily treatments with similar effectiveness and little to no side effects. DTPA introduced by intravenous injection has a short half-time of 19 minutes where it may be effective for possibly 6 to 10 hours when considering the molar ratio in relation to a ^{239}Pu intake of 1 to 1,000 Bq. Regardless multiple treatments are recommended. Other alternatives include DTPA being introduced as an aerosol where it

has a longer residence time (i.e., 75 minute half-time). It may also be applied directly to wounds in aiding the absorption of plutonium followed by its excretion. Aerosol treatments following a plutonium inhalation may enhance urinary excretion by increasing the absorption experienced in the GI tract 1,000 times. Also of note is that aerosol treatment provides approximately a third of the chelation benefit afforded by an injection; therefore, aerosol treatment accompanied by an injection would be recommended. Modeling the effectiveness of either Ca-DTPA or Zn-DTPA using the available data should provide similar results since historically, Ca-DTPA was initially administered and both Ca-DTPA and Zn-DTPA have approximately the same effectiveness for continued treatments. Occupational intakes result in a monomeric form of plutonium being introduced into the circulatory system, where liver decorporation is likely. This is associated with mechanisms similar to those involved with iron metabolism involving the interaction of hepcidin and ferroportin which lead to the introduction of plutonium into circulation.

The mechanism for DTPA influence on liver decorporation remains unclear but evidence suggests that DTPA influences plutonium clearance from the hepatocyte via the liver-biliary pathway.

2.4 Animal Studies

The current biokinetic models are heavily influenced by animal studies due to the insufficient human data on plutonium incorporation. Leggett (2003) had indicated that there was a large uncertainty when extrapolating biokinetic data from laboratory animals to man, especially for the liver due to large differences among species in liver organ

kinetics. Investigators have demonstrated a faster liver clearance in rats than experienced by human. It appears that beagle dog liver kinetics are similar to those of humans (ICRP 1972). Many of the early experiments injected significantly higher plutonium concentrations than experienced by occupational workers. This may have inadvertently triggered a different biokinetic pattern than one would anticipate at the lower concentrations experienced by workers. This was recognized by some researchers and an upper activity concentration of 0.1 μCi kg^{-1} (3.7 kBq kg^{-1}) was chosen to distinguish normal exposures for use in biokinetic model development (Arnold and Jee 1962, Lloyd et al. 1984, Polig et al. 2000). Lloyd et al. (1984) had discovered in experiments with beagle dogs, that the activity concentration of americium was directly proportional to the rate of liver clearance, with the lowest dose of 0.1 μCi kg^{-1} (3.7 kBq kg^{-1}) having the longest retention. Arnold and Jee (1962) and Jee et al. (1962) reported further studies of beagle dogs with Pu(IV) citrate injections at various concentrations that affected the skeletal deposition and kinetics. Dogs injected with the highest concentration [2.7 μCi kg^{-1} (100 kBq kg^{-1})] resulted in all of the cells of the endosteal surfaces being destroyed, terminating the remodeling process, where fibrous tissue covered the sites, creating a barrier between the plutonium on the bone surface and the marrow cavity (Arnold and Jee 1962). Injection concentrations of 0.9 μCi kg^{-1} (33 kBq kg^{-1}) continued the remodeling process, although at a reduced rate, large areas of bone cell death, with abnormal bone growth were observed and focal areas of fibrosis tissue in these investigations (Arnold and Jee 1962). Concentrations of 0.3 μCi kg^{-1} (11 kBq kg^{-1}) resulted in an aggressive remodeling of the trabecular bone, with complete remodeling observed 4 years post injection (Arnold and Jee 1962). Under these conditions plutonium activity was observed

to be diffused throughout both the cortical and trabecular bone with localized accumulation of approximately one-third of the total deposition specifically observed in bone macrophages and existing as free aggregates within the marrow (Arnold and Jee 1962). Concentrations of 0.1 μCi kg^{-1} (3.7 kBq kg^{-1}) produced similar observations with the exception of a lack of plutonium activity in macrophages; thus, indicating that at higher concentrations, the macrophages were suffering from radiation damage and not able to metabolize the plutonium (Arnold and Jee 1962). In this instance many of the smaller macrophages were killed and engulfed by larger tissue macrophages (Arnold and Jee 1962).

Little of the actinide deposited in the liver of laboratory rodents or baboons is recirculated, unless the injected amount is large enough to produce radiation damage (Durbin and Schmidt 1985). The initial liver deposit is secreted to the bile and eliminated by the GI tract; however, at long times after administration, the livers of rodents and primates appear to be mainly circulatory feedback from the bone (Durbin and Schmidt 1985). Leggett (1992) indicated that americium bound to the transferrin protein appeared to shift to the iron-storage protein ferritin in the liver upon a review of a beagle dog study. Within a short period of days or weeks, americium in liver cells was associated with subcellular organelles and indigestible residues of autophagic activity that accumulate in the cells (Leggett 1992). Tissue distribution in rats of various plutonium compounds were equivalent for low doses and varied for higher doses with an increased deposition in the liver and spleen and a corresponding decrease in skeletal deposition that appeared to be influenced by the subacutely lethal dose given (ICRP 1972). Higher

injected doses appeared to increase the polymerization of monomeric plutonium, thus affecting the tissue distribution (ICRP 1972).

Rosenthal et al. (1972) reported the results of a rabbit study where both monomeric and polymeric plutonium were introduced by intravenous injection [0.3 to 0.4 $\mu Ci\ kg^{-1}$ (11 to 15 $kBq\ kg^{-1}$)]. The animals were sacrificed after 3 days and then tissues analyzed. It was observed that polymeric plutonium had a 17-fold higher concentration in the marrow due to tissue macrophages than the monomeric form (Rosenthal et al. 1972). Polymeric plutonium was taken up by tissue macrophages, primarily involving the liver, spleen and bone marrow (Rosenthal et al. 1972). Similar bile and blood concentrations at 3 days were observed for both forms of plutonium (Rosenthal et al. 1972). The liver had a notably higher percentage of the injected concentration for the monomeric form, with 66% compared to 47% of the polymeric form (Rosenthal et al. 1972). The urine excretion was approximately 3 times greater for polymeric plutonium, with 8.5% excreted compared to 3.9% for the monomeric form (Rosenthal et al. 1972). The fecal excretion being similar, 0.74% of the polymeric form was observed compared to 0.55% of the monomeric form (Rosenthal et al. 1972).

These observations indicate that caution should be used when extending animal data to human biokinetic models, because differences due to metabolism, contaminant chemistry, and concentration are significant. Occupational intakes are primarily due to a monomeric form of plutonium that is absorbed into the circulatory system. Many animals such as mice, rats and primates, have a faster liver clearance than that experienced by adult humans. Polig et al. (2000) presented a biokinetic model for the adult beagle dog that paralleled that of the human model in many aspects and therefore

was able to provide a basis for analysis of survival and relative risks, but only when the experimental results from animal investigation produced dosages low enough to not cause acute toxic effects (i.e., dosage levels ranging from 0.026 to 3.5 kBq kg^{-1}) (Polig et al. 2000). Some of the early experiments had higher dosages that introduced acute, non-lethal effects that varied and potentially biased biokinetic expectations for lower doses. These were often drastic changes such as stopping the bone remodeling process, or killing the liver cells resulting in a faster clearance. Therefore, animal studies can provide insight but caution should be used, such as that exercised by Polig et al (2000), when extending their results into human models.

2.5 Biokinetic Models

Biokinetic models provide mathematical representations of the human body that are used for calculating a contaminant's distribution, retention and clearance. The U.S. Department of Energy (DOE) currently employs the ICRP 66 human respiratory tract model, the ICRP 67 systemic model, the ICRP 30 gastrointestinal tract model, and the NCRP 156 wound biokinetic model. Each is described in the following sections:

2.5.1 ICRP 67 Plutonium Systemic Model

The ICRP 67 systemic model for plutonium was largely adopted from Leggett (1992) with a second liver compartment added to model a longer retention that may be associated with the liver Kupffer cells (ICRP 1993). The systemic model is typical of soluble plutonium but the model can be modified to account for insoluble forms of plutonium that are phagocytized by Kupffer cells in the liver and tissue macrophages in the bone marrow for long durations (Leggett 1985). The systemic model consists of

compartments explaining contaminant retention in the liver, skeleton, soft tissues, gonads, kidneys and bladder with the blood compartment acting as the central compartment for the contaminant distribution, including urinary and fecal excretion compartments.

The first liver compartment receives 21% of the activity leaving the blood compartment and transports 93% to the second liver compartment and 7% to the small intestine through the liver-biliary pathway (ICRP 1993). The retention half-time for the first and second liver compartments are 1 year and 9 years, respectively. The soft tissues are represented as 3 compartments (i.e., ST0, ST1 and ST2) where the ST0 compartment (extracellular fluids) receives 30% of the blood compartment activity with a half-time of 1 day, while the ST1 compartment (intermediate retention) and ST2 compartment (tenacious retention) receive 12.5% and 2% of the blood compartment activity with half times of 2 years and 100 years, respectively (ICRP 1993). The ICRP 67 systemic model includes a clearance pathway from the ST1 compartment to the bladder that accounts for half of the plutonium cleared from the ST1 compartment that was necessary to explain experimental observation from human and animal experiments (ICRP 1993). The testes receive a fraction of 0.025% for adults (0.0077% for ovaries) from circulation and recycles back to circulation with a half-time of 10 years, which was based on beagle and monkey long-term data (ICRP 1993, Leggett 1992). The kidneys receive approximately 1% from the blood compartment that is divided with a third going to the kidney tissue and two thirds contributing to the urinary path (ICRP 1993). The bladder receives 2% of the activity from circulation with contributions from the kidney urinary path and ST1 compartment (ICRP 1993).

The skeleton is characterized as 80% cortical and 20% trabecular bone with each consisting of bone volume, surface and marrow (Leggett 1985). Contaminant is only received by the skeleton in the surface compartment, which assumes that the contaminant is largely in a monomeric form, with subsequent transfer of one-third to the bone volume and two-thirds to the marrow compartments (ICRP 1993). The trabecular and cortical surfaces receive 21% and 14% of the activity from circulation, respectively (ICRP 1993). Bone resorption of the bone surface and bone volume enters the bone marrow, with plutonium likely expected to be in a polymeric form, where it is phagocytized by the bone tissue macrophages, with a slow clearance half-time of 91 days to the blood compartment (ICRP 1993, Leggett 1985). The ICRP 67 plutonium systemic model is represented in Figure 11.

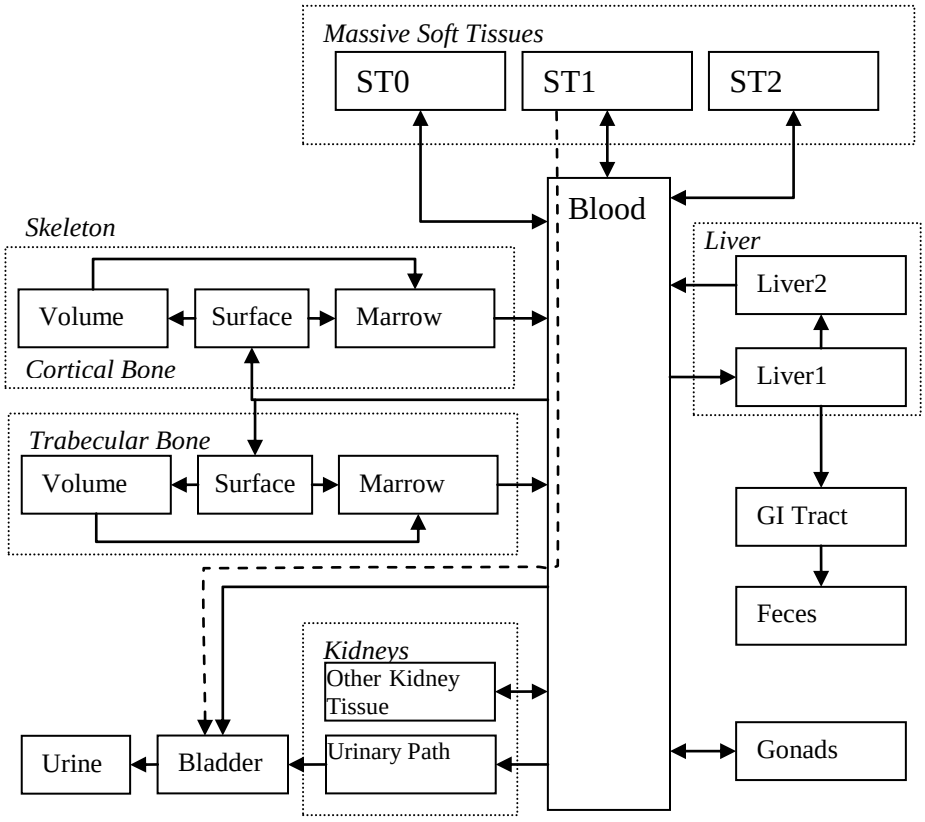

Figure 11: Representation of ICRP 67 systemic compartment model (ICRP 1993, 1997).

Much of the data supporting the current ICRP 67 plutonium systemic model originated from animal studies and humans that were injected with soluble plutonium (ICRP 1993, Langham et al. 1980, Leggett 1985). Suggested updates to the ICRP 67 model have been made since its inception. Polig (1997) and Luciani and Polig (2000, 2007) recommended changes in compartment pathways, and transfer rates for the skeleton, while the Leggett 2005 model added additional blood and liver compartments with some modification to the transfer rates. Table 4 represents a comparison of the recommended changes to the model compared to the ICRP 67 recommended transfer rates.

Table 4: Plutonium systemic model transfer rates (d^{-1}) compared to various contributions (ICRP 1993, Leggett 2005, Luciani and Polig 2000, 2007, Polig 1997).

Compartments	ICRP 67	Polig (1997)	Luciani and Polig (2000)	Leggett et al (2005)
Blood$^{(1)}$ to liver	0.1941	0.120		0.462
Blood$^{(1)}$ to cortical surface	0.1294	0.0952		0.0878
Blood$^{(1)}$ to trabecular surface	0.1941	0.226		0.125
Blood$^{(1)}$ to cortical volume		0.00448		0.00462
Blood$^{(1)}$ to trabecular volume		0.0716		0.01386
Blood$^{(1)}$ to bladder	0.0129		0.00946	
Blood$^{(2)}$ to bladder				3.5
Blood$^{(2)}$ to blood$^{(1)}$				67.55
Blood$^{(1)}$ to kidney (urinary path)	0.00647		0.00992	0.0077
Blood$^{(1)}$ to other kidney tissue	0.00323			0.000385
Blood$^{(1)}$ to ULI contents	0.0129		0.008	0.0116
Blood$^{(1)}$ to testes	0.00023			0.00027
Blood to ovaries	0.000071			0.000085
Blood$^{(2)}$ to ST0	0.2773			29
Blood$^{(1)}$ to ST1	0.0806			0.0185
Blood$^{(1)}$ to ST2	0.0129			0.0231
ST0 to Blood$^{(1)}$	0.693		0.139	0.099
Kidneys (urinary path) to bladder	0.01386		0.0102	0.0173
Urinary bladder content to excretion	12			
Other kidney tissue to blood$^{(2)}$	0.00139			0.000127
ST1 to blood$^{(2)}$	0.000475		0.000950	0.00139
ST1 to bladder	0.000475		(deleted)	
ST2 to blood$^{(2)}$	0.000019			0.000127
Trabecular surface to volume	0.000247	(deleted)		0.000123
Trabecular surface to marrow	0.000493	0.00159		0.000493
Trabecular volume to marrow	0.000493	0.00159		0.000493
Trabecular marrow to blood$^{(2)}$	0.0076	0.0076		0.0076
Cortical surface to volume	0.0000411	(deleted)		0.0000205
Cortical surface to marrow	0.0000821	0.000156		0.0000821
Cortical volume to marrow	0.0000821	0.0000821		0.0000821
Cortical marrow to blood$^{(2)}$	0.0076	0.0076		0.0076
Liver 1$^{(0)}$ to Liver 2$^{(1)}$	0.00177		0.01	0.045286
Liver 1$^{(0)}$ to Small Intestine	0.000133		0.0004	0.0009242
Liver 2$^{(1)}$ to blood$^{(2)}$	0.000211		0.0004	0.00152
Liver$^{(1)}$ to Liver$^{(2)}$				0.00038
Liver$^{(1)}$ to blood$^{(2)}$				0.00152
Liver$^{(2)}$ to blood$^{(2)}$				0.0001266
Gonads to blood$^{(2)}$	0.00019			0.00038

Note: Luciani and Polig (2007) modified Polig's (1997) model by specifying values for an adult of 35 years age, with the values doubled at 60 years and linear interpolation employed between 35 to 60 years. The superscripts $^{(0)}$, $^{(1)}$ and $^{(2)}$ refer to the Leggett 2005 model compartment model designation and are ignored otherwise.

The transfer rates represented the product of the activity fraction going to a specific organ and removal half-time of the primary compartment (Leggett 1992, Luciani and Polig 2007). Leggett et al. (2005) had indicated that the two separate blood

compartments represent two different forms of plutonium in the blood with different excretion rates. The two blood compartment model was also conceived by Durbin et al. (1972) as the proposed model upon her study with rats. Durbin et al. (1972) had indicated that the blood compartments represent plutonium either bound to the transferrin protein or not bound, with each having different kinetics in the model, while Leggett et al. (2005) had included an additional blood compartment to reflect the higher urinary excretion exhibited from resorbed plutonium.

Luciani and Polig (2007) presented a beagle dog study that illustrated the changes in kinetics between beagle dogs and humans with respect to the different models [i.e., ICRP 67, Polig (1997) and Leggett et al. (2005)]. From this comparison the beagle dog clearance rate appeared to emulate Polig (1997) model with subtle differences when compared to the ICRP 67 and the Leggett 2005 model. Luciani and Polig (2007) state that there is no clear physiological basis in adults for bone surfaces to bone volume; therefore, Polig (1997) model assumed there was no transfer and added a transfer path directly from the blood compartment. Leggett et al. (2005) maintained the transfer from the skeleton surface to volume pathway, while also adopting the transfer path directly from the blood compartment. Both models mathematically appear to provide a good representation with observed urinary excretion (Polig 1997, Leggett et al. 2005).

Leggett et al. (2005) also introduced a third liver compartment in order to explain retention in Kupffer cells with a retention half-time of 15 years. The Leggett 2005 model was used as a benchmark for modifying the ICRP 67 systemic model with the goal of maintaining the basic structure of the ICRP 67 systemic model without the addition of the

2^{nd} blood compartment and 3^{rd} liver compartment, in order to maintain simplicity with coupling to the NCRP 156 wound model and for supporting intravenous injections.

2.5.2 ICRP 66 Lung Model

The ICRP 66 lung model redesigned the ICRP 30 lung model to reflect newly acquired information from human studies to provide a better representation of lung biokinetics. The ICRP 66 lung model is represented in Figure 12.

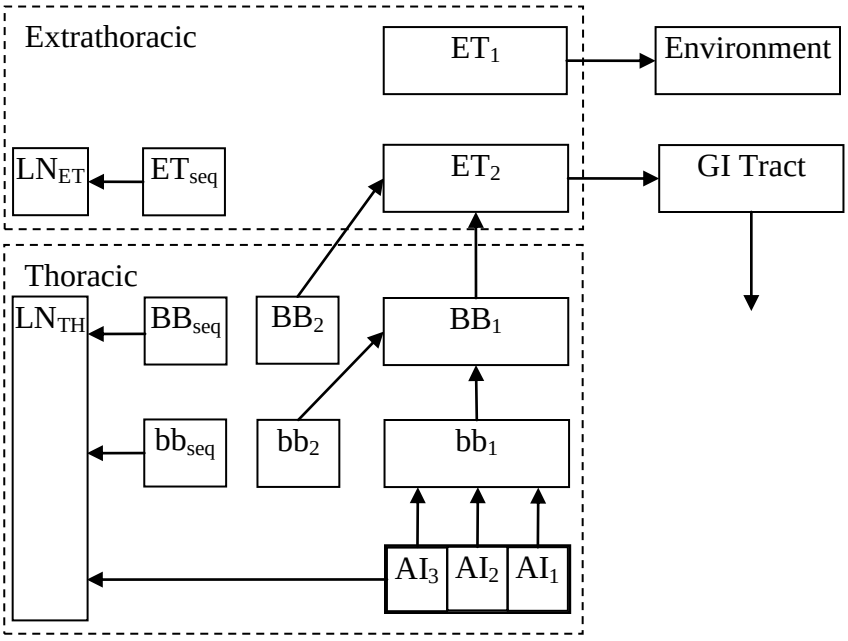

Figure 12: ICRP 66 lung model (ICRP 1994).

Figure 12 displays the lung compartments and the clearance pathways for each compartment.

The nomenclature used in Figure 12:

ET: Extrathoracic Region consisting of the anterior (ET_1) and posterior nasal (ET_2), along with the sequestered particles in the ET region (ET_{seq}) that is cleared to the ET lymph nodes (LN_{ET}) with a half-time of 693 days. The

ET_1 compartment is assumed to clear to the environment with a half-time of 0.693 days; while the ET_2 compartment is assumed to clear to the GI Tract with a half-time of 10 minutes.

BB: Bronchial Region where BB_1 represents the fast mucous clearance with a half-time of 100 minutes, BB_2 represents the slow mucous clearance with a half-time of 23 days, and the BB_{seq} represents the sequestered particles in the BB region that are assumed to clear to the thoracic lymph nodes (LN_{TH}) with a half-time of 69 days.

bb: Bronchiolar Region is similar to the BB region, where bb_1 represents the fast mucous clearance with a half-time of 500 minutes, bb_2 represents the slow mucous clearance with a half-time of 23 days, and the bb_{seq} represents the sequestered particles in the bb region that are assumed to clear to the thoracic lymph nodes (LN_{TH}) with a half-time of 69 days.

AI: Alveolar-Interstitial (AI) Region consists of three AI compartments with different clearance rates. Compartments AI_1 and AI_2 clear to the GI tract with half-times of 35 and 693 days, respectively, while AI_3 clears to both the GI tract and the thoracic lymph nodes (LN_{TH}), with half-times of 19 and 95 years, respectively.

The effective compartment clearance rate includes the particle translocation rate, the absorption rate into the body fluids and the rate of decay. The effective mean residence time is determined from its inverse (i.e., λ_E^{-1}) using Equation 1 (Cember & Johnson 2009):

$$\lambda_E = \lambda_{ab} + S_S + \lambda_R \quad (1)$$

Where:

λ_E = effective clearance rate constant (d^{-1})

λ_{ab} = clearance rate constant from compartment a to compartment b (d^{-1})

S_S = slow absorption into the blood (assumed to be 0.0001 d^{-1} for Type S)

λ_R = radiological decay constant (d^{-1})

Table 5 displays the clearance rate constants and the mean residence times for each compartment for ^{239}Pu.

Table 5: ICRP 66 lung model clearance rates with the respective mean residence times for each compartment.

Region	Compartment	To	λ_{ab} (d^{-1})	λ_R (d^{-1})	S_S (d^{-1})	λ_E (d^{-1})	MRT (d)
ET_1	ET_1	Environment	1	7.9E-08	0.0001	1.0001	1.00
ET_2	ET_2	GI Tract	100	7.9E-08	0.0001	100.0001	0.01
ET_2	ET_{seq}	LN_{ET}	0.001	7.9E-08	0.0001	0.0011	909.03
BB	BB_1	ET_2	10	7.9E-08	0.0001	10.0001	0.10
BB	BB_2	ET_2	0.03	7.9E-08	0.0001	0.0301	33.22
BB	BB_{seq}	LN_{TH}	0.01	7.9E-08	0.0001	0.0101	99.01
bb	bb_1	BB_1	2	7.9E-08	0.0001	2.0001	0.50
bb	bb_2	BB_1	0.03	7.9E-08	0.0001	0.0301	33.22
bb	bb_{seq}	LN_{TH}	0.01	7.9E-08	0.0001	0.0101	99.01
AI	AI_1	bb_1	0.02	7.9E-08	0.0001	0.0201	49.75
AI	AI_2	bb_1	0.001	7.9E-08	0.0001	0.0011	909.03
AI	AI_3	bb_1	0.0001	7.9E-08	0.0001	0.0002	4543.82
AI	AI_3	LN_{TH}	0.00002	7.9E-08	0.0001	0.0001	8327.85
LN_{ET}	LN_{ET}	Body Fluids		7.9E-08	0.0001	0.0001	9992.10
LN_{TH}	LN_{TH}	Body Fluids		7.9E-08	0.0001	0.0001	9992.10

The ICRP 66 lung model also describes a particle transformation from initial intake, to either a bound state or a transformed state. This transformation applies to all compartments in the ICRP 66 lung model with the exception of the ET_1 compartment.

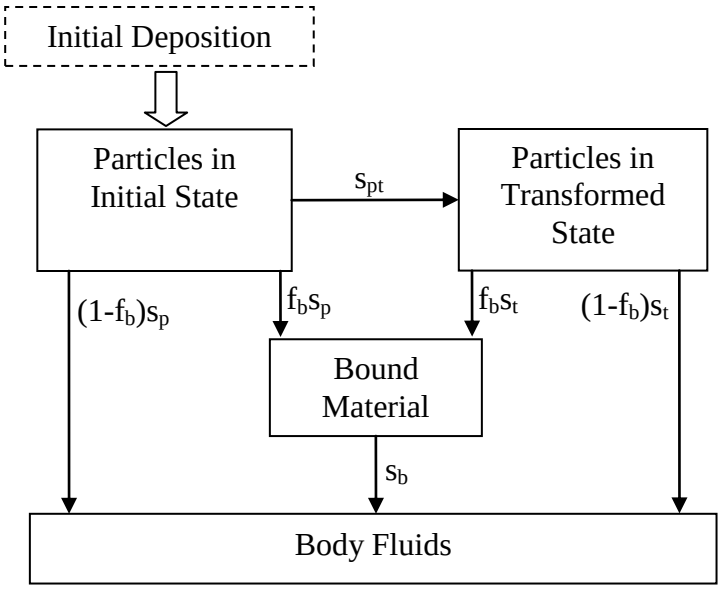

Figure 13: Particle dissolution, absorption and transformation kinetics in ICRP 66 lung model (ICRP 1994).

The particle dissolution, absorption and transformation rates in Figure 13 are presented in Table 6.

Table 6: Particle dissolution, absorption and transformation parameters (d^{-1}) in ICRP 66 lung model (ICRP 1994).

Absorption Type	F (fast)	M (moderate)	S (slow)
s_p	100	10	0.1
s_{pt}	0	90	100
s_t	-	0.005	0.0001
s_b	-	-	-

Where s_p and s_t are the particle dissolution rates, s_{pt} is the particle transformation rate from the initial state to a particle transformed state, and s_b is the particle absorption rate from the bound compartment. The ICRP 66 default assumption is that there is no

bound fraction (f_b), and no default bound particle absorption rate (s_b) was suggested. The bound particle absorption rate must be uniquely determined based on the case characteristics. Another important difference of particles in the bound state is that these particles are assumed to be engulfed by stationary alveolar macrophages where the only clearance is due to absorption following dissolution, with no particle translocation (ICRP 1994, 2002b).

ICRP publication 66 recommends a default inhalation particle size for occupational workers in uncharacterized areas of 5-μm activity median aerodynamic diameter (AMAD); and 1-μm AMAD for the general public (ICRP 1994). Table 7 presents the deposition fraction in each of the ICRP 66 lung model compartments for a 5-μm AMAD particle (ICRP 1994).

Table 7: Lung compartment deposition using the ICRP 66 lung model (ICRP 1994).

Region	Compartment	Compartment Fraction	5- μm Regional Deposition	Total Assigned
ET_1	ET_1	1	0.34	0.34
ET_2	ET_2	0.9995	0.4	0.3998
ET_2	ET_{seq}	0.0005	0.4	0.0002
BB	BB_1	0.663	0.0179	0.0118677
BB	BB_2	0.33	0.0179	0.005907
BB	BB_{seq}	0.007	0.0179	0.0001253
bb	bb_1	0.593	0.011	0.006523
bb	bb_2	0.4	0.011	0.0044
bb	bb_{seq}	0.007	0.011	0.000077
AI	AI_1	0.3	0.053	0.0159
AI	AI_2	0.6	0.053	0.0318
AI	AI_3	0.1	0.053	0.0053

The compartment deposition and clearance rates were specified for a 5-μm AMAD particle size and Type S absorption, which is considered the default parameters

for insoluble ^{239}Pu for an occupational worker. Modifications of the absorption type, particle size and compartment deposition were specified in ICRP (1994) and integrated into the compartment model for this research. Although the default specification for the particle bound state was assumed to be zero, this was revisited during this research and determined for the specific case studied.

2.5.3 ICRP 30 Gastrointestinal Tract Model

Figure 14 illustrates the GI tract model as defined in ICRP 30 and its integration with the ICRP 66 lung model and the ICRP 67 systemic model.

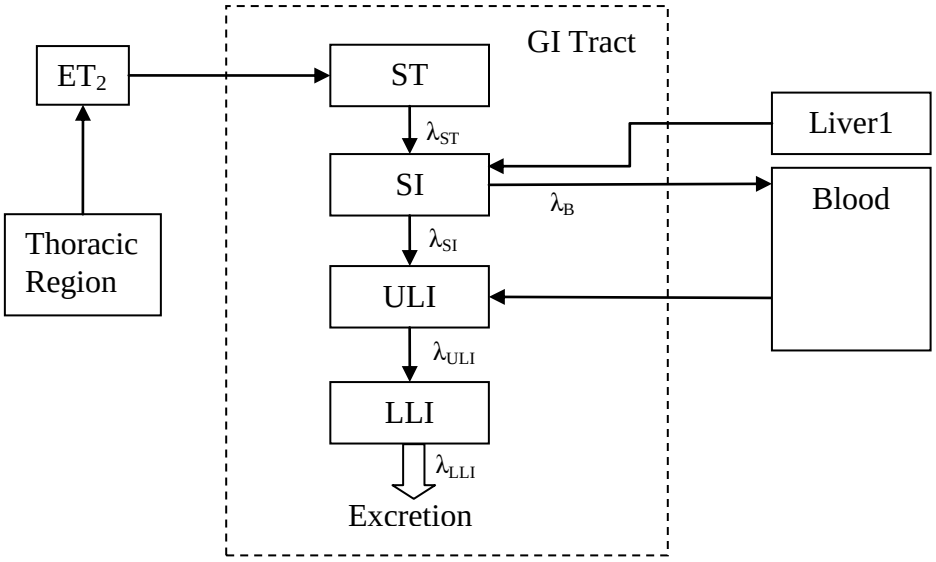

Figure 14: ICRP 30 GI tract model (ICRP 1979) in relation to the ICRP 66 lung model and ICRP 67 systemic model.

Figure 14 illustrates the relationship of the GI tract model to the ICRP 66 lung model and the ICRP 67 systemic model. The GI tract model is made up of the stomach (ST), small intestine (SI), upper large intestine (ULI), and the lower large intestine (LLI), with respective clearance rate constants as defined below (ICRP 1979):

$\lambda_{ST} = 24\ d^{-1}$

λ_{SI} = $6\ d^{-1}$

λ_{ULI} = $1.8\ d^{-1}$

λ_{LLI} = $1\ d^{-1}$

λ_B = $\frac{f_1 \lambda_{SI}}{1 - f_1}$ (if f_1 is assumed to be 0.01 then $\lambda_B = 0.06\ d^{-1}$)

The liver contributes to the GI tract through the liver-biliary pathway; while the blood contributes by desquamated intestinal cells. The blood absorbs from the small intestine via the hepatic portal vein after liver filtration. The thoracic and extrathoracic airways clear to the GI tract, which is a dominant path for insoluble and moderately soluble particles following inhalation. There is very little absorption of actinides in the GI Tract, with a typical f_1 value of 0.00001 for insoluble ^{239}Pu, and 0.0005 for moderately soluble ^{239}Pu, where most of the actinides are excreted (ICRP 1991). The sampling of fecal excretion is important for inhalations of insoluble and moderately soluble actinides due to being the dominant excretion pathway for the initial thoracic airway clearance.

2.5.4 NCRP 156 Wound Model

The wound biokinetic model was designed primarily through the use of experimental animal data due to the lack of available human data where contaminant retention was not influenced by medical intervention, such as tissue excision and DTPA administration (NCRP 2007). The initial partitioning between the soluble and colloidal interstitial state was influenced by the element's tendency to hydrolyze at neutral pH, which affects the contaminants ability to bind locally to tissue molecules (NCRP 2007).

The vast majority of industrial-related contaminated wound cases involved actinides (uranium, plutonium, and americium), with puncture wounds accounting for the majority of the injuries, in which the wound model was developed (NCRP 2007).

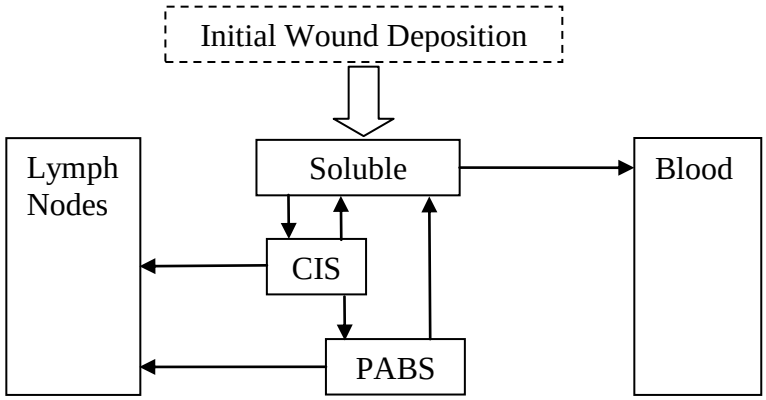

Figure 15: Soluble material wound compartment model (NCRP 2007).

Figure 15 illustrates the wound compartment model for soluble material intakes that include weak, moderate, strong and avid retention characteristics. Soluble radionuclides are initially deposited in the soluble compartment where a percentage will transform particle states with the colloid and intermediate state (CIS) and particles, aggregates and bound state (PABS) compartment. Absorption is illustrated with the transfer from the soluble compartment to the blood compartment. Long term retention is illustrated by transfer to the lymph nodes from the CIS or PABS compartments, in which there is no consideration for absorption or recycling to the other wound compartments. The retention transfer rates are described by NCRP (2007) for various radionuclides, which fit into one of four quantitatively distinct wound retention classes: weak-, moderate-, strong- or avid-retention. Table 8 presents radionuclides according to these groupings.

Table 8: Retention class designation for soluble radionuclides (NCRP 2007).

Retention Class	Radionuclides
Weak	^{131}I, ^{71}Ge (GeO_3), ^{74}As ($AsCl_5$), ^{124}Sb (SbO_3), ^{75}Se (SeO_4), $^{95,96}Tc$ ($TcCl_6$), ^{191}W (WO_4), ^{86}Rb, ^{137}Cs, ^{45}Ca, ^{90}Sr, ^{140}Ba, ^{64}Cu, and ^{230}U (UO_2)
Moderate	^{110}Ag, ^{223}Ra, ^{48}V (VO_3), ^{105}Rh ($RhCl_6$), ^{127m}Te (TeO_4), $^{191,193}Pt$ ($PtCl_4$), and ^{188}Os (OsO_5)
Strong	^{106}Ru ($RuCl_5$), ^{7}Be, ^{51}Cr, ^{67}Ga, ^{88}Y, ^{95}Nb, ^{114m}In, ^{140}La, ^{143}Ce, ^{143}Pr, ^{147}Nd, ^{147}Pm, $^{154,155}Eu$, ^{160}Tb, ^{170}Tm, ^{227}Ac, ^{241}Am, $^{242,244}Cm$, ^{210}Po, ^{238}Pu, ^{239}Pu
Avid	^{46}Sc, ^{95}Zr, ^{113}Sn, ^{233}Pa, and $^{228,234}Th$

Additional wound retention modeling was developed for colloids, particles and fragments, which have a much longer retention time in the wound (NCRP 2007). Plutonium was classified as a strong-retention radionuclide in Table 8. The wound compartment model uses the parameters specified in Table 9 with the initial concentration specified for the compartment relative to the wound type, such as 100% deposited in the soluble compartment for wound types weak, moderate, strong and avid.

Table 9: NCRP 156 Default transfer rates (d^{-1}) for various wound types (NCRP 2007).

Transfer Path	Weak	Moderate	Strong	Avid	Colloids[2]	Particles[2]	Fragments[2]
Soluble to Blood	45	45	0.67	7.0	0.5	100	
Soluble to CIS	20	30	0.6	30	2.5		
CIS to Soluble	2.8	0.4	0.024	0.03	0.025		
CIS to PABS	0.25	6.5×10^{-2}	1×10^{-2}	10	5×10^{-2}		
CIS to lymph nodes	2×10^{-5}	2×10^{-5}	2×10^{-5}	2×10^{-5}	2×10^{-3}		
PABS to soluble	0.08	0.02	0.0012	0.005	0.0015	2×10^{-4}	
PABS to lymph nodes	2×10^{-5}	2×10^{-5}	2×10^{-5}	2×10^{-5}	4×10^{-4}	3.6×10^{-3}	0.004
PABS to TPA[1]						0.04	0.7
TPA[1] to PABS						0.0036	5×10^{-4}
Lymph nodes to blood					0.03	6×10^{-4}	0.03
Fragment to soluble							
Fragment to PABS							0.008

[1] Trapped particle and aggregates compartment
[2] Colloids, Particles and Fragments deposit into the CIS, PABS and fragment compartment, respectively.

The wound compartment model transfer path and associated transfer rates are provided in Table 9 for radionuclides exhibiting soluble, colloidal and fragment characteristics. Figure 15 displayed the compartment model for soluble radionuclides, where some modification would be necessary to accommodate colloids, particles and fragments. Although NCRP (2007) specifically classifies radionuclides with default transfer rates, radionuclides may exhibit traits from several categories, such as americium exhibiting characteristics of both moderate and strong retention categories. The IDEAS (Castellani et al. 2013) guidelines suggested a mix of categories using the default values when attempting to fit actual data. This research included optimization of the strong-retention transfer rates for IDEAS Case 123 with improved results that are discussed in Chapter 4.1.

2.6 Available human data

Published results of human injection studies were used in this research for modifying the ICRP 67 model that included urine, fecal, blood and liver bioassays. The daily mean bioassay measurement data were used for model comparison. Two individual cases (i.e., IDEAS Case 123 and USTUR Case 0269) supported development and validation of the Pu-DTPA model. These are described in the following sections.

2.6.1 Langham Data

Langham et al. (1980) reported on the results of a human study contracted by the Manhattan Engineer District (i.e., Los Alamos Scientific Laboratory of the University of California) and the Atomic Energy Commission (i.e., University of Rochester School of

Medicine and Dentistry). The study involved intravenous injection of trace quantities of ^{239}Pu(IV) citrate in twelve patients (i.e., Hp-1 to Hp-12), with ten that were over the age of 45 years, each with chronic disorders where the life expectancy beyond 10 years was unlikely (Langham et al. 1980). Langham et al. (1980) also reported on four additional results (i.e., Chi-I, Chi-II, Chi-III, Cal. I) obtained from a human study performed at Chicago and Berkeley. Durbin (1971) provided additional details of the Langham et al. (1980) study that included two additional studies performed at Berkeley. There were three occupational intakes Langham et al. (1980) had included from Los Alamos in the study that are omitted from this analysis due to the excretion being based from a predicted intake amount instead of a known quantity. Incremental blood, daily urine and composited 4-day fecal samples were collected following injection, with higher frequency during the first few days (Langham et al. 1980). Durbin (1971) had indicated that there were liver anomalies reported for two cases (i.e., HP-11 and Chi-2), and that several cases (i.e., HP-1, H-7, Hp-9, Hp-12, Chi-I, Chi-II, Cal-I) were anemic, with some having abnormal kidney function (i.e., Hp-4, Chi-I, Chi-II, and Cal-I). Cases Hp-12, Chi-III and Cal-I had excretion provided for much later periods, and were used by Durbin (1971). Durbin (1971) placed emphasis on excretion data obtained from Hp-2, Hp-3, Hp-5, Hp-6, Hp-8 and Hp-10 since they did not have liver or kidney abnormalities. Langham et al. (1980) had identified anomalous data in the study that were not included in the mean bioassay data for this work. This research had considered Durbin's (1971) recommendation to work with a limited subset of the data, but chose to apply the discretion that Langham et al. (1980) had used and kept all of the case data while

removing the previously identified anomalous data. The Langham et al. (1980) data was provided in Appendix 3.

2.6.2 UK Data I

Talbot et al. (1993, 1997) studied the metabolism of ^{237}Pu(IV) citrate injected intravenously in 12 healthy volunteers. Six of the subjects were male (Cases A to F) that ranged in age from 26 to 70 years, and six were female (Cases G to L) that ranged in age from 35 to 57 years, with 4 males and 4 females over the age of 45 years (Talbot et al. 1993, 1997). Incremental excretion samples were collected for blood, urine and feces for 21 days, with several samples collected in later time periods up to 106 days, 97 days and 93 days, respectively (Talbot et al. 1993, 1997). Additionally, the liver uptake was also determined for these subjects by *in vivo* measurements using a single, uncollimated 200-mm diameter Na(I)Tl/CsI(Tl) dual scintillator Phoswich detector (Newton et al. 1998). The activity was determined from venous blood samples that consisted of a 20-mL volume, where the activity was normalized as a percent of the injected dose per kilogram of blood volume, and adjusted to the total blood volume determined for each individual (Talbot et al. 1993, 1997). Talbot et al. (1997) reported the injection percent in the total blood volume for the 28 to 31 minute collection periods for each case, which was used to determine the total blood volume for other periods. The UK Data I was provided in Appendix 3.

2.6.3 UK Data II

Ham and Harrison (2000) studied the gastro-intestinal absorption of ^{244}Pu(IV) citrate administered by ingestion followed by intravenous injection six-months later in

five healthy adult males. The administered ingested and injected amount was 40 ng and 0.8 ng, respectively (Ham and Harrison 2000). Ham and Harrison (2000) calculated an average absorption fraction of 6×10^{-4} that ranged from 1.2 to 8.9×10^{-4} between all subjects that was consistent with ICRP 67 recommendations of 5×10^{-4}. Intravenous injection was performed at six-months where it was determined that the urinary excretion activity due to ingestion was < 0.1% of the expected urinary excretion due to the injection (Ham and Harrison 2000). Initial systemic absorption of the ingested quantity was approximately 3% of the injection quantity. The subjects ranged in age from 36 to 64 years with 3 over the age of 45 years (Ham and Harrison 2000). Incremental urinary excretion samples were collected daily up to 6 years following intravenous injection and reported in percent of injection (Ham and Harrison 2000). The UK Data II was provided in Appendix 3.

2.6.4 Langham's later data

Rundo et al. (1976) reported on the excretion data collected in 1973 from 3 members of the original Langham et al. (1980) study (i.e., Hp-3 and Hp-6) and Durbin (1971) report (Cal-3) who were injected with known quantities of plutonium in 1945 to 1947. Two members were injected intravenously with ^{239}Pu(IV) in a citrate complex, while one (Cal-3) received an intramuscular injection of ^{238}Pu(VI) as a nitrate complex in a leg that was amputated 4 days later (Rundo et al. 1976). The urinary excretion rates of the first two subjects were 7.60 and 4.68 pCi d^{-1}, which accounted for 0.00252% and 0.00141%, at 9,934 and 10,008 days following initial injection, respectively for Hp-3 and Hp-6 (Rundo et al. 1976). The fecal excretion accounted for 40% of the urinary excretion, with 3.17 and 1.77 pCi d^{-1}, respectively (Rundo et al. 1976). Urinary excretion

activity from Cal-3 was 0.06 pCi d^{-1}, which accounted for 0.00012% of the initial activity 9,474 days after injection (Rundo et al. 1976). The third subject still contained 50% of the activity at the injection site 4 days following injection, which would have explained the observed decrease in excretion due to the leg amputation (Rundo et al. 1976). The Cal-3 data was excluded from this work due to the leg amputation and the results being approximately 10 times less than expected and not consistent with the long-term excretion of the other two cases.

2.6.5 IDEAS Case 123

The CONRAD task group studied Case 123 in the IDEAS database (Hurtgen et al. 2006) for optimizing the fit of chelation being applied to the model since this case had early excretion data prior to DTPA administration (Breustedt et al. 2009, 2010). IDEAS Case 123 had a hand wound caused by broken glass with a pH 1 solution of hexavalent ^{239}Pu.[2] Surface decontamination reduced the contamination from 2.22 MBq to 555 kBq, and tissue excision reduced it further to about 74 kBq. The IDEAS database provided urine and fecal excretion, wound assessments, blood activity and the days chelation (DTPA) was administered by intravenous injection. The Pu-DTPA compartment model transfer rates were derived by studying this case. The IDEAS Case 123 data was provided in Appendix 3.

[2] Information was provided in IDEAS database (Hurtgen et al. 2006) with a reference to Jeanmaire 1964 Case 1. IDEAS database was available online at: http://www.sckcen.be/ideas/ ; accessed on January 31, 2013.

2.6.6 USTUR Case 0269

The United States Transuranium and Uranium Registries (USTUR) case 0269 involved an occupational worker that was exposed to an aerosol form of soluble plutonium nitrate in 1956 (James et al. 2007). The worker was promptly treated intravenously with Ca-EDTA that lasted over the course of several years, with variations of oral administration and a late introduction of Ca-DTPA treatments (James et al. 2007). James et al. (2007) reported tissue sample results for USTUR case 0269 for ^{239}Pu 38-years (14,054 days) post intake, with the final tissue and organ burden presented in Table 10.

Table 10: USTUR Case 0269 Autopsy Results (James et al. 2007).

Organ/Tissue	Activity (Bq)
Lungs, larynx, trachea	26.7
Thoracic lymph nodes	0.19
Skeleton	1197
Trabecular	~230*
Cortical	~970*
Liver	937
Kidneys	1.7
Testes	0.83*
Other Soft Tissues	180
Total Systemic burden	2317

*James et al. (2007) had approximated the trabecular and cortical bone deposition from an earlier study. James et al. (2007) had reported two values for the testes activity of 0.83 Bq and 0.83 kBq. The 0.83 Bq was determined to be the correct quantity based on expected ICRP 67 model predictions.

The Pu-DTPA compartment model was validated based on a study of USTUR Case 0269, using the excretion data that was provided in Appendix 3, and comparison with the final tissue and organ burden. This case was unique since it extended the Pu-DTPA model from a wound case to an inhalation case, illustrating the universal application of the model.

2.7 Literature Review Summary

In summary, this chapter presented the biochemistry and distribution of plutonium, briefly described the basic human physiology and histology important for plutonium contamination, provided an in depth discussion of DTPA that included results of animal studies, discussed the various internal dosimetry biokinetic models and included a discussion of the human data and cases that were used in this research. Some highlights included the understanding of the plutonium complex, how it is initially considered in a monomeric form and changes state within the body following physiological processes, such as bone remodeling and macrophage dissolution, and its interaction with endogenous ligands. Calcium and iron homeostasis was also introduced with a discussion of how these can influence plutonium distribution.

Discussions with DTPA included the differences and effectiveness of both Ca-DTPA and Zn-DTPA, where both are considered providing a similar benefit for protracted treatments, while Zn-DTPA was the safer alternative. Animal studies indicated that multiple intra-day Zn-DTPA treatments provided an improved benefit of decorporation than a single injection, and that the liver could be fully decorporated with frequent protracted treatments, while observing a reduction of the skeleton burden. The animal studies supported the idea of liver decorporation that was added to the Pu-DTPA compartment model. The skeleton physiology and the animal studies supported the idea that reduction of the skeleton burden was due to prevention rather than actual decorporation, being based on the skeletal membrane, resorption involving polymeric plutonium being released, and the bone glycoproteins having a higher affinity for plutonium than DTPA.

There was a complete discussion of the biokinetic models representing the absorption, distribution, retention and excretion of plutonium within the human body. This research relied on an integration of these models for studying actual human cases. This chapter concluded with a discussion of the available human data and cases that were used in this research in development of the Pu-DTPA biokinetic model and for proposing a revision to the ICRP 67 systemic model. The mean of the human data was used in the regression of the ICRP 67 proposed revision. The Leggett 2005 model was discussed since it was used as a benchmark for modifying the ICRP 67 model with a goal of keeping the basic structure. Benchmarking included using the long-term blood, liver and skeleton organ burdens to fill in the gap where human data was unavailable, which was important since it relied on the accuracy of the predictions provided by the Leggett 2005 model.

Chapter 3: Methodology

3.1 Compartment Model Calculations

The biokinetic model is described in several ICRP publications, such as ICRP 66 for the lung model and ICRP 67 for the systemic model. Birchall and James (1989) had presented how to perform compartment model calculations that included recycling between compartments. This involved a square rate matrix with the diagonal representing the initial compartment quantity, for an instantaneous acute intake, and the off-diagonals representing the transfer rate among compartments. During this effort rate matrices were developed by integrating the NCRP 156 wound model and the ICRP 66 lung model, each coupled with the ICRP 67 systemic model and the ICRP 30 GI-tract model.

3.1.1 Wound Model

The NCRP 156 wound compartment model rate matrix was specified in Table 11 for plutonium, with strong-retention wound parameters.

Table 11: Wound rate matrix for strong-retention (units in d^{-1}) (NCRP 2007).

	Soluble	CIS	PABS	LN	Blood
Soluble	1	0.6			0.67
CIS	0.024	0	0.01	2×10^{-5}	
PABS	0.0012		0	2×10^{-5}	
LN				0	
Blood					0

The rate matrix presented in Table 11 was arranged with defined pathways, where the contaminant leaves compartments assigned to the left column and enters

compartments specified in the top header. The compartment intake quantities are specified on the diagonal, where Table 11 uses a default intake activity of 1 Bq deposited in the Soluble compartment. This approach was used to calculate intake retention fractions. The compartment transfer rates (λ_i) were specified in the off-diagonal elements. Figure 16 illustrates the rate matrix in relation to the abbreviated NCRP 156 compartment wound model.

Compartment Model

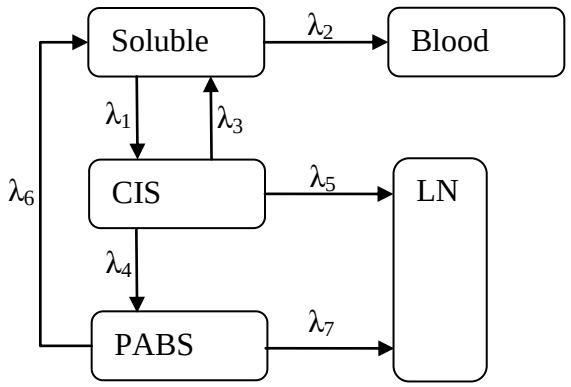

Compartment Rate Matrix

	Soluble	CIS	PABS	LN	Blood
Soluble	1	λ_1			λ_2
CIS	λ_3	0	λ_4	λ_5	
PABS	λ_6		0	λ_7	
LN					
Blood					

Figure 16: Compartment model and rate matrix for a soluble radionuclide wound illustration.

The rate matrix was defined in a Microsoft Excel spreadsheet, coupled with the ICRP 67 systemic and ICRP 30 GI-tract models that was presented in Appendix 6.

The compartment transfer rates are specified in the ICRP and NCRP recommendations with the compartment model; however, they encompass the compartment retention half-time and the fraction designated for each compartment path. The compartment retention half-time is the natural log of 2 divided by the sum of all specified transfer rates leaving the compartment, which would be $\ln(2)/1.27\ d^{-1}$, resulting in a half-time of 0.55 days for the soluble compartment. The distribution fractions can be determined by dividing each path's transfer rate by the total compartment transfer rate, which would be 0.6/1.27 = 0.47 for the Soluble to CIS compartment path. Specifying

compartment fractions and total retention half-times were important for the development and revision of biokinetic models in this research.

3.1.2 Lung Model

The ICRP 66 lung model rate matrix was specified in Figure 17 for the initial and transformed particle compartments that represented a total inhalation activity of 1 Bq for a 5-μm AMAD ^{239}Pu particle size with a Type-S absorption quality.

Compartments	AI1	AI2	AI3	bb1	bb2	bbseq	BB1	BB2	BBseq	LNTH	ET2	ETseq	LNET	ET1	AI1t	AI2t	AI3t	bb1t	bb2t	bbseqt	BB1t	BB2t	BBseqt	LNTHt	ET2t	ETseqt	LNETt	GI ST	GI SI	Blood	Envir
AI1	0.0159			0.02											100															0.1	
AI2		0.0318		0.001												100														0.1	
AI3			0.0053	0.0001						2E-05							100													0.1	
bb1				0.006523			2											100												0.1	
bb2					0.004		0.03												100											0.1	
bbseq						0.000077				0.01										100										0.1	
BB1							0.0118677				10										100									0.1	
BB2								0.005907			0.03											100								0.1	
BBseq									0.000125	0.01													100							0.1	
LNTH										0														100						0.1	
ET2											0.3998														100			100		0.1	
ETseq												0.0002	0													100				0.1	
LNET													0														100			0.1	
ET1														0.34																	1
AI1t																		0.02												0.0001	
AI2t																		0.001												0.0001	
AI3t																		0.0001						2E-05						0.0001	
bb1t																					2									0.0001	
bb2t																					0.03									0.0001	
bbseqt																								0.01						0.0001	
BB1t																									10					0.0001	
BB2t																									0.03					0.0001	
BBseqt																								0.01						0.0001	
LNTHt																								0						0.0001	
ET2t																												100		0.0001	
ETseqt																										0.001				0.0001	
LNETt																											0			0.0001	
GI ST																													24		
GI SI																														6.00E-05	
Blood																															
Envir																															

Figure 17: Rate matrix for plutonium lung model for Type S absorption.

This abbreviated rate matrix was illustrated for discussion purposes, but to be complete, integration with the particle bound compartments, systemic and GI-tract models into the rate matrix would be necessary. Verification of the lung model rate matrix and calculations were performed with comparison to IAEA Safety Reports Series No. 37 (2004) in Appendix 2 for an inhalation characteristic of a 5-μm AMAD ^{239}Pu particle with a Type-S absorption that provided consistent results. Plutonium absorption can also be considered to be Type M for more soluble compounds, such as plutonium-nitrate aerosols.

3.1.3 Compartment Model Solution

Birchall and James (1989) provided insight into solving a compartment model matrix. Once the rate matrix had been specified, then the next step was to transform the rate matrix into an A matrix as described by Birchall and James (1989) as follows:

The compartment model linear first-order differential equation can be described by Equation 2:

$$\frac{dx_i}{dt} = \sum_{\substack{j=1 \\ j \neq i}}^{N} r_{ji} x_j - x_i \sum_{\substack{j=1 \\ j \neq i}}^{N} r_{ij} \tag{2}$$

Where, $r_{ji}x_j$ describes the instantaneous fraction of the content of compartment j that enters compartment i according to the specified transfer rate r_{ji} per unit time. The following substitution is made:

$a_{ij} = r_{ji}$, for i, j = 1 to N and $i \neq j$

$$a_{ii} = -\sum_{\substack{j=1 \\ j \neq i}}^{N} r_{ij} \text{ , for i = 1 to N}$$

Using substitution:

$$\frac{dx_i}{dt} = \sum_{\substack{j=1 \\ j \neq i}}^{N} a_{ij} x_j + a_{ii} x_i$$

$$\frac{dx_i}{dt} = \sum_{j=1}^{N} a_{ij} x_j$$

In matrix notation:

$$\frac{dx}{dt} = [A]x \tag{3}$$

Birchall and James (1989) solved Equation 3 in the following way:

$$x_i(t) = e^{[A]t} x_i(0) \tag{4}$$

And, when the interest is the number compartment decays:

$$u_i(t) = \lambda [A]^{-1} \left[e^{[A]t} - I \right] x_i(0) \tag{5}$$

Where:

[A]: is a matrix representing the transpose of the R matrix with the diagonal being the negative sum of each row's rate constants including the radioactive decay constant

$[A]^{-1}$: is the inverse of matrix A

$x_i(0)$: is the column vector representing the initial compartment (i) quantity

$x_i(t)$: is the column vector representing the compartment (i) quantity at time (t)

$u_i(t)$: is the accumulated number of transformations that have occurred in compartment (i) at time (t)

λ: radioactive decay constant

I: identity matrix

The matrix exponential can be solved using Taylor series approximations or employing eigen-decomposition. Taylor series approximation can be accomplished by:

$$e^{At} = \sum_{i=0}^{\infty} \frac{[At]^i}{i!} = I + At + \frac{[At]^2}{2!} + \ldots \tag{6}$$

Birchall and James (1989) provided a unique solution for abbreviating the steps required for convergence that can be accomplished by the following analogy:

$$e^{At} = \left[e^{(At)/2^n} \right]^{2^n} \tag{7}$$

Where, the denominator (2^n) functions to reduce the members of the A matrix so that the largest element in the A matrix is less than 0.2. Recursive exponential matrix multiplications will also reduce the number of calculations from 2^n to n times that also dramatically shorten the computation time (Birchall and James 1989).

Some software programs can accommodate solving the matrix exponential using the Taylor series approximation. Eigen-decomposition also provides a unique solution as described by Polig (2001), and is also available in several software packages. Eigen-decomposition of the square matrix [A] results in:

$$[A] = u[I\lambda]u^{-1} \tag{8}$$

Where, matrices u and [Iλ] are the eigenvector and eigenvalue solutions for matrix [A], respectively (Lattin et al. 2003, Polig 2001). The eigenvalue matrix described here is simply the product of an identity matrix with the unit vector of eigenvalues that results in a diagonal matrix with the eigenvalues (λ) on the diagonal and 0 for all off-diagonals. Solving for a function of [A] would only require manipulating the eigenvalue matrix. Such as for solving for $e^{[A]}$:

$$e^{[A]} = ue^{I\lambda}u^{-1} = u\begin{bmatrix} e^{\lambda_1} & 0 \\ 0 & e^{\lambda_2} \end{bmatrix}u^{-1} \tag{9}$$

This may also be represented by the following general equation (Polig 2001):

$$f(A) = uf(I\lambda)u^{-1} \tag{10}$$

In the past, there were limited software programs available for solving a matrix exponential. Today, there are several statistical software packages where solving the matrix exponential may be easily performed. For example in the R programming

language, obtaining an exponential of a matrix can simply be obtained using the syntax "expm(A)" when the expm package is installed. This function uses Ward's diagonal Pade' approximation to resolve the matrix (Goulet et al. 2012). Eigenvalues and eigenvectors may also be used for verification or as an alternate means. By obtaining these values of "eigen(A)" which is provided as part of the base R package, one may solve the matrix exponential.

3.1.4 The R Environment[3]

The R environment includes a statistical software package (R Core Team 2013, Venables et al. 2012) that can be used to determine compartment quantities and transformations using the rate matrix as described in Birchall and James (1989) and Polig (2001). Figure 18 presents an R function [decays] that was used for calculating compartment quantities and transformations.

[3] R is a freely available open-source software utility that can be downloaded at: http://www.r-project.org/ with the following recommended user interface: http://www.rstudio.com/.

```
decays = function (R,t,h)                #function requires input of rate matrix (R), time (t), and half-life (h)
in days
{
        X0=diag(as.matrix(R))            #provides the initial quantity vector
        lam=log(2)/h                     #decay constant (lambda)
        A=t(R)                           #A is created from the transpose of R

        #the following for loop specifies the A diagonal as the (-)sum of each row (excluding initial
        quantity)
        N = dim(R)[1]
        for (i in 1:N) {
        A[i, i] = -sum(R[i, -i]) - lam   } #subtracts the radiological decay constant from each diagonal
        element

        # eigen-decomposition method
        V = eigen(A)$vectors
        D.exp = diag(exp(eigen(A)$values * t))
        A.exp = V %*% D.exp %*% solve(V)

        # alternative to the eigen-decomposition method is A.exp=expm(A*t), but requires the expm
        package

        B=A.exp-diag(1,dim(A)[1])        #subtracts the identity matrix from the exponential matrix
        A
        trans=lam*solve(A) %*% B %*% X0  #calculates the total compartment transformations
        X=A.exp %*% X0                   #performs matrix calculation for the quantity left in each
        compartment
        X[N-1]=X[N-1]+trans[N-1]         #adds back in the atoms experiencing decay in the fecal compartment
        X[N]=X[N]+trans[N]               # adds back in the atoms experiencing decay in the urine
        compartment

        ttl = cbind(X0, X, trans)
        colnames(ttl) = c("initial", "atoms", "decays")
        row.names(ttl) = colnames(R)
        structure(list(summary = ttl), class = "decays") }#used to return results
```

Figure 18: R function [decays] for calculating compartment quantities and transformations for a specified time.

The R function [decays] required input by specifying the rate matrix (R), time of interest (t), and radionuclide half-life (h), with all time units in days. The function requires that the urine compartment be specified in the last row and column, and the fecal compartment be specified in the adjacent row and column of the rate matrix. The R functions and rate matrices created and used in this research were provided in Appendix 1 and 4, respectively, with an example rate matrix construction provided in Appendix 6.

The following example was used to demonstrate the concepts presented. The example was provided by Birchall and James (1989) and also used for initial verification. Consider the biokinetic compartment model for ^{131}I in Figure 19.

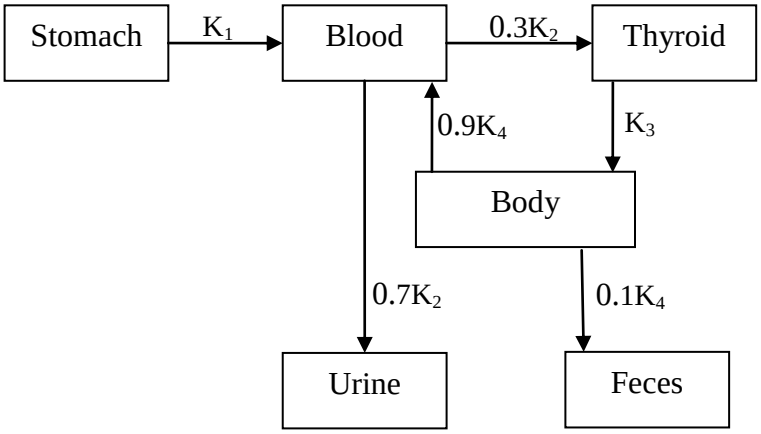

Figure 19: ICRP metabolic model for ^{131}I in adults (Birchall and James 1989).

All transfer rates K_i are in units of d^{-1} and are specified as $K_1=24$, $K_2=\ln(2)/0.25$, $K_3=\ln(2)/80$, and $K_4=\ln(2)/12$. Also, the radioactive decay constant lam = $\ln(2)/8.04$ d^{-1} for ^{131}I, and the initial quantity deposited in the stomach for ingestion was 1 Million atoms, with 0 elsewhere. The calculation was performed in the R programming language as illustrated in Figure 18, using the [decays] function previously described.

Setup the rate matrix as follows:

```
> R=matrix(rep(c(0,0,0,0,0,0),6),nrow=6,byrow=TRUE)
> R[1,1]=1e6
> R[1,2]=24
> R[2,3]=0.3*log(2)/0.25
> R[2,5]=0.7*log(2)/0.25
> R[3,4]=log(2)/80
> R[4,2]=0.9*log(2)/12
> R[4,6]=0.1*log(2)/12
> row.names(R)=c("Stomach","Blood","Thyroid","Body","Urine","Feces")
> colnames(R)=c("Stomach","Blood","Thyroid","Body","Urine","Feces")
> R
        Stomach       Blood   Thyroid       Body    Urine       Feces
Stomach   1e+06 24.00000000 0.0000000 0.00000000 0.000000 0.000000000
Blood     0e+00  0.00000000 0.8317766 0.00000000 1.940812 0.000000000
Thyroid   0e+00  0.00000000 0.0000000 0.00866434 0.000000 0.000000000
Body      0e+00  0.05198604 0.0000000 0.00000000 0.000000 0.005776227
Urine     0e+00  0.00000000 0.0000000 0.00000000 0.000000 0.000000000
Feces     0e+00  0.00000000 0.0000000 0.00000000 0.000000 0.000000000
```

Using the decays function created earlier for 5000 days and 8.04 day half-life, to obtain the compartment quantities and decays:

```
> decays(R,5000,8.04)
$summary
        initial          atoms     decays
Stomach   1e+06  0.000000e+00   3579.323
Blood     0e+00 4.153739e-198  30339.956
Thyroid   0e+00 1.319421e-195 265988.092
Body      0e+00 2.210497e-196  16007.068
Urine     0e+00  6.830131e+05 683013.088
Feces     0e+00  1.072474e+03   1072.474

attr(,"class")
[1] "decays"
```

Figure 20: Thyroid compartment model example using the R program to obtain compartment quantity and transformations.

According to Birchall and James (1989) the thyroid experienced 2.675 x 10^5 transformations, which is in close agreement with the results provided above of 2.66 x 10^5. This example validated the compartment transformation calculation that was provided by the decay function. This function was relied upon frequently during this research and provided intake retention fraction tables that were used for further validation of compartment quantities in Appendix 2.

3.2 Model Development

3.2.1 Pu-DTPA Model

The Pu-DTPA model was developed starting with the model and specified parameters from the CONRAD project (Breustedt et al. 2009), which was illustrated in Figure 21.

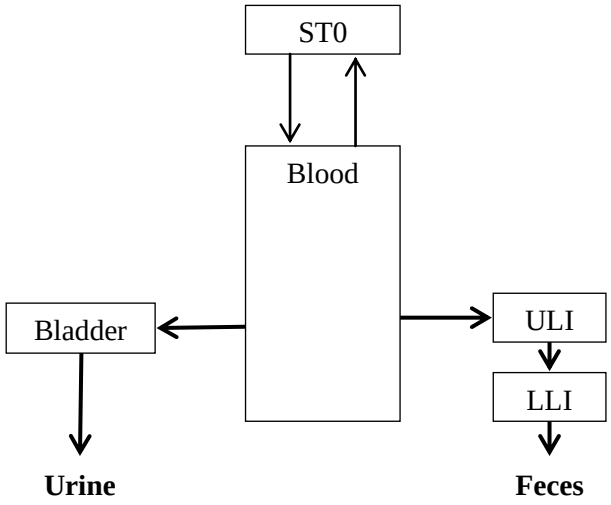

Figure 21: CONRAD proposed compartment structure for DTPA (Breustedt et al. 2009).

The CONRAD task group adapted the Stather et al. (1983) DTPA compartment model, which included the blood and extracellular fluid compartments to the Leggett 2005 model and the ICRP 30 GI tract model (Breustedt et al. 2009). A second-order kinetics mechanism was introduced to the series of first-order differential equations to describe the formation of the Pu-DTPA complex in the model (Breustedt et al. 2009, 2010). The CONRAD task group recommended the initial parameters presented in Table 12, which were based on DTPA kinetics with the assumption that the Pu-DTPA complex would have similar characteristics (Breustedt et al. 2009):

Table 12: CONRAD task group recommended transfer rates (Breustedt et al. 2009).

Compartment Pathway	Transfer Rate (d^{-1})
Blood to interstitium	145
Interstitium to blood	64
Interstitium to lymph	0.0123
Lymph to blood	0.405
Blood to urinary bladder	45.7

Table 12 refers to interstitium that is represented by the ST0 compartment (Leggett et al. 2008). The lymph system was considered part of the ST1 compartment. The blood to urinary bladder represents approximately a 20-minute retention half-time. The CONRAD model did not provide parameters for the blood to fecal excretion pathway, but indicated that there was an increase in fecal excretion (Breustedt et al. 2009).

The compartment model presented in Figure 22 was used in this research, which is a variation of the CONRAD model with the addition of the ST1 and Liver compartments and the Pu-DTPA transitional compartments.

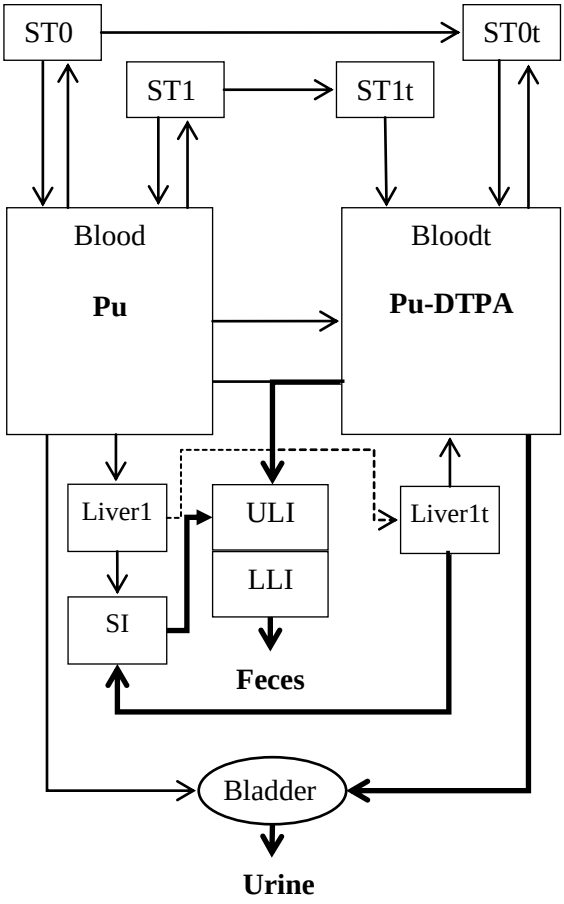

Figure 22: Pu-DTPA biokinetic model. Bolded lines illustrate the Pu-DTPA excretion pathway.

The model was developed with the understanding that the Pu-DTPA complex would exhibit different kinetics than unbound plutonium, using a similar approach as described for the ICRP 66 lung model particle transformation kinetics. Compartments Bloodt, ST0t, ST1t and Liver1t are considered transitional compartments that account for the plutonium quantity upon being complexed with the DTPA ligand. The Pu-DTPA content in these compartments will continue to be tracked, which will assist in accounting for DTPA late excretion periods beyond the first day. The parameters for the compartment model are provided in Table 13 on days that DTPA is administered as either a calcium or zinc salt complex. No distinction was made between the kinetics of Ca-

DTPA or Zn-DTPA complexes which was due to Ca-DTPA normally being administered on the first day and both the calcium and zinc DTPA complexes were considered having the same effect for subsequent days (IAEA 1978). Adjustments to the model transfer rates would be required if Zn-DTPA was administered on the first day since it would have less decorporation potential than Ca-DTPA. The default ICRP 67 transfer rates were used in all normal compartments.

Table 13: Compartment initial transfer rate parameters for use on days DTPA was administered.

Compartment Pathway	Initial Transfer Rate (d^{-1})
ST0 to ST0t	100
ST1 to ST1t	0
Liver1 to Liver1t	0
Blood to Bloodt	100
ST0t to Bloodt	64
ST1t to Bloodt	0
Liver1t to Bloodt	0
Liver1t to SI	0
Bloodt to ST0t	145
Bloodt to ULI	2.3
Bloodt to Bladder	45.7

The ST1t and Liver1t compartments were initially omitted and sequentially introduced during regression with IDEAS Case 123 in the process of discovering an optimum model that was able to best describe the observed urine and fecal excretion. The specified rate matrix was coupled with the NCRP 156 wound or the ICRP 66 lung model, with the ICRP 30 GI tract and ICRP 67 systemic model that required an additional four compartments to be added to the rate matrix.

3.2.2 Modified ICRP 67 model

The ICRP 67 systemic model was reviewed for a physiological basis with hopes of improving the fecal excretion and blood compartment activities when compared to observations from human studies. The model also needed to predict organ and tissue

activity for early and late periods. The ICRP 67 systemic model was specified for monomeric plutonium intakes, which is consistent for occupational exposures. Upon initial absorption, monomeric plutonium complexes primarily with the transferrin protein, and is taken up mostly by the liver hepatocytes, and trabecular regions of bone where the plutonium ion is released from the transferrin protein for local deposition on bone surfaces. A small percentage may be excreted, taken up by soft tissues, or incorporated into Kupffer cells and tissue macrophages.

Trabecular bone surface regions are continuously being remodeled, where resorbed plutonium is assumed to be in a polymeric form that is taken up by the local tissue macrophages and subsequently released in a monomeric form after dissolution. Monomeric plutonium released from tissue macrophages can participate in local bone mineralization, be transported to remote regions of bone and deposit on bone surfaces undergoing some level of mineralization, form a polymeric complex in circulation and be taken up by liver Kupffer cells or tissue macrophages, be filtered by the kidneys and excreted in a monomeric form, or be bound to plasma proteins and circulated to receptor sites. Figure 23 illustrates these basic concepts.

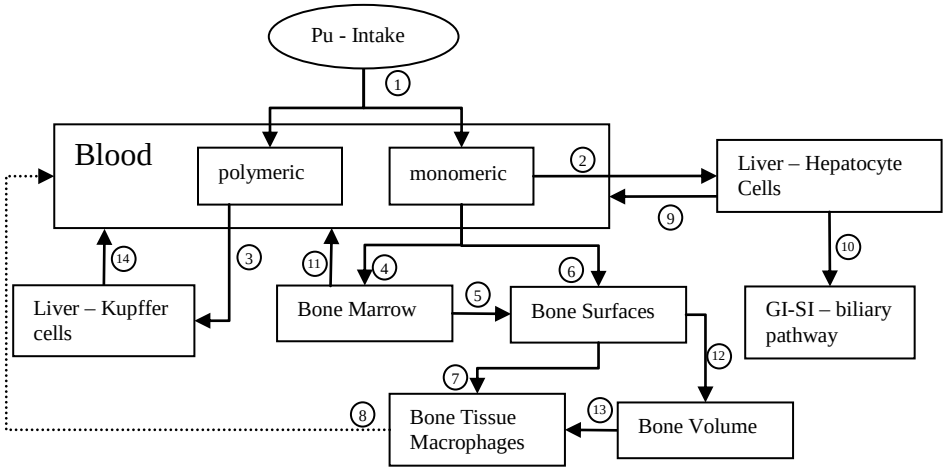

Figure 23: Plutonium distribution basic concepts**.**

Figure Note: (1) Plutonium intake is normally in a monomeric form. Some plutonium molecules may enter in a polymeric form (i.e., $PuNO_3$ or PuO_2) within the blood or extracellular fluids; (2) Some of the plutonium bound to the transferrin protein will have an affinity for the liver hepatocytes and be transferred to the ferritin protein; (3) The Kupffer cells, predominantly in the liver, will engulf polymeric plutonium in circulation; (4) Plutonium bound to the transferrin protein initially attempting red-blood cell incorporation; (5) Plutonium upon being released by the transferrin protein after a failed attempt for red-blood cell incorporation that is expected to be prevalent in the trabecular marrow; (6) Plutonium in a monomeric or ion form will enter the bone fluid via the channels, created by the tight-junctions of adjacent bone-lining cells, with a concentration dependent on the mineralization phase; (7) Plutonium that has been resorbed from the bone surface in a polymeric form will be engulfed by local tissue macrophages, also located in the bone marrow; (8) Monomeric plutonium released by tissue macrophages and reentering circulation; (9) Plutonium released from hepatocyte cells that reenter circulation; (10) Plutonium released from hepatocyte cells via the biliary pathway for excretion in the GI tract small intestine (SI); (11) Plutonium released from the transferrin protein after a failed attempt of red-blood cell incorporation, reentering circulation; (12) Plutonium that is bound to the surface and buried due to further bone mineralization; (13) Resorbed polymeric plutonium will be engulfed by local tissue macrophages; and (14) Monomeric plutonium released by Kupffer cells and reentering circulation.

Figure 23 describes the plutonium distribution that is applicable to a typical occupational exposure based on current understanding. Differences between the concepts presented in Figure 23 and the ICRP 67 systemic model include the transport from blood circulation to bone marrow, bone marrow to bone surfaces, and separate liver compartments. The bone surfaces and bone volume path to the tissue macrophages are considered in the ICRP 67 systemic model as the bone marrow compartment. With this

in mind, the proposed modification to the ICRP 67 systemic model is illustrated as Figure 24.

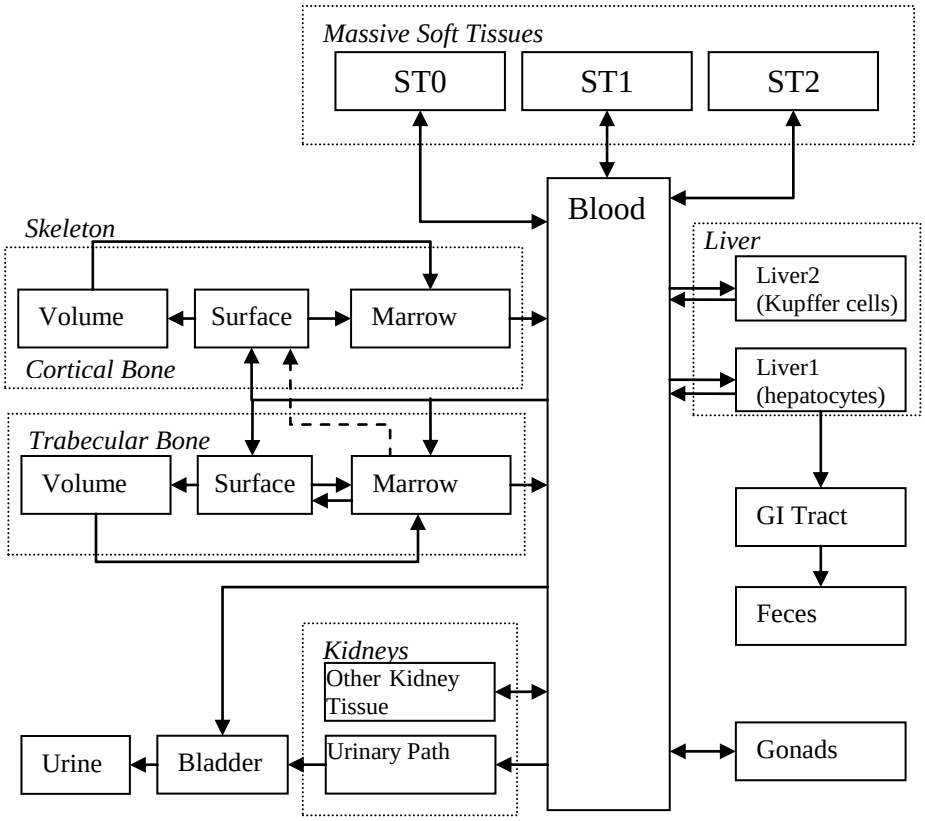

Figure 24: First consideration for modification of the ICRP 67 systemic model.

Figure 24 is the first general consideration of the intricate model advocated within Figure 23 that includes an added pathway from the blood compartment to the trabecular marrow compartment, and pathways from the trabecular marrow to both the cortical and trabecular bone surfaces. The revised model represented by Figure 24 also separates the liver into two compartments with a separate return to the blood compartment. The pathway from the ST1 to the bladder compartment was also removed due to the lack of a physiological basis. The Pu-Tf path from circulation to the bone marrow was originally considered but omitted due to the insignificant residence time in the bone marrow. Plutonium was modeled to include a path directly to the bone volume compartments from

circulation, bypassing the bone surface compartments, which served to represent the initial bone mineralization phase that occurs rapidly over the first few weeks, and was consistent with the Leggett 2005 model and Polig (1997) model assumptions. Therefore, to include all of these considerations, the model was again revised. Figure 25 is a representation of this revised model.

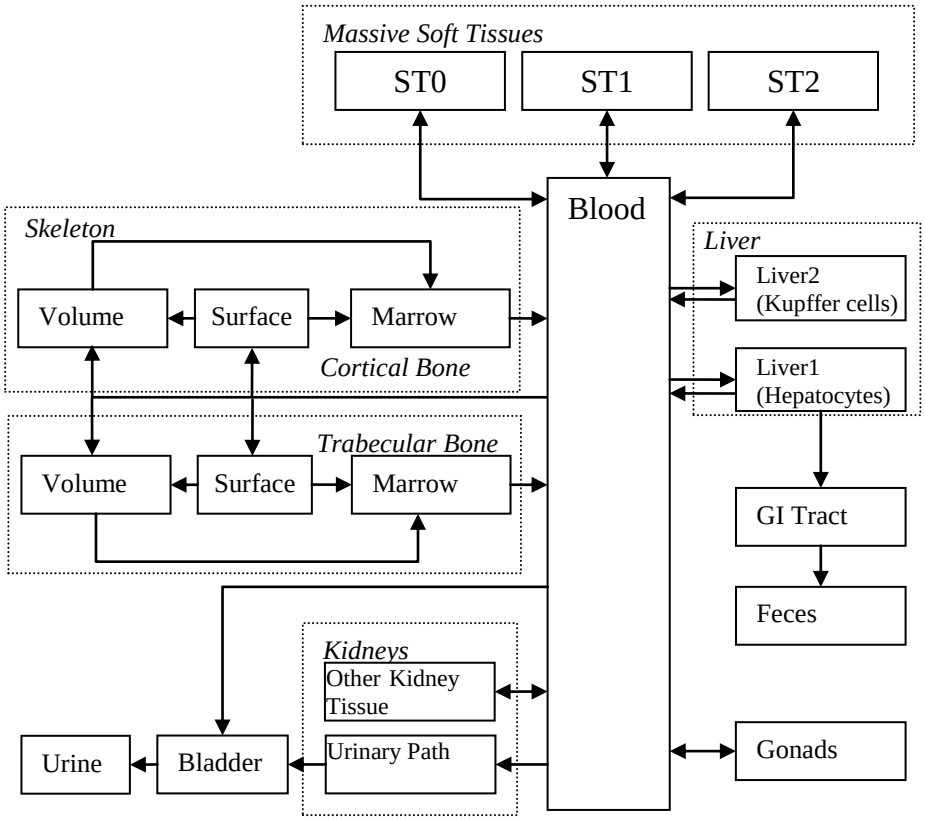

Figure 25: Final modification of the ICRP 67 systemic model.

The initial compartment transfer rates were adopted from the ICRP 67 systemic model for plutonium with inclusion of the Leggett 2005 model transfer rates for the blood compartment to the skeleton compartments. The original transfer rate from the ST1 to the bladder compartment was removed and added to the transfer rate for the ST1 to the blood compartment path. The fractional uptake from the blood compartment to the bone surface and volume compartments was adopted from the Leggett 2005 model and

maintained fixed during optimization. The fraction of activity departing from circulation to the Liver and Skeleton compartments of 21% and 35%, respectively, was adopted from the ICRP 67 systemic model. The Liver1 to Liver2 transfer rate was removed and added to the Liver1 to blood compartment transfer rate. The transfer rates from the blood to both liver compartments were specified with 83% partitioned to the Liver1 compartment and the remaining going to the Liver2 compartment. The soft tissues received 40% of the activity leaving the blood compartment that was also based on the ICRP 67 systemic model. Table 14 illustrated construction of the initial rate matrix prior to optimization.

Table 14: Initial rate matrix specification for the modified ICRP 67 model.

Path	Source	Destination	Transfer Rate (d^{-1})	Row	Column
1	ST0	Blood	0.693	1	20
2	ST1	Blood	0.00095	2	20
3	ST2	Blood	1.9×10^{-5}	3	20
4	Kidneys.other	Blood	0.00139	4	20
5	Liver2	Blood	0.000211	5	20
6	Testes	Blood	0.00019	6	20
7	CortVol	CortMarrow	8.21×10^{-5}	7	9
8	CortSurf	CortVol	4.11×10^{-5}	8	7
9	CortSurf	CortMarrow	8.21×10^{-5}	8	9
10	CortMarrow	Blood	0.0076	9	20
11	TrabVol	TrabMarrow	0.000493	10	12
12	TrabSurf	TrabVol	0.000247	11	10
13	TrabSurf	TrabMarrow	0.000493	11	12
14	TrabMarrow	Blood	0.0076	12	20
15	Liver1	GI.SI	0.000133	13	15
16	Liver1	Blood	0.00177	13	20
17	GI.ST	GI.SI	24	14	15
18	GI.SI	GI.ULI	6	15	16
19	GI.SI	Blood	6.00×10^{-5}	15	20
20	GI.ULI	GI.LLI	1.8	16	17
21	GI.LLI	Feces	1	17	21
22	Kidneys.Urine	Bladder	0.01386	18	19
23	Bladder	Urine	12	19	22
24	Blood	ST0	0.2773	20	1
25	Blood	ST1	0.0806	20	2
26	Blood	ST2	0.0129	20	3
27	Blood	Kidneys.other	0.00323	20	4
28	Blood	Liver2	0.032	20	5
29	Blood	Testes	0.00023	20	6
30	Blood	CortVol	0.006421	20	7
31	Blood	CortSurf	0.122	20	8
32	Blood	TrabVol	0.019444	20	10
33	Blood	TrabSurf	0.175	20	11
34	Blood	Liver1	0.16	20	13
35	Blood	GI.ULI	0.0129	20	16
36	Blood	Kidneys.Urine	0.00917	20	18
37	Blood	Bladder	0.0129	20	19

The ICRP 67 rate matrix was optimized to the available human data for urine, fecal, blood and liver bioassays that was described in Chapter 2. The mean bioassay data, excluding the anomalous data, was used in the regression process. The blood and liver bioassays were from a limited data set with the longest observation being 106 and 437 days, respectively, and required further supplementation for modeling long-term effects. Furthermore, there was no skeleton bioassay data available. The Leggett 2005 model

expectations were used to supplement the blood and liver data for later periods, and provided benchmark data for the skeleton. The mean data from the human studies was used for optimizing the transfer rates using regression techniques based on minimizing the weighted sum of square residuals between the model prediction and the compiled data set for all bioassay types. The IDEAS guidelines (Castellani et al. 2013) were used as a basis for specifying the statistical results that were used as a metric for model performance, discussed later in this chapter.

3.3 Model Fitting

Compartment model calculations supported estimating the compartment transfer rates by comparison of the biokinetic model prediction with published results of human injection studies. Biological retention and excretion data provided by human studies with knowledge of the initial intake quantity and contaminant characteristics provide arguably the highest quality data for model construction. Secondly, experimental data from animals with similar biokinetic properties as humans provide useful information for model building as long as care is taken to account for differences in metabolism especially when these may differ greatly from those of humans. Furthermore, it is well understood that biokinetics may be influenced in animal experiments when significant doses are delivered as a consequence of the experimental protocol. Such experiences are unlikely when considering occupational intakes and should not be included in development of the biokinetic model. Evaluating the fit of the compartment model to the chosen data sets with suitable statistical measures provided assurance of the models performance.

The model fitting process involved minimizing the weighted sum of the squared residuals between the model prediction results with the observed data by modifying a set of unknown parameter values. The parameters represent compartment transfer rates that describe the fractional quantity distribution and retention half-time for the translocation between compartments. Influential parameters, chosen by sensitivity analysis and biokinetic knowledge, were altered during the fitting process to achieve an optimal solution. The solved biokinetic model was evaluated by the chi-squared statistic described by the IDEAS guidelines (Castellani et al. 2013). Models were tested against each other using the same data set, and their chi-squared statistic values were compared to each other.

3.3.1 Regression Approach

Regression was performed by minimizing a weighted least-squares fit of the residuals while adjusting the unknown parameter values. The standard weight alternated between use of the actual or predicted measurement. Additional weighting was applied by squaring the weight when emphasis was needed for lower magnitude data. The weights, although chosen in a somewhat ad hoc manner, were chosen to satisfy the equal variance assumption over the range of the data. The sum of weighted least-squares, referred to in this effort as a chi-square goodness of fit indicator, was presented in Equation 11 (Beal and Shiner 1988, Bevington and Robinson 2003, Garcia-Torano 1996, Luciani and Polig 2000):

$$\chi^2 = \sum_{i=1}^{n} \frac{\left[y_i - y(x_i)\right]^2}{w_i^p} \tag{11}$$

Where:

χ^2 = chi-square goodness of fit indicator

n = number of data points or observations

y_i = actual measurement

$y(x_i)$ = predicted measurement at x_i

w_i = weight (i.e., actual or predicted measurement)

p = power applied to the weight (e.g., 1 or 2)

Evaluation of the model fit performance was determined using the IDEAS guidelines described in the following section.

3.3.2 Model evaluation using the IDEAS guidelines

The IDEAS guidelines were established to improve consistent evaluations for internal dosimetry cases (Castellani et al. 2013, Doerfel et al. 2006). These guidelines recommend performing a natural log transformation of the excretion data since measurements are normally assumed to be lognormally distributed (Castellani et al. 2013, Doerfel et al. 2006). A natural log transformation of the observed and predicted data was included in the analysis and used as part of the model fit evaluation for the case evaluations.

Scattering Factor

The IDEAS guidelines describe equations that use a scattering factor (SF) that was an analog of the geometric standard deviation and determined by Equation 13.

$$SF_i = \exp\sqrt{\left[\ln(SF_A)\right]^2 + \left[\ln(SF_B)\right]^2} \quad (13)$$

The scattering factor is derived from the counting uncertainties with a Poisson distribution (i.e., Type A errors, SF_A) and other uncertainties such as measurement geometry (i.e., Type B errors, SF_B) (Castellani et al. 2013, Doerfel et al. 2006). A review of the examples provided in the IDEAS guidelines indicated that the Type B uncertainties dominated the Type A uncertainties in bioassay measurements and have the largest influence on the total scattering factor (Castellani et al. 2013). The IDEAS guidelines indicated that the SF_B estimated for urine bioassays ranged from 1.3 to 1.8, with an average of 1.6 for 24-hour normalized samples, and fecal samples ranged from 2 to 5, averaging 3 for a 24-hour sample (Castellani et al. 2013, Doerfel et al. 2006). This work adopted the average SF_B of 1.6 and 3 for urine and fecal bioassay, respectively, from the IDEAS guidelines as the overall SF since SF_A was unknown and would likely have little influence on the overall SF determination. The scattering factor for blood samples was undefined, which was likely due to blood measurements rarely being used for dose determination. IDEAS case 123 had 46 samples taken up to 493-days post intake that required an estimate of the scattering factor.

Marsh et al. (2007) determined the scattering factor by calculating the geometric standard deviation of measurement data that were uninfluenced by chelation using Equations 14 and 15.

$$\sigma^2 = \frac{\sum_{i=1}^{n}\left[\ln(M_i) - \ln(p_i)\right]^2}{n - z} \quad (14)$$

$$SF = \exp(\sigma) \quad (15)$$

Where M_i is the bioassay sample measurement, p_i is the sample prediction using the regression model, and n and z is the number of samples and regression model parameters, respectively.

Using Marsh et al.'s (2007) process in deriving the SF, the blood was regressed to a linear combination of exponential functions using the data from Talbot et al. (1997) in which blood sample results were normalized to fractions of the original intake. The plot of the regression model to the blood data was illustrated in Figure 26.

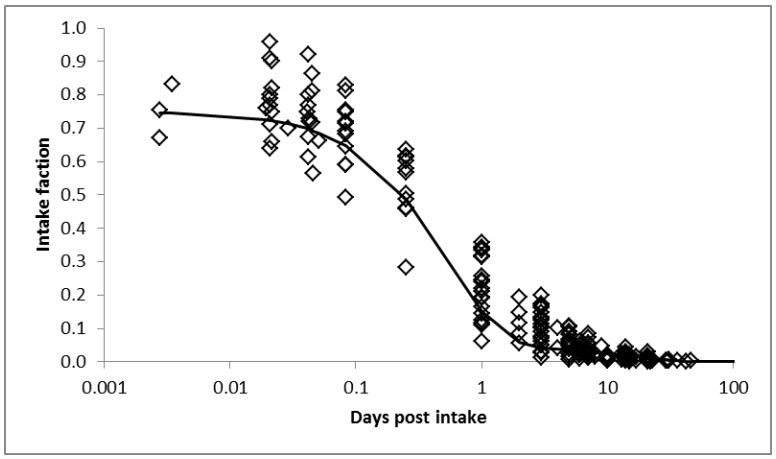

Figure 26: Regression of Talbot et al. (1997) blood data to a linear combination of exponential functions. The regression line was based on estimating 6 parameters that resulted in a scattering factor of 2.1.

Using IDEAS guidelines (Castellani et al. 2013) and Marsh et al. (2007), the scattering factor for the blood samples were determined to be 2.1. Table 15 presents the regression equations and coefficients used in the regression model.

Table 15: Prediction models for deriving blood sample scattering factor.

	Regression Model
Function	$f(t)_2 = \sum_{i=1}^{3} A_i \exp(-\lambda_i t)^i$
Coefficients	A_1: 0.8, λ_1=2 A_2: 0.05, λ_2=0.037 A_3: -0.1, λ_3=1
Scattering Factor	2.1

Likewise, the scattering factor for the liver was required for use in fitting the human liver measurements to the ICRP 67 model. The same method was used in deriving the scattering factor for the liver based on Newton et al.'s (1998) liver *in vivo* measurements that were normalized to fractions of the original intake. Figure 27 illustrates the regression results of fitting a sum of natural log functions.

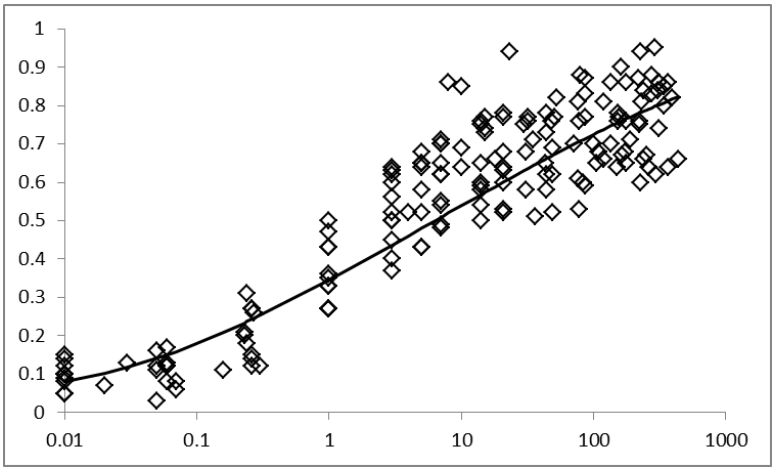

Figure 27: Regression of Newton et al. (1998) liver data to a sum of natural log functions. The regression line was based on estimating 7 parameters that resulted in a scattering factor of 1.3.

Using IDEAS guidelines (Castellani et al. 2013) and Marsh et al. (2007), the scattering factor for the liver samples were determined to be 1.3. The regression line was derived from a sum of natural log functions and derived by minimizing the sum of

squared residuals between the regression line and actual data. Table 16 presents the regression equation and coefficients.

Table 16: Prediction model for deriving liver sample scattering factor.

	Regression Model
Function	$f(t) = \left[\sum_{i=1}^{3} A_i \ln(\lambda_i t)^i \right] + A_4$
Coefficients	A_1: 0.076, λ_1=1 A_2: 0.001, λ_2=48 A_3: -0.0005, λ_3=0.3 A_4: 0.33
Scattering Factor	1.3

Chi-Squared statistic per IDEAS Guidelines

The IDEAS guidelines recommended Equation 16 for determining the chi-squared statistic from a lognormal distribution (Castellani et al. 2013):

$$\chi_0^2 = \sum_{i=1}^{n} \left(\frac{\ln(M_i) - \ln[\mathrm{Im}(t_i)]}{\ln(SF_i)} \right)^2 \tag{16}$$

Where, M_i is the actual bioassay measurement, and $Im(t_i)$ is the predicted value. The chi-squared statistic uses N-1-z degrees of freedom where z is the number of transfer rates found by optimization. Castellani et al. (2013) recommended that all bioassay types should be simultaneously fitted to the model by using a total chi-squared statistic for each bioassay type.

Autocorrelation

An autocorrelation test provided insight into the measure of temporal residual dispersion that was also used for model comparison. The autocorrelation was determined for each bioassay type and for the combined groups using the methods as described by Puncher et al (2007), supplemented by Gregoratto and Marsh (2013) that was also adopted by Castellani et al. (2013) for the IDEAS guidelines. The autocorrelation statistic (ρ) was determined using Equation 17 where the standardized residual (R_i) was used for determining the covariance with a lag of 1 and then divided by the variance.

$$\rho = \frac{\sum_{i=1}^{N-1} R_i R_{i+1}}{\sum_{i=1}^{N} R_i^2} \tag{17}$$

The standardized residual (R_i) was determined from taking the natural log transformation of each measurement (M_i) compared to its predicted value [$Im(t_i)$] (Castellani et al. 2013):

$$R_i = \frac{\ln(M_i) - \ln[\mathrm{Im}(t_i)]}{\ln(SF)} \tag{18}$$

The covariance involving the lag of 1 was the product of R_i with R_{i+1}. The standardized residual (R_{i+1}) was determined by substituting $Im(t_{i+1})$ (representing the subsequent bioassay prediction) in place of $Im(t_i)$ in Equation 18 and solving. The mean and the standard deviation of the autocorrelation for one bioassay type were determined using Equations 19 and 20 (Castellani et al. 2013).

$$\mu = -\frac{1}{n} \tag{19}$$

$$\sigma = \frac{n-2}{n\sqrt{n-1}} \tag{20}$$

Gregoratto and Marsh (2013) suggested that when confronted with multiple bioassay types that one should combine the residuals and treat them as if representing one sample. This process is robust and should provide consistent results with standardized residuals despite unequal variances. There is a slight variation with crossover data that varies depending on the serial order of the bioassay types due to variation in the SF. This occurs when different bioassay data types are combined. For example, fecal bioassay measurements, known to have a large SF, combined with urine bioassay measurements can influence the standardized residual in the denominator for the crossover data by assigning the fecal bioassay SF. However, Gregoratto and Marsh 2013) considered this effect and found it usually to be insignificant. During model development and parameter optimization, the individual group autocorrelation values for each bioassay type were inspected for evaluating the individual bioassay fit. The overall autocorrelation was used to assess the complete fit for the final recommended model. Puncher et al. (2007) had indicated that the autocorrelation should be based on the upper one tail test and rejected at the 5% level. Since the autocorrelation test ranged from -1 to 1, a two tailed-test was employed with rejection at the upper and lower tail at the 0.025 significance level. An assessment of the fit was determined by establishing the critical value at the $\mu \pm 1.96\sigma$, based on a normal distribution. Autocorrelation values within this range were characteristic of an adequate fit.

Scattering Factor Influence

The scattering factor was found to have a significant influence on both the chi-squared statistic and autocorrelation using the IDEAS guidelines. Higher assigned scattering factors resulted in a lower chi-squared statistic and autocorrelation. Since the chi-squared statistic and autocorrelation are sensitive to the defined scattering factor, the scattering factors must be carefully chosen and supported by default assumptions according to the IDEAS guidelines or they must be derived from existing data sets as was performed for the blood and liver samples in this section.

3.3.3 Intake Prediction

The Maximum Likelihood method was used in deriving the predicted individual intake after optimization of the compartment model transfer rates. In some cases references were made to the maximum likelihood result, which assumes a lognormal distribution of the measurement results using the following probability function (Doerfel et al. 2006):

$$f(\ln(M_i)) = \frac{1}{\sqrt{2\pi} M_i \ln(SF_i)} \exp\left[-\frac{(\ln(M_i) - \ln(\mathrm{Im}(t_i))^2}{2\ln^2(SF_i)} \right] \tag{21}$$

The predicted individual intake was determined with Equation 22 where the individual intake (I_i) was derived from each bioassay measurement (M_i) divided by its predicted intake retention fraction [$m(t_i)$] for each of the sample times.

$$\hat{I} = \left[\prod_{i=1}^{n} \left(M_i \Big/ m(t_i) \right) \right]^{1/n} = \left[\prod_{i=1}^{n} \hat{I}_i \right]^{1/n} \tag{22}$$

The predicted individual intake was determined for each bioassay type during the compartment model optimization and used to calculate the intake analysis of variance. This was particularly important during optimization of the Pu-DTPA model since there were sufficient urine, fecal and blood samples to predict the intake; thereby, the Pu-DTPA model was derived with the assumption that the model was correct for each bioassay type.

Castellani et al. (2013) recommended Equation 23 for predicting the overall combined intake for urine and fecal bioassay due to differing variances of each bioassay type:

$$\ln(I) = \frac{\sum_{i=1}^{n_u} \frac{\ln(I_i)}{(\ln(SF_u))^2} + \sum_{j=1}^{n_f} \frac{\ln(I_j)}{(\ln(SF_f))^2}}{\frac{n_u}{(\ln(SF_u))^2} + \frac{n_f}{(\ln(SF_f))^2}} \tag{23}$$

Where each intake estimate ($I_{i,j}$) is calculated from the respective measurement (M_i) divided by the predicted value ($m(t_i)$) for a unit intake as represented by Equation 24.

$$\ln(I) = \frac{\frac{\sum_{i=1}^{n_u} \ln\left(M_i / m(t_i)\right)}{(\ln(SF_u))^2} + \frac{\sum_{j=1}^{n_f} \ln\left(M_j / m(t_j)\right)}{(\ln(SF_f))^2}}{\sum_{b=1}^{N_b} \frac{n_b}{(\ln(SF_b))^2}} \tag{24}$$

Where b represents the bioassay type and N_b represents the total bioassay types used in determining the estimated intake.

The SF that was based on the average value presented in the IDEAS guidelines for the urine and fecal bioassays, and that was previously derived for the liver and blood bioassays was assumed to remain constant in this work. The total combined predicted intake was determined during compartment model optimization to assist in determining the fit quality and for final reporting with the optimized parameters and the regression results.

Analysis of Variance

The analysis of variance assumes that the errors are independent and normally distributed with a mean of zero and variance of σ^2, and represented by the statistical model shown in Equation 25 (Rice 2007):

$$Y_{ij} = \mu + \alpha_i + \varepsilon_{ij} \tag{25}$$

Where, Y_{ij} is the intake based on the j^{th} bioassay sample of the i^{th} bioassay type, μ is the overall intake mean based on all bioassay types, α_i is the differential effect of the i^{th} bioassay type and normalized to $\sum\alpha_i = 0$, and ε_{ij} is the random error in the j^{th} bioassay sample of the i^{th} bioassay type. The null hypothesis assumes that all of the group means (i.e., predicted intake for each bioassay type) are equal. The alternative hypothesis is that at least one mean is different. An F-test can be used to test these hypotheses, with a large F, producing a small p-value, providing evidence the means are not all the same.

Boxplot Comparison of Intakes

A visual representation was included for the intake measurement comparison using boxplots. Figure 28 is an example boxplot that was used for the ICRP 67 model predicted intakes.

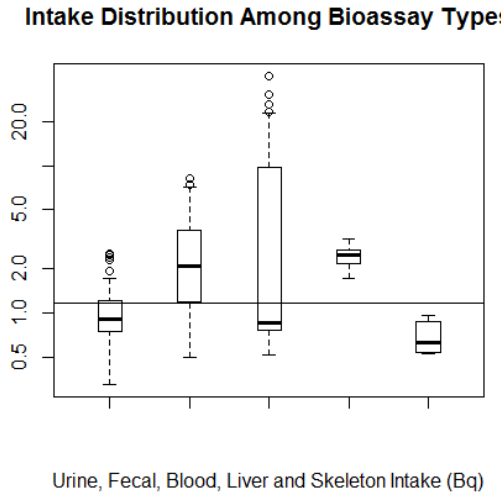

Figure 28: ICRP 67 systemic model comparison of intake predictions for the urine, fecal, blood, liver and skeleton. The ordinate represents the intake amount (Bq) on a log scale. The boxplot indicates the distribution of the predicted intakes, with a combined intake estimate of 1.19 Bq.

In Figure 28 the urine and fecal plots represent a normal distribution, while the liver and skeleton show a slight skewness to the data. The blood in particular showed an extreme positive skewness with the median located near the expected intake of 1.0 Bq and the estimated intakes extending beyond an intake value of 20 Bq. Statistical measures, such as chi-square, are typically based on normality assumptions that may require data transformations in order to achieve normality. The boxplots in Figure 28 are displayed on a log scale, illustrating that a log-transformation of the data resulted in normality assumptions being satisfied for most of the bioassay types.

3.3.4 Parameter optimization

An optimization method was derived in order to expedite the optimization process in a way that required the fewest number of iterations. Optimization was performed by setting initial parameter values and specifying necessary constraints. The parameters were calculated based on the model prediction regressed against the compiled human data set. The parameters were worked on sequentially with the objective of reducing the chi-square goodness of fit indicator (χ^2) between the compartment model prediction and the compiled data. The assigned parameter value (θ) was positioned in the center of a 5 element vector array. The initial range was chosen to be $1/3^{rd}$ θ to $5/3^{rd}$ θ (i.e., $\theta/3$, $2\theta/3$, θ, $4\theta/3$, $5\theta/3$). The χ^2 was determined for each parameter estimate and the value corresponding to the lowest χ^2 was repositioned to the center and the process repeated. Once each parameter was optimized, meaning that there was no improvement on the χ^2 value, the next parameter was evaluated and the process was repeated until that parameter was optimized. Once all parameters were optimized on the first run, then the process was repeated to optimize the earlier parameters that may have been affected by fitting the later parameters. In this way order bias was minimized. Once completed, the process began again by taking 5 equidistant values between the second and fourth position of the previous step (i.e., $4\theta/6$, $5\theta/6$, θ, $7\theta/6$ to $8\theta/6$), ensuring retention of the best θ value. The process was repeated until the desired precision was achieved in the final parameter estimate. The optimization process was represented as a function using Big-R notation, where the symbol 'R' represented iterations, similar to the symbol '$\sum$' representing a summation (Wang 2008). Equation 26 demonstrates its use for 10 complete iterations (j) of 5 equidistant values (i) for describing the optimization process.

$$f(\mathrm{p}) = \mathop{\mathrm{R}}_{\mathrm{j}=1}^{10} \mathop{\mathrm{R}}_{\mathrm{i}=1}^{5} \left(\frac{i - 3 + 3 \times 2^{j-1}}{3 \times 2^{j-1}} \right) \theta \qquad (26)$$

Table 17 presented an example optimization using Equation 26.

Table 17: Optimization method accuracy.

j	i(1)	i(2)	i(3)	i(4)	i(5)	Accuracy
1	1/3	2/3	3/3	4/3	4/3	1/3 (0.33)
2	2/3	5/6	6/6	7/6	4/3	1/6 (0.17)
3	5/6	11/12	12/12	13/12	7/6	1/12 (0.083)
4	11/12	23/24	24/24	25/24	13/12	1/24 (0.042)
5	23/24	47/48	48/48	49/48	25/24	1/48 (0.021)
6	47/48	95/96	96/96	97/96	49/48	1/96 (0.010)
7	95/96	191/192	192/192	193/192	97/96	1/192 (0.0052)
8	191/192	383/384	384/384	385/384	193/192	1/384 (0.0026)
9	383/384	767/768	768/768	769/768	385/384	1/768 (0.0013)
10	767/768	1535/1536	1536/1536	1537/1536	769/768	1/1536 (0.00065)

The optimization illustrated in Table 17 shows how each value of j provides a spread of data that covers the previous j's inner 3 data elements. With this method, the best value is always located in the center and the best estimate is expected to fall within the range of the 2nd and 4th data positions. Therefore, using this optimization approach, an accuracy of 1/100th of the original value should result with a value appropriate at 3 significant figures, using a j value range up to 6, as illustrated in Equation 26. This optimization approach was designed to minimize the number of iterations required for parameter estimation; however, it also assumed only one model minima existed. There was enough variation in the optimization process where the parameters were evaluated over wide ranges and re-evaluated upon changes in other compartment parameters that it was considered robust for parameter estimation; however, it was still possible for the parameter to be optimized against a local minimum. Each optimization presented a plot of the fit for inspection where expert judgment was introduced into the fitting process.

Although it was possible that the optimization may have culminated on a local minimum, this was occasionally experienced and was evident by visual inspection that required a different optimization approach, such as revising the weighting or parameter specification. Optimization was performed using the following R functions [Rmod.opt4, Rmod.mult, Rmod.mult2 and Rmod.67FLS] as elaborated upon in Appendix 1.

3.3.5 Sensitivity Analysis

A sensitivity analysis of the parameters was performed to identify the parameters that had the largest effect on the observed data (e.g., urine excretion, fecal excretion, blood compartment quantity and organ retention). Methods were used as described by Luciani et al. (2001) in Equation 27 where the sensitivity coefficient (S_i) was defined as the ratio of the dependent variable (u) rate of change to relative changes made with the respective transfer rate (λ_i).

$$S_i = \frac{\partial u}{\partial \lambda_i}\frac{\lambda_i}{u} \cong \frac{\Delta u}{\Delta \lambda_i}\frac{\lambda_i}{u} \tag{27}$$

The relative change to the transfer rate was approximated in 0.01 increments that were determined to be sufficient for approximating the partial derivative and identifying the sensitive parameters (Luciani et al. 2001). This method was particularly useful for developing and revising the ICRP 67 and the Pu-DTPA biokinetic models when there were more than a few transfer rate parameters to optimize.

The sensitivity was determined by increasing the transfer rate parameter by 1 percent to observe the accumulated changes in urine and fecal bioassays over various time periods. Table 18 illustrates the sensitivity analysis results for various time periods

using the default strong-retention wound intake parameters described in NCRP 156 incorporated with the ICRP 67 systemic model and the ICRP 30 GI tract model for plutonium.

Table 18: Sensitivity analysis for urine and feces for several time periods of interest for a wound intake.

	Accumulated Urine (Days)						Accumulated Feces (Days)				
Comp. Pathway	1	10	100	1000	10000	Comp. Pathway	1	10	100	1000	10000
Blood to Bladder	0.99	0.92	0.61	0.29	0.18	Blood to GI.ULI	1.00	0.97	0.85	0.53	0.45
Soluble to Blood	0.82	0.45	0.27	0.13	0.02	Soluble to Blood	0.87	0.46	0.26	0.12	0.02
Blood to ST1	-0.02	-0.09	0.03	0.42	0.52	GI.LLI to Feces	0.80	0.04	0.00	0.00	0.00
Blood to Liver1	-0.06	-0.27	-0.30	-0.32	-0.30	GI.ULI to GI.LLI	0.68	0.02	0.00	0.00	0.00
Soluble to CIS	-0.16	-0.42	-0.27	-0.13	-0.02	Liver1 to GI.SI	0.00	0.01	0.13	0.43	0.45
ST1 to Bladder	0.00	0.02	0.15	0.43	0.30	Soluble to CIS	-0.11	-0.43	-0.26	-0.12	-0.02
Blood to Trab.Surf	-0.06	-0.27	-0.30	-0.27	-0.12	Blood to Trab.Surf	-0.04	-0.26	-0.30	-0.26	-0.12
Blood to Cort.Surf	-0.04	-0.18	-0.20	-0.22	-0.28	Liver1 to Liver2	0.00	0.00	-0.01	-0.24	-0.41
Blood to Kidneys.Urine	0.00	0.03	0.20	0.14	0.09	Blood to Cort.Surf	-0.03	-0.17	-0.20	-0.22	-0.28
ST1 to Blood	0.00	0.00	0.00	-0.07	-0.25	Blood to Liver1	-0.04	-0.25	-0.17	0.12	0.21
CIS to Soluble	0.00	0.06	0.17	0.09	0.01	Blood to ST1	-0.02	-0.11	-0.12	-0.11	-0.15
Liver2 to Blood	0.00	0.00	0.00	0.02	0.17	CIS to Soluble	0.00	0.05	0.18	0.09	0.01
Bladder to Urine	0.13	0.00	0.00	0.00	0.00	Liver2 to Blood	0.00	0.00	0.00	0.02	0.17
Kidneys.Urine to Bladder	0.00	0.04	0.11	0.00	0.00	CIS to PABS	0.00	0.00	-0.08	-0.07	-0.01

Table 18 presents the sensitivity analysis results for a wound intake. The transfer rate parameter sensitivities are illustrated for each of the compartment pathways related to its effect on accumulated urine and fecal bioassay. The top 14 sensitive parameters were shown across all time frames, with positive and negative values indicating the appropriate effect on excretion based on a 1% increase in the transfer rate value.

The compartment transfer pathways most sensitive for urine excretion are the blood compartment to the bladder and the wound soluble compartment to the blood compartment. The blood compartment to the ST1 and cortical bone surface compartments, and the ST1 to the bladder compartment become important for later time

periods. The compartment transfer pathways most sensitive for the fecal excretion are the blood compartment to the upper large intestine and the wound soluble compartment to the blood. The liver1 to the small intestine and to the liver2 compartments become important for later time periods. Furthermore, a sensitivity analysis was performed on the bone surface transformations over 50 years and illustrated in Table 19 that was consistent for all time periods investigated.

Table 19: Sensitivity analysis on the bone surface transformations over 50 years, with a 1% increase in transfer rate.

Positive Effect		Negative Effect	
Compartment Path	Sensitivity	Compartment Path	Sensitivity
Blood to Cort.Surf	0.47	Blood to Liver1	-0.28
Liver2 to Blood	0.17	Cort.Surf to Cort.Marrow	-0.19
Blood to Trab.Surf	0.14	Blood to ST1	-0.17
ST1 to Blood	0.08	Cort.Surf to Cort.Vol	-0.15
Liver1 to Liver2	0.05	Trab.Surf to Trab.Marrow	-0.09
Trab.Vol to Trab.Marrow	0.03	Trab.Surf to Trab.Vol	-0.08
Cort.Vol to Cort.Marrow	0.02	ST1 to Bladder	-0.07
Soluble to Blood	0.01	Blood to GI.ULI	-0.05
PABS to Soluble	0.01	Blood to Bladder	-0.05
CIS to Soluble	0.01	Blood to ST2	-0.04

The largest positive changes occurred with the compartment transfer pathways from the blood compartment to the cortical and trabecular bone surfaces and the liver2 compartment to the blood compartment, which illustrates a direct relationship with increases in the transfer rate. The largest negative changes occurred with the compartment transfer pathways from the blood compartment to the liver1 compartment and the ST1 compartment, and the cortical bone surface to the cortical marrow and cortical volume compartments, which illustrates an indirect relationship with increases in the transfer rate. This sensitivity analysis was important when determining the transfer rate parameters that have the largest effect on the transformations occurring to the bone

surfaces. The sensitivity analysis was performed with the R function [Sens] in Appendix 1.

3.3.6 Model Comparison

Model development required a statistical measure to both compare models to the data and to each other. This was accomplished with use of the chi-squared statistic and the associated p-value. The chi-squared statistic was calculated for each bioassay type and summed to provide a total chi-squared statistic for the model fit. Additionally, the associated p-value was determined for each chi-squared statistic based on using N-1-z degrees of freedom (df) that was consistent with the IDEAS guidelines (Castellani et al. 2013). The degrees of freedom included the number of modified parameters for model comparison in cases where parameters were added or optimized to fit the data being evaluated.

Using the IDEAS guidelines (Castellani et al. 2013) a good model would look reasonable by eye when displayed graphically, have a χ_0^2 p-value of 0.05 or greater, and have an auto-correlation value within 95% of the expected confidence range. A more nuanced treatment of p-values, which exist on a continuum, suggest p-values less than 0.01 represent poor fit of the model to the data, and p-values larger than 0.10 represent a good fit of the model to the data, with p-values in between representing various shades of gray (Ramsey and Schafer 2002). These guidelines were suggested as possibilities for evaluating a model fit and were used in this research in evaluating the Pu-DTPA model and modifications to the ICRP 67 model. Since this research focused on comparing models, it was decided to compare the p-values. P-values can be used both to assess the

fit of each model and to compare models. The model with the largest p-value being the one that best fits the data.

3.3.7 DTPA Effectiveness Evaluation

Once the Pu-DTPA model had been optimized and benchmarked using a real case (i.e., IDEAS Case 123 and USTUR Case 0269) then the effectiveness of various DTPA treatments were studied.

Internal dose is based on a 50-year committed dose for occupational workers following intake. This is referred to as the committed effective dose (E) for the whole body, which is based on a summation of individual organ doses with appropriate tissue weighting factors (w_T) applied as recommended by ICRP publication 60 (1991), which is related to the fractional organ dose contribution to the whole body. The committed effective dose is determined from Equation 28.

$$E = \sum_T w_T \sum_R w_R D_{T,R} \tag{28}$$

The individual organ doses is referred to as the committed equivalent dose (CEqD), which is directly related to the number of radionuclide transformations occurring in the organ or tissue that includes the assigned radiation weighting factor (w_R). The committed equivalent dose is determined from Equation 29.

$$CEqD = \sum_R w_R D_{T,R} \tag{29}$$

Where the absorbed dose ($D_{T,R}$) is the accumulated dose determined over a 50-year time period. The w_R is assigned from ICRP (1991) based on the radiological biological effectiveness due to the radiation emitted from the radionuclide

transformation. Alpha particles have a w_R of 20 (compared to electrons and photons of 1) and deposit their energy locally in tissue. The transformation of ^{239}Pu results in an average alpha particle emission of 5.15 MeV that is accompanied with low energy photons and electrons averaging less than 20 keV. With this knowledge, the difference in absorbed dose to the local tissue and organ can be determined. The absorbed dose is clearly dominated by the alpha particle emission, and is directly proportional to the number of transformations.

The effectiveness of DTPA administration was determined by reviewing the difference in compartment transformations to the bone surfaces occurring over a 50-year period. The value is directly related to the bone surface CEqD, which is the limiting organ for ^{239}Pu intakes. The difference in the number of organ transformations with and without treatment (i.e., CEqD savings) was determined for several treatment strategies to derive the DTPA effectiveness. This research evaluated early and late chelation treatment for ^{239}Pu intakes for wounds and for inhalations. Questions pertaining to how late treatment can be started and still be effective, and the continued effectiveness of protracted treatments were investigated.

Chapter 4: Results and Discussion

4.1 Pu-DTPA Model

The proposed Pu-DTPA compartment model was optimized using IDEAS Case 123 (as described in Chapter 2). IDEAS Case 123 was chosen since this had been previously studied by the CONRAD task group and had several bioassay sample types collected that could be used for evaluation. The Pu-DTPA biokinetic model described in Chapter 3 was optimized with IDEAS Case 123 for urine and fecal excretion with the R function [Rmod.opt4] in Appendix 1.

4.1.1 Optimization with IDEAS Case 123

The CONRAD task group recommended parameters that were initially used for DTPA clearance for the recycling between the blood and extracellular fluid (ST0) compartments, and the blood to bladder excretion pathway. It was assumed that the Pu-DTPA complex was formed with a transfer rate of 100 d^{-1} (i.e., equivalent to a 10 minute half-time). The intermediate soft tissue (ST1) compartment was initially omitted, with plans for subsequent use, and the blood to upper large intestine (GI.ULI) was initially estimated to be 5% of the urinary excretion. Case 123 from the IDEAS database (2013) was evaluated with chelation taking place on days 3, 4, 5, 6, 7, 10, 27, 28, 29, 30, 90, 92, 94, 120, 124, 128 and 133. For the compartment model calculations, the chelation days were increased by 1 so as to indicate the enhanced excretion starting with the sample submitted on the 4^{th} day, which assumed a 24-hour sample collection beginning on day 3. Additional details included that the wound was excised, reducing the contamination from 555 kBq to 74 kBq; however, it was unclear on when the excision took place due to the

61st day wound count was 78 kBq. Case 123 also included wound *in vivo* counts, fecal bioassays and blood analysis, which could be used for further analysis. Case 123 is unique since it started chelation late, thus providing initial bioassays that were not influenced by chelation on days 1, 2 and 3. The R function [Rmod.opt4] included the transitional paths (i.e., ST0 to ST0t, ST1 to ST1t, Blood to Bloodt, Liver1 to Liver1t) with their associated transfer rates during days of chelation, and set the transfer rates to 0 for days chelation was not administered, while still accounting for the transitional compartment quantities to continue their outflow kinetics. Figure 29 represents the actual urinary excretion to the model fit using these assumptions.

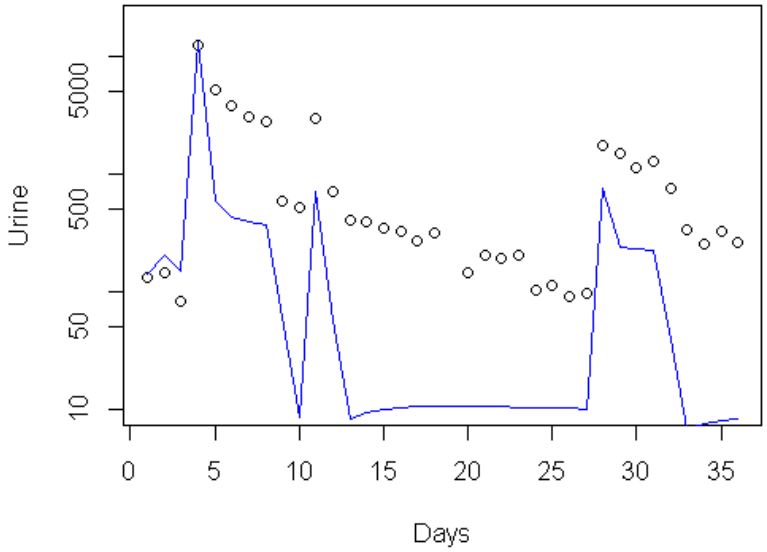

Figure 29: Case 123 urine excretion (Bq d^{-1}) compared to initial compartment assumptions.

Figure 29 illustrated that the model fit was not a good representation of the actual urine excretion results, which was similar to what the CONRAD task group had experienced (Breustedt et al. 2010). For this analysis, the ICRP 67 systemic model was used since it had been reviewed and approved for use by the U.S. DOE. The initial excretion enhancement was well represented for day 4, but the subsequent excretion amounts fell considerably below expectation. The various NCRP (2007) wound retention

models were reviewed and it was determined that the fit had characteristics similar to a strong-retention and possibly a colloidal particle. Therefore, in an attempt to represent this, the strong-retention parameters were retained, with initial amounts divided between the Solubility and CIS compartment. Figure 30 illustrates the model fit using these assumptions.

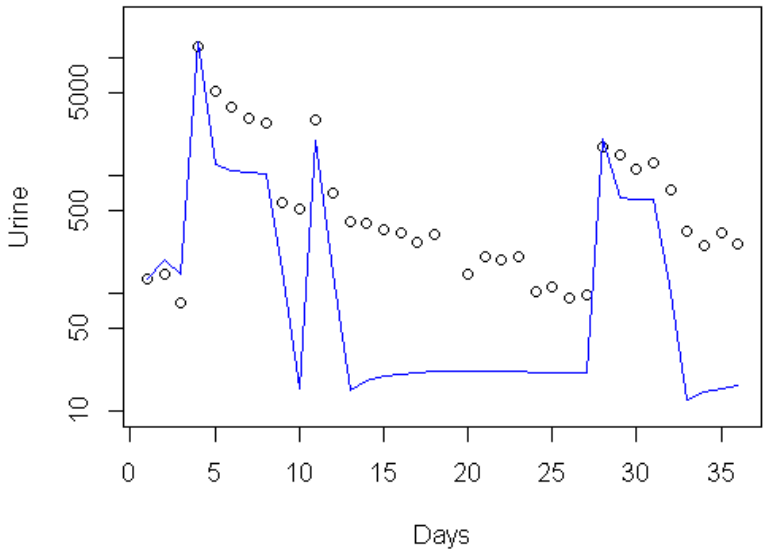

Figure 30: Case 123 urine excretion (Bq d^{-1}) compared to interim compartment assumptions varying the wound parameters.

Upon visual inspection, this simulation had promising characteristics compared to the previous fit, and was used as a start for further optimization. The visual inspection indicated that there was more retention of the Pu-DTPA complex with a slower excretion, which was also suggested by the CONRAD task group (Breustedt 2009). Since a literature review had suggested that DTPA complexes may be formed in soft tissues, it was decided to include the intermediate soft tissue compartment (ST1) for inspection. The Pu-DTPA complex was assumed to have a longer retention in the transitional ST1 compartment (ST1t) compared to the ST0t compartment. Also, there was no feedback considered from the Pu-DTPA complex from the blood (Bloodt) to the ST1t

compartment. The transfer rates for transition from the blood and ST0 compartments were held constant. The transition from ST1 to ST1t, which represented the Pu-DTPA complex formation in the ST1 compartment, and ST1t to Bloodt were set at 1.8 and 0.2, respectively. Figure 31 illustrates the model fit with these assumptions.

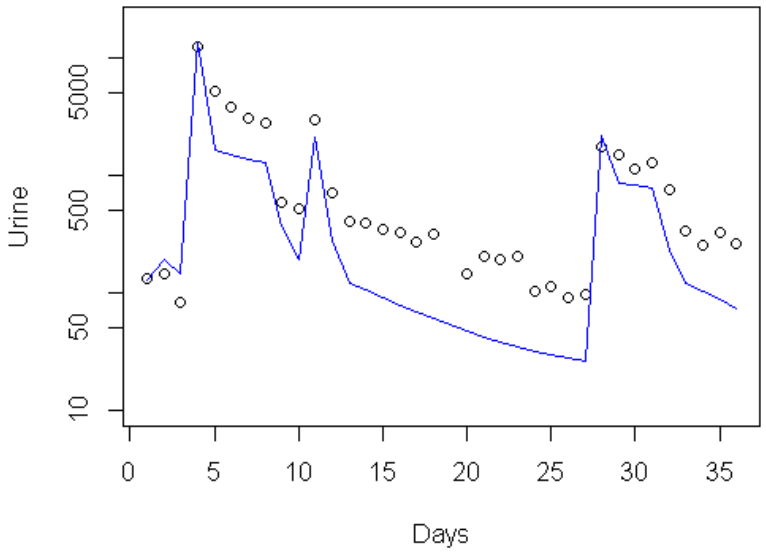

Figure 31: Case 123 urine excretion (Bq d^{-1}) compared to compartment assumptions with ST1 included.

This model fit appeared to provide some explanation for the delayed Pu-DTPA excretion, thus explaining the benefit of including the ST1 compartment. Since the original model parameters assumed that the Pu-DTPA complex had the same kinetics as Ca-DTPA, optimization was performed by allowing the Pu-DTPA transitional parameters to change. This was presented in Figure 32.

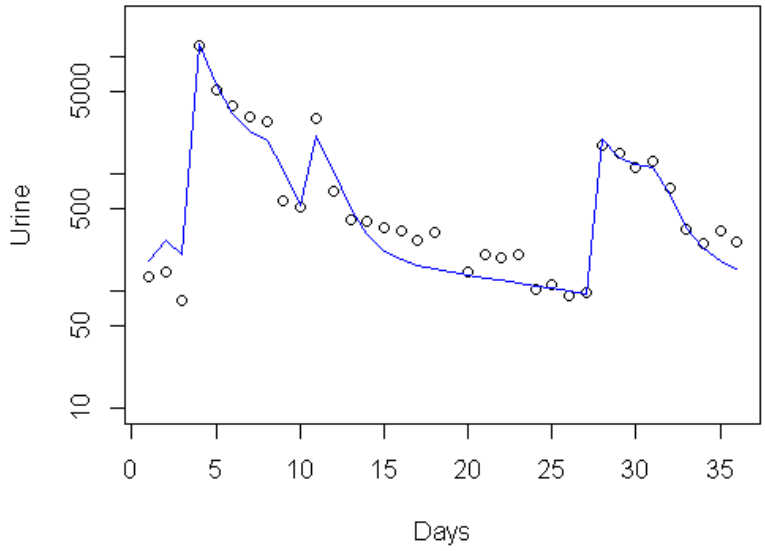

Figure 32: Case 123 urine excretion (Bq d^{-1}) compared to interim compartment assumptions varying several compartment parameters.

Once optimization had been performed with the ST1 compartment, it was decided to introduce the liver1 compartment due to published sources indicating that liver decorporation was evident. The liver1 transitional compartment was optimized with an equivalent distribution to the blood and the small intestine since this was uncertain. Final optimization was presented in Figure 33.

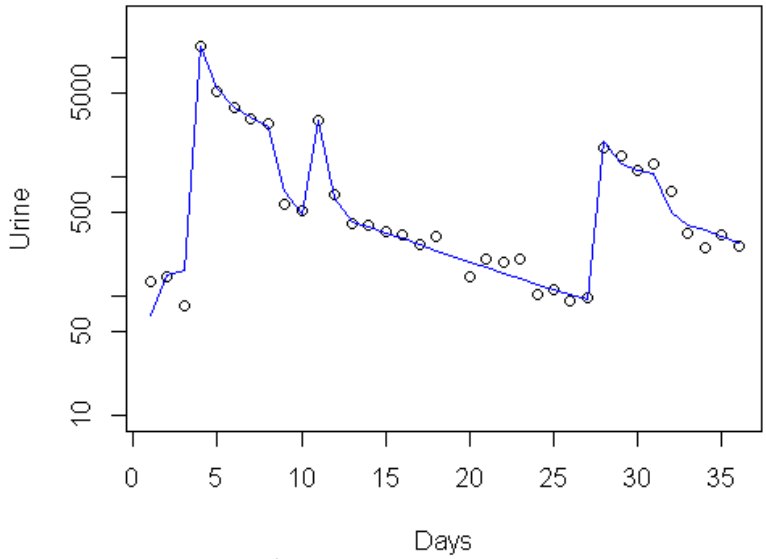

Figure 33: Case 123 urine excretion (Bq d^{-1}) compared to final compartment assumptions after optimization.

The transfer rate parameters specified in Table 20 were developed following optimization of the wound compartment transfer rates with the initial intake equally divided between the Soluble and CIS compartments that was specific to IDEAS Case 123.

Table 20: Pu-DTPA suggested compartment model transfer rate parameters (R.123).

Compartment Pathway	Transfer Rate (d^{-1})	Compartment Pathway	Transfer Rate (d^{-1})
ST0 to ST0t	3.65	Bloodt to Bladder	45.7
ST1 to ST1t	1.925	Liver1 to Liver1t	2.2
Blood to Bloodt	1.378 (2.76 when enhanced)[a]	Liver1t to Bloodt	0.067
ST0t to Bloodt	300	Liver1t to SI	0.067
ST1t to Bloodt	0.12	Wound: Soluble to Blood	0.241
Bloodt to ST0t	145	Wound: Soluble to CIS	0.094
Bloodt to ULI	4	Wound: CIS to Soluble	0.026

[a]An enhanced transfer rate is used for DTPA treatment methods with enhanced chelation effectiveness, such as multiple intra-day treatments.

The transfer rates in Table 20 indicated that DTPA formed a complex with the plutonium activity that was present in the ST0 (83%), Blood (54%), ST1 (85%) and Liver1 (89%) compartments. This supported the physiological understanding of DTPA having a brief beneficial effect in circulation for complexing with plutonium due to the short biological half-time and competition with endogenous proteins, while plutonium continued to be absorbed from the wound contamination and added due to resorption. The suggested enhanced transfer rate for the Pu-DTPA complex in the blood was assumed to increase the beneficial duration of DTPA that accounted for 73% of the plutonium in the Blood compartment without influencing other compartments. Both the ST1 and Liver1 compartments had long retention properties where the DTPA had an opportunity to influence most of the stored contaminant. Pu-DTPA translocated from the Bloodt compartment with a half-time of approximately 5 minutes with 74%, 24% and 2% directed towards the ST0t, Bladder and ULI compartments, respectively. The ST0t compartment returned the Pu-DTPA back to the Bloodt compartment with a half-time of approximately 3 minutes, which supported the rapid exchange between these compartments in circulation. The ST1t and Liver1t explained the long retention observations of Pu-DTPA with half-times of 5.8 days and 5.2 days, respectively, which

supported experimental observation of a delayed excretion, with half of the Liver1t compartment departing to the small intestine.

The optimized parameter transfer rates for the formation of the Pu-DTPA complex may be explained since DTPA has a short half-time and is available for the first 6 to 10 hours due to its molar concentration, with the assumption that this individual was administered DTPA by an intravenous injection once per day. The case did not specify whether DTPA was administered in a calcium or zinc salt complex and was treated the same in the optimization process. It is unclear on how much of the Liver Pu-DTPA complex departed the liver by the biliary transport path versus being resorbed into the circulatory system; however, animal studies appeared to indicate that the biliary transport path dominated the resorption. This assumption was considered but did not compare well with the compartment model results, since the decorporated liver activity also influenced the urinary excretion; therefore, in the absence of further data it was decided to maintain equal contributions of the Pu-DTPA complex for both pathways from the liver. The assumption of plutonium having partial colloidal properties were due to the possibility of the liquid being of a plutonium nitrate complex, which is discussed in NCRP (2007) as being a partial colloid when injected into animals. The wound parameter changes were specific to this case; however, other cases should consider starting with the default wound parameter transfer rates and refine as necessary to fit the situation. Optimization was performed for a truncated period of 36 days with regression against the urine excretion data. The long-term performance was inspected and plotted in Figure 34 for comparison with the urine bioassays, with inclusion of the fecal regression fit that was based on the intake amount derived from the urine regression.

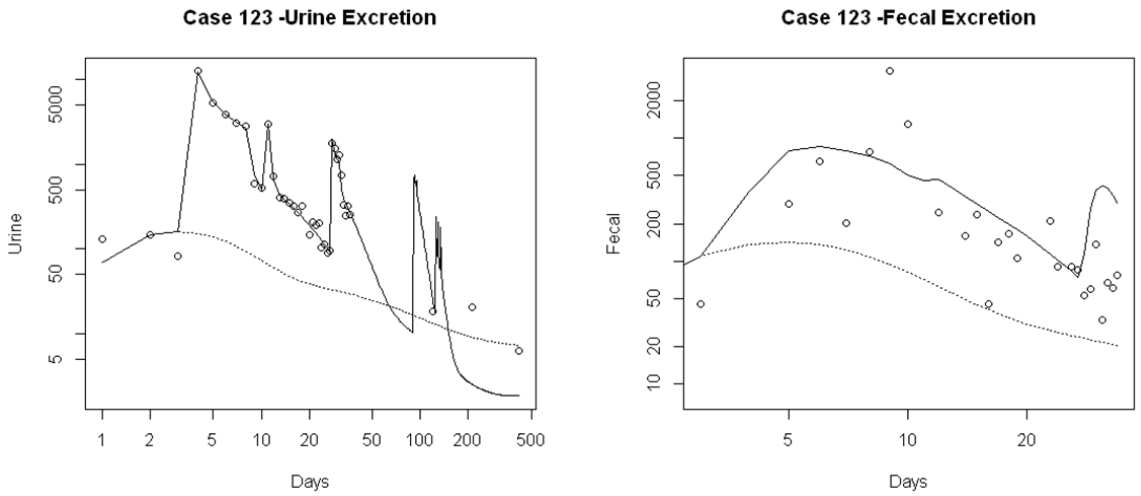

Figure 34: Case 123 urine (left) and fecal (right) excretion compared to final compartment assumptions (solid line) after optimization, with ordinate units in Bq. The dashed line in both figures represents the expected excretion without enhancement due to DTPA. Both models are representative of an intake of 148 kBq.

The final optimized model results were evaluated using the R function [Rmod.mult2] and illustrated in Figure 34. The chi-squared statistic was based on the IDEAS guidelines on a log-transformation of the measurement data, with a specified scattering factor of 1.6 and 3 for the urine and fecal bioassays, respectively. The chi-squared statistic of the log-transformed data for the urine and fecal bioassays resulted in 65 (with 37 degrees of freedom) and 25 (with 24 degrees of freedom), with p-values of 0.003 and 0.41, respectively. Later urine bioassay measurements were above expectation for an unperturbed sample and lacked sufficient samples taken on days surrounding the late chelation treatment that could have been used for further study. It was noteworthy that the chi-squared statistic performed of the urine samples with omission of the final 3 measurements resulted in 8.1 with a p-value of 1.

The autocorrelation results were -0.19 and 0.62 for the urine and fecal bioassay, respectively, which indicated an acceptable performance of the urine bioassay prediction but indicated bias in the fecal bioassay prediction when compared against the 95%

threshold values. The visual appearance of the plots in Figure 34 indicated that the model prediction of the urine bioassays was a very close approximation to the actual data, but the model prediction of the fecal bioassays was hard to judge due to the larger variance of the data about the prediction. The higher variance for the fecal bioassay was expected since the optimization was performed for the urine excretion, and there typically is a larger variance in sample collection and results for fecal bioassays. There are a few noteworthy items in the optimized model. Since the intake involved both soluble and colloidal characteristics, the initial quantity was divided between the soluble and CIS compartment, which explained the initial increase on the fourth day. The early urine excretion compared well to the optimized model; however, it became less desirable for later periods beyond 200 days. It was feasible that the individual possibly received additional uptakes that may have attributed to this elevation. The model prediction of the fecal excretion was elevated due to representing the intake quantity predicted by the urine.

The wound activity was also reviewed in relation to the Pu-DTPA model results.

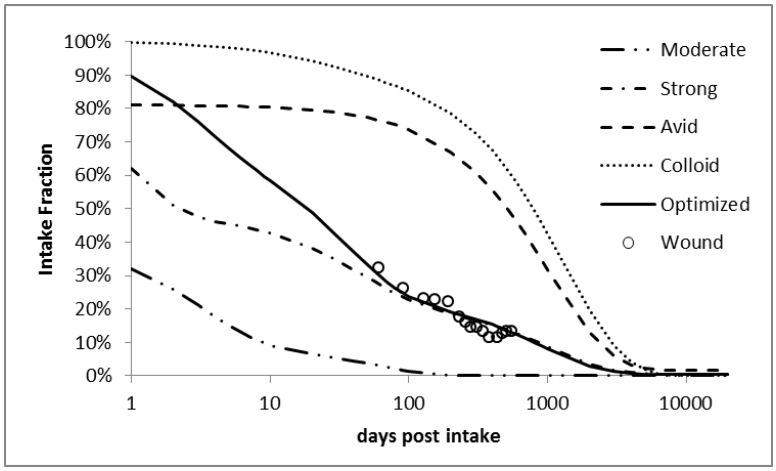

Figure 35: IDEAS Case 123 wound count fraction of an initial estimated intake of 240,000 Bq compared to default and optimized wound retention factors.

Figure 35 illustrated the wound measurement as a fraction of an initial estimated intake of 240,000 Bq in order to compare the trend to the NCRP (2007) default and optimized intake retention fractions. Both the strong-retention and optimized wound results provided a close relationship for the days the wound was measured, where the initial trend appeared to have a closer resemblance to the optimized results. Both the avid-retention and colloid retention fractions illustrate a slow decrease up to 100 days post intake followed by a rapid decline that differed from the actual measurements. The wound intake estimate in relation to the strong-retention and optimized model was approximately 60% higher than expected when compared to the urine bioassay prediction of 148,000 Bq. It was unclear when the wound activity was excised by the case description. It was indicated that the activity after excision was 74,000 Bq; whereas the first wound activity recorded on day 61 was 77,700 Bq.

Another comparison was made with the IDEAS Case 123 blood bioassays in relation to the Pu-DTPA model prediction, which was presented in Figure 36.

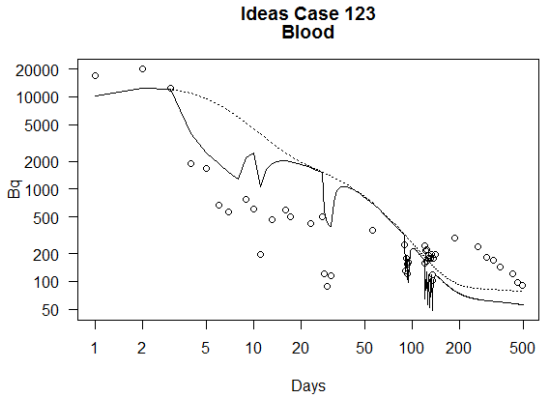

Figure 36: 500 day Pu-DTPA model prediction (solid line) compared with the IDEAS Case 123 blood bioassays that also included comparison to the ICRP 67 model prediction without chelation (dashed line) for an intake of 148,000 Bq. The plot was adjusted to represent the assigned intake.

Figure 36 illustrates the Pu-DTPA model prediction of the blood quantity compared to the ICRP 67 model based on an intake of 148,000. The Pu-DTPA model

appeared to overestimate the blood compartment activity concentration during the chelation days from 4 to 56 and underestimate the activity from days 187 to 294. The chi-squared statistic for the blood samples was 68 with 45 degrees of freedom with a p-value of 0.015, indicating a relatively poor fit to the data. The autocorrelation for the fit of the blood samples was 0.92, indicating bias in the temporal fit of the data.

There are several compartments that contribute to the blood quantity; however, the wound in this case was assumed to be the largest contributor. The predicted line, with no apparent influence from DTPA seemed to follow the observations for the initial days and the days near the end of the sampling period. It was evident that the blood bioassay measurements were higher than expected starting at 200 days post intake, which was consistent with the urine bioassay results.

The bone surface transformations were studied with the R function [Pu.CEDref] to determine the transformations experienced with the cortical and trabecular bone surfaces for a 50 year period with IDEAS Case 123. The Pu-DTPA model resulted in a total bone surface transformation for a 1 Bq intake of 2.79×10^{8} with a 39% reduction when compared to no chelation treatment. The Pu-DTPA model accounted for the removal of plutonium from: circulation, liver and soft tissues; thus reducing the quantity available for skeleton deposition. The reduction of transformations experienced on the bone surfaces are a good approximation of the dose saved for the individual.

4.1.2 Comparison of Pu-DTPA with ICRP 67 for IDEAS Case 123

The Pu-DTPA model optimized to IDEAS Case 123 was compared to the ICRP 67 model using the strong-retention wound default parameters with no optimization or

credit for chelation. This resulted in the regression plots provided in Figure 37 for IDEAS Case 123.

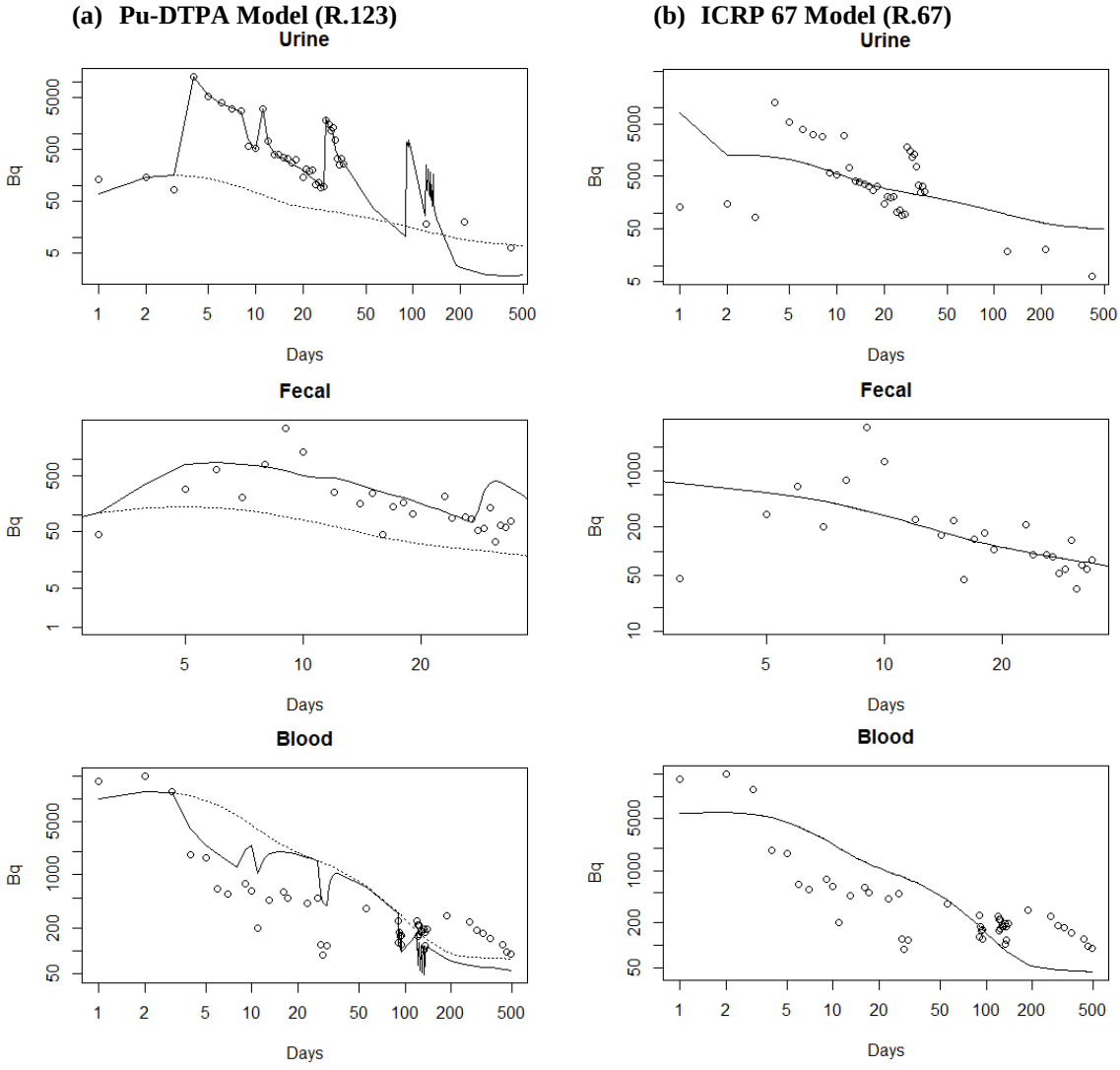

Figure 37: 500 day fitted bioassay plot comparison of the Pu-DTPA model fitted with the (a) optimized parameters for IDEAS Case 123 with a specified intake of 148,000 Bq based on initial optimization, and (b) ICRP 67 without applying chelation influence, with the intake determined from maximum likelihood methods. The solid and dashed lines in (a) indicate the Pu-DTPA model and ICRP 67 model with and without chelation, respectively.

The Pu-DTPA model was compared to the ICRP 67 biokinetic model using the R function [Rmod.mult2], with statistics provided for the log-transformation of the data and a specified intake of 148,000 Bq shown in Figure 37(a). Figure 37(b) illustrates the

results of applying the ICRP 67 model without considering chelation influence. This resulted when using the urine bioassay data in a prediction of intake of 1.1 Million Bq. This is a prediction that is 7 times higher than the initial intake prediction. Visually, the optimized Pu-DTPA model prediction appears to be a better fit to the actual observations than the ICRP 67 model without chelation influence. The boxplots were also compared in Figure 38.

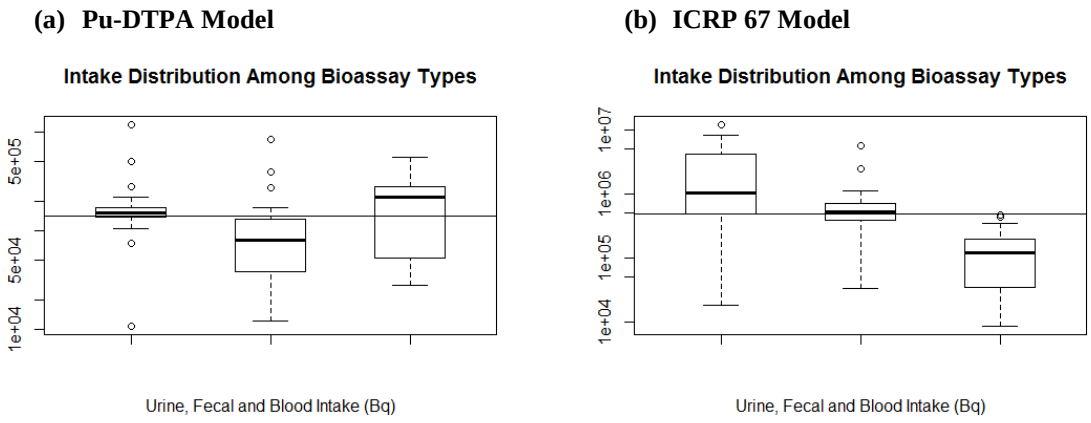

Figure 38: Boxplots representing the residual distribution of the Pu-DTPA model (a) and (b) ICRP 67 systemic model for the urine, fecal and blood on a log scale. The horizontal line represents a combined intake of (a) 142,000 Bq and (b) 480,000 Bq determined from the maximum likelihood of all bioassay types.

The boxplots were created with the R function [Rmod.mult2]. These figures illustrate the dispersion of predicted intake observations about the predicted total combined intake of 142,000 Bq and 480,000 Bq for the Pu-DTPA model and the ICRP 67 model, respectively. The observed variance visually appeared to differ between bioassay types. The boxplots also indicated the median values of the urine, fecal and blood bioassays in relation to the combined intake estimate. The boxplots of the urine and fecal distributions of the Pu-DTPA model and the fecal distribution of the ICRP 67 model illustrated a normal distribution of the individual predicted intakes on a log scale, hence describing them as lognormal distributions. The blood distribution of both models

and the urine distribution of the ICRP 67 model revealed skewness of the individual predicted intakes. The model fit statistics were provided in Table 21.

Table 21: Comparison of Pu-DTPA model with the ICRP 67 model without DTPA influence.

Biokinetic Model	Pu-DTPA[2] χ_0^2	ICRP67[2] χ_0^2	Observations	Original Est.Intake (Bq)	ICRP 67 Est.Intake (Bq)	Intake[1] AOV: F-Test
Urine:	65 (21 df)	335 (32 df)	38	153,000	1,099,000	Pu-DTPA: F=1.71
Fecal:	25 (24 df)	17 (24 df)	25	81,000	517,000	ICRP 67: F=3.08
Blood:	68 (45 df)	100 (45 df)	46	140,000	85,000	
			Summary Results			
Total Chi-Sq:	159 (90 df) (p<0.001)	453 (101 df) (p<0.001)	109			
Autocorrelation:	0.39 (-0.19 urine)	0.59 (0.49 urine)		95% range (-0.189 to 0.175)		

[1] The intake analysis of variance (AOV) F-Test was determined from all bioassay type specified intakes in relation to each other.

[2] The degrees of freedom accounted for 5 fitted NCRP 156 parameters for both models and 11 additional parameters in the Pu-DTPA model when optimized to the urine excretion data.

The total chi-squared statistic comparison indicated that the Pu-DTPA model coupled with the ICRP 67 model (χ_0^2/df = 1.77, p-value essentially zero) resulted in an improved bioassay prediction involving chelation when compared to solely the ICRP 67 model (χ_0^2/df = 4.49, p-value essentially zero). Both models fit the data poorly, but the Pu-DTPA model performed better. The poor fit of the final three urine bioassays contributed to this failure. The autocorrelation indicated there was a bias in the combined fit of all bioassay types, while the urine bioassay fit was significant in the Pu-DTPA model (i.e., -0.19) with a 95% critical range of -0.33 to 0.28. The AOV F-test of the predicted intakes for the Pu-DTPA model (F-Test = 1.71, p-value = 0.19) and the ICRP 67 model (F-Test = 3.08, p-value = 0.05) demonstrate the Pu-DTPA model has a higher level of internal consistency than the ICRP 67 model, as reflected in the higher p-value from the F-test. The Pu-DTPA model clearly improved the fit and internal consistency of the ICRP 67 model.

4.2 Modified ICRP 67 Model

The ICRP 67 biokinetic model was investigated for possible changes that included removing the ST1 to Bladder pathway. A baseline was established with no change, then with the ST1 to Bladder pathway removed. Figure 39 illustrates the significance of removing the ST1 to Bladder pathway.

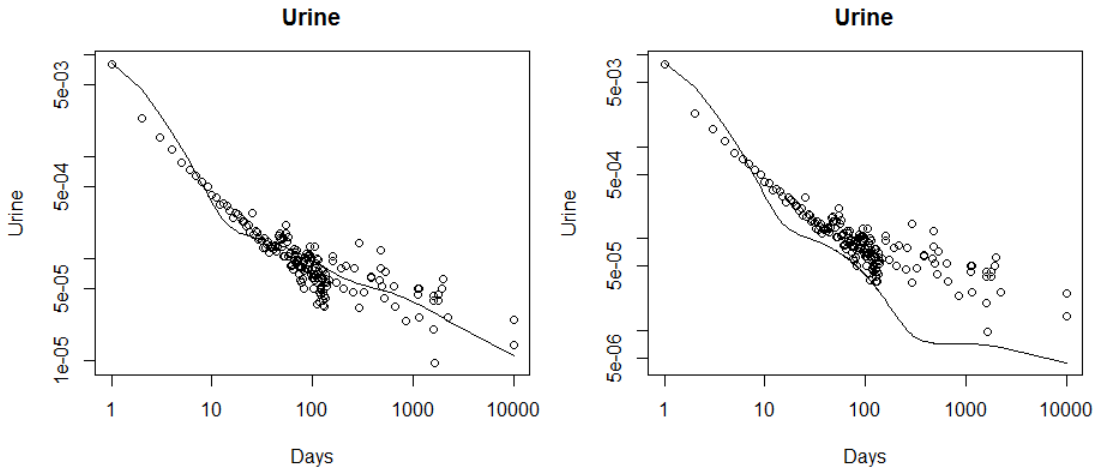

Figure 39: Incremental urine excretion predicted intake retention fraction curve (solid line) calculated from the ICRP 67 rate matrix with the ST1 to bladder path included on the left figure and removed in the right figure, compared to the mean human case data results.

As can be seen from Figure 39, the ST1 to bladder path was fairly significant and had a dramatic affect when compared to the human case mean data when it was removed. Both Luciana and Polig (2000) and Leggett et al. (2005) had proposed revisions to the model that removed the ST1 to bladder path. In an attempt to modify the ICRP 67 model, some of Leggett et al.'s (2005) recommended transfer rates were adopted with the exception of the second blood compartment and 3rd liver compartment in an effort to retain the basic structure of the ICRP 67 systemic model. The R function [Rmod.67FLS] was used for the optimization analysis.

The modification proposed new solutions to the liver compartments by splitting both the Liver 1 and Liver 2 compartment, with each representing the hepatocytes and Kupffer cells, respectively. The Liver 1 compartment included pathways to the small intestine that represented clearance of plutonium through the biliary pathway, and also included a return to the blood compartment that represented monomeric plutonium released back into circulation. The Liver 2 compartment only included a pathway back to the blood compartment that represented monomeric plutonium released from the Kupffer cells. The modification included transfer paths from the blood compartment to both cortical and trabecular bone volume compartments using the established ratios described in Leggett et al. (2005). Constraints were adopted during the fitting process that maintained the blood to bone surface and volume compartment ratios fixed for cortical and trabecular bone, and the transfer rates from the trabecular surface and volume to marrow compartments, and marrow compartments to the blood compartment were kept constant. The total blood outflow was also kept constant during the fitting process, while several contributions to the blood compartment were allowed to vary. The blood contribution to the testes and kidney tissues were also maintained constant.

The human data were limited in that there were up to 106 days of blood measurements and 437 days of liver measurements, with no skeleton measurements. The human data were supplemented with derived intake retention fractions from the Leggett 2005 model for plutonium injection (Appendix 5) for the periods beyond the existing data up to 20,000 days to ensure the model's performance for long periods post intake. The initial model prediction plots were illustrated in Figure 40.

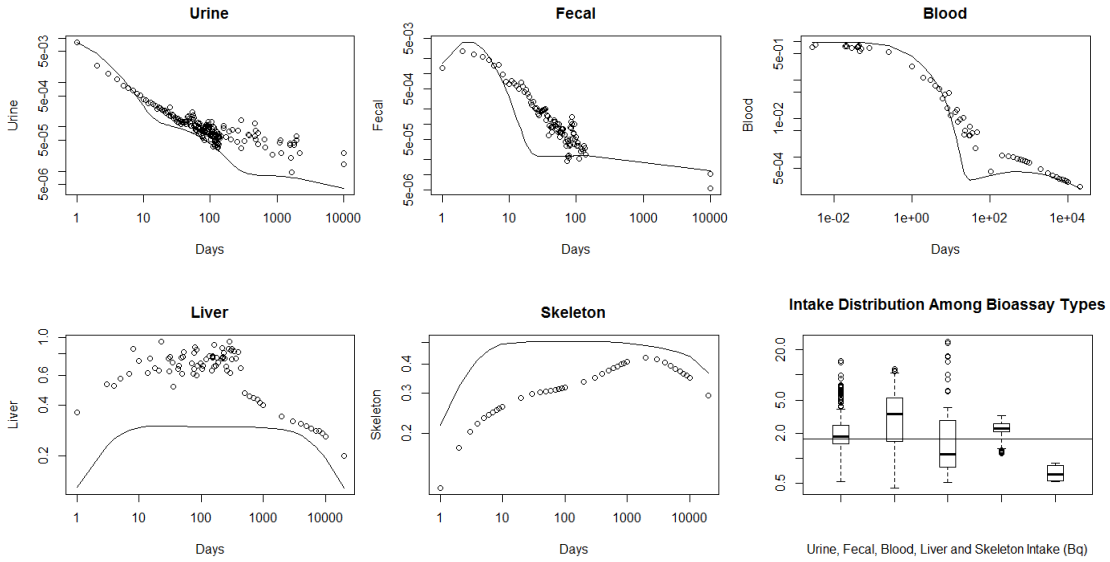

Figure 40: Initial model prediction plots for the urine, fecal, blood, liver and skeleton, with ordinate units based on the fractional amount of a unit intake. The boxplot indicates the distribution of the predicted intakes, with an expectation of 1.0, on a log scale. Plots obtained from R function [Rmod.67FLS].

Figure 40 illustrated the challenges required of the optimization process in order to provide a reasonably accurate prediction for the human data bioassay measurements and the additional supplemented data from the Leggett 2005 model predictions for liver and blood bioassays. It was apparent that the urine, fecal, blood and liver model predictions were below expectation, while the skeleton exceeded expectation for early measurement periods. A sensitivity analysis was performed of the revised compartment rate matrix to determine the significant parameters with respect to time. Figure 41 was generated to provide a visual representation of the significant compartment pathways.

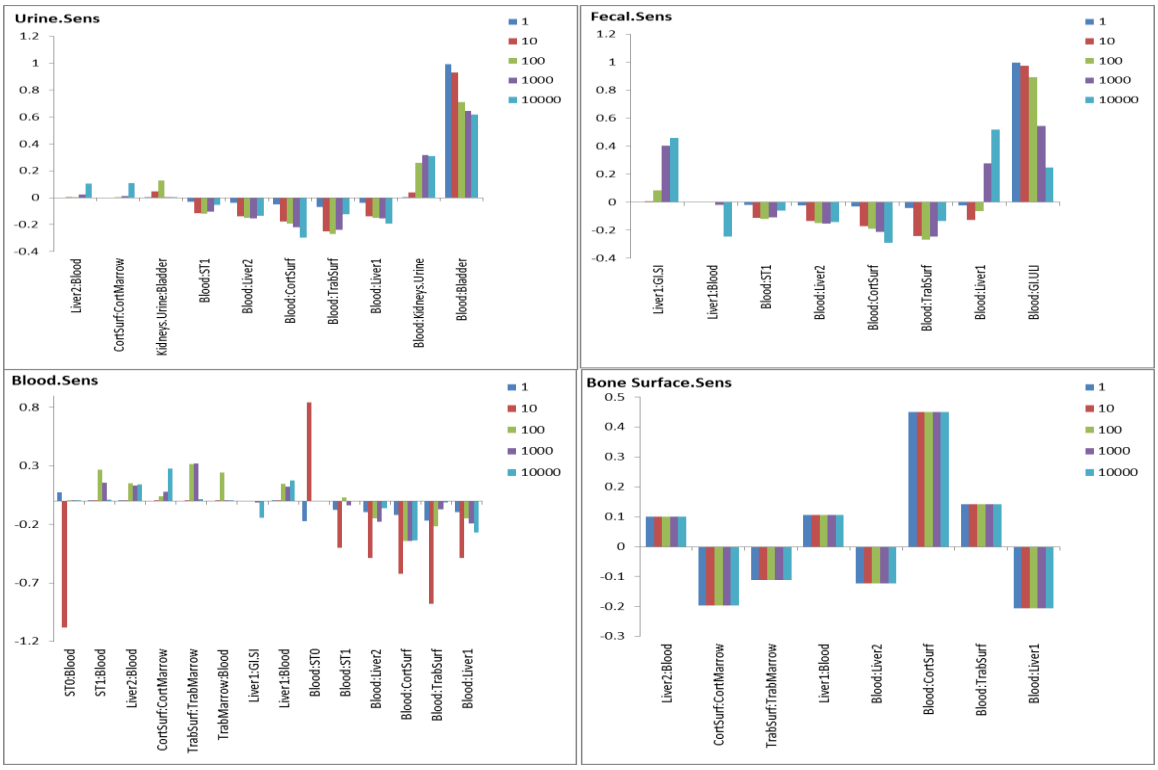

Figure 41: Sensitivity analysis of the urine, fecal, blood and bone surfaces for 1, 10, 100, 1,000 and 10,000 days post intake with the initial modified ICRP 67 rate matrix.

The sensitivity analysis determined that the blood to bladder pathway (i.e., Blood.Bladder) was significant for urine bioassays across all time periods. The blood to both liver compartments and bone surfaces were significant for all bioassay types across most time periods. Additionally, the exchange with the blood and extracellular fluids and intermediate soft tissue compartments were important during the early collection periods for the blood bioassays.

Initial predictions indicated that the liver compartment was lower than expected, while the skeleton compartment was higher than expected. This required an optimization process that allowed the liver contribution from circulation to increase while decreasing the skeleton contribution but also keeping the skeleton fractions constant with respect to cortical and trabecular bone and maintaining the ratio of bone volumes with respect to the

bone surfaces. The soft tissues were also partly reduced in an attempt to maintain the ratio between each of the soft tissues that were adopted from both the ICRP 67 systemic model and the Leggett 2005 model.

Optimization was performed using R function [Rmod.67FLS], which resulted in Figure 42.

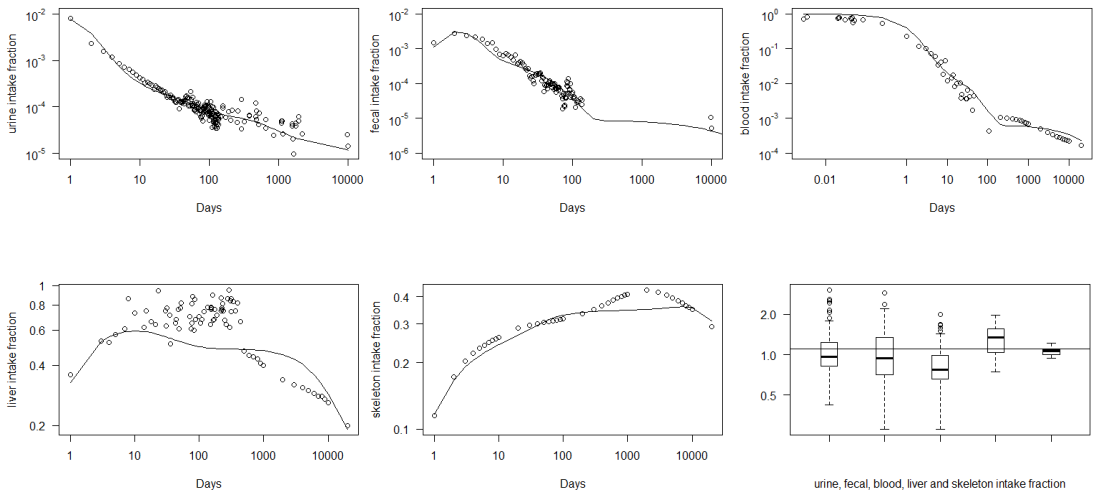

Figure 42: Final optimization of the modified ICRP 67 model in comparison to the urine, fecal, blood, liver and skeleton comparison data, with ordinate units based on the fractional amount of a unit intake. The boxplot indicated the distribution of the predicted intakes, with a combined intake estimate of 1.11.

Figure 42 indicated that the modified model demonstrated some minor differences from the actual mean observations. The boxplots illustrated the spread of predicted intakes compared to the total combined intake mean value of 1.11, indicating that most of the observed data were within an intake value of 1 about the mean. The boxplots indicated that each of the bioassay intake estimates were either normal or had a slight skewness when inspected on a log-scale, supporting the assumption of a lognormal distribution. The data spread indicated a wider dispersion of the urine and fecal intake estimates with several observations that exceeded the expected data distribution, which

were illustrated as separate points beyond the boxplot whisker. The boxplots also represented that the median values of the urine, fecal, liver and skeleton estimated intakes were consistent, with a narrow dispersion of the inner quartiles. The intakes due to urine, fecal, blood, liver and skeleton bioassays were 0.99, 0.97, 0.80, 1.27 and 1.06, respectively.

The model assumed that 74% of the activity in the blood compartment would be translocated to the skeleton and liver with three-fourths directed to the liver compartments. The soft tissues, bladder and kidneys urinary pathway received 21.5%, 1.35% and 2.33% of the blood compartment quantity, respectively. The kidney tissues initially received 0.05% from circulation as was proposed in the Leggett 2005 model; however, the long-term kidney retention was approximately three times higher than expected using the original ICRP 67 model; therefore, the kidney tissue fraction was reduced to 0.015% to address the kidney burden. The testes received 0.025% from the blood compartment with the transfer rate retained from the Leggett 2005 model. The ovaries were not included in the rate matrix but were assumed to also remain consistent with the Leggett 2005 model. The cortical volume and trabecular volume received 5% and 10% of the blood compartment quantity directed to the cortical (40%) and trabecular (60%) bones, respectively. The cortical and trabecular surface to the respective bone volumes were adopted from Leggett 2005 model, while the other skeleton transfer rates were maintained consistent with both the Leggett 2005 model and the ICRP 67 model. The transfer rates were specified in Table 22.

Table 22: Transfer rates specified for the modified ICRP 67 model.

Source	Destination	Transfer Rate (d^{-1})	Source	Destination	Transfer Rate (d^{-1})
ST0	Blood	**$3.42x10^{-1}$**	Bladder	Urine	$1.2x10^{-1(1)}$
ST1	Blood	$9.5x10^{-4(1)}$	Blood	ST0	**$1.53x10^{-1}$**
ST2	Blood	$1.9x10^{-5(1)}$	Blood	ST1	**$4x10^{-2}$**
Kidneys other	Blood	$1.27x10^{-4(2)}$	Blood	ST2	**$6x10^{-3}$**
Liver2	Blood	**$3.56x10^{-4}$**	Blood	Kidneys other	$1.39x10^{-4(2)}$
Testes	Blood	$3.8x10^{-4(2)}$	Blood	Liver2	**$2.587x10^{-1}$**
Cortical volume	Cortical marrow	$8.21x10^{-5(1)}$	Blood	Testes	$2.695x10^{-4(2)}$
Cortical surface	Cortical volume	$2.05x10^{-5(2)}$	Blood	Ovaries	$8.47x10^{-5(2)}$
Cortical surface	Cortical marrow	$8.21x10^{-5(1)}$	Blood	Cortical volume	**$3.5x10^{-3}$**
Cortical marrow	Blood	$7.6x10^{-3(1)}$	Blood	Cortical surface	**$6.72x10^{-2}$**
Trabecular volume	Trabecular marrow	$4.93x10^{-4(1)}$	Blood	Trabecular volume	**$1.06x10^{-2}$**
Trabecular surface	Trabecular volume	$1.23x10^{-4(2)}$	Blood	Trabecular surface	**$9.55x10^{-2}$**
Trabecular surface	Trabecular marrow	$4.93x10^{-4\ (1)}$	Blood	Liver1	**$2.457x10^{-1}$**
Trabecular marrow	Blood	$7.6x10^{-3\ (1)}$	Blood	Upper large intestine	**$9.2x10^{-3}$**
Liver1	small intestine	**$8.33x10^{-4}$**	Blood	Kidneys urine	**$2.15x10^{-2}$**
Liver1	Blood	**$4.05x10^{-2}$**	Blood	Bladder	**$1.25x10^{-2}$**
Kidneys urine	Bladder	**$1.8x10^{-3}$**			

Bold transfer rates were determined during optimization.
(1) adopted from ICRP 67 model
(2) adopted from Leggett 2005 model

An analysis of this effort indicated a combined bioassay normalized chi-squared statistic of the log-transformed data of 2,237/2,145 = 1.04 with 2,145 degrees of freedom with a p-value of 0.08, suggesting a marginal fit to the data. (Note: chi-squared statistic results were based on comparison of the model to the actual observations without the supplemented data). An additional comparison was made with the optimized results to that expected by both the ICRP 67 and the Leggett 2005 models, which were presented in Figure 43.

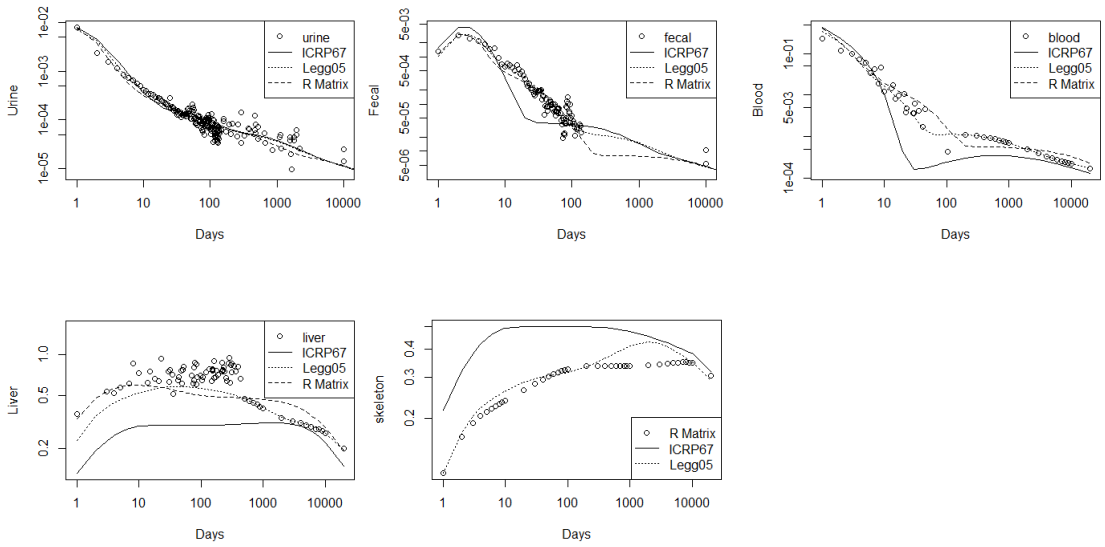

Figure 43: Modified ICRP 67 model (R Matrix R.67Mod24) for the urine, fecal, blood, liver and skeleton compared to the ICRP 67 and the Leggett 2005 model (Legg05) models with the actual mean observations, and supplemented data from the Leggett 2005 model for the blood, liver and skeleton. Supplemented measurements were provided for the blood and liver bioassays for 200 and 500 days up to 20,000 days, respectively. R function [compare.IRF] was used for the plot comparison.

Figure 43 indicated that the modification to the ICRP 67 model results compared well with the actual mean observations and closely approximated the Leggett 2005 model. The modified ICRP 67 model had favorable experimental qualities in that it was able to be compared to multiple bioassay types, with removal of the ST1 to bladder pathway, while also maintaining one blood compartment.

An analysis was performed of the ICRP 67 original transfer rates for comparison to the recommended model fitted to the actual mean observations. Figure 44 illustrated these results.

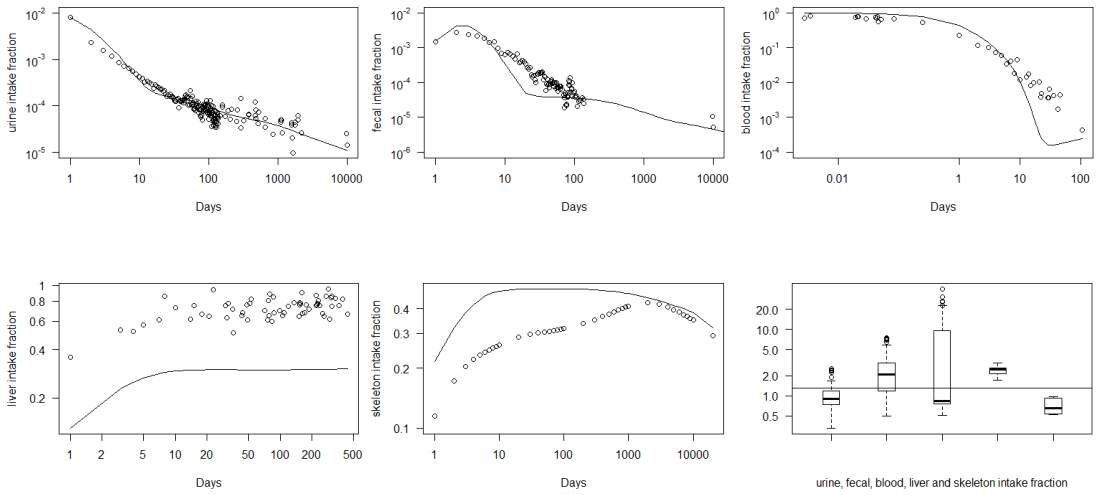

Figure 44: ICRP 67 systemic model comparison plots for the urine, fecal, blood, liver and the skeleton. The skeleton was the simulated data based on the Leggett 2005 model. The boxplot indicates the distribution of the predicted intakes, with a combined intake estimate of 1.31, on a log scale.

Figure 44 indicated that the model fit the urine excretion well, but failed to provide an adequate visual fit for the fecal, blood and liver observations. The skeleton was based off of the Leggett 2005 model and it was understood that the ICRP 67 model would not fit this based on discussion in the referenced publication regarding the early distribution to the liver compartment, an assessment known to be contrary to earlier predictions. The boxplots presented in Figure 44 illustrated the dispersion of observations about the predicted total combined intake of 1.31 and the variance between the bioassay type predictions indicating that the observed data had a wide dispersion about the mean which was significant for the fecal and blood estimated intakes. The boxplots indicated that each of the bioassay intake estimates were either normal or had a slight skewness, with exception of the blood estimated intakes that demonstrated even a higher significant positive skewness. The data spread indicated a wider dispersion of the urine and fecal intake estimates with several measurements exceeding 99% of the expected data distribution. The boxplots also indicated that the median values of each

bioassay type intake estimate varied significantly, with a wide dispersion of the inner quartiles observed for the fecal and blood estimated intakes. The intakes predicted based upon urine, fecal and blood bioassay data were determined as 0.91, 2.00 and 2.07, respectively. These results indicated a combined bioassay chi-squared statistic of the log-transformed data of 4,776 with 2,169 degrees of freedom thus leading to rejection of the null hypothesis and implying that the model was not representative of the observed data.

The proposed modified ICRP 67 model was compared to the original ICRP 67 model and the Leggett 2005 model with the results illustrated in Table 23.

Table 23: Modified ICRP 67 comparison to original and the Leggett 2005 model.

Biokinetic Model	Total Chi-Square [2]	Autocorrelation 95% range (-0.042 to 0.042)	Estimated Intake[1]	AOV F-Test Significance
Modified ICRP 67 [3]	2,237: p=0.08 (df=2145)	0.26	T:1.11, U:0.99, F:0.97, B:0.80, L:1.27, S:1.06	Intake: F=18.9 (p<0.01)
Original ICRP 67 [3]	4,776: p<0.001 (df=2169)	0.65	T:1.31, U:0.91, F:2.00, B:2.07, L:2.11, S:0.70	Intake: F=3.7 (p<0.01)
Leggett 2005 Model [3]	2,316: p=0.014 (df=2169)	0.28	T:1.08, U:0.92, F:1.02, B:1.08, L:1.26, S:1.00	Intake: F=12.3 (p<0.01)

[1] The estimated intake is provided for the total combined intake (T), urine bioassay (U), fecal bioassay (F), blood samples (B), liver *in vivo* measurements (L), and comparison with Leggett et al. (2005) skeleton model prediction (S).

[2] Chi-squared statistic values were performed without the liver, blood and skeleton supplemented values. The degrees of freedom accounted for 24 fitted parameters in the modified ICRP 67 model.

[3] Results obtained using rate matrices (R.67Mod24, R.67 and R.Leg) for the modified ICRP 67, original ICRP 67 and Leggett 2005 model, respectively.

The total chi-squared statistic comparison indicated that the modified ICRP 67 model (normalized χ_0^2 = 1.04, p-value = 0.08) resulted in an improved bioassay prediction when compared to the original ICRP 67 model (normalized χ_0^2 = 2.20, p-value essentially zero). In comparison, the Leggett model (normalized χ_0^2 = 1.07, p-value = 0.014) resulted in a slightly poorer performance than the modified ICRP 67 model. None of the models fitted the data as much as one might hope, but the modified ICRP 67 model

was clearly best with the largest p-value and the normalized chi-square closest to 1.0. The skeleton and supplemented data for the blood and liver measurements were excluded from the chi-squared statistic results due to being based on comparison with another prediction model instead of actual data. The autocorrelation showed temporal bias in all models, with the modified ICRP 67 model having the lowest value of 0.26, followed by the Leggett 2005 model having a value of 0.28. The AOV F-test results for the intakes being equivalent for each of the models resulted in rejecting the null hypothesis for all models. This suggests that all the models failed to demonstrate internal consistency between the intake estimates derived from the different bioassay types.

The modified ICRP 67 model predicted an intake from urine of 0.99, with the original ICRP 67 and Leggett 2005 models having 0.91 and 0.92, respectively, where the expected intake was 1.0. The modified ICRP 67 model also predicted an intake of 0.97 and 0.80 from the fecal and blood compartments, with the original ICRP 67 model predicting 2.00 and 2.07, respectively, and the Leggett 2005 model predicting 1.02 and 1.08, respectively. All models fell short of predicting the intake due to the liver *in vivo* measurements with the modified ICRP 67, Leggett 2005 model and ICRP 67 model predicting 1.27, 1.26 and 2.11, respectively. The total combined intake (i.e., the estimated intake derived from evaluating all bioassay types) for the modified ICRP 67 model resulted in 1.11 that was comparable to the Leggett 2005 model of 1.08, with an expectation of a unit intake. Additionally, the original ICRP 67 model resulted in an estimated intake of 1.31 based on evaluating all bioassay types.

The long-term plots were compared between each of the models in Table 24 to illustrate the significance of the long-term performance:

Table 24: Comparison of long-term bioassay prediction plots with the Modified and Original ICRP 67, and Leggett 2005 model.

(a) Modified ICRP 67	(b) Original ICRP 67	(c) Leggett 2005 model
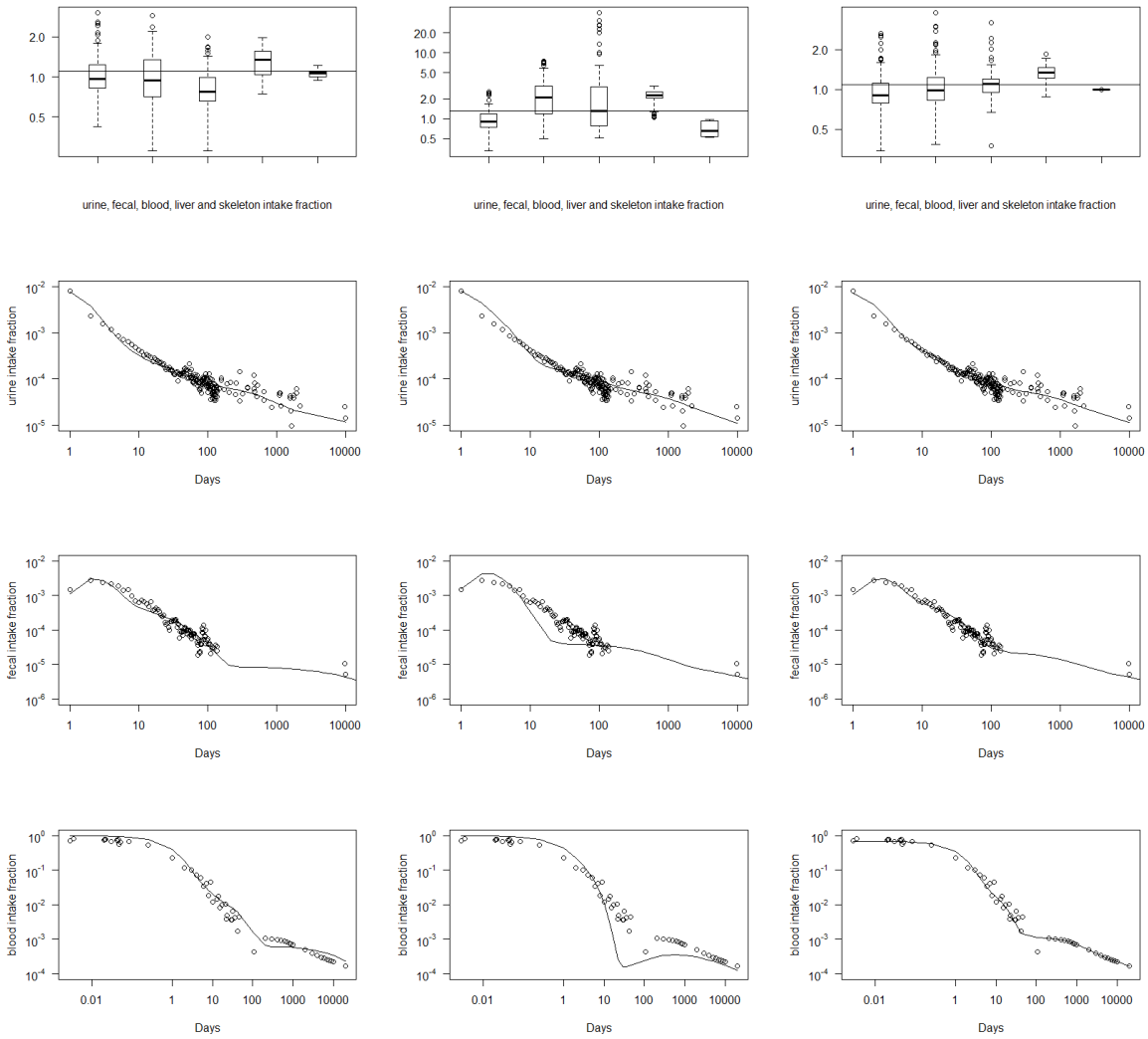		

Table 24 continued.

(a) Modified ICRP 67	(b) Original ICRP 67	(c) Leggett 2005 model
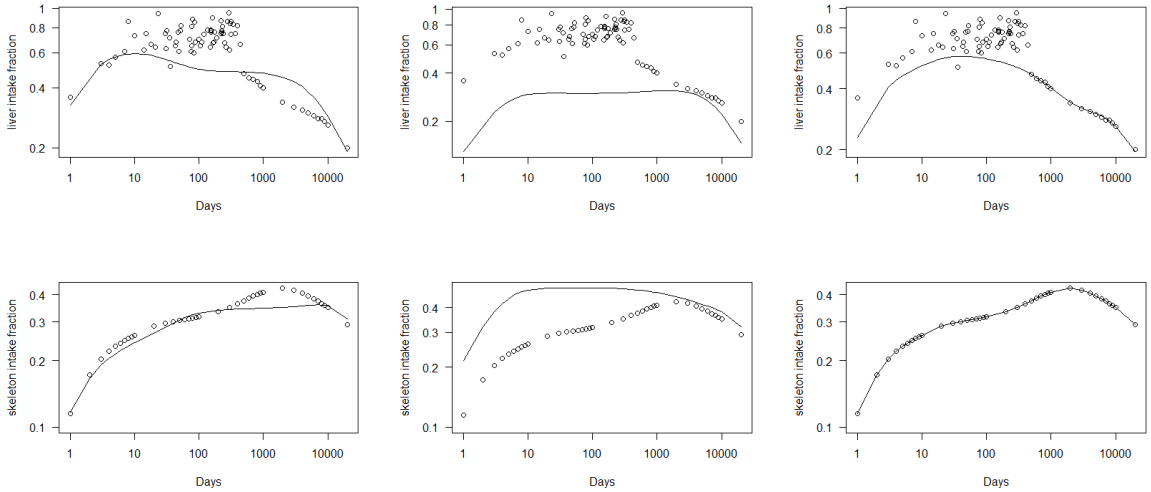		

Table 24 illustrates a comparison between the ICRP 67 model and Leggett 2005 model with the modified ICRP 67 model. Comparison of the boxplots indicated that the modified ICRP 67 and the Leggett 2005 models had a low overall dispersion of predicted intake results. The urine prediction was similar in all models, with observed variations in the fecal prediction between all models. The blood prediction appeared to perform best with the Leggett 2005 model and secondly with the modified ICRP 67 model based on visual inspection of the data. The liver prediction provided by the modified ICRP 67 model indicated a good visual fit of the data up to 100 days with the Leggett 2005 model appearing to provide better results for later time periods up to 500 days with the actual data. The Leggett 2005 model skeleton prediction matched the baseline reference since the data was originally provided by the Leggett 2005 model. The modified ICRP 67 model appeared to provide a better visual approximation to the skeleton burden compared

to the original ICRP 67 model. The long-term prediction was similar in all models with slight variations visible in the blood, fecal and liver bioassays.

In summary, the modified ICRP 67 biokinetic model was substantially better than the original ICRP 67 model, with the modified ICRP 67 model having the best overall fit that was demonstrated by having the largest p-value for goodness of fit. Bioassay programs often rely primarily on urine and fecal bioassay measurements when considering occupational exposures and therefore it is important for practical purposes to make certain that the biokinetic models are representative of these two bioassay types. The analysis in this section used only data from human injection studies. The human data used in this research (Appendix 3) should be considered the gold standard in developing and optimizing systemic biokinetic models for plutonium intakes. However, due to insufficient blood, liver and skeleton human data obtained over long time periods, these data were augmented by predicted values from the Leggett 2005 model. The results indicated that the modified ICRP 67 biokinetic model provided a close approximation of the urine and fecal measurement predictions compared to the mean of the actual observed data from human injection studies. The modified ICRP 67 model maintained the basic structure of the original ICRP 67 model that continued to support the efficient coupling with intake biokinetic models. Furthermore, the modified ICRP 67 model included physiological improvements to the original ICRP 67 model that resulted in better performance.

4.3 Pu-DTPA Model with Modified ICRP 67 Model

4.3.1 Pu-DTPA Model with IDEAS Case 123

The Pu-DTPA model was coupled with the modified ICRP 67 model using the optimized wound parameters determined in Section 4.1.1. Plots of the model prediction with the actual bioassay data were presented in Figure 45.

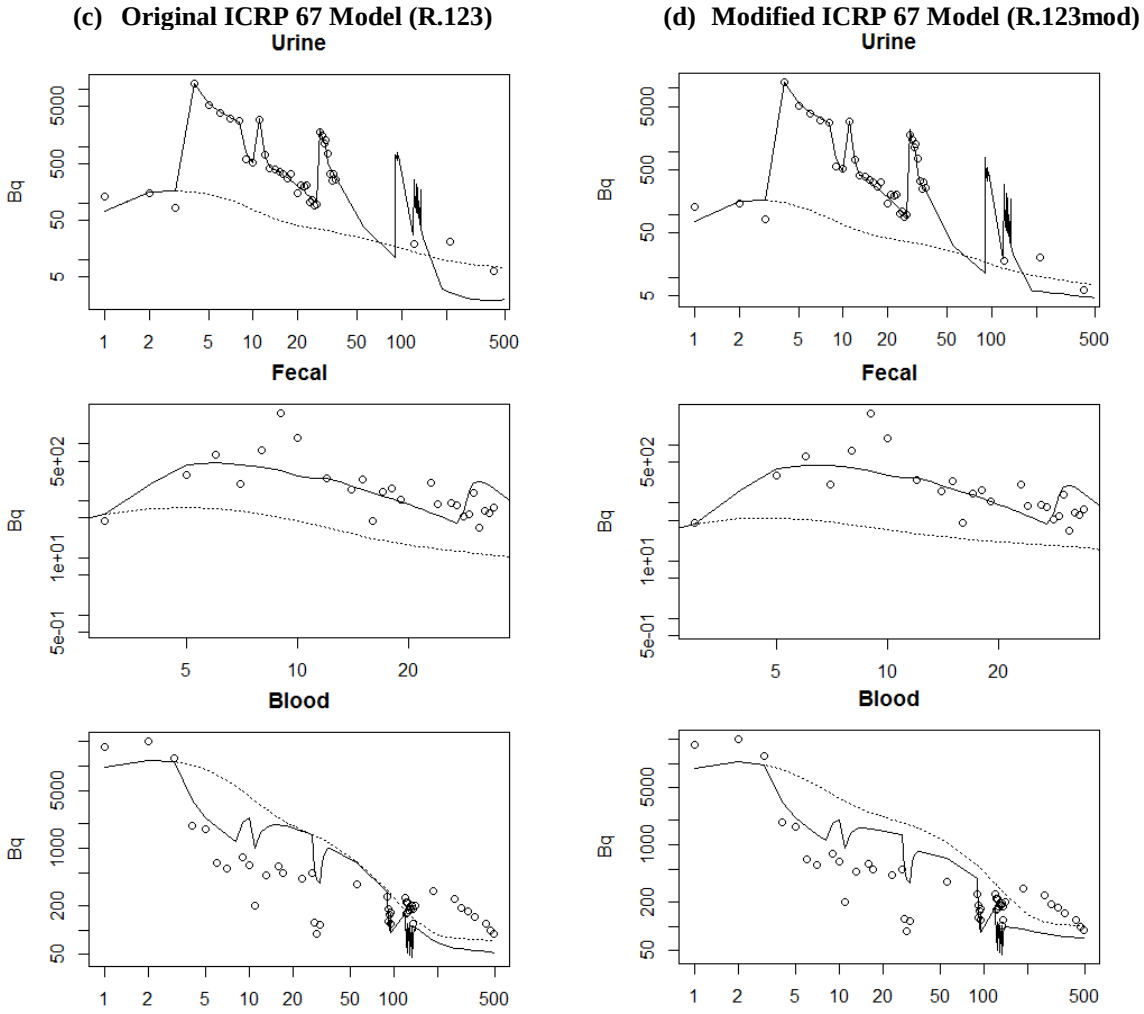

Figure 45: 500 day fitted bioassay plot comparison of the Pu-DTPA model fitted with the (a) original (R.123) and the (b) modified (R.123mod) ICRP 67 model using the optimized wound parameters for both models. The solid and dashed lines indicate the standard model with and without chelation, respectively.

The model comparison was performed using R function [Rmod.mult2]. The boxplots were also compared in Figure 46.

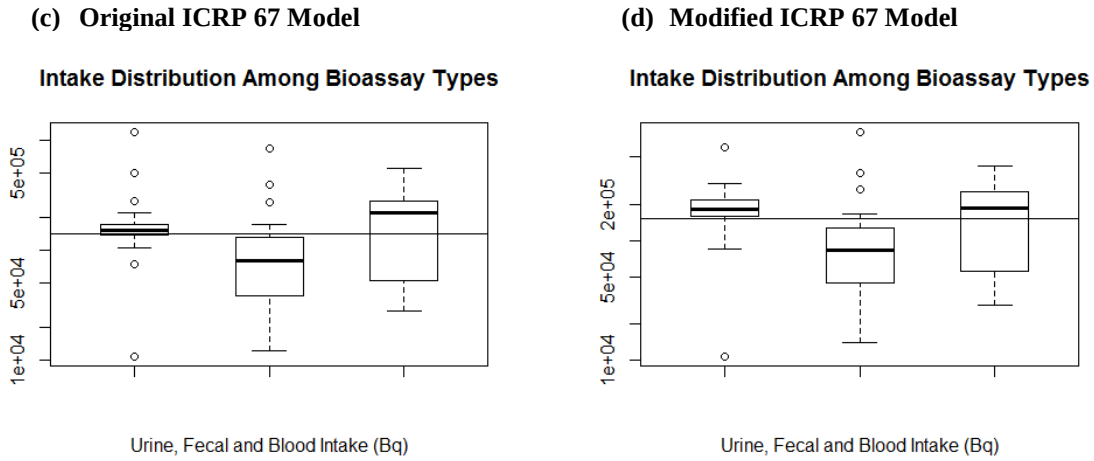

Figure 46: Boxplots representing the distribution of the Pu-DTPA model coupled with the (a) original and (b) modified ICRP 67 systemic model for the urine, fecal and blood on a log scale. The horizontal line represents the combined intake determined from fitting to the urine, fecal and blood bioassays.

The boxplots illustrated the dispersion of observations about the predicted total combined intake of 142,000 Bq and 152,000 Bq for the Pu-DTPA model coupled with the original (R.123) and modified (R.123mod) models, respectively. The boxplots indicated that the median and dispersion of the urine, fecal and blood bioassays for the original and modified models were similar. The model fit statistics were provided in Table 25.

Table 25: Comparison of Pu-DTPA model with the original and modified ICRP 67 model.

Biokinetic Model	Original [2] ICRP67 χ_0^2	Modified [2] ICRP67 χ_0^2	Observations	Original Est.Intake (Bq)	Modified Est.Intake (Bq)	Intake[1] AOV F-Test
Urine:	65 (32 df)	51 (32 df)	38	153,000	174,000	Original ICRP67: F=1.71 (p=0.19)
Fecal:	18 (24 df)	16 (24 df)	25	81,000	83,000	
Blood:	68 (45 df)	57 (45 df)	46	140,000	132,000	Modified ICRP67: F=5.06 (p<0.01)
			Summary Results			
Total Chi-Sq:	151 (p<0.001)	124 (p=0.06)	109			
	(df=101 df)	(df=101)				
Autocorrelation:	0.38	0.34	95% range (-0.189 to 0.175)			
	(-0.19 urine)	(-0.30 urine)				

[1] The intake AOV F-Test was determined from all bioassay type specified intakes in relation to each other.
[2] The degrees of freedom accounted for 5 optimized NCRP 156 wound parameters fitted to the urine excretion.

The total chi-squared statistic comparison indicated that the Pu-DTPA model coupled with the modified ICRP 67 model (normalized χ_0^2 = 1.23, p-value = 0.06) resulted in an improved bioassay prediction involving chelation when compared to being coupled with the original ICRP 67 model (normalized χ_0^2 = 1.50, p-value = 0.0009). The Pu-DTPA model coupled with the original ICRP 67 model was a very poor fit to the data, whereas the Pu-DTPA model coupled with the modified ICRP 67 model provided a marginal fit to the data. This indicates that the Pu-DTPA model coupled with the modified ICRP 67 model was preferred compared to being coupled with the original ICRP 67 model. The autocorrelation based on the combined bioassay intake comparison was 0.38 and 0.34, respectively, which indicated bias in both models; however, the autocorrelation of the urine bioassay fit of -0.19 was significant for the original ICRP 67 model with a 95% critical range of -0.33 to 0.23. The AOV p-value of the predicted intakes indicated that the Pu-DTPA model coupled with the original ICRP 67 model (F = 1.71, p-value = 0.19) showed internal consistency between the blood, urine and feces

estimates of intake; whereas, the p-value when coupled with the modified ICRP 67 model ($F = 5.06$, p-value = 0.008) demonstrates the model had little internal consistency between blood, urine and feces intake estimates. It was likely that the F-test analysis of variance of the Pu-DTPA model coupled with the modified ICRP 67 model was influenced by having a smaller variance within the bioassay types, thereby elevating the F-test. Both models appeared to work well with IDEAS Case 123 and were not significantly different in important structural ways.

The bone surface transformations were studied with the R function [Pu.CEDref] to determine the cortical and trabecular bone response for a 50-year period with IDEAS Case 123 using both models. The Pu-DTPA model combined with the original ICRP 67 model resulted in a 38.9% reduction in total bone surface transformations due to chelation, compared to a 38.7% reduction when combined with the modified ICRP 67 model. The transformation reduction experienced on the bone surfaces is a good approximation of the dose saved for the individual using the various models. Both models provided a similar prediction of the dose saved to the bone surfaces.

4.4 USTUR Case 0269 Validation

USTUR Case 0269 involved an inhalation of soluble plutonium nitrate followed by treatment of various chelating agents and administration methods that included Ca-EDTA and late Ca-DTPA treatments. The R functions [MLE.lung, Pu.lung3 and Pu.lung3B] were created to evaluate inhalation cases that required input of a rate matrix that included the ICRP 66 lung model coupled with the ICRP 67 systemic model, the ICRP 30 GI tract model and the Pu-DTPA biokinetic model. The R function

[MLE.lung] allowed for specifying an aerosol size, solubility type and particle bound fraction. For USTUR Case 0269, the particle solubility was suspected of being classified as a Type M (moderate) absorption due to inhalation of a soluble plutonium nitrate aerosol. The intake was estimated by inspection of the early fecal data for the first several days. This was possible since the chelation influence of the fecal activity was considered insignificant during the first several days due to the lung clearance dominating the fecal excretion pathway. The analysis considered the first 5 days. Furthermore, the early fecal activity was not influenced greatly due to solubility differences based on inspection of the published intake retention fractions (IRFs) in IAEA (2004); however, the intake varied depending on particle size. The intake was derived from the early fecal bioassay measurements, presented in Table 26.

Table 26: Initial intake estimated from early fecal samples using the IRFs in IAEA (2004).

Day	Fecal (Bq)	Type M (5 μm) Fecal IRF	Type M (5 μm) Intake (Bq)	Type M (1 μm) Fecal IRF	Type M (1 μm) Intake (Bq)
1	5,000	0.11	45,000	0.058	86,000
2	4,833	0.15	32,000	0.084	58,000
4	2,333	0.034	69,000	0.019	123,000
5	500	0.013	38,000	0.008	63,000
		Average	*46,000*	*Average*	*83,000*

The average intake was determined to be 46,000 Bq and 83,000 Bq for a Type M intake due to a particle size of 5-μm and 1-μm AMAD, respectively. Using these two estimated intakes, the urine enhancement was determined from the expected excretion using the IAEA (2004) IRF tables.

Table 27: Derivation of urine bioassay enhancement ratio due to chelation using the IRFs provided in IAEA (2004).

Day	Urine (Bq)	Type M (1 μm) Urine IRF	Type M (1 μm) Expected for 83,000 Bq	Enhancement Ratio (1 μm)	Type M (5 μm) Urine IRF	Type M (5 μm) Expected for 46,000 Bq	Enhancement Ratio (5 μm)
1	48.7	2.0×10^{-4}	16.6	2.9	2.3×10^{-4}	10.6	4.6
2	72.2	1.1×10^{-4}	9.1	7.9	1.3×10^{-4}	6.0	12
3	111.3	7.1×10^{-5}	5.9	19	7.8×10^{-5}	3.6	31
4	59.8	5.0×10^{-5}	4.2	14	5.3×10^{-5}	2.4	25
5	14.7	3.8×10^{-5}	3.2	4.6	3.9×10^{-5}	1.8	8.2
6	2.1	3.1×10^{-5}	2.6	0.8	3.0×10^{-5}	1.4	1.5
7	3.4	2.6×10^{-5}	2.2	1.5	2.4×10^{-5}	1.1	3.1
8	3.5	2.3×10^{-5}	1.9	1.8	2.0×10^{-5}	0.9	3.9
9	3.0	2.1×10^{-5}	1.7	1.8	1.7×10^{-5}	0.8	3.8

The enhancement ratio was higher for the 5-μm particle size when combined with an estimated intake of 46,000 Bq for the first several days, with a high of 31 compared to 19 for the 1-μm particle size for an 83,000 Bq intake. An inspection of the Type S solubility IRFs would have resulted in an estimated 100 fold increase for the enhancement ratio. For example, the Type S IRF for urine on day 3 was 8.3×10^{-7} (IAEA 2004), which resulted in a urine bioassay estimate of 0.038 Bq for a 46,000 Bq intake, and an enhancement ratio of 2,915, far beyond expectation. These results supported the Type M solubility classification.

The solubility was evaluated further by comparing the ratio of the fecal to urine excretion for the first several days in hopes of bounding the particle absorption type and possibly the particle size, with the results provided in Table 28.

Table 28: Comparison of urine and fecal excretion for determining absorption type using the provided IRFs in IAEA (2004) for a 1- and 5-μm AMAD particle size (2004).

Day	Urine (Bq)	Type M Expected	Fecal (Bq)	Fecal/Urine Ratio	Expected Ratio (Type M)	Expected Ratio (Type S)
			1-μm AMAD (83,000 Bq)			
1	48.7	16.6	5,000	301	290	30,500
2	72.2	9.1	4,833	531	764	73,000
3	111.3	5.9	No Sample			
4	59.8	4.2	2,333	555	380	33,000
5	14.7	3.2	500	156	211	17,000
			5-μm AMAD (46,000 Bq)			
1	48.7	10.6	5,000	472	478	48,000
2	72.2	6.0	4,833	806	1,150	114,000
3	111.3	3.6	No Sample			
4	59.8	2.4	2,333	972	642	59,000
5	14.7	1.8	500	277	333	31,000

From inspection of Table 28 it was apparent without further analysis that the particle solubility resembled a Type M absorption by examining the expected ratio compared to the Fecal/Urine ratio. The average residual between the 1-μm and 5-μm particle size resulted in 119 and 184, respectively, which indicated that the 1-μm particle size may be a better fit, and was also closer to James et al. (2007) prediction of 2 μm.

The autopsy results indicated that the lungs and thoracic lymph nodes were 26.7 Bq and 0.19 Bq, respectively, with a systemic burden of 2,317 Bq. The lung burden ratio to the systemic burden was 0.012; however, James et al. (2007) had determined that the systemic burden was decreased approximately 50% due to chelation without affecting the lungs, the unperturbed ratio was determined to be approximately 0.006. The standard ICRP 66 lung model would have predicted a lung intake retention fraction of 8.1×10^{-25} for 10,000 days post intake for a Type M absorption, assuming a 1-μm AMAD particle size (IAEA 2004). Furthermore, the original ICRP 67 model predicted the total body intake retention fraction of 0.06 for 10,000 days post intake for a Type M absorption that resulted in a lung to total body intake ratio of 1×10^{-21} (IAEA 2004). This indicated that some of the intake appeared to be bound to the lungs to account for the final lung burden. James et al. (2007) had determined that a bound fraction of 8% was appropriate with additional particle solubility transfer rate adjustments to the standard model. The bound fraction was rounded to 10% in order to stay close to that predicted by James et al. (2007), but to remain with the default compartment transfer rates while adjusting the bound particle absorption rate, which was performed in the following section.

4.4.1 Pu-DTPA Analysis with original ICRP 67 model

The performance of the Pu-DTPA biokinetic model coupled with the original ICRP 67 model was investigated due to its current recommended use for long-term applicability (Konzen and Brey 2014 submitted). The oral chelation administered during days 46 to 51 days and 93 to 102 days, and the decholin treatment during days 5,959 and 5,963 were omitted due to little or no observable enhancement indicating its ineffectiveness in influencing the bioassay excretion. The chelation performed with Ca-EDTA and Ca-DTPA were treated as having the same effect using the transfer rates defined for Ca-DTPA administration. There was no record of Zn-DTPA being administered. The models were fit to the urine and fecal excretion using R function [MLE.lung] with the rate matrix (R.LungPu.orig67b). Analysis indicated that a particle bound fraction of 10% with a corresponding transfer rate of 0.00023 d^{-1} would provide a lung to systemic burden ratio of 0.006 and a lung burden of 27.1 Bq, for an intake of 83,000 Bq. Furthermore, the thoracic lymph nodes burden resulted in 0.056 Bq, approximately 30% of the expected quantity at autopsy. The urine and fecal plots for 2,000 days were provided in Figure 47 using R function [MLE.lung] with the (R.LungPu.orig67b) rate matrix:

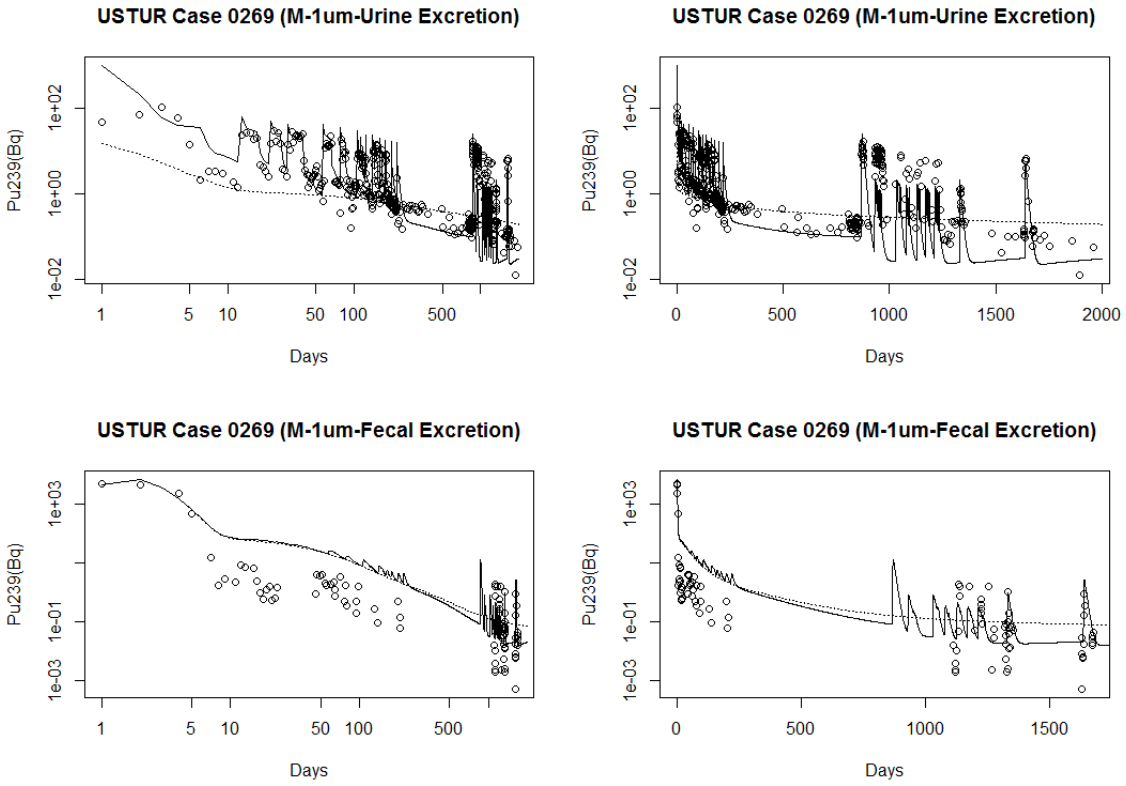

Figure 47: USTUR Case 0269 urine and fecal excretion observations compared to the predicted model (solid line) and standard model without chelation (dashed line), against a log-log scale and semilog scale on the left and right figures, respectively. The prediction model was fitted to an initial intake of 83,000 Bq with a 1-µm AMAD particle size, Type M absorption and 10% bound fraction for the first 2,000 days post intake.

The urine plots in Figure 47 appear to follow the observations for the first 1,000 days with the base of the predicted curve descending below the actual observations around 1,000 days post intake, with an adequate enhancement that represented the chelation performed on 1,331 and 1,640 days post intake. The initial urine prediction was approximately 20 times higher than actual, which may have been due to a delayed absorption into the blood from the lungs. The fecal excretion activity was elevated during the first 500 days when compared to the actual measurements that was due to relying on the default ICRP 66 lung model translocation rates without optimization; however, the late chelation enhancement and baseline provided a better fit. Plots were

also performed for all of the urine and fecal data for inspecting the long-term prediction with both bioassay types in Figure 48.

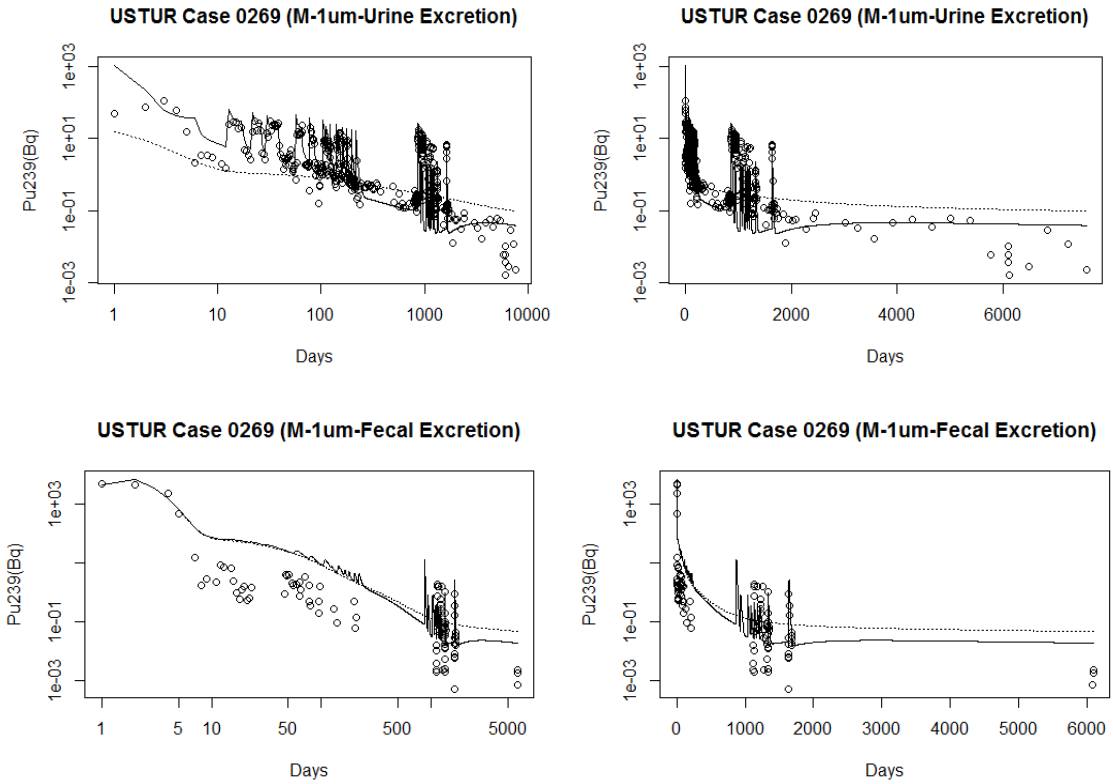

Figure 48: USTUR Case 0269 urine and fecal excretion observations compared to the predicted model (solid line) and standard model without chelation (dashed line), against a log-log scale and semilog scale on the left and right figures, respectively. The prediction model was fitted to an initial intake of 83,000 Bq with a 1-µm AMAD particle size, Type M absorption and 10% bound fraction for all of the urine and fecal excretion data.

The urine plots in Figure 48 illustrated a lower baseline around 2,000 days that was previously discussed. Furthermore the late prediction around 6,000 days was higher than the actual measurements for both urine and fecal bioassays due to the observed drop in bioassay excretion following decholin administration during 5,959 to 5,963 days.

Final Tissue Analysis

The organ burden was determined with R function [Pu.lung3C] and (R.LungPu.orig67b) rate matrix using the ICRP 66 lung model for a 1-µm AMAD

particle, Type M absorption and a 10% bound fraction with a bound transfer rate of 2.3 x 10^{-4} d^{-1} that was coupled with the original ICRP 67 systemic model for plutonium. Table 29 illustrates a comparison of these results with the final organ and tissue burden.

Table 29: USTUR Case 0269 organ burden comparison using Pu-DTPA model with original ICRP 67 model.

Organ/tissue	Activity at Death (Bq)	Expected without DTPA (Bq)	Saved (%)	Predicted with DTPA (Bq)	Comparison with Autopsy (%)
Lungs, larynx, trachea	26.7	27.1	None expected	27.1	+1.5%
Thoracic lymph nodes (LNth)	0.19	0.056	None expected	0.056	-71%
Skeleton	1,197	2,686	55%	1,181	-1.3%
Trabecular	~230	540		219	-4.8%
Cortical	~970	2,146		962	-0.8%
Liver	937	1,409	33%	522	-44%
Kidneys	1.7	2.82	40%	1.15	-32%
Testes	0.83	1.80	54%	0.77	-7.2%
All other soft tissues	180	473	62%	214	+19%
Systemic	2,317	4,575	49%	1,920	-17%
		Summary Results for Pu-DTPA with Urine Excretion			
Total Chi-Sq:		3,593	475 (95% critical value)		
Autocorrelation:		0.77	range (-0.097 to 0.092)		
Degrees of Freedom		426			
Model Predicted Intake:		103,000 Bq			

The model predicted well the lung burden; however, under predicted the thoracic lymph nodes by 71%, which had the expected ratio with the lungs when evaluating against the standard model. The reduced quantity, illustrated in the saved column in Table 29, due to the chelation therapy treatment ranged from 33% for the liver to 62% for all soft tissues, with the systemic burden being reduced by 49%, when compared to predicted results. The Pu-DTPA biokinetic model had predicted the final organ quantities well when compared to the autopsy case, with the skeleton and liver being under predicted by 1.3% and 44%, respectively, while the systemic burden was under predicted by 17%. The model also was able to predict an intake of 103,000 Bq based on

the maximum likelihood method that was within 25% of the specified intake of 83,000 Bq based on regression of the urine bioassay results. These results indicate that the skeleton burden could be reasonably predicted by the Pu-DTPA model without considering additional skeleton decorporation; whereas, the liver decorporation was higher than expected and could result in a lower dose assignment of approximately one-half of the actual results. These analyses demonstrated the benefit of using the Pu-DTPA model coupled with the original ICRP 67 systemic model based upon an autopsy case while using the default Pu-DTPA model parameters. Further research was necessary in order to study the liver burden, which was likely biased due to flaws identified with the ICRP 67 model regarding liver retention (Leggett et al. 2005).

4.4.2 Pu-DTPA Analysis with the modified ICRP 67 model

The performance of the Pu-DTPA biokinetic model was investigated while it was coupled with the modified ICRP 67 model for comparison with the original model results. The models were regressed to the urine and fecal excretion data using R function [MLE.lung] with the rate matrix (R.LungPu.origbv1) for the first 2,000 days to highlight interim enhancement performance in Figure 49.

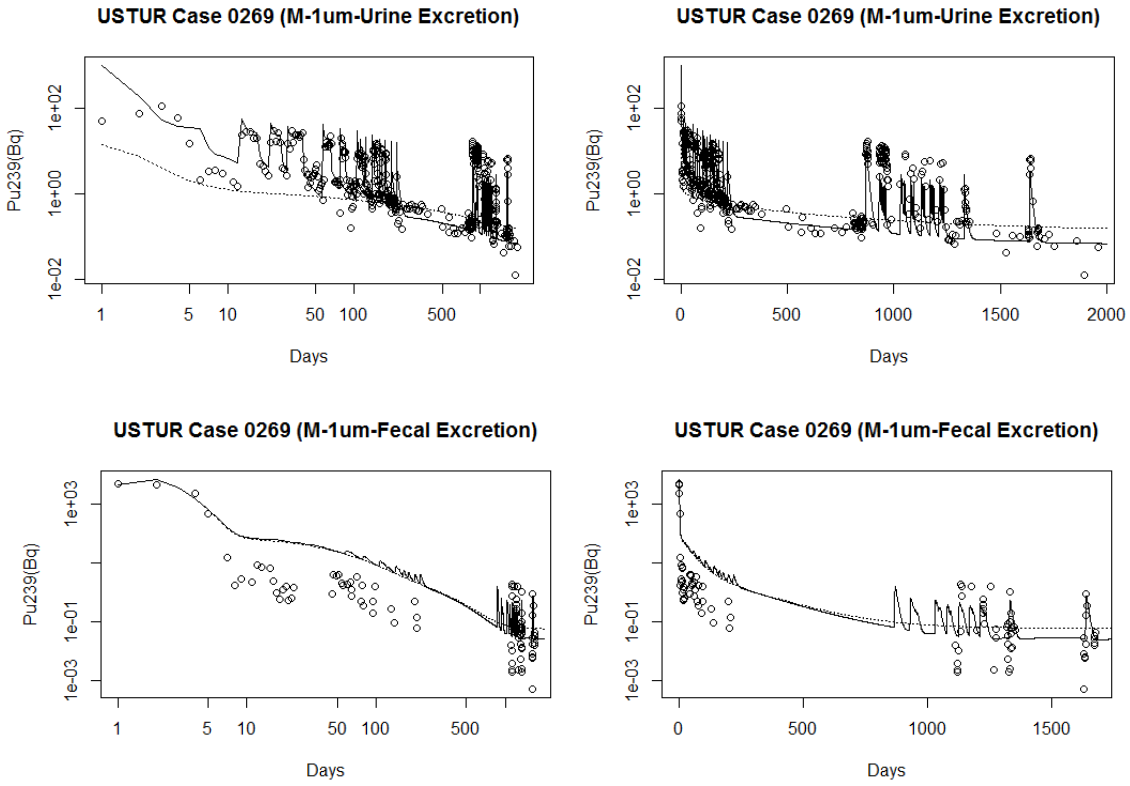

Figure 49: USTUR Case 0269 urine and fecal excretion observations compared to the predicted model (solid line) and modified ICRP 67 model without chelation (dashed line), against a log-log scale and semilog scale on the left and right figures, respectively. The prediction model was fitted to an initial intake of 83,000 Bq with a 1-µm AMAD particle size, Type M absorption and 10% bound fraction for the first 2,000 days post intake.

The urine plots in Figure 49 indicate that the predicted model with the modified ICRP 67 model provided a significant improvement for the late excretion results observed around 1,000 to 1,500 days due to a raised baseline. The initial urine prediction was approximately 20 times higher than actual, which may have been due to a delayed absorption into the blood from the lungs. The fecal prediction baseline was higher than expected for the initial samples that was due to relying on the default ICRP 66 lung model translocation rates without optimization. However this was as expected for the later period beyond 1,000 days. Plots were also generated and provided in Figure 50 for all of the urine and fecal data, thus providing a means for visually inspecting the long-term prediction with both bioassay types.

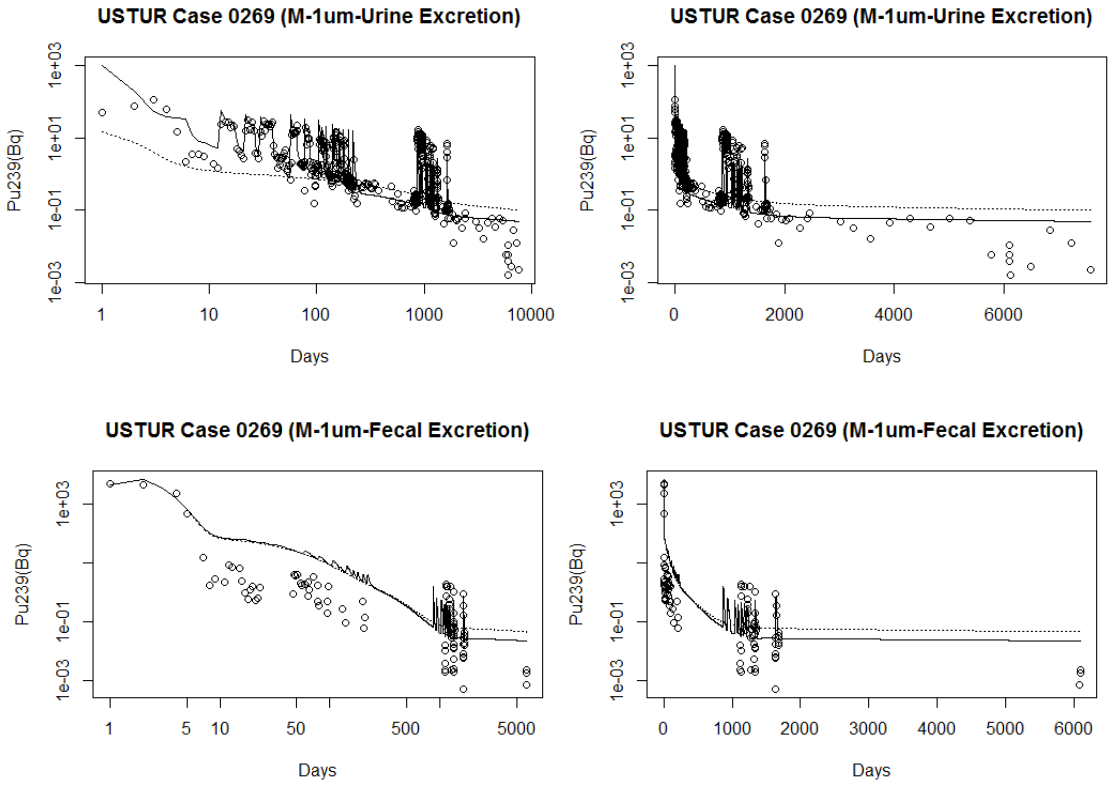

Figure 50: USTUR Case 0269 urine and fecal excretion observations compared to the predicted model (solid line) and modified ICRP 67 model without chelation (dashed line), against a log-log scale and semilog scale on the left and right figures, respectively. The prediction model was fitted to an initial intake of 83,000 Bq with a 1-µm AMAD particle size, Type M absorption and 10% bound fraction for all of the urine and fecal excretion data.

The urine plots in Figure 50 illustrated a visually improved baseline compared to using the original ICRP 67 model. The late prediction, around 6,000 days, was higher than the actual measurements for both urine and fecal bioassays. This is attributed to the observed drop in bioassay excretion following decholin administration during 5,959 to 5,963 days.

Final Tissue Analysis

The organ burden was determined using the R function [Pu.lung3C] and (R.LungPu.origbv1) rate matrix using the modified ICRP 67 model coupled with the ICRP 66 lung model for a 1-µm AMAD particle, Type M absorption and a 10% bound

fraction with a bound transfer rate of 2.3 x 10^{-4} d^{-1}. Table 30 presented a comparison of the predicted results to the final organ and tissue burden.

Table 30: USTUR Case 0269 organ burden comparison using Pu-DTPA model with modified ICRP 67 model.

Organ/tissue	Activity at Death (Bq)	Expected without DTPA (Bq)	Saved (%)	Predicted with DTPA (Bq)	Comparison with Autopsy (%)
Lungs, larynx, trachea	26.7	27.1	None expected	27.1	+1.5%
Thoracic lymph nodes (LNth)	0.19	0.056	None expected	0.056	-71%
Skeleton	1,197	2,558	53%	1,235	+3.2%
Trabecular	~230	552		270	+17%
Cortical	~970	2,007		965	-0.5%
Liver	937	1,829	49%	895	-4.5%
Kidneys	1.7	2.84	40%	1.37	-19%
Testes	0.83	1.76	53%	0.86	+3.6%
All other soft tissues	180	379	53%	183	+1.7%
Systemic	2,317	4,802	52%	2,330	+0.6%
		Summary Results for Pu-DTPA with Urine Excretion			
Total Chi-Sq:		2,743	475 (95% critical value)		
Autocorrelation:		0.69	range (-0.097 to 0.092)		
Degrees of Freedom		426			
Model Predicted Intake:		97,000 Bq			

The model predicted the lung burden and burden of the thoracic lymph nodes to be the same as shown with the last section. This is true because there were no changes made to the ICRP 66 model parameters. The reduced quantity, illustrated in the saved column in Table 30, due to the chelation therapy treatment for the skeleton was 53% with the systemic burden being reduced 52%, when compared to predicted results. The quantity saved in the soft tissues, kidneys and testes were 53%, 40% and 53%, respectively. The Pu-DTPA biokinetic model had predicted the skeleton and liver within 3.2% and 4.5%, respectively, while the systemic burden was predicted within 1% of the autopsy results. The model also was able to predict an intake of 97,000 Bq based on the

maximum likelihood method that was within 20% of the specified intake of 83,000 Bq based on regression of the urine bioassay results.

The autopsy results indicated that the liver and skeleton made up 92% of the systemic burden that was divided between the skeleton and liver by 52% and 40%, respectively, with the soft tissues making up the remaining 8%. These results were consistent with the modified ICRP 67 model prediction where the liver and skeleton made up 91% of the systemic burden with 53% due to the skeleton, 38% due to the liver and 8% due to the soft tissue contribution. The modified ICRP 67 model provided consistent results with the autopsy results, with remarkable improvements compared to being coupled with the original ICRP 67 systemic model.

4.4.3 Summary of Pu-DTPA Model Results for USTUR Case 0269

A comparative review of the Pu-DTPA model with respect to the original and modified ICRP 67 model is presented in Table 31.

Table 31: USTUR Case 0269 organ burden comparison using the Pu-DTPA model with the original and modified ICRP 67 systemic model for an intake of 83,000 Bq.

Organ/tissue	Activity at Death (Bq)	Original ICRP 67 (Bq):(% Difference)	Modified ICRP 67 (Bq):(% Difference)
Lungs, larynx, trachea	26.7	27.1(+1.5%)	27.1(+1.5%)
Thoracic lymph nodes (LNth)	0.19	0.056(-71%)	0.056(-71%)
Skeleton	1,197	1,181(-1.3%)	1,235(+3.2%)
Trabecular	~230	219(-4.8%)	270(+17%)
Cortical	~970	962(-0.8%)	965(-0.5%)
Liver	937	522(-44%)	895(-4.5%)
Kidneys	1.7	1.15(-32%)	1.37(-19%)
Testes	0.83	0.77(-7.2%)	0.86(+3.6%)
All other soft tissues	180	214(+19%)	183(+1.7%)
Systemic	2,317	1,920(-17%)	2,330(+0.6%)

The summary provided in Table 31 demonstrates that the Pu-DTPA model coupled with the modified ICRP 67 model provided the closest results, with the skeleton,

liver, testes, soft tissues and systemic burden, which is within 5% of the final quantity determined at the autopsy. The observed ratio between the trabecular and cortical bone were similar to that reported by James et al (2007); although it was also acknowledged that these burdens were approximated and not actually based on autopsy measurements. The cumulative number of skeleton transformations is considered to be a good indicator for determining the influence of chelation. The Pu-DTPA model coupled with either the original or modified ICRP 67 model, adequately perform this comparison. The liver burden was predicted within 5% of actual autopsy results when the Pu-DTPA model was coupled with the modified ICRP 67 model, which improved the prediction of 44% when coupled with the original ICRP 67 model. This difference is apparently due to inadequacies of the ICRP 67 systemic model.

Figure 51 illustrates a comparison of the organ quantities predicted by the various model arrangements.

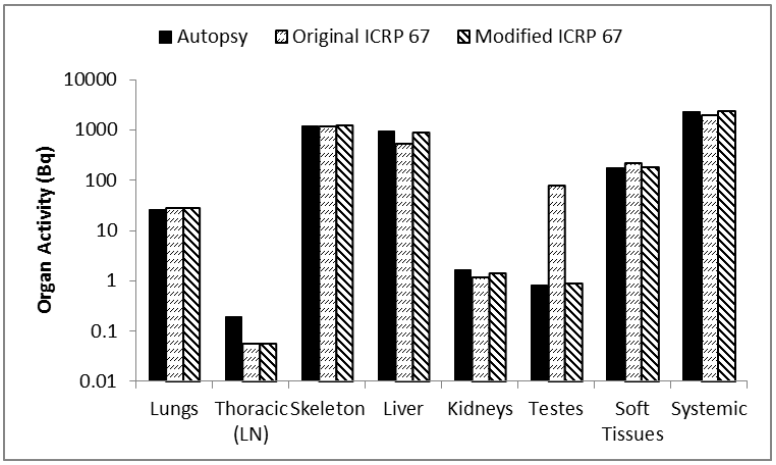

Figure 51: Plot of USTUR organ quantity comparison with autopsy and predictions with the original and modified ICRP 67 models.

The original and modified ICRP 67 predictions were similar to the autopsy results for the lungs and skeleton, with notable differences in the liver and testes. The modified ICRP 67 model provided predictions closer to observations in this case.

A formal analysis was performed of the Pu-DTPA model coupled with original and modified ICRP 67 model with comparison to the USTUR Case 0269 excretion data as shown in Table 32.

Table 32: Comparison of the Pu-DTPA model coupled with the ICRP 67 model, illustrating the chi-squared statistic (χ_0^2) of the log-transformed data and the autocorrelation (ac) for urine and feces with USTUR Case 0269 excretion data.

ICRP 67 Model:	Original χ_0^2	Modified χ_0^2	df	Original (ac)	Modified (ac)	Autocorrelation critical range
Urine:	3,593	2,743	426	0.77	0.69	95% range (-0.097 to 0.092)
Fecal:	497	471	92	0.75	0.74	95% range (-0.21 to 0.19)
Total:	4,090	3,212	518	Not Performed	Not Performed	

The Pu-DTPA model coupled with the modified ICRP 67 model (normalized χ_0^2 = 6.2, p-value <0.001) resulted in an improved bioassay prediction involving chelation when compared to being coupled with the original ICRP 67 model (normalized χ_0^2 = 7.9, p-value <0.001), although both model predictions provided a poor fit to the data upon inspection of the resultant p-values. The autocorrelations of the urine and fecal exceeded the 0.05 significance level indicating that there was a bias in the predicted model to the actual observations; however, the Pu-DTPA model coupled with the modified ICRP 67 model indicated the lowest autocorrelation of 0.69 when compared to the urine excretion measurements.

The USTUR Case 0269 was used for validating the Pu-DTPA models and illustrated adequate performance in predicting the final organ and tissue burden. It is likely that the ICRP 67 model will be revisited and revised sometime in the near future, and may resemble something close to the modified ICRP 67 model; therefore, effort should be placed on developing a model that would perform well with the modified ICRP 67 model. Since the model predicted the skeleton burden well (i.e., 3.2% of the autopsy

result), there was no identified benefit of including skeleton decorporation in the Pu-DTPA model. The significant organs for determining committed effective dose rely primarily on an accurate prediction of the skeleton, liver and testes burden with application of the ICRP 60 (1991) tissue weighting factors. The Pu-DTPA model performed well with both the original and modified ICRP 67 models, but was able to provide a better prediction of the liver (i.e., 4.5% compared to 44%) and testes (i.e., 3.6% compared to 7.2%) final quantities for USTUR Case 0269 when coupled with the modified ICRP 67 model.

4.5 Treatment Strategies

Once the Pu-DTPA model was determined to be credible for wounds and inhalation cases, treatment strategies were developed to provide guidance on early and protracted chelation therapy. An assessment of DTPA effectiveness was based on the Pu-DTPA model coupled with the ICRP 67 systemic model without modification because this is the currently accepted model for the U.S. DOE, and the effectiveness was based on the number of bone surface transformations, a value that was consistent with both the original and modified ICRP 67 models.

4.5.1 DTPA Effectiveness for Wounds

Contaminant retention in wounds is affected by tissue excision, wound irrigation and systemic absorption. Transuranic radionuclides exhibit strong-retention properties (NCRP 2007) which are illustrated in Figure 52 with the corresponding blood compartment quantity in relation to the initial intake.

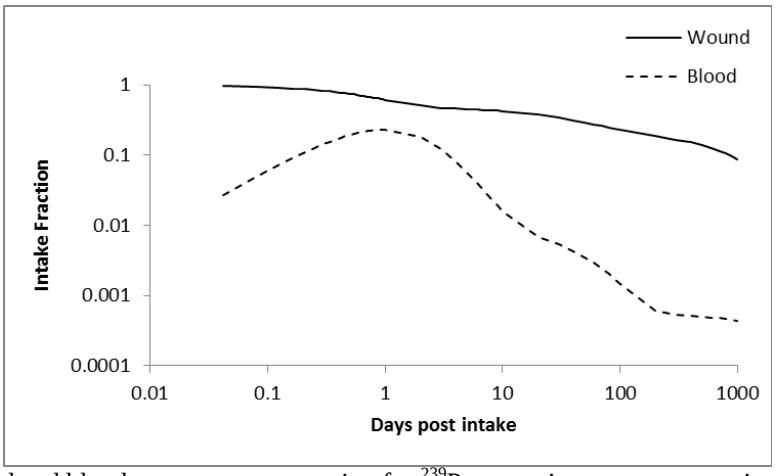

Figure 52: Wound and blood compartment retention for ^{239}Pu assuming a strong-retention wound type (NCRP 2007).

Figure 52 illustrated the wound and blood compartment retention for ^{239}Pu, using strong-retention transfer rate parameters from the NCRP 156 wound model coupled with the ICRP 67 systemic model. The blood compartment quantity reached a peak of ~23% of the initial intake at the end of the first day without intervention. The initial blood compartment uptake was influenced by the declining wound activity, where the first few days were important with respect to chelation effectiveness. Systemic absorption of radioactivity from a wound, as illustrated in Figure 52, is likely to continue for several years and may require protracted treatment and monitoring for large intakes.

The default NCRP 156 wound parameters were used for deriving an initial estimate and potential benefit for DTPA administration. Table 33 illustrated the local wound activity experienced by a strong-retention type of wound, with a corresponding conservative tissue uptake without chelation influence.

Table 33: Wound activity relation to tissue uptake for ^{239}Pu using default NCRP 156 parameters without DTPA influence.

Time Period (days)	Wound Activity	Wound Activity Decrease	Total Body Burden	Tissue Uptake
1st Day	62%	38%	99.8%	37.8%
2nd Day	51%	11%	99.4%	48.4%
(3-4) Days	46%	5%	98.6%	52.6%
(5-10) Days	43%	3%	97.8%	54.8%
(11-20) Days	38%	5%	97.4%	59.4%
(21-30) Days	35%	3%	97.1%	62.1%
(31-40) Days	32%	3%	96.8%	64.8%
(41-60) Days	28%	4%	96.4%	68.4%
(61-100) Days	23%	5%	95.8%	72.8%
(101-200) Days	19%	4%	94.6%	75.6%
(201-300) Days	17%	2%	93.8%	76.8%
(301-400) Days	15%	2%	93.0%	78.0%
(401-500) Days	14%	1%	92.3%	78.3%
(501-600) Days	13%	1%	91.6%	78.6%
(601-700) Days	12%	1%	91.0%	79.0%
(701-800) Days	11%	1%	90.4%	79.4%
(801-900) Days	10%	1%	89.8%	79.8%
(901-1000) Days	9%	1%	89.2%	80.2%
(1001-2000) Days	4%	5%	84.7%	80.7%
(2001-3000) Days	2%	2%	81.4%	79.4%
(3001-4000) Days	1%	1%	78.7%	77.7%

Table 33 results are applicable to strong-retention wound types that have a long radiological half-life. Items of note are the periods where chelation influence would provide a potential benefit. The first 2 days are the important in that approximately 48% of the tissue uptake potential could be prevented. Another 5% could be prevented up to day 4 and 3% up to day 10, with 3 to 5% for each 10 day treatment period up to 40 days post intake. Later periods would require extended treatment periods to realize a 4 to 5% treatment benefit.

DTPA effectiveness was determined for wounds and inhalation intakes by using the Pu-DTPA model coupled with the NCRP 156 model for a strong-retention wound and the original ICRP 67 systemic model. The DTPA effectiveness was determined by reviewing the reduction in the bone surface transformations for a 50 year period, relative to the CEqD, due to chelation influence compared to no treatment, using the R function

[Pu.CEDref]. The benefit of different treatment starting periods was reviewed for either a single injection or a series of 3 daily administrations for a strong-retention wound intake of ^{239}Pu. Further enhancement was also included to account for multiple intra-day treatments or intramuscular injection. The results were presented in Table 34.

Table 34: DTPA benefit for ^{239}Pu strong wound retention for single injection or 3-day series injections. Enhanced injections (i.e., application by intramuscular injection or multiple intra-day injections) were included.

Day Start	One Injection	Enhanced Injections	3 day Series	Enhanced 3-day Series
1	19.22%	26.04%	40.44%	45.50%
2	27.67%	33.40%	37.39%	40.92%
3	25.87%	29.51%	31.46%	33.62%
4	22.86%	25.16%	26.90%	28.28%
5	20.38%	21.92%	23.79%	24.75%
6	18.59%	19.68%	21.70%	22.42%
7	17.35%	18.16%	20.30%	20.87%
8	16.50%	17.13%	19.35%	19.82%
9	15.93%	16.44%	18.71%	19.12%
10	15.56%	15.97%	18.29%	18.65%

Table 34 illustrated the effects of a single injection providing a dose reduction benefit of 19% on the first day, which was based on treatment starting promptly after intake. If treatment started on the second day, there is an indication that there would be approximately a 28% dose reduction benefit, which initially appeared contrary to suggested treatment; however, DTPA studies were primarily developed by intravenous injection of the contaminant where prompt treatment would be appropriate. In this case, the NCRP 156 wound model indicated that the contaminant is slowly absorbed; reaching a peak blood quantity at the end of the first day for a strong-retention wound type. Thus the model simulates DTPA treatment at the start of the second day when the blood quantity was at its peak and where early treatment is a greater benefit. This analysis does not recommend waiting until the second day to begin treatment, but it illustrates the importance of continuing treatment on the second day. According to the 3-day series

treatment, the largest benefit of 40% was realized with 3 consecutive treatments that began promptly after intake. There was a 3% reduction in benefit if treatment was delayed until the second day.

The enhanced injections illustrated in Table 34 were calculated by doubling the transitional blood compartment transfer rate value, which simulated additional treatments during the course of the day. The action of providing a fractionated dose of a single treatment at spaced time intervals extends the chelation therapy. DTPA in circulation would be maintained at beneficial levels for most of the day. Enhanced treatment could also be administered by intramuscular injection of DTPA where it was expected to have a slower rate of absorption into the blood, thus extending the DTPA levels for a longer period. The enhanced treatment methods were described in Chapter 2 based on experimental evidence. The results of the enhanced treatment were important during the initial few days, adding up to another 5 to 7% dose reduction benefit. The simulated enhanced treatment calculations used in the Pu-DTPA model, with the results illustrated in Table 34, were considered conservative and it may be possible that a further benefit would be realized. According to the model prediction, the benefit of enhanced injections is important for the first several days with little benefit for later time periods. Research has indicated that Ca-DTPA administered in fractionated doses had negative consequences with protracted treatment, which were not observed with Zn-DTPA.

Table 34 results were plotted in Figure 53 to illustrate the dose reduction benefit of DTPA treatment and the benefit of delayed treatment.

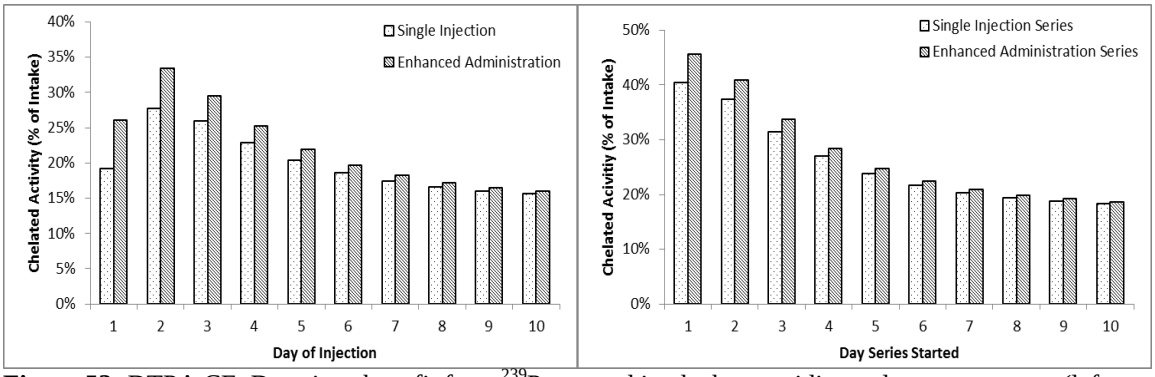

Figure 53: DTPA CEqD savings benefit for a ^{239}Pu wound intake by providing only one treatment (left figure), and by a 3-day treatment series starting on the day specified (right figure), that includes comparison with enhanced techniques.

Figure 53 illustrates the benefit of when to perform a single injection, compared to the enhanced administration method (e.g., multiple intra-day injections or intramuscular injection) providing a noticeable difference during the first several days. The series administration assumes daily injections for a series of three continuous days, in which most of the chelation effect may be observed. A series of three injections were chosen since the chelation effectiveness on the 4th day was 1 to 2% of the initial intake and provided little benefit in this illustration; however, this should not preclude treatments beyond three continuous days.

The Pu-DTPA model was studied to determine an optimum treatment schedule. Weekly treatment strategies were compared for 20 weeks of protracted treatment for one, three or five treatments per week. Figure 54 presented the model prediction for the different treatment strategies. This resulted in five treatments per week being the most effective with a bone surface dose reduction of 62% when continued for 20 weeks.

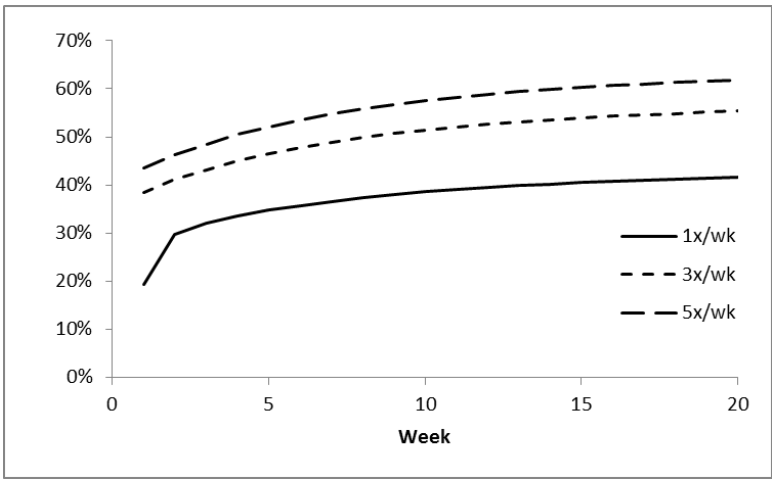

Figure 54: Protracted treatment comparison of cumulative bone surface CEqD savings for various DTPA treatments of 1 time to 5 times per week up to 20 weeks for a ^{239}Pu contaminated wound uptake.

Figure 54 illustrates the dose reduction benefit of protracted treatments up to 20 weeks post intake. Multiple treatments of 5 treatments per week provided the largest benefit, and by inspection of Figure 54 the slope of the 3 treatments per week was similar beyond five weeks, which would support reducing the treatment frequency.

Another comparison study reviewed late chelation treatment that was similar to Cohen et al.'s (1974) baboon study, where treatments were provided for three weeks. Incremental monthly treatments ranged from one application per month to five times per week for a total of three weeks.

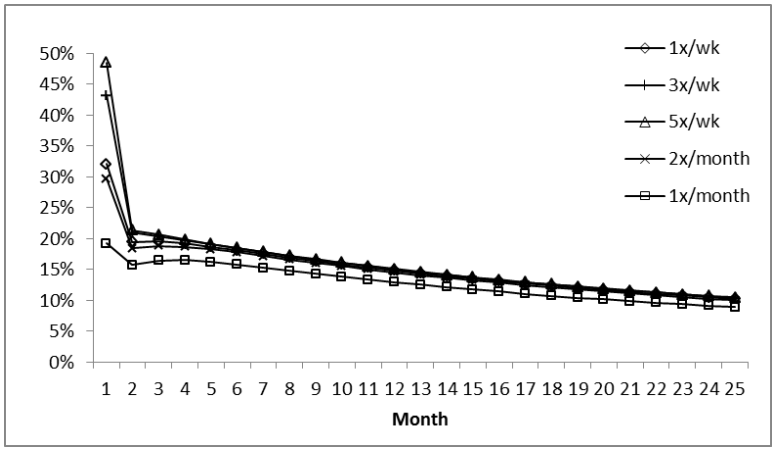

Figure 55: Late incremental DTPA treatment comparison of bone surface CEqD savings for 1 to 5 times per week for a 3-week period, and 1 to 2 treatments per month for a ^{239}Pu contaminated wound uptake.

Figure 55 illustrates that DTPA administered five times per week for three weeks provided the best strategy for the first month, with little additional benefit afforded for later months. Late months were shown to be comparable for treatments ranging from 2 to 15 treatments per month. According to this and the previous analysis, treatment could be tapered to 3 times per week after the first month, and tapered again to 2 times per month beginning possibly on the 4^{th} month. Also shown in Figure 55 is the dose reduction benefit of one treatment per month, which visibly did not perform well to the other treatments, and also indicates that the chelation compartments (i.e., liver, blood, ST0 and ST1) partially replenishes within a few weeks due to resorption.

An additional review compared the different protracted treatment methods. Figure 56 illustrated starting the protracted treatments on the second month following an initial 3-day series treatment on the first month, which resulted in a 52%, 54% and 57% bone surface dose savings for two treatments per month, one treatment per week and five treatments per week, respectively, up to a total treatment period of one year. This indicated that there is small additional benefit when providing frequent administrations during protracted treatments.

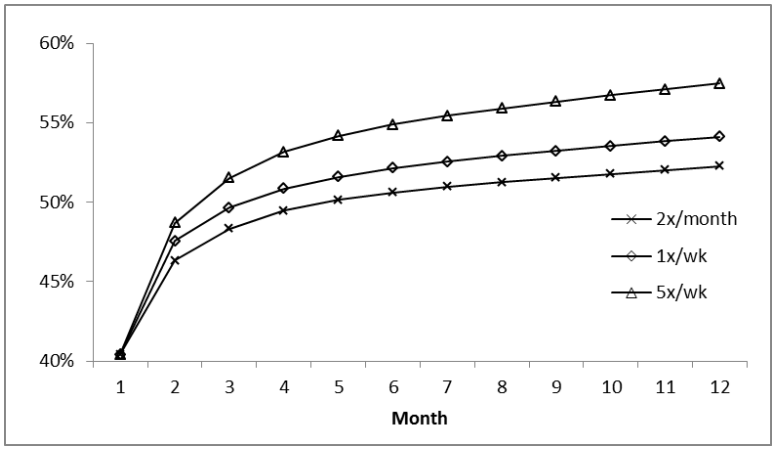

Figure 56: Protracted treatment comparison of cumulative bone surface CEqD savings for the first year, starting with a 3-day series treatment for the first month, followed by various treatments.2 treatments per month (2x/month), 1 treatment per week (1x/wk) and 5 treatments per week for 3 weeks per month (5x/wk) for a ^{239}Pu contaminated wound uptake.

Figure 56 illustrated one possibility of delayed treatments following an initial 3-day series of consecutive treatments administered promptly after intake, with no additional treatment until the start of the second month. The slopes of the lines were similar for 1 treatment per week and 2 treatments per month beyond 3 months.

In summary, this research supported the continued practice of early treatment with 3 consecutive treatments recommended for wound intakes, supplemented by enhanced treatments. A summary of the chelation benefit for wounds was presented in Figure 57 for a typical plutonium wound.

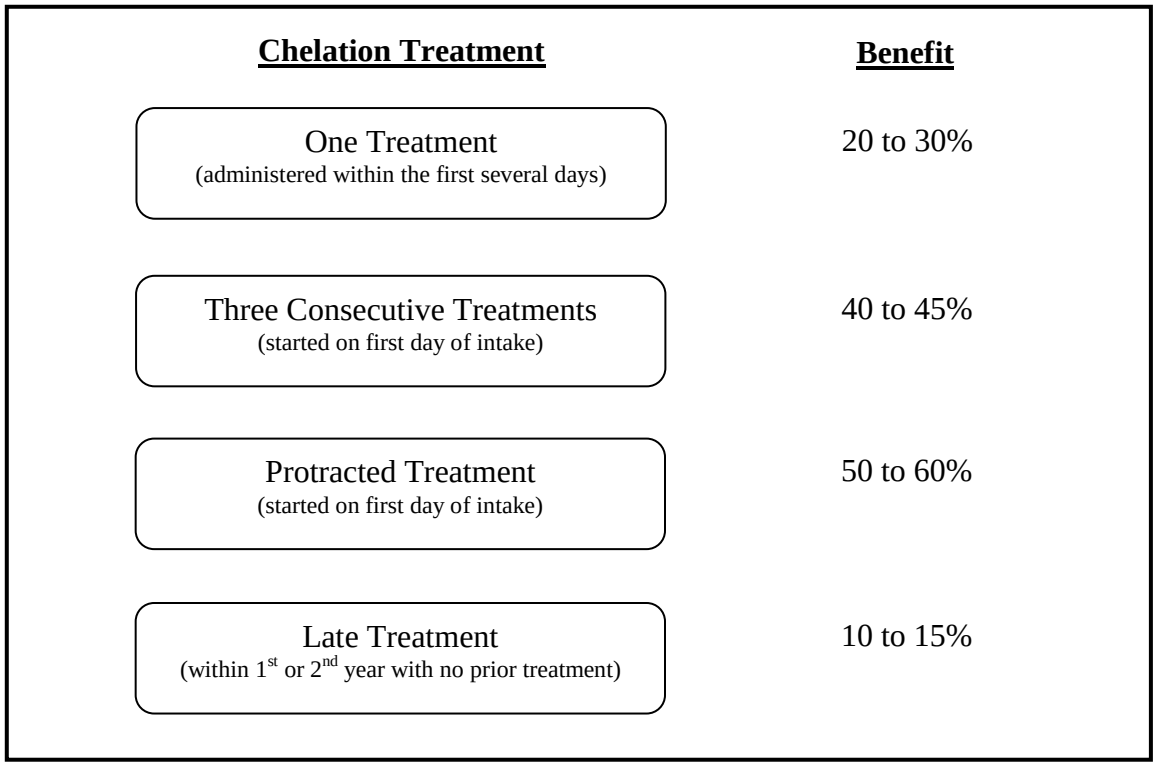

Figure 57: Summary of the chelation benefit for a plutonium contaminated wound.

This research determined that chelation could provide up to approximately a 50 to 60% benefit for long protracted treatment which was also confirmed with the USTUR autopsy case. Therefore, wounds involving a large intake should also consider the value of early tissue excision. Since approximately 50% of the plutonium activity is absorbed within the first few days, priority should be placed on arranging for tissue excision within the first several hours of the incident. The Pu-DTPA model could be used to study different treatment strategies that would provide the best dose savings while also minimizing the burden on the individual, such as reducing the extent of necessary treatments to a tolerable frequency.

4.5.2 Contaminated Inhalation Intakes

Lung intakes of insoluble and moderately soluble particles are cleared primarily via the gastro-intestinal (GI) tract during the first few days; while experiencing some absorption depending on the particles solubility characteristics (ICRP 1994). Figure 58 illustrated the lung burden and blood compartment retention of the reference worker with an aerosol size of 5-µm AMAD using the ICRP 66 lung model coupled with the ICRP 67 systemic model.

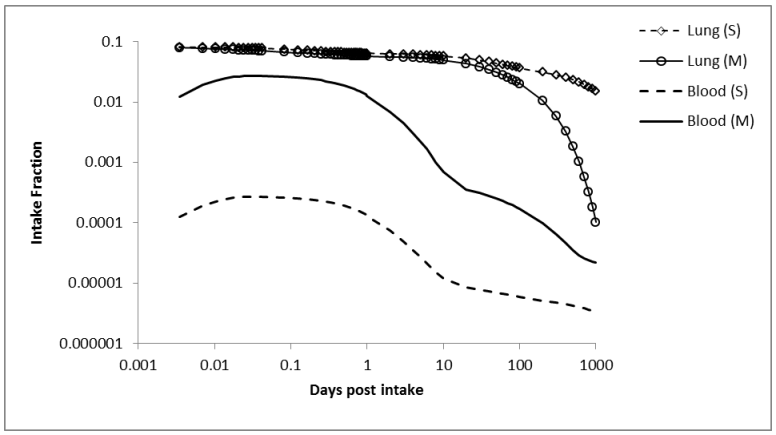

Figure 58: Lung and blood compartment retention for a Type M and Type S absorption.

The blood compartment will reach a peak of approximately 2.7% and 0.03% of the initial intake within the first hour following a moderate (Type M) and insoluble (Type S) intake, respectively. The initial blood compartment uptake indicated that the first day is important with respect to DTPA effectiveness. Chelation treatment is normally not recommended for an insoluble (Type S) intake, where a lung lavage may be advised for significant intakes.

The effectiveness of DTPA administration was studied by reviewing the reduction in compartment transformations to the bone surfaces occurring over a 50-year period

based on one or two treatments that was directly related to the bone surface CEqD. DTPA effectiveness was illustrated in Figure 59 for a Type M and Type S absorption.

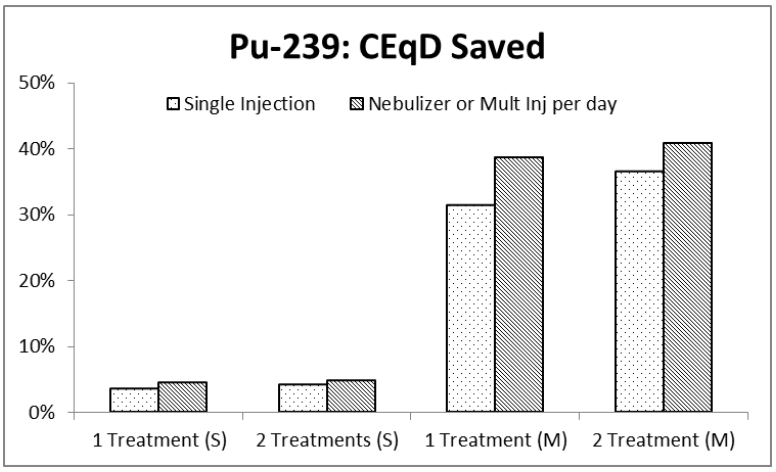

Figure 59: Dose reduction due to DTPA administration for a Type M or Type S absorption.

Figure 59 illustrated that treatment of an inhalation of a Type M absorption could save approximately 30 to 40% of the CEqD for one or two treatments, respectively, while a Type S absorption could save up to 5% of the CEqD. An increased benefit due to enhanced treatments (e.g., application by nebulizer or multiple intra-day injections) was suggested for a single treatment. Another point to consider is that absorption types of mixtures may not be exact and may fall between classifications, such as a mixture of plutonium and americium. It has been observed that some Type S inhalations may have a Type M component, and DTPA treatment may need to be considered for large intakes.

Treatment protocols were also reviewed for a ^{239}Pu Type M absorption inhalation with the results presented in Figure 60.

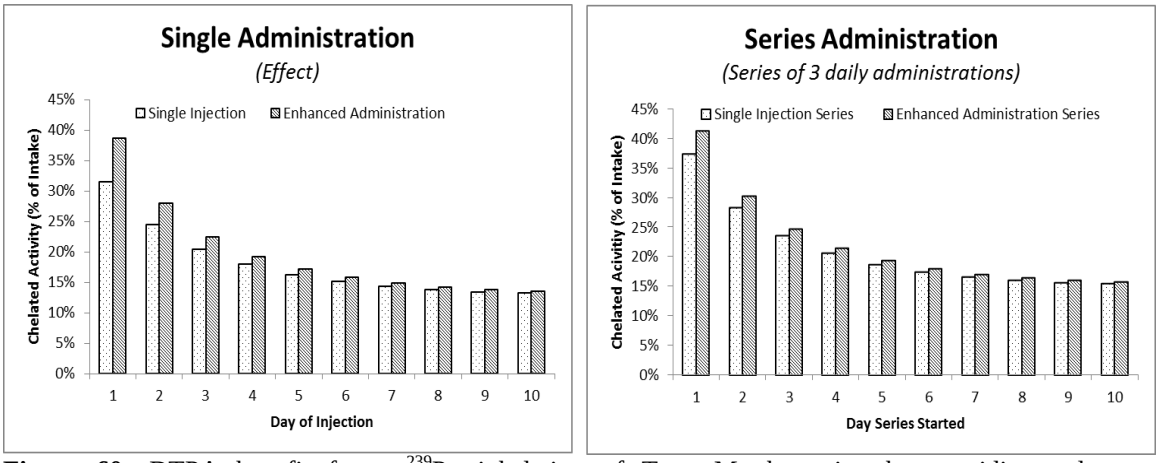

Figure 60: DTPA benefit for a ^{239}Pu inhalation of Type M absorption by providing only one administration, by single or 3-day series injections, including enhanced administration techniques.

Figure 60 illustrates how administration on the first day appears to be substantially better than starting on the second day, of approximately 10%. The best approach would be to use an enhanced DTPA administration on the first day in order to realize the largest benefit. This reflects a Type M absorption, such as Plutonium-nitrate or Americium. A Type S absorption was not studied since there was only a maximum benefit of 5% protracted treatment during the first week.

In summary, this research supported the continued practice of early treatment for an inhalation of a Type M (or unknown) particle absorption, with subsequent treatments on the second and third days for significant intakes. This research also supported enhanced treatment, such as supplementing DTPA administration by injection with nebulized treatment.

Chapter 5: Conclusion

This research goal was to develop a Pu-DTPA model that could be used for estimating intakes based on bioassays that were influenced by chelation. The Pu-DTPA model was developed from a case study of a wound intake and validation performed with a USTUR autopsy case. The Pu-DTPA model integrated with the ICRP 67 model resulted in an improved bioassay prediction involving chelation when compared solely to the ICRP 67 model for IDEAS Case 123. This research also proposed a modification to the ICRP 67 model without requiring additional compartments, thus presenting a parsimonious model that could be easily adopted for use and which provides an improved prediction of compartment distributions. The proposed ICRP 67 modification included a significant adjustment by splitting the liver compartments based on physiological assumptions of separating the hepatocyte activity from the Kupffer cells. The proposed ICRP 67 modification resulted in an improved bioassay prediction when compared to the ICRP 67 model for the human data used in this research. Both the Pu-DTPA model and the proposed modification to the ICRP 67 model also resulted in an improved bioassay prediction when compared to IDEAS Case 123 and USTUR Case 0269. The prediction of the final tissue burden compared well with the final tissue autopsy analysis. Predictions were within 5% of the total skeleton, liver, testes, soft tissues and systemic burden. This research concluded that there was no benefit in adding skeleton decorporation to the Pu-DTPA model due to the close agreement of the predicted skeleton activity to the USTUR autopsy case. This supports the idea that reduction of the skeleton activity was likely related to decreasing the systemic burden by decorporating soft tissues, liver, blood and extracellular fluids.

A Pu-DTPA biokinetic model was developed for estimating plutonium intakes with recommended treatment strategies for intakes due to wounds and inhalations for providing an optimum decorporation benefit. Treatment for a plutonium wound intake included a 3-day series of initial treatments and prompt treatment for Type M particle absorption inhalation, with further enhancement possible based on treatment application. Ca-DTPA administration introduces the potential of negative side effects that increase with extended treatment and administering fractionated doses over the course of a day; however, it had the greatest decorporation benefit on the first day following a plutonium intake. Treatment with Zn-DTPA did not result in negative side effects and provided the same decorporation benefit following the first day. Treatment of occupational intakes is likely to only reduce the stochastic risk of cancer by approximately 50% with extended treatment with the largest treatment benefit occurring the first several days. The methods presented are recommended methods and may vary depending on the specifics of each case regarding the intake quantity, route of intake, and nature of the contaminant.

Chapter 6: References

Anderson CP, Shen L, Eisenstein RS, Leibold EA. Mammalian iron metabolism and its control by iron regulatory proteins. Biochim Biophys Acta. 1823(9): 1468-1483; 2012.

Arnold JS, Jee WSS. Pattern of long term skeletal remodeling revealed by radioautographic distribution of Pu^{239} in dogs. Health Physics 8:705-707; 1962.

Babiker MM. Binding of [^{51}Cr]Ethylenediaminetetraacetate to proteins of human plasma. J Physiol. 374: 117-122; 1986.

Barrett KE, Barman SM, Boitano S, Brooks HL. Ganong's Review of Medical Physiology-24th Ed., McGraw-Hill Lange Medical, United States; 2012.

Beal SL, Sheiner LB. Heteroscedastic nonlinear regression. Technometrics 30:327-338; 1988.

Bevington PR, Robinson DK. Data reduction and error analysis for the physical sciences. 3rd Ed. McGraw-Hill Companies, Inc., New York; 2003.

Bhattacharyya MH, Peterson DP, Lindenbaum A. Action of DTPA on hepatic plutonium: 1. Quantitation of the DTPA-induced biliary excretion of plutonium in the rat. Radiation Research 74:179-185; 1978.

Bilezikian JP, Raisz LG, Martin TJ. Principles of bone biology – third edition, Academic Press, San Diego; 2008.

Birchall A, James AC, A microcomputer algorithm for solving first-order compartmental models involving recycling, Health Phys. 56(6): 857-868; 1989.

Boonrungsiman S, Gentleman E, Carzaniga R, Evans ND, McComb DW, Porter AE, Stevens MM. The role of intracellular calcium phosphate in osteoblast-mediated bone apatite formation. PNAS 109(35): 14170-14175; 2012.

Breustedt B, Blanchardon E, Berard P, Fritsch P, Giussani A, Lopez MA, Luciani A, Nosske D, Piechowski J, Schimmelpfeng J, Serandour AL. Biokinetic modeling of DTPA decorporation therapy: the CONRAD approach. Radiation Protection Dosimetry 134(1):38-48; 2009.

Breustedt B, Blanchardon E, Berard P, Fritsch P, Giussani A, Lopez MA, Luciani A, Nosske D, Piechowski J, Schimmelpfeng J, Serandour AL. The CONRAD approach to biokinetic modeling of DTPA decorporation therapy. Health Phys. 99(4):547-552; 2010.

Bridges KR, Cudkowicz A. Effect of iron chelators on the transferrin receptor in K562 cells. J Biological Chemistry 259(21): 12970-12977; 1984.

Carbaugh EH, Decker WA, Swint MJ. Medical and health physics management of a plutonium wound. Radiation Protection Dosimetry 26(1):345-349; 1989.

Castellani CM, Marsh JW, Hurtgen C, Blanchardon E, Berard P, Giussani A, Lopez MA. IDEAS guidelines (version 2) for the estimation of committed doses from incorporation monitoring data. European Radiation Dosimetry Group e.V., EURADOS-2013-01, Branschweig; 2013.

Catsch A. (moderator). Diagnosis and treatment of incorporated radionuclides: round table discussion. IAEA Proceedings, Vienna :617-625; 1976.

Cheng Y, Zak D, Alsen P, Harrison SC, Walz T. Structure of the human transferrin receptor-transferrin complex. Cell 116(4):565-576; 2004.

Chipperfield AR, Taylor DM. Binding of plutonium to glycoproteins in vitro. Radiation Research 43:393-402; 1970.

Chipperfield AR, Taylor DM. The binding of thorium(IV), plutonium(IV), americium(III), and curium(III) to the constituents of bovine cortical bone in vitro. Radiation Research 51:15-30; 1972.

Clarke B. Normal bone anatomy and physiology. Clin J Am Soc Nephrol 3:S131-S139; 2008.

Cohen N, Guilmette RA, Wrenn ME. Chelation of 241Am from the liver and skeleton of adult baboon. Radiation Research 58:439-447; 1974.

Crabtree RH. The organometallic chemistry of the transition metal, 4th Ed. John Wiley and Sons, Inc. Hoboken; 2005.

De Domenico I, McVey Ward D, Kaplan J. Hepcidin and ferroportin: the new players in iron metabolism. Semin Liver Dis. 31(3): 272-279; 2011.

Doerfel H, Andrasi A, Bailey M, Berkovski V, Blanchardon E, Castellani CM, Hurtgen C, LeGuen B, Malatova I, Marsh J, Stather J. General guidelines for the estimation of committed effective dose from incorporation monitoring data. Wissenschaftliche Berichte FZKA 7243, Forschungszentrum Karlsruhe in der Helmholtz-Gemeinschaft; 2006.

Durbin PW. Plutonium in man: a twenty-five year review. Lawrence Radiation Laboratory, Division of Biology and Medicine, University of California, UCRL 20850, Berkeley; 1971.

Durbin PW. Plutonium in mammals: influence of plutonium chemistry, route of administration, and physiological status of the animal of initial distribution and long-term metabolism. Health Phys. 29:495-510; 1975.

Durbin PW. Lauriston S. Taylor Lecture: The quest for therapeutic actinide chelators. Health Phys. 95(5): 465; 2008.

Durbin PW, Schmidt, CT. Part V: Implications for metabolic modeling, Health Phys. 49(4): 623-661, 1985.

Durbin PW, Schmidt CT. Dosimetric Models: Physiologically based pharmacokinetics: Predicting the kinetics of chelating agents in man from animal data, Health Physics 57 (Sup. 1): 165-174; 1989.

Durbin PW, Jeung N. Collected original data on distribution of ^{238}Plutonium in plasma and excreta of monkeys. Division of Research Medicine and Radiation Biophysics, Lawrence Berkeley Laboratory. LBL-28651; 1990.

Durbin PW, Horovitz MW, Close ER. Plutonium deposition kinetics in the rat. Health Phys. 22:731-741; 1972.

Durbin PW, Kullgren B, Xu J, Raymond KN. Development of decorporation agents for the actinides. Radiation Protection Dosimetry 79(1-4):433-443; 1998.

Fawcett DW. Bloom and Fawcett: Concise Histology, Chapman and Hall, New York; 1997.

Flora SJS, Pachauri V. Chelation in metal intoxication. Int. J. Environ. Res. Public Health 7: 2745-2788; 2010.

Forejtnikova H, Vieillevoye M, Zermati Y, Lambert M, Pellegrino RM, Guihard S, Gaudry M, Camaschella C, Lacombe C, Roetto A, Mayeux P, Verdier F. Transferrin receptor 2 is a component of the erythropoietin receptor complex and is required for efficient erythropoiesis. Blood 116(24):5357-5367; 2010.

Fritsch P, Serandour AL, Gremy O, Phan G, Tsapis N, Fattal E, Benech H, Deverre JR, Poncy JL. Structure of a single model to describe plutonium and americium decorporation by DTPA treatments. Health Phys. 99(4):553-559; 2010.

Ganong WF. Review of medical physiology – 21st Ed. McGraw-Hill Companies, Inc., United States; 2003.

Garcia-Torano E. A comparative study of minimization methods in the fitting of alpha-particle spectra. Nucl. Instr. And Meth. A 369: 608-612; 1996.

Ghoti H, Fibach E, Westerman M, Gordana O, Ganz T, Rachmilewitz E. Increased serum hepcidin levels during treatment with deferasirox in iron-overloaded patients with myelodysplastic syndrome. British Journal of Haemotology 153:118-120; 2011.

Goulet V, Dutang C, Maechler M, Firth D, Shapira M, Stadelmann M. expm: Matrix exponential. R package version 0.99-0; available at: http://CRAN.R-project.org/package=expm; 2012.

Grappin L, Berard P, Menetrier F, Carbone L, Courtay C, Castagnet X, Le Goff JP, Neron MO, Piechowski J. Treatment of actinide exposures: A review of Ca-DTPA injections inside CEA-COGEMA plants, Radiation Protection Dosimetry 127(1-4): 435-439; 2007.

Gregoratto D, Marsh JW. Note on the autocorrelation coefficient as a test statistic for assessment of the goodness-of-fit of biokinetic models to multiple bioassay data sets. Radiation Protection Dosimetry 157(3): 442-445; 2013.

Gremy O, Tsapis N, Chau Q, Renault D, Abram MC, Van der Meeren A. Preferential decorporation of americium by pulmonary administration of DTPA dry powder after inhalation of aged PuO_2 containing americium in rats. Radiation Research 174:637-644; 2010.

Gropper SS, Smith JL, Groff JL. Advanced Nutrition and Human Metabolism, 5th ed., Wadsworth Cengage Learning, Belmont, CA; 2009.

Grube BJ, Stevens W, Atherton DR. The retention of plutonium in hepatocytes and sinusoidal lining cells isolated from rat liver. Radiation Research 73:168-179; 1978.

Hall RM, Poda GA, Fleming RR, Smith JA. A mathematical model for estimation of plutonium in the human body from urine data influenced by DTPA therapy. Health Phys. 34:419-431; 1978.

Hall JE, Guyton and Hall textbook of medical physiology – 12th Ed. Saunders Elsevier, Philadelphia; 2011.

Ham GJ, Harrison JD. The gastrointestinal absorption and urinary excretion of plutonium in male volunteers. Radiat Prot Dosimetry 87(4): 267-272; 2000.

Hameln Pharmaceuticals. Prescribing information for pentetate calcium trisodium and pentetate zinc trisodium injections. Hameln Pharmaceuticals, Hameln; 2004.

Hershko C. A study of the chelating agent diethylenetriaminepentaacetic acid using selective radioiron probes of reticuloendothelial and parenchymal iron stores. J Lab Clin Med 85(6):913-921; 1975.

Hurtgen C, Andrasi A, Bailey M, Blanchardon E, Berkovski V, Castellani CM, Doerfel H, Jourdain JR, LeGuen B, Malatova I, Marsh J, Puncher M. IDEAS internal contamination database: a compilation of published internal contamination cases. A tool for the internal dosimetry community. Radiation Protection Dosimetry 125(1-4):520-522; 2006.

International Atomic Energy Agency. Diagnosis and treatment of incorporated radionuclides. Proceedings of an international seminar on diagnosis and treatment of incorporated radionuclides, 8-12 December 1975: International Atomic Energy Agency, Vienna; 1976.

International Atomic Energy Agency. Treatment of incorporated transuranium elements. IAEA Technical Report Series No. 184: International Atomic Energy Agency, Vienna; 1978.

International Atomic Energy Agency. Methods for assessing occupational radiation doses due to intakes of radionuclides. IAEA Safety Report Series No. 37: International Atomic Energy Agency, Vienna; 2004.

International Commission on Radiological Protection. The metabolism of compounds of plutonium and other actinides. Oxford: Pergamon Press; ICRP Publication 19; 1972.

International Commission on Radiological Protection. Limits on intakes of radionuclides by workers. Oxford: Pergamon Press; ICRP Publication 30, Part 1; Ann ICRP 2(3/4); 1979.

ICRP. 1990 recommendations of the International Commission on Radiological Protection. ICRP Publication 60; Ann ICRP 21(1-3); 1991.

International Commission on Radiological Protection. Age dependent doses to members of the public from intake of radionuclides: Part 2 Ingestion dose coefficients. Oxford: Pergamon Press; ICRP Publication 67; Ann ICRP 23(3/4); 1993.

International Commission on Radiological Protection. Human respiratory tract model for radiological protection. Oxford: Pergamon Press; ICRP Publication 66; Ann ICRP 24(1-3); 1994.

International Commission on Radiological Protection. Basic anatomical and physiological data for use in radiological protection reference values. Oxford: Pergamon Press; ICRP Publication 89; Ann ICRP 32(3-4); 2002a.

International Commission on Radiological Protection. Guide for the Practical Application of the ICRP Human Respiratory Tract Model, ICRP Supporting Guidance 3. Pergamon Press; (Volume 32, Issues 1-2); 2002b.

James AC, Sasser LB, Stuit DB, Glover SE, Carbaugh EH. USTUR whole body case 0269: demonstrating effectiveness of I.V. Ca-DTPA for Pu. Radiation Protection Dosimetry 127 (1-4):449-455; 2007.

Jee WSS, Distribution and toxicity of ^{239}Pu in bone. Health Phys. 22: 583-595; 1972.

Jee WSS, Stover BJ, Taylor GN, Christensen WR. The skeletal toxicity of Pu^{239} in adult beagles. Health Phys. 8: 599-607; 1962.

Jensen MP, Gorman-Lewis D, Aryal B, Paunesku T, Vogt S, Rickert PG, Seifert S, Lai B, Woloschak GE, Soderholm L. An iron-dependent and transferrin-mediated cellular uptake pathway for plutonium. Nat Chem Biol 7(8): 560-565; 2012.

Kawabata H, Nakamaki T, Ikonomi P, Smith RD, Germain RS, Koeffler HP. Expression of transferrin receptor 2 in normal and neoplastic hematopoietic cells. Blood 98(9):2714-2719; 2001.

Konzen K, Brey R. Development of the plutonium-DTPA biokinetic model. Health Phys. Manuscript submitted for publishing; 2014.

Konzen K, Brey R, Guilmette R. Early blood plutonium retention in nonhuman primates compared to the NCRP 156 wound biokinetic model. Health Phys. Manuscript in press; 2014.

Langham WH, Bassett SH, Harris PS, Carter RE. Distribution and excretion of plutonium administered intravenously to man. Health Phys. 38:1031-1060; 1980.

Lattin J, Carroll JD, Green PE. Analyzing Multivariate Data. Brooks/Cole, Cengage Learning, Belmont; 2003.

Leggett RW. A model of the retention, translocation and excretion of systemic Pu, Health Physics 49(6): 1115-1137; 1985.

Leggett RW. A retention-excretion model for americium in humans. Health Physics 62(4):288-310; 1992.

Leggett RW. Reliability of the ICRP's dose coefficients for members of the public. III. Plutonium as a case study of uncertainties in the systemic biokinetics of radionuclides. Radiation Protection Dosimetry 106(2):103-120; 2003.

Leggett RW, Eckerman KF, Khokhryakov VF, Suslova KG, Krahenbuhl MP, Miller SC. Mayak Worker Study: An improved biokinetic model for reconstructing doses from internally deposited plutonium, Radiat. Res. 164:111–122; 2005.

Lloyd RD, Mays CW, McFarland SS, Taylor GN, Atherton DR. A comparison of Ca-DTPA and Zn-DTPA for chelating ^{241}Am in Beagles. Health Phys. 31: 281-284; 1976.

Lloyd RD, Mays CW, Jones CW, Atherton DR, Bruenger FW, Shabestari LR, Wrenn ME. Retention and dosimetry of injected ^{241}Am in beagles. Radiation Research 100: 564-575; 1984.

Luciani A, Polig E. Verification and modification of the ICRP-67 model for plutonium dose calculation, Health Phys. 78(3): 303-310; 2000.

Luciani A, Polig E. Surface-seeking radionuclides in the skeleton: Current approach and recent developments in biokinetic modeling for humans and beagles, Radiation Protection Dosimetry 127(1-4): 140-143; 2007.

Luciani A, Doerfel H, Polig E. Sensitivity analysis of the urinary excretion of plutonium. Radiation Protection Dosimetry 93(2): 179-183; 2001.

Luciani A, Polig E, Lloyd RD, Miller SC. Americium in the beagle dog: biokinetic and dosimetric model. Health Phys. 90(5): 459-470; 2006.

Marsh JW, Blanchardon E, Castellani CM, Desai AD, Dorrian MD, Hurtgen C, Koukouliou V, Lopez MA, Luciani A, Puncher M, Andrasi A, Bailey MR, Berkovski V, Birchall A, Bonchug Y, Doerfel H, Malatova I, Molokanov A, Ratia H. Evaluation of scattering factor values for internal dose assessment following the ideas guidelines: preliminary results. Radiation Protection Dosimetry 127(1-4): 339-342; 2007.

Matsuo K, Irie N. Osteoclast-osteoblast communication. Archives of Biochemistry and Biophysics 473:201-209; 2008.

Mayle KM, Le AM, Kamei DT. The intracellular trafficking pathway of transferrin. Biochimica et Biophysica Acta 1820:264-281; 2012.

Mays CW, Lloyd RD, Taylor GN, Wrenn ME. Cancer incidence and lifespan vs. α-particle dose in beagles. Health Phys. 52:617-624; 1987.

McCorry LK. Essentials of Human Physiology for Pharmacy, 2nd Ed. CRC Press: Taylor and Francis Group, Boca Raton, FL; 2009.

Metzler D. Biochemistry: the chemical reactions of living cells. Academic Press, San Diego, CA; 2001.

Moore RC, Gasser M, Awwad N, Holt KC, Salas FM, Hasan A, Hasan MA, Zhao H, Sanchez CA. Sorption of plutonium(VI) by hydroxyapatite. Journal of Radioanalytical and Nuclear Chemistry 23(1):97-101; 2005.

National Council on Radiation Protection and Measurements. Development of a biokinetic model for radionuclide contaminated wounds and procedures for their assessment, dosimetry and treatment. Bethesda, MD: NCRP; NCRP Report No. 156; 2007.

Newton D, Talbot RJ, Kang C, Warner AJ. Uptake of plutonium by the human liver. Radiat Prot Dosimetry 80(4): 385-395; 1998.

O'Boyle NC, Nicholson GP, Piper TJ, Taylor DM, Williams DR, Williams G. A review of plutonium(IV) selective ligands, Appl. Radiat. Isot. 48(2): 183-200; 1997.

Palaneeswari S, Ganesh M, Karthikeyan t, Manjula Devi A, Mythili S. Hepcidin – minireview. Journal of Clinical and Diagnostic Research 7(8):1767-1771; 2013.

Phan G, Ramounet-Le Gall B, Manceau J, Fanet M, Benech H, Fritsch P, Fattal E, Deverre JR. Targeting of diethylene triamine pentaacetic acid encapsulated in liposomes to rat liver: an effective strategy to prevent bone deposition and increase urine elimination of plutonium in rats. Int J Radiat Biol 80(6):413-422; 2004.

Pippard MJ, Jackson MJ, Hoffman K, Petrou M, Modell CB. Iron chelation using subcutaneous infusions of diethylene triamine penta-acetic acid (DTPA). Scand J Haematol 36: 466-472; 1986.

Polig E. Labels of surface-seeking radionuclides in the human skeleton, Health Phys. 72(1): 19-33; 1997.

Polig E., Modeling the distribution and dosimetry of internal emitters: A review of mathematical procedures using matrix methods, Health Phys. 81(5):492–501; 2001.

Polig E, Bruenger FW, Lloyd RD, Miller SC. Microdistribution of ^{239}Pu in the beagle skeleton. Health Phys. 75(3):251-258; 1998.

Polig E, Bruenger FW, Lloyd RD, Miller SC. Biokinetic and dosimetric model of plutonium in the dog. Health Phys. 78(2):182-190; 2000.

Pounds JG, Long GJ, Rosen JF. Cellular and molecular toxicity of lead in bone. Environmental Health Perspectives 91:17-32; 1991.

Puncher M, Birchall A, Marsh JW. The autocorrelation coefficient as a tool for assessing goodness of fit between bioassay predictions and measurement data. Radiation Protection Dosimetry 127(1-4): 370-373; 2007.

R Core Team. R: A language and environment for statistical computing (Version R-2.15.2). R Foundation for Statistical Computing, Vienna, Austria. ISBN 3-900051-07-0. Retrieved January 19, 2013. Available from http://www.R-project.org/; 2013.

Raisz LG. Physiology and pathophysiology of bone remodeling. Clinical Chemistry 45(8):1353-1358; 1999.

Ramsey FL, Schafer DW. The statistical sleuth: a course in methods of data analysis (2nd ed), Duxbury; 2002.

Rice JA, Mathematical Statistics and Data Analysis – Third Edition, Brooks/Cole, Cengage Learning, Belmont; 2007.

Richardson RB. A physiological skeletal model for radionuclide and stable element biokinetics in children and adults. Health Phys. 99(4):471-482; 2010.

Roedler HD, Nosske D, Ohlenschlager L, Schieferdecker H, Doerfel H, Renz K. Incorporation of ^{241}Am: effectiveness of late DTPA chelation therapy. Radiation Protection Dosimetry 26(1-4):377-379; 1989.

Rosenthal MW, Lindenbaum A. Influence of DTPA therapy on long-term effects of retained monomeric plutonium: comparison with polymeric plutonium. Radiation Research 31:506-521; 1967.

Rosenthal MW, Lindenbaum A, Russell JJ, Moretti E, Chladek D. Metabolism of monomeric and polymeric plutonium in the rabbit; comparison with the mouse. Health Physics 23:231-238; 1972.

Ross MH, Pawlina W. Histology: a text and atlas: with correlated cell and molecular biology - 6th Ed., Wolter Kluwer, Lippincott Williams & Wilkins, Baltimore; 2011.

RStudio. RStudio: Integrated development environment for R (Version 0.97.310). Boston, MA. Retrieved January 19, 2013. Available from http://www.rstudio.org/; 2013.

Rundo J, Starzyk PM, Sedlet J, Larsen RP, Oldham RD, Robinson JJ. The excretion rate and retention of plutonium 10,000 days after acquisition. In Diagnosis and Treatment of Incorporated Radionuclides. IAEA-SR-6/23, Vienna: 15-22; 1976.

Russell CD, Bischoff PG, Rowell KL, Kontzen F, Lloyd LK, Tauxe WN, Dubovsky EV. Quality control of Tc-99m DTPA for measurement of glomerular filtration: concise communication. J Nucl Med 24: 722-727; 1983.

Sanders CL, Maintenance of phagocytic function following $^{239}PuO_2$ particle administration. Health Phys. 18: 82-85; 1970.

Schimmelpfeng J. Physiology-based modeling in radiation research: The biokinetics of plutonium, Radiation Protection Dosimetry 136(2): 74-81; 2009.

Schubert J, Fried JF, Rosenthal MW, Lidenbaum A. Tissue distribution of monomeric and polymeric plutonium as modified by a chelating agent. Radiation Research 15:220-226; 1961.

Sims NA, Gooi JH. Bone remodeling: multiple cellular interactions required for coupling of bone formation and resorption. Seminars in Cell & Developmental Biology 19:444-451; 2008.

Sohn Y, Mitterstiller A, Breuer W, Weiss G, Cabantchik Z. Rescuing iron-overloaded macrophages by conservative relocation of the accumulated metal. British Journal of Pharmacology 164:406-418; 2011.

Stather JW, Smith H, Bailey MR, Birchall A, Bulman A, Crawley FEH. The retention of ^{14}C-DTPA in human volunteers after inhalation or intravenous injection. Health Phys. 44(1):45-52; 1983.

Talbot RJ, Newton D, Warner AJ. Metabolism of injected plutonium in two healthy men. Health Phys 65(1): 41-46; 1993.

Talbot RJ, Newton D, Dmitriev SN. Sex-related differences in the human metabolism of plutonium. Radiat Prot Dosimetry 71(2): 107-121; 1997.

Talmage DW, Talmage RV. Calcium homeostasis: how bone solubility relates to all aspects of bone physiology. J Musculoskelet Neuronal Interact 7(2):108-112; 2007.

Taylor DM. Interactions between transuranium elements and the components of cells and tissues. Health Phys. 22: 575-581; 1972.

Taylor DM. The bioinorganic chemistry of actinides in blood. Journal of Alloys and Compounds 6-10:271-273; 1998.

Taylor GN, Williams JL, Roberts L, Atherton DR, Shabestari L. Increased toxicity of Na_3CaDTP when given by protracted administration. Health Phys. 27: 285-288; 1974.

Taylor GN, Lloyd RD, Boseman JJ, Atherton DR, Mays CW. Removal of plutonium from beagles using Ca-DTPA and Zn-DTPA: effects of initial DTPA injection. Health Physics 35:201-210; 1978.

Teti A, Zallone A. Do osteocytes contribute to bone mineral homeostasis? Osteocytic osteolysis revisited. Bone 44:11-16; 2009.

Thomson BM, Smith CL, Busch RD, Siegel MD, Baldwin C. Removal of metals and radionuclides using apatite and other natural sorbents. Journal of Environmental Engineering 129(6):492-499; 2003.

U.S. Department of Energy (DOE). Linking Legacies: Connecting the cold war nuclear weapons production processes to their environmental consequences. U.S. Department of Energy Office of Environmental Management, DOE/EM-0319, Washington D.C.; 1997.

U.S. Department of Health and Human Services (DHHS). Toxicological profile for plutonium, Public Health Service Agency for Toxic Substances and Disease Registry, Atlanta GA; 2010.

Venables WN, Smith DM, R Core Team. An introduction to R. Notes on R: a programming environment for data analysis and graphics Version 2.15.2; 2012.

Volf V, Luz A, Schaffer E, Muller WA, Rencova J. Effect of oral ZnDTPA on late effects of injected plutonium in rat, Int. J. Radiat. Biol. 75(8):929-941; 1999.

Wang Y. On the Big-R notation for describing iterative and recursive behaviors. Int'l Journal of Cognitive Informatics and Natural Intelligence 2(1):17-28; 2008.

Wisse E, Braet F, Luo D, De Zanger R, Jans D, Crabbe E, Vermoesen A. Structure and function of sinusoidal lining cells in the liver. Toxicologic Pathology 24(1): 100-111; 1996.

Appendixes

Appendix 1: R Functions

Introduction:

The following R functions were created for use in this research. The function should be able to be installed into R by copying and pasting the function. Each function provides a description on its purpose. This research used R version 3.0.2, with RStudio (2013) version 0.98.501, both of which are available at http://cran.r-project.org/ and http://www.rstudio.com/, respectively. Most of the functions require input of the rate matrix with some requiring the bioassay sample results and input of treatment days, which are assigned on the day bioassay is collected. For example, if treatment is given on day 0 and a urine bioassay is collected on day 1, then the chelation day was specified as day 1. The R programming language requires some knowledge of its use which can be obtained by formal instruction or by studying the many tutorials available, such as at the http://cran.r-project.org/.

When installing a function, the function can be copied from this document and pasted into R, or one may type ">fix(<<insert function name>>)" and enter the function excluding the function name. This method can also be used for editing the function. Tip: the R language is case sensitive; therefore, if a function is capitalized, such as "Chi.sq", calling the function by "chi.sq" would not be recognized. Defined functions, assigned tables and matrices can be inspected by ">ls()".

Load

This function loads a rate matrix into the R programming platform. This requires the specified square matrix to be copied from a spreadsheet, such as from MS Excel, to the clipboard prior to calling the function.

Example: To specify a rate matrix as ‘R1’, select all of the column and row headers with the associated transfer rates and select copy from the spreadsheet, then open R and enter:

>R1=load()$R

This function translates the table into a matrix, assigns “0” for nonspecified cells, and ensures that the row and column headers are the same.

Function:

```
load = function(R) {
R=read.table("clipboard",sep="\t",header=T)
R=R[,-1]
row.names(R)=colnames(R)
head(R)
N = dim(R)[1]
for (i in 1:N) {
   for (j in 1:N) {
      if (is.na(R[i, j]))
         R[i, j] = 0
   }
}
structure(list(R=R))
}
```

Decays

This function analyzes the rate matrix (R) based on time (t) of interest and half-life (h), both specified in days, providing compartment quantities and transformations based on methods described by Birchall and James (1989) algorithm. The rate matrix was constructed for an intake of 1 Bq. This function requires the 'expm' package to be installed for performing the matrix exponential. If the 'expm' package is unavailable, then the function can be modified to use the eigen function that is provided in the base package, by commenting (i.e., insert '#' in front of the step) the expm steps and removing the commenting for the eigen steps.

Example: To obtain a list of compartment quantities and transformations for a strong-retention wound intake of ^{239}Pu at 100 days post intake, enter:

>decays(R=R1, t=100, h=24065*365)

Function:

```
decays = function (R, t, h)
#R is rate matrix, t is time of interest (days) and h is halflife (days).
{
  require(expm)
   R = as.matrix(R)
   X0 = diag(R)
   lam = log(2)/h
   A = t(R)
   N = dim(R)[1]
   for (i in 1:N) {A[i, i] = -sum(R[i, -i]) - lam}
   #V = eigen(A)$vectors
   #D = diag(eigen(A)$values)
   #D.exp = diag(exp(eigen(A)$values * t))
   #A.exp = V %*% D.exp %*% solve(V)
   A.exp=expm(A*t)
   B = A.exp - diag(1, dim(A)[1])
   trans = lam * solve(A) %*% B %*% X0
   trans=trans/lam*86400
   X = A.exp %*% X0
   X[N - 1] = X[N - 1]+trans[N-1]
   X[N] = X[N]+trans[N]
   ttl = cbind(X0, X, trans)
```

```
colnames(ttl) = c("Initial (Bq)", "Final (Bq)", "decays")
row.names(ttl) = colnames(R)
structure(list(summary = ttl), class = "decays")}
```

Sens

This function performs a sensitivity analysis over all the rate matrix specified compartments for the time periods of interest, while also segregating the most influential compartments for urine, feces, blood and skeleton. The input requires the rate matrix to be specified with the time period of interest.

Example: To find the important compartments for the 100th day for the R.Pu rate matrix:
>Sens(R=R.Pu, t=100)

Function:

```
Sens=function (R=R,t=10)
{
#the rate matrix must have urine in the last row and feces in the second to last row
#the rate matrix must have Cort.Surf and Trab.Surf as headers for the bone surfaces
val=matrix(c(0,0,0,0,0,0,0,0,0,0,0,0),nrow=1,byrow=T)
colnames(val)=c("coef","compartment.1","compartment.2","transfer.rate","row","col","U.sens","F
.sens","B.sens","BS.sens","k1","k2","k3")
val=val[-1,]
h.days=24131*365.25
tf=50*365.25
t=t
N=dim(R)[1]
for(i in 1:N){
   if(colnames(R)[i]=="Cort.Surf" || colnames(R)[i]=="CortBS" || colnames(R)[i]=="CortSurf")
k1=i
   if(colnames(R)[i]=="Trab.Surf" || colnames(R)[i]=="TrabBS" || colnames(R)[i]=="TrabSurf")
k2=i
   if(colnames(R)[i]=="Blood") k3=i
}

p=1
for(i in 1:N){
        for(j in 1:N){
                if(R[i,j]>0 && i!=j) {
                u1=decays(R, t, h.days)$summary[N, 2];
                f1=decays(R,t,h.days)$summary[N-1,2];
                s1=decays(R,tf,h.days)$summary[k1,3] + decays(R,tf,h.days)$summary[k2,3];
                b1=decays(R,t,h.days)$summary[k3,2];
                op=R[i,j];
                dp=R[i,j]*1.01;
                R[i,j]=dp;
                u2=decays(R, t, h.days)$summary[N, 2];
                f2=decays(R,t,h.days)$summary[N-1,2];
                s2=decays(R,tf,h.days)$summary[k1,3] + decays(R,tf,h.days)$summary[k2,3];
                b2=decays(R,t,h.days)$summary[k3,2];
                R[i,j]=op;
```

```
                su=round((u2-u1)/u1/0.01,digits=5);
                sf=round((f2-f1)/f1/0.01,digits=5);
                ss=round((s2-s1)/s1/0.01,digits=5);
                sb=round((b2-b1)/b1/0.01,digits=5);

                val=rbind(val,matrix(c(p,row.names(R)[i],colnames(R)[j],R[i,j],i,j,su,sf,sb,ss,k1,
                k2,k3), nrow=1,byrow=T));
                p=p+1;
                }
        }
}
val=as.data.frame(val)
U.val=val[order(abs(as.numeric(as.matrix(val[,7]))),decreasing=TRUE),]
F.val=val[order(abs(as.numeric(as.matrix(val[,8]))),decreasing=TRUE),]
B.val=val[order(abs(as.numeric(as.matrix(val[,9]))),decreasing=TRUE),]
S.val=val[order(abs(as.numeric(as.matrix(val[,10]))),decreasing=TRUE),]

structure(list(val=val,U.val=U.val[1:10,],F.val=F.val[1:10,],B.val=B.val[1:10,],S.val=S.val[1:10,])
)
}
```

R.spec

This function is used to inspect the rate matrix and prints out the rate matrix compartment transfer rates with the corresponding row and column designations.

Example: To inspect the R.Pu rate matrix enter the following:

>R.spec(R=R.Pu)

Function:

```
R.spec=function (R=R)
{
val=matrix(c(0,0,0,0,0,0),nrow=1,byrow=T)
colnames(val)=c("coef","compartment.1","compartment.2","transfer.rate","row","col")
val=val[-1,]

p=1
for(i in 1:dim(R)[1]){
        for(j in 1:dim(R)[2]){
            if(R[i,j]>0) {
                val=rbind(val,matrix(c(p,row.names(R)[i],colnames(R)[j],R[i,j],i,j),nrow=1,byro
        w=T));
                p=p+1;
                }
        }
}
val=as.data.frame(val)
structure(list(val=val))
}
```

Pu.univ

This function provides the compartment quantities for a plutonium rate matrix for a wound with various dimensions that searches for compartments that are universal, including DTPA transitional compartments. The function requires that the rate matrix is defined for the following row and column headers “Blood”, “Bloodt”, “ST0”, “ST0t”, “CortVol”, “Liver1”, and “Liver2”, for compartment specification. The “CortVol” compartment must be the first specified skeleton compartment with the next 5 specified compartments encompassing all of the skeleton compartments. This function requires input of a rate matrix specified for plutonium that includes DTPA compartments, chelation days as a unit vector (d), time in days of interest (t), and halflife in years (h).

Example:

```
>Pu.univ(R=R.PuDTPA, d=c(1,2,3), t=10, h=24065)
```

Function:

```
Pu.univ= function (R=R,d=chel,t=10,h=24065)
{

#this function can take an undefined rate matrix dimensions for DTPA, where d is the chelation
matrix
#and t is the time period of interest.
#this function relies on the following:
#compartment specifications "Blood", "Bloodt", "CortVol" being the first skeleton compartment,
#"Liver1", "Liver2"

   h.days = h * 365.25

#set rate matrices with and without dtpa
   R.dtpa=R
   R.wo=R
#find paths to clear for bare rate matrix
   a=0;b=0;c=0;dd=0;
   for(i in 1:dim(R)[1]){if(colnames(R)[i]=="ST0t")a=i;
   if(colnames(R)[i]=="Bloodt")b=i;
   if(colnames(R)[i]=="Blood")c=i;
   if(colnames(R)[i]=="ST0")dd=i;}
   R.wo[dd:c,a:b]=0;

#set compartment location for urine, feces, blood, liver and skeleton
```

```
ku=dim(R)[1]
kf=ku-1

for(kk in 1:ku){
   if(colnames(R)[kk]=="Blood"){kb1=kk;
                        for(kk2 in (kb1:ku)){
                           if(colnames(R)[kk2]=="Bloodt")kb2=kk2}}
   if(colnames(R)[kk]=="Liver2"){kl1=kk;
                        for(kk2 in (kl1:ku)){
                           if(colnames(R)[kk2]=="Liver1")kl2=kk2}}
   if(colnames(R)[kk]=="CortVol" || colnames(R)[kk]=="Cort.Vol"){ks1=kk;ks2=ks1+5;}
}

Pu.atoms = matrix(c(0, 0, 0, 0, 0, 0,0,0), nrow = 1, byrow = T)
colnames(Pu.atoms) = c("Time(d)", "Urine", "Faeces", "Tot.Body",
   "Skeleton", "Liver","Blood","Wound")
Pu.atoms = Pu.atoms[-1, ]


for (i in 1:t) {
        R=R.wo
        for(j in 1:length(d)){
                if(i==d[j]) R = R.dtpa}
        k = 1;n=I;

        last=decays(R,k,h.days)$summary[,2]

        pu.1 = last[ku] - decays(R,k - 1, h.days)$summary[ku, 2] #incremental urine
        pu.2 = last[kf] - decays(R,k - 1, h.days)$summary[kf, 2] #incremental feces
        pu.3 = sum(last[1:(kf-1)]) #whole body quantity
        pu.4 = sum(last[ks1:ks2])  #total skeleton quantity
        pu.5 = sum(last[kl1],last[kl2]) #,last[27]) #liver quantity
        pu.6 = sum(last[kb1],last[kb2]) #blood quantity
        pu.7 = sum(last[1:4]) #wound quantity
        pu.new = matrix(c(n, pu.1, pu.2, pu.3, pu.4, pu.5,pu.6,pu.7), nrow = 1, byrow = T)
        Pu.atoms = rbind(Pu.atoms, pu.new)

        #Update R matrix diagonal amounts based on last run
        for(j in 1:length(last)){R.dtpa[j,j]=last[j];R.wo[j,j]=last[j];}

}
structure(list(Pu.atoms = Pu.atoms))
}
```

Pu.univF

This function is a variation of Pu.univ that improves optimization time by only providing results specified in the cd matrix for days of interest (i.e., bioassay collection days, chelation treatment days). This function is used with the Rmod.mult2 optimization function.

Example:

```
>Pu.univF(R=R.PuDTPA, d=c(1,2,3), t=10, h=24065, cd=c(1,2,3,4,5,7,9))
```

Function:

```
function (R=R,d=chel,t=10,h=24065,cd=cd)
{

#this function can take an undefined rate matrix dimensions for DTPA, where d is the chelation
matrix
#and t is the time period of interest.
#this function relies on the following:
#compartment specifications "Blood", "Bloodt", "CortVol" being the first skeleton compartment,
#"Liver1", "Liver2"

   h.days = h * 365.25


#set rate matrices with and without dtpa
   R.dtpa=R
   R.wo=R
#find paths to clear for bare rate matrix
   a=0;b=0;c=0;dd=0;
   for(i in 1:dim(R)[1]){if(colnames(R)[i]=="ST0t")a=i;
   if(colnames(R)[i]=="Bloodt")b=i;
   if(colnames(R)[i]=="Blood")c=i;
   if(colnames(R)[i]=="ST0")dd=i;}
   R.wo[dd:c,a:b]=0;
   #R.wo[5:23,25:30]=0
   #R.wo[24,31]=0


#set compartment location for urine, feces, blood, liver and skeleton
   ku=dim(R)[1]
   kf=ku-1

   for(kk in 1:ku){
      if(colnames(R)[kk]=="Blood"){kb1=kk;
          for(kk2 in (kb1:ku)){
              if(colnames(R)[kk2]=="Bloodt")kb2=kk2}}
      if(colnames(R)[kk]=="Liver2"){kl1=kk;
           for(kk2 in (kl1:ku)){
```

```
                if(colnames(R)[kk2]=="Liver1")kl2=kk2}}
            if(colnames(R)[kk]=="CortVol" || colnames(R)[kk]=="Cort.Vol"){ks1=kk;ks2=ks1+5;}
        }

        Pu.atoms = matrix(c(0, 0, 0, 0, 0, 0,0,0), nrow = 1, byrow = T)
        colnames(Pu.atoms) = c("Time(d)", "Urine", "Faeces", "Tot.Body",
            "Skeleton", "Liver","Blood","Wound")
        Pu.atoms = Pu.atoms[-1, ]


        for (i in 1:length(cd)) {
            dU=cd[i]
            if(i>1 && (dU-cd[i-1])>1) k=dU-cd[i-1] else k=1
            R=R.wo
                for(j in 1:length(d)){
                        if(dU==d[j]) R = R.dtpa}

                n=dU

                last=decays(R,k,h.days)$summary[,2]

                pu.1 = last[ku] - decays(R,k - 1, h.days)$summary[ku, 2] #incremental urine
                pu.2 = last[kf] - decays(R,k - 1, h.days)$summary[kf, 2] #incremental feces
                pu.3 = sum(last[1:(kf-1)]) #whole body quantity
                pu.4 = sum(last[ks1:ks2])  #total skeleton quantity
                pu.5 = sum(last[kl1],last[kl2]) #,last[27]) #liver quantity
                pu.6 = sum(last[kb1],last[kb2]) #blood quantity
                pu.7 = sum(last[1:4]) #wound quantity
                pu.new = matrix(c(n, pu.1, pu.2, pu.3, pu.4, pu.5,pu.6,pu.7), nrow = 1, byrow = T)
                Pu.atoms = rbind(Pu.atoms, pu.new)

    #Update R matrix diagonal amounts based on last run
                for(j in 1:length(last)){R.dtpa[j,j]=last[j];R.wo[j,j]=last[j];}

        }
structure(list(Pu.atoms = Pu.atoms))
}
```

Rmod.opt4

This function was used in discovering the Pu-DTPA model using IDEAS Case 123. The rate matrix was specified for the ICRP 67 systemic model coupled with the NCRP 156 wound model with DTPA compartments. This function was upgraded to Rmod.mult and Rmod.mult2 for later analysis. This function was used to optimize the Pu-DTPA model only to the urine bioassay that was specified in a table (C.urine). The function required frequent editing and revising of initial compartment transfer rates. The function optimized compartments that were specified by the 'param' in the input statement that had to match the designations within the function, which varied from the rate matrix compartment names. Standard statistics were provided in the results with an inspection of variable changes during the optimization process. The chelation days were specified in the 'chel' row vector. Intake may be specified within the function. A least squares fitting function 'lm' was used for fitting the parameters. Optimization input parameters included the number of times to repeat all parameter optimizations when one is changed (times); the sensitivity of the chi-square goodness of fit result (sens); the optimization function denominator (opt: set to 3); the precision of the parameter estimate (tight); and specifying either to optimize using the singular weight (weight= 1) or a squared weight (weight=2) in the denominator of the chi-square goodness of fit indicator. If the intake was specified within the function then opt.int ="TRUE", otherwise opt.int= "FALSE" and the intake was calculated.

Example:

```
>Rmod.opt4(R=R.67DTPA.0v1, chel=chel, param=c("ST0.ST0t","BL.BLt"),
times=2,sens=1, opt=3,tight=3,weight=1,opt.int="FALSE")
```

Function:

```
Rmod.opt4= function(R=R.Pu.dtpa,chel=chel,param=c("ST0.ST0t","BL.BLt"),times=2,sens=1, opt=3,tight=3,
weight=1,opt.int="FALSE")
{

#The R matrix is specified, chel is the row vector of days that were chelated, param are the parameters to be fitted,
#times indicates the number of times to cycle through all fitted parameters whenever one changes,
#sens is the change in chi-square value between two parameter values, if less than this amount then the lower one will
#be used for the next iteration, opt is the divisor in the optimization function (normally 3, but can be higher)
#tight relates to how many sig figs are needed, such as 6 will give 2 sig figs, and 9 will give 3, based on the optimization
#function, weight can be 1 for single weight, and 2 for squared weight in the chi-square fitting
#opt.int indicates if the optimization is to include a known intake value, specified as "TRUE" or "FALSE"

  p=length(param)
  cnt=0

  #set initial parameter values
  ST0.ST0t=3.65      #8.32 0.042
  ST1.ST1t=1.93      #8.32
  ST0t.BLt=300      #0.462
  ST1t.BLt=0.12  #0.116
  BL.BLt=1.38        #3.69
  BLt.ULI=0.0     #0.7
  BLt.BLA=45.7    #10
  BLt.ST0t=145    #2.5  3.24
  Sol.BL=0.74     #0.67
  CIS.Sol=0.073   #0.024
  Sol.CIS=0.47     #0.6
  PABS.Sol=.0012
  CIS.PABS=0.01
  A1.Sol=0.4  #0.5   #1
  A2.CIS=0.6  #0.5   #0
  A3.PABS=0.0  #0.0
  L1.L1t=0.649        #0.6
  L1t.BLt=0       #0.609
  L1t.SI=0.27        #0.077
  BLt.L1t=0       #2.67


val=matrix(c(ST0.ST0t,ST1.ST1t,ST0t.BLt,ST1t.BLt,BL.BLt,BLt.ULI,BLt.BLA,BLt.ST0t,Sol.BL,CIS.Sol,Sol.CIS,PABS.Sol,CIS.P
ABS,A1.Sol,A2.CIS,A3.PABS,L1.L1t,L1t.BLt,L1t.SI,BLt.L1t),nrow=1,byrow=T)

colnames(val)=c("ST0.ST0t","ST1.ST1t","ST0t.BLt","ST1t.BLt","BL.BLt","BLt.ULI","BLt.BLA","BLt.ST0t","Sol.BL","CIS.Sol","S
ol.CIS","PABS.Sol","CIS.PABS","A1.Sol","A2.CIS","A3.PABS","L1.L1t","L1t.BLt","L1t.SI","BLt.L1t")

  #place initial parameter values into matrix
  R[5,25]=val[1,1] #ST0.ST0t
  R[6,26]=val[1,2] #ST1.ST1t
  R[25,28]=val[1,3] #ST0t.BLt
  R[26,28]=val[1,4] #ST1t.BLt
  R[24,28]=val[1,5] #BL.BLt
  R[28,20]=val[1,6] #BLt.ULI
  R[28,23]=val[1,7] #BLt.BLA
  R[28,25]=val[1,8] #BLt.ST0t
  R[1,24]=val[1,9]  #Sol.BL
  R[2,1]=val[1,10]  #CIS.Sol
  R[1,2]=val[1,11]  #Sol.CIS
  R[3,1]=val[1,12]  #PABS.Sol
  R[2,3]=val[1,13]  #CIS.PABS
  R[1,1]=val[1,14]  #A1.Sol
  R[2,2]=val[1,15]  #A2.CIS
  R[3,3]=val[1,16]  #A3.PABS
  R[17,27]=val[1,17] #L1.L1t
  R[27,28]=val[1,18] #L1t.BLt
  R[27,19]=val[1,19] #L1t.SI
  R[28,27]=val[1,20] #BLt.L1t
```

```
   #specify modification step
   t=opt

   #specify sensitivity
   s=sens
   times=times
   loops=1

   #specify weight vector of original urine results
   w=1/C.urine[,2]
   w2=w^2

   if(weight==1){ww=w}else{ww=w2}

   #specify row vectors
   q=matrix(c(0,0,0,0,0),nrow=1,byrow=T)
   X=matrix(c(rep(0,p)),nrow=1,byrow=T)

   colnames(X)=param
   chi=matrix(c(0,0,0,0,0),nrow=1,byrow=T)
   change=chi
   change=change[-1,]

   kk=1
while (kk<=tight){
   loops=1
   while(loops<=times){
      for(z in 1:p){
         again=1

          if(param[z]=="ST0.ST0t")k=1
          if(param[z]=="ST1.ST1t")k=2
          if(param[z]=="ST0t.BLt")k=3
          if(param[z]=="ST1t.BLt")k=4
          if(param[z]=="BL.BLt")k=5
          if(param[z]=="BLt.ULI")k=6
          if(param[z]=="BLt.BLA")k=7
          if(param[z]=="BLt.ST0t")k=8
          if(param[z]=="Sol.BL")k=9
          if(param[z]=="CIS.Sol")k=10
          if(param[z]=="Sol.CIS")k=11
          if(param[z]=="PABS.Sol")k=12
          if(param[z]=="CIS.PABS")k=13
          if(param[z]=="A1.Sol")k=14
          if(param[z]=="A2.CIS")k=15
          if(param[z]=="A3.PABS")k=16
          if(param[z]=="L1.L1t")k=17
          if(param[z]=="L1t.BLt")k=18
          if(param[z]=="L1t.SI")k=19
          if(param[z]=="BLt.L1t")k=20

         while(again==1){
            for(i in 1:5){
               q[i]=(i-3+t*2^(kk-1))/(t*2^(kk-1))*val[1,k];

               if(param[z]=="ST0.ST0t")R[5,25]=q[i]
               if(param[z]=="ST1.ST1t")R[6,26]=q[i]
               if(param[z]=="ST0t.BLt")R[25,28]=q[i]
               if(param[z]=="ST1t.BLt")R[26,28]=q[i]
               if(param[z]=="BL.BLt")R[24,28]=q[i]
               if(param[z]=="BLt.ULI")R[28,20]=q[i]
               if(param[z]=="BLt.BLA")R[28,23]=q[i]
               if(param[z]=="BLt.ST0t")R[28,25]=q[i]
               if(param[z]=="Sol.BL")R[1,24]=q[i]
               if(param[z]=="CIS.Sol")R[2,1]=q[i]
                if(param[z]=="Sol.CIS")R[1,2]=q[i]
                if(param[z]=="PABS.Sol")R[3,1]=q[i]
                if(param[z]=="CIS.PABS")R[2,3]=q[i]
                if(param[z]=="A1.Sol")R[1,1]=q[i]
                if(param[z]=="A2.CIS")R[2,2]=q[i]
```

```
            if(param[z]=="A3.PABS")R[3,3]=q[i]
            if(param[z]=="L1.L1t")R[17,27]=q[i]
            if(param[z]=="L1t.BLt")R[27,28]=q[i]
            if(param[z]=="L1t.SI")R[27,19]=q[i]
            if(param[z]=="BLt.L1t")R[28,27]=q[i]

           X.s=Pu.univ(d=chel,t=36,R=R)$Pu.atoms[,1:3]
           Xs.urine=X.s[-19,-3]
           X.lm=lm(C.urine[,2]~Xs.urine[,2]-1)
           X.U=Xs.urine
           X.U[,2]=X.U[,2]*summary(X.lm)$coefficients[1]
           res=summary(X.lm)$residuals^2
            intake=summary(X.lm)$coefficients[1]
            if(weight==1){int.factor=abs(intake-136000)*2/100}else{int.factor=abs(intake-136000)/10000}
           if(opt.int=="FALSE")int.factor=0
            chi[i]=t(as.matrix(res)) %*% ww + int.factor
            chi.o = t(as.matrix(res)) %*% w

         }
         cnt=cnt+1
         again=0
         low=chi[3]
         X[z]=q[3]

         for(i in 1:5){if(chi[i]<low-s){again=1;val[1,k]=q[i];low=chi[i];}
         }
         change=rbind(change,chi)

         #ensure the R matrix has the best values
          R[5,25]=val[1,1] #ST0.ST0t
          R[6,26]=val[1,2] #ST1.ST1t
          R[25,28]=val[1,3] #ST0t.BLt
          R[26,28]=val[1,4] #ST1t.BLt
          R[24,28]=val[1,5] #BL.BLt
          R[28,20]=val[1,6]
          R[28,23]=val[1,7] #BLt.BLA
          R[28,25]=val[1,8] #BLt.ST0t
          R[1,24]=val[1,9]  #Sol.BL
          R[2,1]=val[1,10] #CIS.Sol
          R[1,2]=val[1,11] #Sol.CIS
          R[3,1]=val[1,12]  #PABS.Sol
          R[2,3]=val[1,13]  #CIS.PABS
          R[1,1]=val[1,14]  #A1.Sol
          R[2,2]=val[1,15]  #A2.CIS
          R[3,3]=val[1,16]  #A3.PABS
          R[17,27]=val[1,17] #L1.L1t
          R[27,28]=val[1,18] #L1t.BLt
          R[27,19]=val[1,19] #L1t.SI
          R[28,27]=val[1,20] #BLt.L1t
       }
     }

     loops=loops+1
   }
   kk=kk+1
}

#run intake again based on best parameters
X.s=Pu.univ(d=chel,t=36,R=R)$Pu.atoms[,1:3]
Xs.urine=X.s[-19,-3]
X.lm=lm(C.urine[,2]~Xs.urine[,2]-1)
intake=summary(X.lm)$coefficients[1]

#plot results
plot(C.urine,log="y",ylim=c(10,20000))
lines(X.U,typ="l",col="blue")

structure(list(X=val,cnt=cnt,chi.low=low,intake=intake,chi.w=chi,chi=chi.o,int.factor=int.factor,q=q))
}
```

Rmod.mult

This function was used to optimize the Pu-DTPA model that included comparison to 3 bioassay types (i.e., urine, fecal and blood). Normal statistics are provided in the results with plots of each bioassay fit. The function optimized compartments that were specified by the 'param' in the input statement. Bioassay table results were provided with the first column being a chronological listing of the measurement days, and the second being the corresponding results in units of Bq. The input assumed that the 'case' was the urine bioassay table, while the bio2 and bio3 were the fecal and blood bioassays, respectively. This function required all three bioassay types to be entered. The rate matrix was specified for a plutonium wound that included DTPA transitional compartments. The chelation days were specified in the 'chel' row vector. Intake may be specified, typically in units of Bq when known, or left as 1 where the function will predict the intake. Optimization requires 2 parameters to be specified in 'param' (which may be the same), and uses a '.' between specified compartments for defining the transfer path. The specified compartments must be consistent with the rate matrix specified compartments. Optimization parameters include the number of times to repeat all parameter optimizations when one is changed (times); the sensitivity of the chi-square goodness of fit result (sens); the optimization function denominator (opt: set to 3); the precision of the parameter estimate (tight); and specifying either to optimize against the normal weight (tg= "FALSE") or a squared weight (tg= "TRUE"). The optimization can be weighted to a bioassay type using a weighted ratio (wr) for each (e.g., wr=cbind(0.5, 0.1, 0.4) for applying 50% weight to urine, 10% to fecal and 40% to blood bioassays). This function also uses a defined scattering factor (SF) for each bioassay type.

Example:

>Rmod.mult(R=R.Pu.dtpa,title="IDEAS Case 123", case=123.urine, bio2=123.fecal, bio3=123.blood, h=24065,t=100,intake=1, d=chel, param=c("ST1.ST1t","Liver1.Liver1t"), times=2,sens=1,opt=3,tight=3,tg="FALSE",wr=cbind(0.5,0.1,0.4), SF=c(1.6,3,2.1))

Function:

```
Rmod.mult=function(R=R.Pu.dtpa,title="",case=case,bio2=bio2,bio3=bio3,h=24065,t=100,intake=1, d=chel,
param=c("ST0.ST0t","Blood.Bloodt"),times=2,sens=1,opt=3,tight=3,tg="FALSE",wr=cbind(0.5,0.1,0.4), SF=c(1.6,3,2.1))
{
#The R matrix is specified, chel is the row vector of days that were chelated, param are the parameters to be fitted,
#case is a 2-dimensional matrix with measurement days in the first column and the bioassay measurement in the second
column,
#h is the contaminant half-life in years, t is the time period to be evaluated from the intial time (e.g., 0 to 100 days).
#times indicates the number of times to cycle through all fitted parameters whenever one changes,
#sens is the change in chi-square value between two parameter values, if less than this amount then the lower one will
#be used for the next iteration, opt is the divisor in the optimization function (normally 3, but can be higher)
#tight relates to the precision of the estimated parameter
#case is reserved for the urine bioassay, where bio2 is fecal bioassay and bio3 is blood bioassay
#tg is "TRUE" when fitting to the target function (squared weight)

   p=length(param)
   cnt=0

   #set initial parameter values
   N = dim(R)[1]
   RC=1:N^2;dim(RC)=c(N,N);

   val2=matrix(c(0,0,0,0),nrow=1,byrow=T)
   val2=val2[-1,]

   #forms pathway matrix (RC) and value matrix (val2) of pathways and associated transfer rates for parameters of interest
   for(p in 1:length(param)){
      for(i in 1:N){
         for(j in 1:N){
            RC[i,j]=paste(row.names(R)[i],colnames(R)[j],sep=".")
            if(RC[i,j]==param[p]){if(R[i,j]==0.0)R[i,j]=10;
                        val2=rbind(val2,matrix(c(R[i,j],RC[i,j],i,j),nrow=1,byrow=T));}
         }}}

   #Define parameter matrix
   val=matrix(c(val2[,1]),nrow=1,byrow=T)
   colnames(val)=c(val2[,2])
   pos=val2[,3:4]


   #setup case dimension for optimization
   Nu=case[dim(case)[1],1]; if(Nu<t)tu=Nu else Nu=t;
   NN=dim(case)[1]
   for(i in NN:1){
      if(case[i,1]>t)case=case[-i,]}

   Nf=bio2[dim(bio2)[1],1]; if(Nf<t)tf=Nf else Nf=t;
   NN=dim(bio2)[1]
   for(i in NN:1){
      if(bio2[i,1]>t)bio2=bio2[-i,]}

   Nb=bio3[dim(bio3)[1],1]; if(Nb<t)tb=Nb else Nb=t;
   NN=dim(bio3)[1]
   for(i in NN:1){
      if(bio3[i,1]>t)bio3=bio3[-i,]}


   #specify modification step
   tt=opt
```

```
#specify sensitivity
s=sens
times=times
loops=1


#specify row vectors
q=matrix(c(0,0,0,0,0),nrow=1,byrow=T)
X=matrix(c(rep(0,p)),nrow=1,byrow=T)

colnames(X)=param
chi=matrix(c(0,0,0,0,0),nrow=1,byrow=T)
change=chi
change=change[-1,]
chi.U=chi; chi.F=chi; chi.B=chi; lchi.U=chi; lchi.F=chi; lchi.B=chi; tchi.U=chi; tchi.F=chi; tchi.B=chi;

#Perform optimization loop
kk=1
while (kk<=tight){
   loops=1
   #loop cycles through all fitted parameters after each is changed to ensure the best fit
   while(loops<=times){
      for(z in 1:p){
         again=1

         while(again==1){
            for(i in 1:5){

               q[i]=(i-3+tt*2^(kk-1))/(tt*2^(kk-1))*as.numeric(val[1,z]);
               a=as.numeric(pos[z,1]);b=as.numeric(pos[z,2]);

               R[a,b]=q[i]


               #Assumes Plutonium matrix
               fst=Pu.univ(R=R,d=d,t=t,h=h)$Pu.atoms
               wod=Pu.univ(R=R,d=0,t=t,h=h)$Pu.atoms
               X.U=fst[,1:2]; X.Uo=wod[,1:2]; X.Uz=X.U;
               X.F=cbind(fst[,1], fst[,3]); X.Fo=cbind(wod[,1], wod[,3]); X.Fz=X.F;
               X.B=cbind(fst[,1], fst[,7]); X.Bo=cbind(wod[,1], wod[,7]); X.Bz=X.B;


               #normalize urine model results for regression
               X.Uz=X.U
               for(ii in t:1){
                  rem=0
                  for(jj in 1:dim(case)[1]){
                     if(X.U[ii,1]==case[jj,1])rem=1}
                  if(rem==0)X.U=X.U[-ii,]
               }

               #normalize fecal model results for regression
               X.Fz=X.F
               for(ii in t:1){
                  rem=0
                  for(jj in 1:dim(bio2)[1]){
                     if(X.F[ii,1]==bio2[jj,1])rem=1}
                  if(rem==0)X.F=X.F[-ii,]
               }

               #normalize fecal model results for regression
               X.Bz=X.B
               for(ii in t:1){
                  rem=0
                  for(jj in 1:dim(bio3)[1]){
                     if(X.B[ii,1]==bio3[jj,1])rem=1}
                  if(rem==0)X.B=X.B[-ii,]
               }

               #specify intake to use
```

```
            if(intake<=1){
               intakeU=exp(sum(log(case[,2]/X.U[,2])/dim(case)[1]))
               intakeF=exp(sum(log(bio2[,2]/X.F[,2])/dim(bio2)[1]))
               intakeB=exp(sum(log(bio3[,2]/X.B[,2])/dim(bio3)[1]))
               sdI=sd(c(intakeU,intakeF,intakeB))
            }
            else{
               intakeU=intake;intakeF=intake;intakeB=intake;
               sdI=0;
            }

            #adjust model prediction wrt intake and obtain residuals and specify weight vector
            X.U[,2]=X.U[,2]*intakeU; X.Uo[,2]=X.Uo[,2]*intakeU; X.Uz[,2]=X.Uz[,2]*intakeU; resU=case[,2]-
              X.U[,2]; lresU=log(case[,2])-log(X.U[,2]); wU=1/X.U[,2]; lwU=1/log(X.U[,2]);
            X.F[,2]=X.F[,2]*intakeF; X.Fo[,2]=X.Fo[,2]*intakeF; X.Fz[,2]=X.Fz[,2]*intakeF; resF=bio2[,2]-X.F[,2];
              lresF=log(bio2[,2])-log(X.F[,2]); wF=1/X.F[,2]; lwF=1/log(X.F[,2]);
            X.B[,2]=X.B[,2]*intakeB; X.Bo[,2]=X.Bo[,2]*intakeB; X.Bz[,2]=X.Bz[,2]*intakeB; resB=bio3[,2]-
              X.B[,2]; lresB=log(bio3[,2])-log(X.B[,2]); wB=1/X.B[,2]; lwB=1/log(X.B[,2]);


            #Determine chi square goodness of fit with or without a specified intake
            chi.U[i]=t(resU^2)  %*% wU; tchi.U[i]=(t(resU) %*% wU)^2; lchi.U[i]=t(lresU^2) %*% lwU;
            chi.F[i]=t(resF^2)  %*% wF; tchi.F[i]=(t(resF) %*% wF)^2; lchi.F[i]=t(lresF^2) %*% lwF;
            chi.B[i]=t(resB^2)  %*% wB; tchi.B[i]=(t(resB) %*% wB)^2; lchi.B[i]=t(lresB^2) %*% lwB;

            #calculate sum of weighted chi's for each bioassay type
            Wchi=chi.U*wr[1]+chi.F*wr[2]+chi.B*wr[3]
            Wtchi=tchi.U*wr[1]+tchi.F*wr[2]+tchi.B*wr[3]
            LWchi=lchi.U*wr[1]+lchi.F*wr[2]+lchi.B*wr[3]

            #obtain the lowest values for final report
            if(i==3){logChi=LWchi;Bst.Intake=cbind(intakeU,intakeF,intakeB);LX.U=X.U;LX.Uo=X.Uo;
              LX.Uz=X.Uz;LX.F=X.F; LX.Fo=X.Fo; LX.Fz=X.Fz;LX.B=X.B; LX.Bo=X.Bo;
              LX.Bz=X.Bz;BWchi=Wchi; BWtchi=Wtchi; Bchi=cbind(chi.U[3], chi.F[3], chi.B[3]);
              Blchi=cbind(lchi.U[3],lchi.F[3],lchi.B[3]);
              Btchi=cbind(tchi.U[3],tchi.F[3],tchi.B[3]);Bsd=sdI;}

         }
         cnt=cnt+1
         again=0
         if(tg=="FALSE"){low=Wchi[3];}else{low=Wtchi[3];}

         #Determine if the 3rd or center chi value is lowest.  If not then repeat cycle with adjusted parameters.
         if(tg=="FALSE"){
            for(ii in 1:5){if(Wchi[ii]<low-s){again=1;val[1,z]=q[ii];low=Wchi[ii];}}}
         else{
            for(ii in 1:5){if(Wtchi[ii]<low-s){again=1;val[1,z]=q[ii];low=Wtchi[ii];}}
         }

         if(tg=="FALSE") change=rbind(change,Wchi) else change=rbind(change,Wtchi)

         #ensure the R matrix has the best values
         R[a,b]=as.numeric(val[1,z])

       }
     }

     loops=loops+1
   }
   kk=kk+1
}


X.U[,2]=LX.U[,2]; X.Uo[,2]=LX.Uo[,2]; X.Uz[,2]=LX.Uz[,2];mU=X.U;mU[,2]=mU[,2]/Bst.Intake[1];
X.F[,2]=LX.F[,2]; X.Fo[,2]=LX.Fo[,2]; X.Fz[,2]=LX.Fz[,2];mF=X.F;mF[,2]=mF[,2]/Bst.Intake[2];
X.B[,2]=LX.B[,2]; X.Bo[,2]=LX.Bo[,2]; X.Bz[,2]=LX.Bz[,2];mB=X.B;mB[,2]=mB[,2]/Bst.Intake[3];

#determine intake from multiple bioassay types
Nu=dim(case)[1];Nf=dim(bio2)[1];Nb=dim(bio3)[1];
lnI1=sum(log(case[,2]/mU[,2]))/(log(SF[1]))^2+sum(log(bio2[,2]/mF[,2]))/(log(SF[2]))^2
```

```
  +sum(log(bio3[,2]/mB[,2]))/(log(SF[3]))^2
lnI2=sum(Nu/(log(SF[1]))^2+Nf/(log(SF[2]))^2+Nb/(log(SF[3]))^2)
lnI=lnI1/lnI2
mI=exp(lnI)

#determine individual intakes
uI=exp(sum(log(case[,2]/mU[,2]))/Nu)
fI=exp(sum(log(bio2[,2]/mF[,2]))/Nf)
bI=exp(sum(log(bio3[,2]/mB[,2]))/Nb)
IM=matrix(c(mI,uI,fI,bI),nrow=1,byrow=T)
colnames(IM)=c("Total","Urine","Fecal","Blood")

#setup individual predicted intake arrays for boxplot
Int.U=case; Int.U[,2]=case[,2]/mU[,2];
Int.F=bio2; Int.F[,2]=bio2[,2]/mF[,2];
Int.B=bio3; Int.B[,2]=bio3[,2]/mB[,2];

#determine analysis of variance for the individual intakes
numI=sum(Nu*(uI-mI)^2+Nf*(fI-mI)^2+Nb*(bI-mI)^2)/2
denI=(sum(((case[,2]/mU[,2])-uI)^2)+sum(((bio2[,2]/mF[,2])-fI)^2)+sum(((bio3[,2]/mB[,2])-bI)^2))/(Nu+Nf+Nb-3)
Ft=numI/denI

#determine autocorrelation
denU=sum((case[,2]-X.U[,2])^2); sResU=(log(case[,2])-log(X.U[,2]))/log(SF[1]);
numU=0
for(i in 1:(dim(case)[1]-1)){
   numU=(case[i,2]-X.U[i,2])*(case[i+1,2]-X.U[i+1,2])+numU
}
acU=numU/denU

denF=sum((bio2[,2]-X.F[,2])^2); sResF=(log(bio2[,2])-log(X.F[,2]))/log(SF[2]);
numF=0
for(i in 1:(dim(bio2)[1]-1)){
   numF=(bio2[i,2]-X.F[i,2])*(bio2[i+1,2]-X.F[i+1,2])+numF
}
acF=numF/denF

denB=sum((bio3[,2]-X.B[,2])^2); sResB=(log(bio3[,2])-log(X.B[,2]))/log(SF[3]);
numB=0
for(i in 1:(dim(bio3)[1]-1)){
   numB=(bio3[i,2]-X.B[i,2])*(bio3[i+1,2]-X.B[i+1,2])+numB
}
acB=numB/denB

ac=cbind(acU,acF,acB)

#determined overall autocorrelation using IDEAS guidelines
sResT=c(sResU,sResF,sResB); numT=0; TN=length(sResT)[1];
for(i in 1:(TN-1)){
   numT=sResT[i]*sResT[i+1]+numT;}
denT=sum(sResT^2)
Tac=numT/denT
Tmean=-1/TN; Tsigma=(TN-2)/(TN*sqrt(TN-1));
TCL95=c(Tmean-1.645*Tsigma,Tmean+1.645*Tsigma);
Tchisq=denT;


#determine individual autocorrelation
numU=0;
for(i in 1:(Nu-1)){
   numU=sResU[i]*sResU[i+1]+numU;}
denU=sum(sResU^2)
acSU=numU/denU

numF=0;
for(i in 1:(Nf-1)){
   numF=sResF[i]*sResF[i+1]+numF;}
denF=sum(sResF^2)
acSF=numF/denF
```

```
                numB=0;
                for(i in 1:(Nb-1)){
                   numB=sResB[i]*sResB[i+1]+numB;}
                denB=sum(sResB^2)
                acSB=numB/denB

                #plot results


plot(case,log="xy",main=c(title,"Urine"),lty=2,ylim=c(min(X.Uo[,2],X.Uz[,2],case[,2]),max(X.Uo[,2],X.Uz[,2],case[,2])))
                lines(X.Uo,typ="l",col="black",lty=3)
                lines(X.Uz[,1:2],typ="l",col="black")


plot(bio2,log="xy",main=c(title,"Fecal"),lty=2,ylim=c(min(X.Fo[,2],X.Fz[,2],bio2[,2]),max(X.Fo[,2],X.Fz[,2],bio2[,2])))
                lines(X.Fo,typ="l",col="black",lty=3)
                lines(X.Fz[,1:2],typ="l",col="black")

                plot(bio3,log="xy",main=c(title,"Blood"),lty=2,
ylim=c(min(X.Bo[,2],X.Bz[,2],bio3[,2]),max(X.Bo[,2],X.Bz[,2],bio3[,2])))
                lines(X.Bo,typ="l",col="black",lty=3)
                lines(X.Bz[,1:2],typ="l",col="black")

                boxplot(Int.U[,2],Int.F[,2],Int.B[,2],log="y",xlab="Urine, Fecal and Blood Intake (Bq)",
                  main="Intake Distribution Among Bioassay Types",boxwex=0.5)
                abline(h=mI)

             structure(list(X=val, cnt=cnt, chi.low=low, Combined.Intake=IM, IntakeSD=Bsd, Ftest=Ft, chi=Bchi, logChiGoF=Blchi,
             Total.logChiGoF=sum(Blchi),WeightedChi=Btchi, autocorrelation=ac, Std.autocorrelation=c(Tac,acSU,acSF,acSB),
             Total.Conf=TCL95, Total.DF=TN-3, Total.logChi=Tchisq))
             }
```

Rmod.mult2

This function is a variation of Rmod.mult that improves optimization time by obtaining predictions for bioassay and chelation days for comparison with actual case, omitting the days in between.

Example:

```
>Rmod.mult2(R=R.123,title="IDEAS Case 123", case=123.urine, bio2=123.fecal,
bio3=123.blood, h=24065,t=100,intake=1, d=chel,
param=c("ST1.ST1t","Liver1.Liver1t"),
times=2,sens=1,opt=3,tight=3,tg="FALSE",wr=cbind(0.5,0.1,0.4), SF=c(1.6,3,2.1))
```

Function:

```
function(R=R.Pu.dtpa,title="",case=C.urine,bio2=C.fecal,bio3=C.blood,h=24065,t=500, intake=1,d=chel,

param=c("ST0.ST0t","Blood.Bloodt"),times=2,sens=1,opt=3,tight=3,tg="FALSE",wr=cbind(0.5,0.1,0.4),SF=c(1.6,3,2.1))
{

#The R matrix is specified, chel is the row vector of days that were chelated, param are the parameters to be fitted,
#case is a 2-dimensional matrix with measurement days in the first column and the bioassay measurement in the second
column,
#h is the contaminant half-life in years, t is the time period to be evaluated from the intial time (e.g., 0 to 100 days).
#times indicates the number of times to cycle through all fitted parameters whenever one changes,
#sens is the change in chi-square value between two parameter values, if less than this amount then the lower one will
#be used for the next iteration, opt is the divisor in the optimization function (normally 3, but can be higher)
#tight relates to the precision of the estimated parameter
#case is reserved for the urine bioassay, where bio2 is fecal bioassay and bio3 is blood bioassay
#tg is "TRUE" when fitting to the target function (weighted chi-square)

  p=length(param)
  cnt=0

  #set initial parameter values
  N = dim(R)[1]
  RC=1:N^2;dim(RC)=c(N,N);

  val2=matrix(c(0,0,0,0),nrow=1,byrow=T)
  val2=val2[-1,]

  #forms pathway matrix (RC) and value matrix (val2) of pathways and associated transfer rates for parameters of interest
  for(p in 1:length(param)){
    for(i in 1:N){
      for(j in 1:N){
        RC[i,j]=paste(row.names(R)[i],colnames(R)[j],sep=".")
        if(RC[i,j]==param[p]){if(R[i,j]==0.0)R[i,j]=10;
                    val2=rbind(val2,matrix(c(R[i,j],RC[i,j],i,j),nrow=1,byrow=T));}
      }}}

  #Define parameter matrix
  val=matrix(c(val2[,1]),nrow=1,byrow=T)
  colnames(val)=c(val2[,2])
  pos=val2[,3:4]

  #setup case dimension for optimization
  Nu=case[dim(case)[1],1]; if(Nu<t)tu=Nu else Nu=t;
  NN=dim(case)[1]
  for(i in NN:1){
```

```
   if(case[i,1]>t)case=case[-i,]}

Nf=bio2[dim(bio2)[1],1]; if(Nf<t)tf=Nf else Nf=t;
NN=dim(bio2)[1]
for(i in NN:1){
   if(bio2[i,1]>t)bio2=bio2[-i,]}

Nb=bio3[dim(bio3)[1],1]; if(Nb<t)tb=Nb else Nb=t;
NN=dim(bio3)[1]
for(i in NN:1){
   if(bio3[i,1]>t)bio3=bio3[-i,]}

#setup case dimension

NN=length(d)
for(i in length(d):1){
   if(d[i]>t)d=d[-i]}

#combine days with dtpa days for combined vector
cd=c(case[,1],bio2[,1],bio3[,1],d)
cd=sort(cd)
cd=unique(cd)

#specify modification step
tt=opt

#specify sensitivity
s=sens
times=times
loops=1


#specify row vectors
q=matrix(c(0,0,0,0,0),nrow=1,byrow=T)
X=matrix(c(rep(0,p)),nrow=1,byrow=T)

colnames(X)=param
chi=matrix(c(0,0,0,0,0),nrow=1,byrow=T)
change=chi
change=change[-1,]
chi.U=chi; chi.F=chi; chi.B=chi; lchi.U=chi; lchi.F=chi; lchi.B=chi; tchi.U=chi; tchi.F=chi; tchi.B=chi;

#Perform optimization loop
kk=1
while (kk<=tight){
   loops=1
   #loop cycles through all fitted parameters after each is changed to ensure the best fit
   while(loops<=times){
      for(z in 1:p){
         again=1

         while(again==1){
            for(i in 1:5){

               q[i]=(i-3+tt*2^(kk-1))/(tt*2^(kk-1))*as.numeric(val[1,z]);
               a=as.numeric(pos[z,1]);b=as.numeric(pos[z,2]);

               R[a,b]=q[i]


               #Assumes Plutonium matrix
               fst=Pu.univF(R=R,d=d,t=t,h=h,cd=cd)$Pu.atoms
               wod=Pu.univF(R=R,d=0,t=t,h=h,cd=cd)$Pu.atoms
               X.U=fst[,1:2]; X.Uo=wod[,1:2]; X.Uz=X.U;
               X.F=cbind(fst[,1], fst[,3]); X.Fo=cbind(wod[,1], wod[,3]); X.Fz=X.F;
               X.B=cbind(fst[,1], fst[,7]); X.Bo=cbind(wod[,1], wod[,7]); X.Bz=X.B;

               t=length(cd)

               #normalize urine model results for regression
```

```
   X.Uz=X.U
   for(ii in t:1){
      rem=0
      for(jj in 1:dim(case)[1]){
         if(X.U[ii,1]==case[jj,1])rem=1}
      if(rem==0)X.U=X.U[-ii,]
   }

   #normalize fecal model results for regression
   X.Fz=X.F
   for(ii in t:1){
      rem=0
      for(jj in 1:dim(bio2)[1]){
         if(X.F[ii,1]==bio2[jj,1])rem=1}
      if(rem==0)X.F=X.F[-ii,]
   }

   #normalize fecal model results for regression
   X.Bz=X.B
   for(ii in t:1){
      rem=0
      for(jj in 1:dim(bio3)[1]){
         if(X.B[ii,1]==bio3[jj,1])rem=1}
      if(rem==0)X.B=X.B[-ii,]
   }

   #specify intake to use
   if(intake<=1){
      intakeU=exp(sum(log(case[,2]/X.U[,2])/dim(case)[1]))
      intakeF=exp(sum(log(bio2[,2]/X.F[,2])/dim(bio2)[1]))
      intakeB=exp(sum(log(bio3[,2]/X.B[,2])/dim(bio3)[1]))
      sdI=sd(c(intakeU,intakeF,intakeB))
   }
   else{
      intakeU=intake;intakeF=intake;intakeB=intake;
      sdI=0;
   }

   #adjust model prediction wrt intake and obtain residuals and specify weight vector
   X.U[,2]=X.U[,2]*intakeU;    X.Uo[,2]=X.Uo[,2]*intakeU;    X.Uz[,2]=X.Uz[,2]*intakeU;    resU=case[,2]-
       X.U[,2]; lresU=log(case[,2])-log(X.U[,2]); wU=1/X.U[,2]; lwU=1/log(X.U[,2]);
   X.F[,2]=X.F[,2]*intakeF;  X.Fo[,2]=X.Fo[,2]*intakeF;  X.Fz[,2]=X.Fz[,2]*intakeF;  resF=bio2[,2]-X.F[,2];
       lresF=log(bio2[,2])-log(X.F[,2]); wF=1/X.F[,2]; lwF=1/log(X.F[,2]);
   X.B[,2]=X.B[,2]*intakeB;    X.Bo[,2]=X.Bo[,2]*intakeB;    X.Bz[,2]=X.Bz[,2]*intakeB;    resB=bio3[,2]-
       X.B[,2]; lresB=log(bio3[,2])-log(X.B[,2]); wB=1/X.B[,2]; lwB=1/log(X.B[,2]);


   #Determine chi square goodness of fit with or without a specified intake
   chi.U[i]=t(resU^2)  %*% wU; tchi.U[i]=(t(resU) %*% wU)^2; lchi.U[i]=t(lresU^2) %*% lwU;
   chi.F[i]=t(resF^2)  %*% wF; tchi.F[i]=(t(resF) %*% wF)^2; lchi.F[i]=t(lresF^2) %*% lwF;
   chi.B[i]=t(resB^2)  %*% wB; tchi.B[i]=(t(resB) %*% wB)^2; lchi.B[i]=t(lresB^2) %*% lwB;

   #calculate sum of weighted chi's for each bioassay type
   Wchi=chi.U*wr[1]+chi.F*wr[2]+chi.B*wr[3]
   Wtchi=tchi.U*wr[1]+tchi.F*wr[2]+tchi.B*wr[3]
   LWchi=lchi.U*wr[1]+lchi.F*wr[2]+lchi.B*wr[3]

   #obtain the lowest values for final report
   if(i==3){logChi=LWchi;Bst.Intake=cbind(intakeU,intakeF,intakeB); LX.U=X.U; LX.Uo=X.Uo;
     LX.Uz=X.Uz; LX.F=X.F; LX.Fo=X.Fo; LX.Fz=X.Fz;LX.B=X.B;  LX.Bo=X.Bo; LX.Bz=X.Bz;
     BWchi=Wchi; BWtchi=Wtchi; Bchi=cbind(chi.U[3], chi.F[3], chi.B[3]);
     Blchi=cbind(lchi.U[3],lchi.F[3],lchi.B[3]);
         Btchi=cbind(tchi.U[3],tchi.F[3],tchi.B[3]);Bsd=sdI;}
     }
cnt=cnt+1
again=0
if(tg=="FALSE"){low=Wchi[3];}else{low=Wtchi[3];}


#Determine if the 3rd or center chi value is lowest.  If not then repeat cycle with adjusted parameters.
```

```
            if(tg=="FALSE"){
               for(ii in 1:5){if(Wchi[ii]<low-s){again=1;val[1,z]=q[ii];low=Wchi[ii];}}}
            else{
               for(ii in 1:5){if(Wtchi[ii]<low-s){again=1;val[1,z]=q[ii];low=Wtchi[ii];}}
            }

            if(tg=="FALSE") change=rbind(change,Wchi) else change=rbind(change,Wtchi)

            #ensure the R matrix has the best values
            R[a,b]=as.numeric(val[1,z])

         }
      }

      loops=loops+1
   }
   kk=kk+1
}


X.U[,2]=LX.U[,2]; X.Uo[,2]=LX.Uo[,2]; X.Uz[,2]=LX.Uz[,2];mU=X.U;mU[,2]=mU[,2]/Bst.Intake[1];
X.F[,2]=LX.F[,2]; X.Fo[,2]=LX.Fo[,2]; X.Fz[,2]=LX.Fz[,2];mF=X.F;mF[,2]=mF[,2]/Bst.Intake[2];
X.B[,2]=LX.B[,2]; X.Bo[,2]=LX.Bo[,2]; X.Bz[,2]=LX.Bz[,2];mB=X.B;mB[,2]=mB[,2]/Bst.Intake[3];

#determine intake from multiple bioassay types
Nu=dim(case)[1];Nf=dim(bio2)[1];Nb=dim(bio3)[1];
lnI1=sum(log(case[,2]/mU[,2]))/(log(SF[1]))^2+sum(log(bio2[,2]/mF[,2]))/(log(SF[2]))^2
  +sum(log(bio3[,2]/mB[,2]))/(log(SF[3]))^2
lnI2=sum(Nu/(log(SF[1]))^2+Nf/(log(SF[2]))^2+Nb/(log(SF[3]))^2)
lnI=lnI1/lnI2
mI=exp(lnI)

#determine individual intakes
uI=exp(sum(log(case[,2]/mU[,2]))/Nu)
fI=exp(sum(log(bio2[,2]/mF[,2]))/Nf)
bI=exp(sum(log(bio3[,2]/mB[,2]))/Nb)
IM=matrix(c(mI,uI,fI,bI),nrow=1,byrow=T)
colnames(IM)=c("Total","Urine","Fecal","Blood")

#setup individual predicted intake arrays for boxplot
Int.U=case; Int.U[,2]=case[,2]/mU[,2];
Int.F=bio2; Int.F[,2]=bio2[,2]/mF[,2];
Int.B=bio3; Int.B[,2]=bio3[,2]/mB[,2];

#determine analysis of variance for the individual intakes
numI=sum(Nu*(uI-mI)^2+Nf*(fI-mI)^2+Nb*(bI-mI)^2)/2
denI=(sum(((case[,2]/mU[,2])-uI)^2)+sum(((bio2[,2]/mF[,2])-fI)^2)+sum(((bio3[,2]/mB[,2])-bI)^2))/(Nu+Nf+Nb-3)
Ft=numI/denI

#determine autocorrelation
denU=sum((case[,2]-X.U[,2])^2); sResU=(log(case[,2])-log(X.U[,2]))/log(SF[1]);
numU=0
for(i in 1:(dim(case)[1]-1)){
   numU=(case[i,2]-X.U[i,2])*(case[i+1,2]-X.U[i+1,2])+numU
}
acU=numU/denU

denF=sum((bio2[,2]-X.F[,2])^2); sResF=(log(bio2[,2])-log(X.F[,2]))/log(SF[2]);
numF=0
for(i in 1:(dim(bio2)[1]-1)){
   numF=(bio2[i,2]-X.F[i,2])*(bio2[i+1,2]-X.F[i+1,2])+numF
}
acF=numF/denF

denB=sum((bio3[,2]-X.B[,2])^2); sResB=(log(bio3[,2])-log(X.B[,2]))/log(SF[3]);
numB=0
for(i in 1:(dim(bio3)[1]-1)){
   numB=(bio3[i,2]-X.B[i,2])*(bio3[i+1,2]-X.B[i+1,2])+numB
}
acB=numB/denB
```

```
ac=cbind(acU,acF,acB)

#determined overall autocorrelation using IDEAS guidelines
sResT=c(sResU,sResF,sResB); numT=0; TN=length(sResT)[1];
for(i in 1:(TN-1)){
   numT=sResT[i]*sResT[i+1]+numT;}
denT=sum(sResT^2)
Tac=numT/denT
Tmean=-1/TN; Tsigma=(TN-2)/(TN*sqrt(TN-1));
TCL95=c(Tmean-1.645*Tsigma,Tmean+1.645*Tsigma);
Tchisq=denT;


#determine individual autocorrelation
numU=0;
for(i in 1:(Nu-1)){
   numU=sResU[i]*sResU[i+1]+numU;}
denU=sum(sResU^2)
acSU=numU/denU

numF=0;
for(i in 1:(Nf-1)){
   numF=sResF[i]*sResF[i+1]+numF;}
denF=sum(sResF^2)
acSF=numF/denF

numB=0;
for(i in 1:(Nb-1)){
   numB=sResB[i]*sResB[i+1]+numB;}
denB=sum(sResB^2)
acSB=numB/denB

#plot results


plot(case,log="xy",main=c(title,"Urine"),lty=2,ylim=c(min(X.Uo[,2],X.Uz[,2],case[,2]),max(X.Uo[,2],X.Uz[,2],case[,2])))
lines(X.Uo,typ="l",col="black",lty=3)
lines(X.Uz[,1:2],typ="l",col="black")


plot(bio2,log="xy",main=c(title,"Fecal"),lty=2,ylim=c(min(X.Fo[,2],X.Fz[,2],bio2[,2]),max(X.Fo[,2],X.Fz[,2],bio2[,2])))
lines(X.Fo,typ="l",col="black",lty=3)
lines(X.Fz[,1:2],typ="l",col="black")

plot(bio3,log="xy",main=c(title,"Blood"),lty=2,
ylim=c(min(X.Bo[,2],X.Bz[,2],bio3[,2]),max(X.Bo[,2],X.Bz[,2],bio3[,2])))
lines(X.Bo,typ="l",col="black",lty=3)
lines(X.Bz[,1:2],typ="l",col="black")

boxplot(Int.U[,2],Int.F[,2],Int.B[,2],log="y",xlab="Urine, Fecal and Blood Intake (Bq)",
  main="Intake Distribution Among Bioassay Types",boxwex=0.5)
abline(h=mI)

structure(list(X=val, cnt=cnt, chi.low=low, Combined.Intake=IM, IntakeSD=Bsd, Ftest=Ft, chi=Bchi, logChiGoF=Blchi,
Total.logChiGoF=sum(Blchi),WeightedChi=Btchi,  autocorrelation=ac, Std.autocorrelation=c(Tac,acSU,acSF,acSB),
Total.Conf=TCL95,Total.DF=TN-3, Total.logChi=Tchisq))
}
```

Rmod.67FLS

Function used for optimizing the modified ICRP 67 model. This function is a variation of the Rmod.mult and Rmod.mult2. This function relies on the mean human data and supplemental data of 5 bioassay measurement types (i.e., urine, fecal, blood, liver and skeleton). These are specified for case, bio2, bio3, bio4 and bio5 for the default values. The skeleton intake retention fractions were based on Leggett 2005 model prediction that was specified in the Legg05.IRF table. The time (t) was the last day used for the model prediction, which compared the model to the provided bioassay values for days of interest. This function also will accommodate rate matrices based on the Leggett 2005 model (e.g., R.Leg in appendix 4) when 'Leg="True").

Example: For optimizing the ICRP 67 rate matrix by adjusting the Soluble and CIS wound compartment transfer rates. The intake is specified at 1.00001 since the bioassay data are provided as intake retention fractions, with 1 as the expectation, and since the model attempts to optimize the parameters to a calculated intake when the intake is specified equal to 1, treating it as unspecified.

```
Rmod.67FLS(R=R.67,title="",case=L2.urine,bio2=L2.fecal,bio3=L3.blood,bio4=L2.liver,
bio5=cbind(Legg05.IRF[,1],Legg05.IRF[,5]),h=24065,t=15000,intake=1.00001,d=0,
param=c("Soluble.CIS","CIS.Soluble"),times=1,sens=0.0001,opt=3,tight=1,tg="FALSE",
wr=cbind(1,1,1,1,1),SF=c(1.6,3,2.1,1.3,1.3),Leg="False")
```

Function:

```
Rmod.67FLS=function(R=R.67M,title="",case=L2.urine,bio2=L2.fecal,bio3=L3.blood,bio4=L2.liver,
bio5=cbind(Legg05.IRF[,1],Legg05.IRF[,5]),h=24065,t=15000,intake=1.00001,d=0,param=c("Soluble.CIS","CIS.Soluble"),
times=1,sens=0.0001,opt=3,tight=1,tg="FALSE",wr=cbind(1,1,1,1,1),SF=c(1.6,3,2.1,1.3,1.3),Leg="False")
{

#The R matrix is specified, chel is the row vector of days that were chelated, param are the parameters to be fitted,
#case is a 2-dimensional matrix with measurement days in the first column and the bioassay measurement in the second column,
#h is the contaminant half-life in years, t is the time period to be evaluated from the initial time (e.g., 0 to 100 days).
#times indicates the number of times to cycle through all fitted parameters whenever one changes,
#sens is the change in chi-square value between two parameter values, if less than this amount then the lower one
#will be used for the next iteration, opt is the divisor in the optimization function (normally 3, but can be higher)
#tight relates to the precision of the estimated parameter
#case is reserved for the urine bioassay, where bio2 is fecal bioassay, bio3 is blood bioassay, bio4 is liver bioassay
```

```
#tg is "TRUE" when fitting to the target function (weighted chi-square)
#Leg is "TRUE" when fitting to Leggett et al. (2005) compartment model matrix


        p=length(param)
        cnt=0
        h=h*365.25

        colnames(bio5)=c("Days","Skeleton")

        #set initial parameter values
        N = dim(R)[1]
        RC=1:N^2;dim(RC)=c(N,N);

        val2=matrix(c(0,0,0,0),nrow=1,byrow=T)
        val2=val2[-1,]

        #forms pathway matrix (RC) and value matrix (val2) of pathways and associated transfer rates for parameters of interest
        for(p in 1:length(param)){
           for(i in 1:N){
              for(j in 1:N){
                 RC[i,j]=paste(row.names(R)[i],colnames(R)[j],sep=".")
                 if(RC[i,j]==param[p]){if(R[i,j]==0.0)R[i,j]=10;
                                 val2=rbind(val2,matrix(c(R[i,j],RC[i,j],i,j),nrow=1,byrow=T));}
              }}}

        #Define parameter matrix
        val=matrix(c(val2[,1]),nrow=1,byrow=T)
        colnames(val)=c(val2[,2])
        pos=val2[,3:4]


        #setup case dimension for optimization
        Nu=case[dim(case)[1],1]; if(Nu<t)tu=Nu else Nu=t;
        NN=dim(case)[1]
        for(i in NN:1){
           if(case[i,1]>t)case=case[-i,]}

        Nf=bio2[dim(bio2)[1],1]; if(Nf<t)tf=Nf else Nf=t;
        NN=dim(bio2)[1]
        for(i in NN:1){
           if(bio2[i,1]>t)bio2=bio2[-i,]}

        Nb=bio3[dim(bio3)[1],1]; if(Nb<t)tb=Nb else Nb=t;
        NN=dim(bio3)[1]
        for(i in NN:1){
           if(bio3[i,1]>t)bio3=bio3[-i,]}

        Nl=bio4[dim(bio4)[1],1]; if(Nl<t)tl=Nl else Nl=t;
        NN=dim(bio4)[1]
        for(i in NN:1){
           if(bio4[i,1]>t)bio4=bio4[-i,]}

        Ns=bio5[dim(bio5)[1],1]; if(Ns<t)ts=Ns else Ns=t;
        NN=dim(bio5)[1]
        for(i in NN:1){
           if(bio5[i,1]>t)bio5=bio5[-i,]}


        #determine location of urine, fecal and blood on matrix
        for(i in 1:dim(R)[1]){
           if(colnames(R)[i]=="Urine") ku=i;
           if(colnames(R)[i]=="Faeces" || colnames(R)[i]=="Feces") kf=i;
           if(colnames(R)[i]=="Blood") kb=i;
           if(colnames(R)[i]=="Liver1") kl=i;
           if(colnames(R)[i]=="CortVol" || colnames(R)[i]=="Cort.Vol"){ks1=kk;ks2=ks1+5;}
        }

        if(Leg=="TRUE"){ku=28; kf=27;kb=25;kb2=26;kl=16;kl2=17;kl3=18;ks1=10;ks2=15;}
```

```
#specify modification step
tt=opt

#specify sensitivity
s=sens
times=times
loops=1


#specify row vectors
q=matrix(c(0,0,0,0,0),nrow=1,byrow=T)
X=matrix(c(rep(0,p)),nrow=1,byrow=T)

colnames(X)=param
chi=matrix(c(0,0,0,0,0),nrow=1,byrow=T)
change=chi
change=change[-1,]
chi.U=chi; chi.F=chi; chi.B=chi; chi.L=chi; chi.S=chi; lchi.U=chi; lchi.F=chi; lchi.B=chi; lchi.L=chi; lchi.S=chi;
tchi.U=chi; tchi.F=chi; tchi.B=chi; tchi.L=chi; tchi.S=chi

#Perform optimization loop
kk=1
while (kk<=tight){
   loops=1
   #loop cycles through all fitted parameters after each is changed to ensure the best fit
   while(loops<=times){
      for(z in 1:p){
         again=1

         while(again==1){
            for(i in 1:5){

               q[i]=(i-3+tt*2^(kk-1))/(tt*2^(kk-1))*as.numeric(val[1,z]);
               a=as.numeric(pos[z,1]);b=as.numeric(pos[z,2]);

               R[a,b]=q[i]


               #obtain data matrix using R matrix
               X.U=matrix(c(0,0),nrow=1,byrow=TRUE)
               colnames(X.U)=c("Days","Urine")
               for (ii in 1:dim(case)[1]){
                  dU=case[ii,1];
                  last=decays(R,dU,h)$summary[ku,2]-decays(R,dU-1,h)$summary[ku,2];
                  X.U=rbind(X.U,c(dU,last));}
               X.U=X.U[-1,]

               X.F=matrix(c(0,0),nrow=1,byrow=TRUE)
               colnames(X.U)=c("Days","Fecal")
               for (ii in 1:dim(bio2)[1]){
                  dF=bio2[ii,1];
                  last=decays(R,dF,h)$summary[kf,2]-decays(R,dF-1,h)$summary[kf,2];
                  X.F=rbind(X.F,c(dF,last));}
               X.F=X.F[-1,]

               X.B=matrix(c(0,0),nrow=1,byrow=TRUE)
               colnames(X.B)=c("Days","Blood")
               for (ii in 1:dim(bio3)[1]){
                  dB=bio3[ii,1];
                  last=decays(R,dB,h)$summary[kb,2];
                  if(Leg=="TRUE"){last=decays(R,dB,h)$summary[kb,2]+decays(R,dB,h)$summary[kb2,2];}
                  X.B=rbind(X.B,c(dB,last));}
               X.B=X.B[-1,]

               X.L=matrix(c(0,0),nrow=1,byrow=TRUE)
               colnames(X.L)=c("Days","Liver")
               for (ii in 1:dim(bio4)[1]){
                  dL=bio4[ii,1];
                  last=decays(R,dL,h)$summary[kl,2]+decays(R,dL,h)$summary[kl-8,2];
```

```
  if(Leg=="TRUE"){last=decays(R,dL,h)$summary[kl,2]+decays(R,dL,h)$summary[kl2,2]+decays(R,dL,h
  )$summary[kl3,2];}
  X.L=rbind(X.L,c(dL,last));}

X.L=X.L[-1,]

X.S=matrix(c(0,0),nrow=1,byrow=TRUE)
colnames(X.S)=c("Days","Skeleton")
for (ii in 1:dim(bio5)[1]){
   dS=bio5[ii,1];
   last=decays(R,dS,h)$summary[,2];
   #last=sum(last[ks1:ks2])
   last1=sum(last[11:16])
   if(Leg=="TRUE"){last1=sum(last[10:15]);}
   X.S=rbind(X.S,c(dS,last1));}
X.S=X.S[-1,]


#specify intake to use
if(intake<=1){
   intakeU=exp(sum(log(case[,2]/X.U[,2])/dim(case)[1]))
   intakeF=exp(sum(log(bio2[,2]/X.F[,2])/dim(bio2)[1]))
   intakeB=exp(sum(log(bio3[,2]/X.B[,2])/dim(bio3)[1]))
   intakeL=exp(sum(log(bio4[,2]/X.L[,2])/dim(bio4)[1]))
   intakeS=exp(sum(log(bio5[,2]/X.S[,2])/dim(bio5)[1]))

   sdI=sd(c(intakeU,intakeF,intakeB,intakeL,intakeS))
}
else{
   intakeU=intake;intakeF=intake;intakeB=intake; intakeL=intake; intakeS=intake;
   sdI=0;
}

#adjust model prediction wrt intake and obtain residuals and specify weight vector
X.U[,2]=X.U[,2]*intakeU; resU=case[,2]-X.U[,2]; lresU=log(case[,2])-log(X.U[,2]); wU=1/X.U[,2]; lwU=1/log(X.U[,2]);
X.F[,2]=X.F[,2]*intakeF; resF=bio2[,2]-X.F[,2]; lresF=log(bio2[,2])-log(X.F[,2]); wF=1/X.F[,2]; lwF=1/log(X.F[,2]);
X.B[,2]=X.B[,2]*intakeB; resB=bio3[,2]-X.B[,2]; lresB=log(bio3[,2])-log(X.B[,2]); wB=1/X.B[,2]; lwB=1/log(X.B[,2]);
X.L[,2]=X.L[,2]*intakeL; resL=bio4[,2]-X.L[,2]; lresL=log(bio4[,2])-log(X.L[,2]); wL=1/X.L[,2]; lwL=1/log(X.L[,2]);
X.S[,2]=X.S[,2]; resS=bio5[,2]-X.S[,2]; lresS=log(bio5[,2])-log(X.S[,2]); wS=1/X.S[,2]; lwS=1/log(X.S[,2]);


#Determine chi square goodness of fit with or without a specified intake
chi.U[i]=t(resU^2)  %*% wU; tchi.U[i]=(t(resU) %*% wU)^2; lchi.U[i]=t(lresU^2) %*% lwU;
chi.F[i]=t(resF^2)  %*% wF; tchi.F[i]=(t(resF) %*% wF)^2; lchi.F[i]=t(lresF^2) %*% lwF;
chi.B[i]=t(resB^2)  %*% wB; tchi.B[i]=(t(resB) %*% wB)^2; lchi.B[i]=t(lresB^2) %*% lwB;
chi.L[i]=t(resL^2)  %*% wL; tchi.L[i]=(t(resL) %*% wL)^2; lchi.L[i]=t(lresL^2) %*% lwL;
chi.S[i]=t(resS^2)  %*% wS; tchi.S[i]=(t(resS) %*% wS)^2; lchi.S[i]=t(lresS^2) %*% lwS;

#calculate sum of weighted chi's for each bioassay type
Wchi=chi.U*wr[1]+chi.F*wr[2]+chi.B*wr[3]+chi.L*wr[4]+chi.S*wr[5]
Wtchi=tchi.U*wr[1]+tchi.F*wr[2]+tchi.B*wr[3]+tchi.L*wr[4]+tchi.S*wr[5]
LWchi=lchi.U*wr[1]+lchi.F*wr[2]+lchi.B*wr[3]+lchi.L*wr[4]+lchi.S*wr[5]


#obtain the lowest values for final report
if(i==3){logChi=LWchi;Bst.Intake=cbind(intakeU,intakeF,intakeB,intakeL,intakeS); LX.U=X.U;LX.F=X.F;
LX.B=X.B;LX.L=X.L;LX.S=X.S; BWchi=Wchi; BWtchi=Wtchi; Bchi=cbind(chi.U[3], chi.F[3],
chi.B[3],chi.L[3],chi.S[3]);
Blchi=cbind(lchi.U[3],lchi.F[3],lchi.B[3],lchi.L[3],lchi.S[3]);Btchi=cbind(tchi.U[3],tchi.F[3],tchi.B[3],tchi.L[3],tchi.S[3]);
Bsd=sdI;}

        }
cnt=cnt+1
again=0
if(tg=="FALSE"){low=Wchi[3];}else{low=Wtchi[3];}


#Determine if the 3rd or center chi value is lowest.  If not then repeat cycle with adjusted parameters.
if(tg=="FALSE"){
```

```
   for(ii in 1:5){if(Wchi[ii]<low-s){again=1;val[1,z]=q[ii];low=Wchi[ii];}}}
else{
   for(ii in 1:5){if(Wtchi[ii]<low-s){again=1;val[1,z]=q[ii];low=Wtchi[ii];}}
}

if(tg=="FALSE") change=rbind(change,Wchi) else change=rbind(change,Wtchi)

#ensure the R matrix has the best values
R[a,b]=as.numeric(val[1,z])

            }
          }

loops=loops+1
       }
kk=kk+1
   }


X.U[,2]=LX.U[,2]; mU=X.U;mU[,2]=mU[,2]/Bst.Intake[1];
X.F[,2]=LX.F[,2]; mF=X.F;mF[,2]=mF[,2]/Bst.Intake[2];
X.B[,2]=LX.B[,2]; mB=X.B;mB[,2]=mB[,2]/Bst.Intake[3];
X.L[,2]=LX.L[,2]; mL=X.L;mL[,2]=mL[,2]/Bst.Intake[4];
X.S[,2]=LX.S[,2]; mS=X.S;mS[,2]=mS[,2]/Bst.Intake[5];

#determine intake from multiple bioassay types
Nu=dim(case)[1];Nf=dim(bio2)[1];Nb=dim(bio3)[1];Nl=dim(bio4)[1];Ns=dim(bio5)[1];
lnI1=sum(log(case[,2]/mU[,2]))/(log(SF[1]))^2+sum(log(bio2[,2]/mF[,2]))/(log(SF[2]))^2+sum(log(bio3[,2]/mB[,2]))/(log
(SF[3]))^2
+sum(log(bio4[,2]/mL[,2]))/(log(SF[4]))^2+sum(log(bio5[,2]/mS[,2]))/(log(SF[5]))^2
lnI2=sum(Nu/(log(SF[1]))^2+Nf/(log(SF[2]))^2+Nb/(log(SF[3]))^2+Nl/(log(SF[4]))^2+Ns/(log(SF[5]))^2)
lnI=lnI1/lnI2
mI=exp(lnI)

#determine individual intakes
uI=exp(sum(log(case[,2]/mU[,2]))/Nu)
fI=exp(sum(log(bio2[,2]/mF[,2]))/Nf)
bI=exp(sum(log(bio3[,2]/mB[,2]))/Nb)
lI=exp(sum(log(bio4[,2]/mL[,2]))/Nl)
sI=exp(sum(log(bio5[,2]/mS[,2]))/Ns)
IM=matrix(c(mI,uI,fI,bI,lI,sI),nrow=1,byrow=T)
colnames(IM)=c("Total","Urine","Fecal","Blood","Liver","Skeleton")

#setup individual predicted intake arrays for boxplot
Int.U=case; Int.U[,2]=case[,2]/mU[,2];
Int.F=bio2; Int.F[,2]=bio2[,2]/mF[,2];
Int.B=bio3; Int.B[,2]=bio3[,2]/mB[,2];
Int.L=bio4; Int.L[,2]=bio4[,2]/mL[,2];
Int.S=bio5; Int.S[,2]=bio5[,2]/mS[,2];

#determine analysis of variance for the individual intakes
numI=sum(Nu*(uI-mI)^2+Nf*(fI-mI)^2+Nb*(bI-mI)^2+Nl*(lI-mI)^2+Ns*(sI-mI)^2)/2
denI=(sum(((case[,2]/mU[,2])-uI)^2)+sum(((bio2[,2]/mF[,2])-fI)^2)+sum(((bio3[,2]/mB[,2])-bI)^2)
+sum(((bio4[,2]/mL[,2])-lI)^2)+sum(((bio5[,2]/mS[,2])-sI)^2))/(Nu+Nf+Nb+Nl+Ns-3)
Ft=numI/denI

#determine autocorrelation
denU=sum((case[,2]-X.U[,2])^2); sResU=(log(case[,2])-log(X.U[,2]))/log(SF[1]);
numU=0
for(i in 1:(dim(case)[1]-1)){
   numU=(case[i,2]-X.U[i,2])*(case[i+1,2]-X.U[i+1,2])+numU
}
acU=numU/denU

denF=sum((bio2[,2]-X.F[,2])^2); sResF=(log(bio2[,2])-log(X.F[,2]))/log(SF[2]);
numF=0
for(i in 1:(dim(bio2)[1]-1)){
   numF=(bio2[i,2]-X.F[i,2])*(bio2[i+1,2]-X.F[i+1,2])+numF
}
acF=numF/denF
```

```
denB=sum((bio3[,2]-X.B[,2])^2); sResB=(log(bio3[,2])-log(X.B[,2]))/log(SF[3]);
numB=0
for(i in 1:(dim(bio3)[1]-1)){
   numB=(bio3[i,2]-X.B[i,2])*(bio3[i+1,2]-X.B[i+1,2])+numB
}
acB=numB/denB

denL=sum((bio4[,2]-X.L[,2])^2); sResL=(log(bio4[,2])-log(X.L[,2]))/log(SF[4]);
numL=0
for(i in 1:(dim(bio4)[1]-1)){
   numL=(bio4[i,2]-X.L[i,2])*(bio4[i+1,2]-X.L[i+1,2])+numL
}
acL=numL/denL

denS=sum((bio5[,2]-X.S[,2])^2); sResS=(log(bio5[,2])-log(X.S[,2]))/log(SF[5]);
numS=0
for(i in 1:(dim(bio5)[1]-1)){
   numS=(bio5[i,2]-X.S[i,2])*(bio5[i+1,2]-X.S[i+1,2])+numS
}
acS=numS/denS

ac=cbind(acU,acF,acB,acL,acS)

#determined overall autocorrelation using IDEAS guidelines
#sResT=c(sResU,sResF,sResB,sResL,sResS); numT=0; TN=length(sResT)[1];
sResT=c(sResU,sResF,sResB,sResL); numT=0; TN=length(sResT)[1];
for(i in 1:(TN-1)){
   numT=sResT[i]*sResT[i+1]+numT;}
denT=sum(sResT^2)
Tac=numT/denT
Tmean=-1/TN; Tsigma=(TN-2)/(TN*sqrt(TN-1));
TCL95=c(Tmean-1.645*Tsigma,Tmean+1.645*Tsigma);
Tchisq=denT;


#determine individual autocorrelation
numU=0;
for(i in 1:(Nu-1)){
   numU=sResU[i]*sResU[i+1]+numU;}
denU=sum(sResU^2)
acSU=numU/denU

numF=0;
for(i in 1:(Nf-1)){
   numF=sResF[i]*sResF[i+1]+numF;}
denF=sum(sResF^2)
acSF=numF/denF

numB=0;
for(i in 1:(Nb-1)){
   numB=sResB[i]*sResB[i+1]+numB;}
denB=sum(sResB^2)
acSB=numB/denB

numL=0;
for(i in 1:(Nl-1)){
   numL=sResL[i]*sResL[i+1]+numL;}
denL=sum(sResL^2)
acSL=numL/denL

numS=0;
for(i in 1:(Ns-1)){
   numS=sResS[i]*sResS[i+1]+numS;}
denS=sum(sResS^2)
acSS=numS/denS

#plot results

plot(case,log="xy",main=c(title,"Urine"),lty=2,ylim=c(min(X.U[,2],case[,2]),max(X.U[,2],case[,2])))
```

```
        lines(X.U[,1:2],typ="l",col="black")

        plot(bio2,log="xy",main=c(title,"Fecal"),lty=2,ylim=c(min(X.F[,2],bio2[,2]),max(X.F[,2],bio2[,2])))
        lines(X.F[,1:2],typ="l",col="black")

        plot(bio3,log="xy",main=c(title,"Blood"),lty=2, ylim=c(min(X.B[,2],bio3[,2]),max(X.B[,2],bio3[,2])))
        lines(X.B[,1:2],typ="l",col="black")

        plot(bio4,log="xy",main=c(title,"Liver"),lty=2, ylim=c(min(X.L[,2],bio4[,2]),max(X.L[,2],bio4[,2])))
        lines(X.L[,1:2],typ="l",col="black")

        plot(bio5,log="xy",main=c(title,"Skeleton"),lty=2, ylim=c(min(X.S[,2],bio5[,2]),max(X.S[,2],bio5[,2])))
        lines(X.S[,1:2],typ="l",col="black")

        boxplot(Int.U[,2],Int.F[,2],Int.B[,2],Int.L[,2],Int.S[,2],log="y",xlab="Urine, Fecal, Blood, Liver and Skeleton Intake
            (Bq)",main="Intake Distribution Among Bioassay Types",boxwex=0.3)
        abline(h=mI)

Structure(list(X=val, cnt=cnt, chi.low=low, Combined.Intake=IM, IntakeSD=Bsd, Ftest=Ft, chi=Bchi, logChiGoF=Blchi,
Total.logChiGoF=sum(Blchi),WeightedChi=Btchi, autocorrelation=ac, Std.autocorrelation=c(Tac,acSU,acSF,acSB,acSL,acSS),
Total.Conf=TCL95,Total.DF=TN-3, Total.logChi=Tchisq))
}
```

Compare.IRF

This function provides plots of the model prediction (without DTPA) to the ICRP 67 and Leggett 2005 models based on intake retention fractions for visual comparison to actual and supplemented human data. The function requires the input of actual and supplemented human data for urine, fecal, blood, liver and skeleton bioassays as a fraction of the initial intake. The function also requires IRF tables derived from the ICRP 67 and Leggett 2005 models, as ICRP67.IRF and Legg05.IRF for the expected urine, fecal, blood, liver and skeleton measurements up to 20,000 days based on logarithmic time periods (i.e., 1 to 10 days in increments of 1 day, 10 to 100 days in increments of 10 days, and so on up to 20,000 days). Rate matrices with DTPA transitional compartments will be revised to nullify the transitional transfer rates.

Example: The following example provides plots for all bioassay types.

```
> compare.IRF(R.67Pu,type="urine")
> compare.IRF(R.67Pu,type="fecal")
> compare.IRF(R.67Pu,type="blood")
> compare.IRF(R.67Pu,type="liver")
> compare.IRF(R.67Pu,type="skeleton")
```

Function:

```
compare.IRF=function(R=R.Pu,type="urine",bio1=L2.urine,bio2=L2.fecal,bio3=L2.blood,bio4=L2.liver,bi
o5=L3. blood,Leg="FALSE"){


    I1=ICRP67.IRF
    I2=Legg05.IRF
    cc=0
    h.days=24065*365.25

    if(type=="urine"){cM=bio1;cc=1;}
    if(type=="fecal"){cM=bio2;cc=2;}
    if(type=="blood"){cM=bio3;cc=3;}
    if(type=="liver"){cM=bio4;cc=4;}
    #if(type=="bloodm"){cM=bio5;cc=5;}

    Xn=matrix(c(0,0),nrow=1,byrow=T)
```

```
   #set rate matrices with and without dtpa

   R.wo=R
   #find paths to clear for bare rate matrix
   a=0;b=0;c=0;dd=0;
   for(i in 1:dim(R)[1]){if(colnames(R)[i]=="ST0t")a=i;
                  if(colnames(R)[i]=="Bloodt")b=i;
                  if(colnames(R)[i]=="Blood")c=i;
                  if(colnames(R)[i]=="ST0")dd=i;}


   #if dtpa compartments are present, then R matrix is respecified
   if(a!=0){R.wo[dd:c,a:b]=0;R=R.wo;}


   #set compartment location for urine, feces, blood, liver and skeleton
   ku=dim(R)[1]
   kf=ku-1

   for(kk in 1:ku){
      if(colnames(R)[kk]=="Blood"){kb1=kk;}
      if(colnames(R)[kk]=="Liver2"){kl1=kk;
                           #for(kk2 in (kl1:ku)){
                           for(kk2 in 1:ku){
                              if(colnames(R)[kk2]=="Liver1")kl2=kk2}}
      if(colnames(R)[kk]=="CortVol" || colnames(R)[kk]=="Cort.Vol"){ks1=kk;ks2=ks1+5;}
      }



   for(i in 1:38){
      d=I1[i,1];
      last=decays(R,d,h.days)$summary[,2]
      if(type=="urine"){ nd=last[ku] - decays(R,d - 1, h.days)$summary[ku, 2]; cn=2;}
      if(type=="fecal"){ nd=last[kf] - decays(R,d - 1, h.days)$summary[kf, 2]; cn=3;}
      if(type=="blood"){nd=sum(last[kb1]); cn=7;if(Leg=="TRUE")nd=nd+last[kb1+1]}
      if(type=="liver"){nd=sum(last[kl1],last[kl2]); cn=6;if(Leg=="TRUE")nd=sum(last[16:18])}
      if(type=="skeleton"){nd=sum(last[ks1:ks2]); cn=5;}
   Xn=rbind(Xn,c(d,nd))}


colnames(Xn)=c("Days",type)
Xn=Xn[-1,]

if(cc>=1 && cc<=4){

plot(cM,log="xy",ylim=c(min(cM[,2],Xn[,2],I1[,cn],I2[,cn]),max(cM[,2],Xn[,2],I1[,cn],I2[,cn])))
   lines(cbind(Xn[,1],I1[,cn]),typ="l")
   lines(cbind(Xn[,1],I2[,cn]),lty=3)
   lines(cbind(Xn[,1],Xn[,2]),lty=2)
   if(cc==4) pos="bottomright" else pos="topright"

   legend(pos,c(type,"ICRP67","Legg05","R Matrix"),pch=c(1,NA,NA,NA),lty=c(NA,1,3,2))
}
else{
```

```
    plot(Xn,log="xy",ylim=c(min(Xn[,2],I1[,cn],I2[,cn]),max(Xn[,2],I1[,cn],I2[,cn])))
    lines(cbind(Xn[,1],I1[,cn]),typ="l")
    lines(cbind(Xn[,1],I2[,cn]),lty=3)

    legend("bottomright",c("R Matrix","ICRP67","Legg05"),pch=c(1,NA,NA),lty=c(NA,1,3))
  }

  structure(list())

}
```

MLE.lung

Function analyzes inhalations with chelation, providing an estimated intake quantity accompanied with the standard statistics and plots with the actual bioassay sample results and the standard model prediction without chelation. The rate matrix is specified with incorporated ICRP 66 and ICRP 67 compartments, and with DTPA compartments specified. The chelation days are specified for 'd', and the time (t) that is the duration up to the specified period in days. This function accommodates particle solubility for 'type', bound fraction 'fb', and the particle's AMAD 'size'. The function will perform a comparison with the urine, fecal, blood, liver or lung bioassay measurements, which is specified by entering the bioassay type with the 'Exc' input criteria. The intake may be specified greater than 1 or set to 1 when the intake estimate is desired. The 'weight' refers to the chi-square goodness of fit indicator with either the 'model' prediction or 'actual' value listed in the denominator of the formula. The scattering factor is used for chi-squared statistic and autocorrelation determination.

Example:

```
>MLE.lung(R=R.lung,d=c(1,2) ,t=50,case=L2.urine,type="S",fb=0,size=5,Exc="urine",h=24065,intake=1,
title="",weight="model",SF=c(1.6,3,2.1,1.3,1.1))
```

Function:

```
MLE.lung=function(R=R.lung,d=chel1,t=50,case=C169U,type="S",fb=0,size=5,Exc="urine",h=24065,inta
ke=1, title="",weight="actual",SF=c(1.6,3,2.1,1.3,1.1)){
   N=case[dim(case)[1],1]
   if(N<t)t=N else N=t

   #truncated case when N>t
   NN=dim(case)[1]
   for(i in NN:1){
      if(case[i,1]>t)case=case[-i,]}

   if(Exc=="urine"){k=2; SF=SF[1];}
   if(Exc=="fecal"){k=3; SF=SF[2];}
   if(Exc=="liver"){k=6; SF=SF[4];}
   if(Exc=="blood"){k=7; SF=SF[3];}
```

```
   if(Exc=="lung"){k=9; SF=SF[5];}

#determine whether Pu or Am by R matrix dimension
if(dim(R)[1]==54){X.s=Pu.lung3(R=R,d=d,t=t,type=type,h=h)$Pu.atoms;
                  X.z=Pu.lung3(R=R,d=0,t=t,type=type,h=h)$Pu.atoms;}

if(dim(R)[1]==53){X.s=Am.lung3(R=R,d=d,t=t,type=type,h=h)$Am.atoms[,1:k];
                  X.z=Am.lung3(R=R,d=0,t=t,type=type,h=h)$Am.atoms[,1:k];}

   #for lung compartment matrix with the bound compartment
if(dim(R)[1]==67){X.s=Pu.lung3B(R=R,d=d,t=t,type=type,fb=fb,size=size,h=h)$Pu.atoms;
                  X.z=Pu.lung3B(R=R,d=0,t=t,type=type,fb=fb,size=size,h=h)$Pu.atoms;}

if(dim(R)[1]==70){X.s=Pu.lung3C(R=R,d=d,t=t,type=type,fb=fb,size=size,h=h)$Pu.atoms;
                  X.z=Pu.lung3C(R=R,d=0,t=t,type=type,fb=fb,size=size,h=h)$Pu.atoms;}

if(dim(R)[1]==66){X.s=Am.lung3B(R=R,d=d,t=t,type=type,fb=fb,size=size,h=h)$Pu.atoms;
                  X.z=Am.lung3B(R=R,d=0,t=t,type=type,fb=fb,size=size,h=h)$Pu.atoms;}


   X.s=cbind(X.s[,1],X.s[,k])
   X.z=cbind(X.z[,1],X.z[,k])
   X.o=X.s

   #normalize results to case days for regression
   for(i in N:1){
      rem=0
      for(j in 1:dim(case)[1]){
         if(X.s[i,1]==case[j,1])rem=1}
      if(rem==0)X.s=X.s[-i,]}


   #specify intake to use
   if(intake<=1){
      intake=exp(sum(log(case[,2]/X.s[,2])/dim(case)[1]))
   }

   intakeU=intake

   X.U=X.s
   X.o[,2]=intake*X.o[,2]
   X.z[,2]=intake*X.z[,2]

   #get final regression stats
   X.U[,2]=X.U[,2]*intakeU; resU=case[,2]-X.U[,2]; lresU=log(case[,2])-log(X.U[,2]); wU=1/X.U[,2];
     lwU=1/log(X.U[,2])

   #determine autocorrelation
   denU=sum((case[,2]-X.U[,2])^2);
   sResU=(log(case[,2])-log(X.U[,2]))/log(SF[1]);
   numU=0
   for(i in 1:(dim(case)[1]-1)){
      numU=(case[i,2]-X.U[i,2])*(case[i+1,2]-X.U[i+1,2])+numU
   }
   acU=numU/denU
```

```
   #determine individual autocorrelation
   Nu=dim(case)[1];
   numU=0;
   for(i in 1:(Nu-1)){
      numU=sResU[i]*sResU[i+1]+numU;}
   denU=sum(sResU^2)
   acSU=numU/denU
   Tac=numU/denU

   #determined overall autocorrelation using IDEAS guidelines
   sResT=sResU; numT=0; TN=length(sResT)[1];
   for(i in 1:(TN-1)){
      numT=sResT[i]*sResT[i+1]+numT;}
   denT=sum(sResT^2)
   Tmean=-1/TN; Tsigma=(TN-2)/(TN*sqrt(TN-1));
   TCL95=c(Tmean-1.645*Tsigma,Tmean+1.645*Tsigma);
   Tchisq=denT;

   #plot results
   low=min(X.o[,2],X.z[,2],case[,2])
   hi=max(X.o[,2],X.z[,2],case[,2])

   plot(case,log="y",ylim=c(low,hi),main=title)
   lines(X.o,typ="l")
   lines(X.z,typ="l",lty=3)
   plot(case,log="xy",ylim=c(low,hi),main=title)
   lines(X.o,typ="l")
   lines(X.z,typ="l",lty=3)

   structure(list(Intake=intake,Std.autocorrelation=Tac,Total.Conf=TCL95,Total.LogChi=Tchisq,DF=TN-
1))

}
```

Pu.CEDref

This function analyzes the bone surface transformations for a specified time frame. The function requires input of the R matrix, days of chelation (d), time (t) in days, and whether the intake is due to inhalation (inh). The function is setup for ^{239}Pu with a half-life of 24,065 years. The time of interest is typically a 50 year period in relation to a committed effective dose for occupational workers. If the intake is due to inhalation, then inh= "TRUE". The results include the change in urine (Delta.U) and fecal (Delta.F) excretion and their associated enhancement (Enh.Urine and Enh.fecal) for the specified time. Bone surface transformations are also provided that factors in the chelation treatments (BStrans), compared to no treatment (NBStrans), with the bone surface transformations reduction due to chelation (BS.saved). Lung transformations are also provided for inhalation intakes (Lung.tr).

Example: The rate matrix was specified for the Pu-DTPA model coupled with the ICRP 67 systemic model and NCRP 156 wound model. Chelation days were specified for IDEAS Case 123 (chel). The time of interest was 50 years (t) in days.

```
>Pu.CEDref(R=R.67DTPA.0v1,d=chel,t=18250,inh="FALSE")$Pu.atoms
```

Function:

```
Pu.CEDref= function (R=R,d=chel,t=10,inh="FALSE")
{
   h.days = 24065 * 365.25
   R.dtpa=R
   R.wo=R
   #find paths to clear for bare rate matrix
   a=0;b=0;c=0;dd=0;
   for(i in 1:dim(R)[1]){if(colnames(R)[i]=="ST0t")a=i;
                  if(colnames(R)[i]=="Bloodt")b=i;
                  if(colnames(R)[i]=="Blood")c=i;
                  if(colnames(R)[i]=="ST0")dd=i;}
   R.wo[dd:c,a:b]=0;
   u=dim(R)[1]
   f=u-1
   for(kk in 1:u){
```

```
    if(colnames(R)[kk]=="Blood"){kb1=kk;
                            for(kk2 in (kb1:u)){
                               if(colnames(R)[kk2]=="Bloodt")kb2=kk2}}
    if(colnames(R)[kk]=="Liver2"){kl1=kk;
                             for(kk2 in (kl1:u)){
                                if(colnames(R)[kk2]=="Liver1")kl2=kk2}}
    if(colnames(R)[kk]=="CortVol" || colnames(R)[kk]=="Cort.Vol"){b1=kk+1;b2=b1+3;}
  }
  trans=matrix(c(rep(0,dim(R)[1])),ncol=1,byrow=TRUE)
  row.names(trans)=row.names(R)
  colnames(trans)="50-year tranformations"
  k = t;n=t;init=0
  R=R.wo

  #find initial values prior to chelation
  Nlast=decays(R,t,h.days)$summary[,2]
  Nlast1=decays(R,t-1,h.days)$summary[,2]
  Ntrans=decays(R,(50*365.25),h.days)$summary[,3]

#choose correct R matrix
    kk=k
    dt=0
    for(a in 1:length(d)){
      R=R.wo
      if(d[a]>init && d[a]<=n){
        rf=d[a]-init
        if(dt==1)rf=d[a]-d[a-1]
        kk=n-d[a]
        last1=decays(R,(rf-1),h.days)$summary[,2]
        trans=trans+decays(R,(rf-1),h.days)$summary[,3]
        for(j in 1:length(last1)){
          R.dtpa[j,j]=last1[j];R.wo[j,j]=last1[j];}
        R=R.dtpa
        last=decays(R,(1),h.days)$summary[,2]
        trans=trans+decays(R,(1),h.days)$summary[,3]
        for(j in 1:length(last)){
          R.dtpa[j,j]=last[j];R.wo[j,j]=last[j];}
        dt=1
        dlast=d[a]
        if(d[a]==n){
                R=R.wo
                trans=trans+decays(R,(50*365.25-dlast),h.days)$summary[,3]}
        }
    }

    if(dt==0){
      last=decays(R,kk,h.days)$summary[,2]
      last1=decays(R,kk-1,h.days)$summary[,2]
      trans=trans+decays(R,(50*365.25),h.days)$summary[,3]
    }
    if(dt==1 && kk>0){
      R=R.wo
      last=decays(R,kk,h.days)$summary[,2]
      last1=decays(R,kk-1,h.days)$summary[,2]
      trans=trans+decays(R,(50*365.25-dlast),h.days)$summary[,3]
    }

    pu.1 = last[u] - last1[u]
    pu.2 = last[f] - last1[f]
    Npu.1= Nlast[u] - Nlast1[u]
    Npu.2= Nlast[f] - Nlast1[f]
    Enh.u=pu.1/Npu.1
```

```
    Enh.f=pu.2/Npu.2
    D.u=pu.1-Npu.1
    D.f=pu.2-Npu.2
    BStrans=sum(trans[b1],trans[b2])
    NBStrans=sum(Ntrans[b1],Ntrans[b2])
    BS.sav=1-BStrans/NBStrans
    Lung.tr=0
    if(inh=="TRUE")Lung.tr=sum(trans[1:10],trans[15:24])
    pu.new = matrix(c(n, D.u, D.f, Enh.u, Enh.f, BStrans, NBStrans, BS.sav,Lung.tr), nrow = 1,
                byrow = T)

    colnames(pu.new)=c("Days",  "Delta.U(Bq)","Delta.F(Bq)",  "Enh.Urine",  "Enh.fecal",  "BStrans",
        "NBStrans", "BS.saved","Lung.tr")
    Pu.atoms = pu.new

  structure(list(Pu.atoms = Pu.atoms))
}
```

Pu.lung

This function evaluated a rate matrix specified for the ICRP 66 lung model without the bound compartments, and included DTPA compartments. The results provided the final results for the time period of interest, and may be evaluated for fractional day periods (df). This function could evaluate either a Type M or Type S inhalation. Chelation days (d) are specified in the input. The rate matrix is specified for a 54 dimension square matrix.

Example: The rate matrix was specified as R.lung for a Type S absorption for 20 days, with chelation on the first 2 days as follows:

> Pu.lung(R.lung, d=c(1,2), t=20, type= “S”)

Function:

```
Pu.lung = function (R=R,d=chel,t=10,df=1,type="S")
{
#R is specified rate matrix that includes dtpa compartments
#d is days that chelation was applied
#df provides the daily fraction for the time(t) specified
#type is absorption type "S" or "M" for Pu

s.p=0.1; s.pt=100; s.t=0.0001;
Lamb=0.00006

if(type=="M"){s.p=10; s.pt=90; s.t=0.005; Lamb=0.003;}

R[1:13,47]=s.p
R[15:27,47]=s.t
R[42,47]=Lamb
for(i in 1:13){R[i,14+i]=s.pt}
h.days = 24065 * 365.25  #Pu-239 half-life in days
R.dtpa=R
R.wo=R
R.wo[28:47,48:51]=0  #removes dtpa influence

   Pu.atoms = matrix(c(0, 0, 0, 0, 0, 0,0,0,0,0), nrow = 1, byrow = T)
   colnames(Pu.atoms) = c("Time(d)", "Urine", "Faeces", "Tot.Body",
      "Skeleton", "Liver","Blood","ST0","lung","ET")
   Pu.atoms = Pu.atoms[-1, ]
   N=(t/df)
   for (i in 1:N) {
         R=R.wo
```

```
        for(j in 1:length(d)){
                if(i==d[j]) R = R.dtpa}

        k = 1*df
        n = i*df
        last=decays(R,k,h.days)$summary[,2]
        last1=last
        last1[53:54]=0
        if(k>=1) last1=decays(R,k-1,h.days)$summary[,2]

        pu.1 = last[54] - last1[54]
        pu.2 = last[53] - last1[53]
        pu.3 = sum(last[1:51])
        pu.4 = sum(last[34:39])
        pu.5 = sum(last[32],last[40],last[50])
        pu.6 = last[47]
        pu.7 = last[28]
        pu.8 = sum(last[1:10],last[15:24])
        pu.9 = sum(last[11:14],last[25:27])
        pu.new = matrix(c(n, pu.1, pu.2, pu.3, pu.4, pu.5,pu.6,pu.7,pu.8,pu.9), nrow = 1, byrow = T)
        Pu.atoms = rbind(Pu.atoms, pu.new)
#Update R matrix diagonal amounts based on last run
        for(j in 1:length(last)){R.dtpa[j,j]=last[j];R.wo[j,j]=last[j];}
   }
   structure(list(Pu.atoms = Pu.atoms))
}
```

Pu.lung2

This function was used for verification against IAEA Safety Report Series No. 37 (2004), with R matrix R.lung. The results provide a table of intake retention fractions for the incremental urine, feces, total body, lung, skeleton, liver and blood, over a period of 20,000 days. The table results were compared to published results for verification of model performance. The model being verified was the decays function for handling matrix exponentials. This function could verify either a Type M or Type S inhalation.

Example: The verification was performed with the R.lung rate matrix for a Type S absorption as follows:

> Pu.lung2(R.lung)

Function:

```
Pu.lung2=function (R=R.lung,type="S")
{
s.p=0.1; s.pt=100; s.t=0.0001;
Lamb=0.00006

if(type=="M"){s.p=10; s.pt=90; s.t=0.005; Lamb=0.003;}

R[1:13,47]=s.p
R[15:27,47]=s.t
R[42,47]=Lamb
for(i in 1:13){R[i,14+i]=s.pt}

R[28:47,48:51]=0  #removes dtpa influence


   h.days = 24065 * 365.25
   Pu.atoms = matrix(c(0, 0, 0, 0, 0, 0, 0, 0), nrow = 1, byrow = T)
   colnames(Pu.atoms) = c("Time(d)", "Urine", "Faeces", "Tot.Body",
                          "Lung", "Skeleton", "Liver", "Blood")
   Pu.atoms = Pu.atoms[-1, ]
   for (i in 1:38) {
      if (i <= 10) k = i
      if (i > 10 && i <= 19) k = (i - 9) * 10
      if (i > 19 && i <= 28) k = (i - 18) * 100
      if (i > 28 && i <= 37) k = (i - 27) * 1000
      if (i == 38) k = (i - 36) * 10000
      pu.1 = decays(R, k, h.days)$summary[54, 2] - decays(R, k - 1, h.days)$summary[54, 2]
      pu.2 = decays(R, k, h.days)$summary[53, 2] - decays(R, k - 1, h.days)$summary[53, 2]
      pu.3 = sum(decays(R, k, h.days)$summary[1:47, 2])
      pu.4 = sum(decays(R, k, h.days)$summary[1:10, 2], decays(R, k, h.days)$summary[15:24, 2])
      pu.5 = sum(decays(R, k, h.days)$summary[34:39, 2])
      pu.6 = sum(decays(R, k, h.days)$summary[32, 2],decays(R, k, h.days)$summary[40, 2])
      pu.7 = sum(decays(R, k, h.days)$summary[47, 2])
      pu.new = matrix(c(k, pu.1, pu.2, pu.3, pu.4, pu.5, pu.6, pu.7),nrow = 1, byrow = T)
      Pu.atoms = rbind(Pu.atoms, pu.new)
```

```
    }
    structure(list(Pu.atoms = Pu.atoms))
}
```

Pu.lung3

This function is a variation of Pu.lung2 that can provide incremental daily results with various plutonium radionuclides. The function requires input of the rate matrix (R), the chelation days (d), the time of interest (t), the fractional daily period to be studied (df), the absorption type as either Type M or Type S (type), and the half-life in years (h). This function is called upon by MLE.lung, but may also be used by itself. The results are in a table of intake retention fractions as described for Pu.lung2.

Example: The following function can be used to provide incremental results for the first 24 hours.

>Pu.lung3(R=R.lung, d=c(1),t=1, df=1/24, type="S",h=24065)

Function:

```
Pu.lung3= function (R=R,d=chel,t=10,df=1,type="S",h=24065)
{
   #R is specified rate matrix that includes dtpa compartments
   #d is days that chelation was applied
   #df provides the daily fraction for the time(t) specified
   #type is absorption type "S" or "M" for Pu

   s.p=0.1; s.pt=100; s.t=0.0001;
   Lamb=0.00006

   if(type=="M"){s.p=10; s.pt=90; s.t=0.005; Lamb=0.003;}

   R[1:13,47]=s.p
   R[15:27,47]=s.t
   R[42,47]=Lamb
   for(i in 1:13){R[i,14+i]=s.pt}

   h.days = h * 365.25  #Pu-239 half-life in days

   R.dtpa=R
   R.wo=R
   R.wo[28:47,48:51]=0  #removes dtpa influence

   Pu.atoms = matrix(c(0, 0, 0, 0, 0, 0,0,0,0,0), nrow = 1, byrow = T)
   colnames(Pu.atoms) = c("Time(d)", "Urine", "Faeces", "Tot.Body",
                          "Skeleton", "Liver","Blood","ST0","lung","ET")
   Pu.atoms = Pu.atoms[-1, ]

   N=(t/df)

   for (i in 1:N) {
      R=R.wo
```

```
    for(j in 1:length(d)){
            if(df<1){
                    if(floor(i*df+1)==d[j]) R = R.dtpa}
            else {if(i==d[j]) R=R.dtpa}
          }

    k = 1*df
    n = i*df

    last=decays(R,k,h.days)$summary[,2]
    last1=last
    last1[53:54]=0
    if(k>=1) last1=decays(R,k-1,h.days)$summary[,2]

    pu.1 = last[54] - last1[54]
    pu.2 = last[53] - last1[53]
    pu.3 = sum(last[1:51])
    pu.4 = sum(last[34:39])
    pu.5 = sum(last[32],last[40],last[50])
    pu.6 = last[47]
    pu.7 = last[28]
    pu.8 = sum(last[1:10],last[15:24])
    pu.9 = sum(last[11:14],last[25:27])
    pu.new = matrix(c(n, pu.1, pu.2, pu.3, pu.4, pu.5,pu.6,pu.7,pu.8,pu.9), nrow = 1,
                byrow = T)
    Pu.atoms = rbind(Pu.atoms, pu.new)

    #Update R matrix diagonal amounts based on last run
    for(j in 1:length(last)){R.dtpa[j,j]=last[j];R.wo[j,j]=last[j];}

  }
  Pu.atoms
  structure(list(Pu.atoms = Pu.atoms))
}
```

Pu.lung3B

This function is a variation of Pu.lung3 but accommodates a 67 dimension square rate matrix that has been expanded for bound compartments in the ICRP 66 lung model, and allows for the specification of the bound fraction (fb) and specification of the standard AMAD particle sizes (i.e., 1,2,3,5,7,10, 15 and 20 microns). Absorption type may be specified as F, M or S. The rate matrix must also have DTPA compartments specified.

Example: The rate matrix R.LungPu.orig67bv1 was specified for the Pu-DTPA model with the original ICRP 67 model. Chelation days were specified for the first 5 days. The bound fraction was specified as 0.1. The particle AMAD particle size was specified as 10 microns. Default values used otherwise. (Note: the function accommodates a square rate matrix of 67 dimensions, where the R.LungPu.orig67b had 70 dimensions. R.LungPu.orig67bv1 reduced the original rate matrix to 67 dimensions by removing the dummy variables for this example.)

>Pu.lung3B(R=R.LungPu.orig67bv1, d=c(1,2,3,4,5), t=10, fb=0.1, size=10)

Function:

```
Pu.lung3B=function (R=R,d=chel,t=10,df=1,type="S",fb=0,size=5,h=24065)
{
   #R is specified rate matrix that includes dtpa compartments
   #d is days that chelation was applied
   #df provides the daily fraction for the time(t) specified
   #type is absorption type "F","M" or "S"
   #fb is fraction going to the bound compartment
   #size is particle size of either 1,2,3,5,7,10,15 or 20 in microns

   #specify particle size deposition from ICRP 66
   AMTD1=matrix(c(1,0.17,0.21,0.0066,0.0058,0.0084,0.0081,0.11),nrow=1,byrow=T)
   AMTD2=matrix(c(2,0.25,0.32,0.0099,0.0074,0.0080,0.0068,0.092),nrow=1,byrow=T)
   AMTD3=matrix(c(3,0.30,0.37,0.011,0.0073,0.0077,0.0060,0.077),nrow=1,byrow=T)
   AMTD5=matrix(c(5,0.34,0.40,0.012,0.0059,0.0066,0.0044,0.053),nrow=1,byrow=T)
   AMTD7=matrix(c(7,0.35,0.40,0.011,0.0046,0.0055,0.0032,0.038),nrow=1,byrow=T)
   AMTD10=matrix(c(10,0.35,0.38,0.0095,0.0031,0.0042,0.0021,0.024),nrow=1,byrow=T)
```

```
AMTD15=matrix(c(15,0.33,0.36,0.0072,0.0018,0.0027,0.0011,0.012),nrow=1,byrow=T)
AMTD20=matrix(c(20,0.32,0.33,0.0055,0.0011,0.0018,0.00066,0.0072),nrow=1,byrow=T)

AMTD=AMTD1
colnames(AMTD)=c("um","ET1","ET2","BBf","BBs","bbf","bbs","AI")
AMTD=rbind(AMTD,AMTD2,AMTD3,AMTD5,AMTD7,AMTD10,AMTD15,AMTD20)

for(i in 1:8){
if(AMTD[i,1]==size)ps=i}

R[1,1]=0.3*AMTD[ps,8] #AI1
R[2,2]=0.6*AMTD[ps,8] #AI2
R[3,3]=0.1*AMTD[ps,8] #AI3
R[4,4]=0.593*(sum(AMTD[ps,6:7])) #bb1
R[5,5]=0.4*(sum(AMTD[ps,6:7])) #bb2
R[6,6]=0.007*(sum(AMTD[ps,6:7])) #bbseq
R[7,7]=0.663*(sum(AMTD[ps,4:5])) #BB1
R[8,8]=0.33*(sum(AMTD[ps,4:5])) #BB2
R[9,9]=0.007*(sum(AMTD[ps,4:5])) #BBseq
R[11,11]=0.9995*AMTD[ps,3] #ET2
R[12,12]=0.0005*AMTD[ps,3] #ETseq
R[14,14]=AMTD[ps,2]  #ET1

#specify solubility transfer rates based on absorption type
s.p=0.1; s.pt=100; s.t=0.0001;
Lamb=0.00006
if(type=="S"){s.p=(1-fb)*0.1;s.pt=100;s.t=(1-fb)*0.0001;Lamb=0.00006;s.pb=fb*0.1;s.tb=fb*0.0001;s.b=0.00001;}
if(type=="M"){s.p=(1-fb)*10;s.pt=90;s.t=(1-fb)*0.005;Lamb=0.003;s.pb=fb*10;s.tb=fb*0.005;s.b=0.00023;}
 # if(type=="M"){s.p=(1-fb)*50;s.pt=50;s.t=(1-fb)*0.02;Lamb=0.003;s.pb=fb*50;s.tb=fb*0.02;s.b=0.0002;}
#James(2007)
if(type=="F"){s.p=(1-fb)*100;s.pt=0;s.t=(1-fb)*0;Lamb=0.003;s.pb=fb*100;s.tb=fb*0;s.b=0.0002;}

R[1:13,60]=s.p
R[15:27,60]=s.t
R[28:40,60]=s.b
R[55,60]=Lamb
for(i in 1:13){R[i,i+14]=s.pt}
for(i in 1:13){R[i,i+27]=s.pb}
for(i in 1:13){R[i+14,i+27]=s.tb}

h.days = h * 365.25  #Pu-239 half-life in days

R.dtpa=R
R.wo=R
R.wo[41:60,61:64]=0  #removes dtpa influence

Pu.atoms = matrix(c(0, 0, 0, 0, 0, 0,0,0,0,0), nrow = 1, byrow = T)
colnames(Pu.atoms) = c("Time(d)", "Urine", "Faeces", "Tot.Body",
                  "Skeleton", "Liver","Blood","ST0","lung","ET")
Pu.atoms = Pu.atoms[-1, ]

N=(t/df)

for (i in 1:N) {
   R=R.wo
   for(j in 1:length(d)){
            if(df<1){
                  if(floor(i*df+1)==d[j]) R = R.dtpa}
            else {if(i==d[j]) R=R.dtpa}
          }

   k = 1*df
```

```
   n = i*df

   last=decays(R,k,h.days)$summary[,2]
   last1=last
   last1[66:67]=0
   if(k>=1) last1=decays(R,k-1,h.days)$summary[,2]

   pu.1 = last[67] - last1[67]
   pu.2 = last[66] - last1[66]
   pu.3 = sum(last[1:64])
   pu.4 = sum(last[47:52])
   pu.5 = sum(last[45],last[53])
   pu.6 = last[60]
   pu.7 = last[41]
   pu.8 = sum(last[1:10],last[15:24],last[28:37])
   pu.9 = sum(last[11:14],last[25:27],last[38:40])
   pu.new = matrix(c(n, pu.1, pu.2, pu.3, pu.4, pu.5,pu.6,pu.7,pu.8,pu.9), nrow = 1,
            byrow = T)
   Pu.atoms = rbind(Pu.atoms, pu.new)

   #Update R matrix diagonal amounts based on last run
   for(j in 1:length(last)){R.dtpa[j,j]=last[j];R.wo[j,j]=last[j];}

}
Pu.atoms
structure(list(Pu.atoms = Pu.atoms))
        }
```

Pu.lung3C

This function is a variation of Pu.lung3 but accommodates a 70 dimension square rate matrix that has been expanded for bound compartments in the ICRP 66 lung model, and allows for the specification of the bound fraction (fb) and specification of the standard AMAD particle sizes (i.e., 1,2,3,5,7,10, 15 and 20 microns). Furthermore, this function provides organ burden information that was studied during this research. Absorption type may be specified as F, M, S or J (which represented James et al. (2007) parameters). The rate matrix must also have DTPA compartments specified. Other differences included reporting the quantity in the liver, blood and ST0 transitional compartments.

Example: The rate matrix R.LungPu.orig67b was specified for the Pu-DTPA model with the original ICRP 67 model. Chelation days were specified for the first 5 days. The bound fraction was specified as 0.1. The particle AMAD particle size was specified as 10 microns. Default values used otherwise.

>Pu.lung3C(R=R.LungPu.orig67b, d=c(1,2,3,4,5), t=10, fb=0.1, size=10)

Function:

```
Pu.lung3C=function (R=R,d=chel,t=10,df=1,type="S",fb=0,size=5,h=24065)
{
   #R is specified rate matrix that includes dtpa compartments
   #d is days that chelation was applied
   #df provides the daily fraction for the time(t) specified
   #type is absorption type "F","M" or "S" or "J" for James et al. (2007) parameters
   #fb is fraction going to the bound compartment
   #size is particle size of either 1,2,3,5,7,10,15 or 20 in microns

   #specify particle size deposition from ICRP 66
   AMTD1=matrix(c(1,0.17,0.21,0.0066,0.0058,0.0084,0.0081,0.11),nrow=1,byrow=TRUE)
   AMTD2=matrix(c(2,0.25,0.32,0.0099,0.0074,0.0080,0.0068,0.092),nrow=1,byrow=TRUE)
   AMTD3=matrix(c(3,0.30,0.37,0.011,0.0073,0.0077,0.0060,0.077),nrow=1,byrow=TRUE)
   AMTD5=matrix(c(5,0.34,0.40,0.012,0.0059,0.0066,0.0044,0.053),nrow=1,byrow=TRUE)
   AMTD7=matrix(c(7,0.35,0.40,0.011,0.0046,0.0055,0.0032,0.038),nrow=1,byrow=TRUE)
   AMTD10=matrix(c(10,0.35,0.38,0.0095,0.0031,0.0042,0.0021,0.024),nrow=1,byrow=TRUE)
```

```
AMTD15=matrix(c(15,0.33,0.36,0.0072,0.0018,0.0027,0.0011,0.012),nrow=1,byrow=TRUE)
AMTD20=matrix(c(20,0.32,0.33,0.0055,0.0011,0.0018,0.00066,0.0072),nrow=1,byrow=TRUE)

AMTD=AMTD1
colnames(AMTD)=c("um","ET1","ET2","BBf","BBs","bbf","bbs","AI")
AMTD=rbind(AMTD,AMTD2,AMTD3,AMTD5,AMTD7,AMTD10,AMTD15,AMTD20)

for(i in 1:8){
if(AMTD[i,1]==size)ps=i}

R[1,1]=0.3*AMTD[ps,8] #AI1
R[2,2]=0.6*AMTD[ps,8] #AI2
R[3,3]=0.1*AMTD[ps,8] #AI3
R[4,4]=0.593*(sum(AMTD[ps,6:7])) #bb1
R[5,5]=0.4*(sum(AMTD[ps,6:7])) #bb2
R[6,6]=0.007*(sum(AMTD[ps,6:7])) #bbseq
R[7,7]=0.663*(sum(AMTD[ps,4:5])) #BB1
R[8,8]=0.33*(sum(AMTD[ps,4:5])) #BB2
R[9,9]=0.007*(sum(AMTD[ps,4:5])) #BBseq
R[11,11]=0.9995*AMTD[ps,3] #ET2
R[12,12]=0.0005*AMTD[ps,3] #ETseq
R[14,14]=AMTD[ps,2]  #ET1

#specify solubility transfer rates based on absorption type
s.p=0.1; s.pt=100; s.t=0.0001;
Lamb=0.00006
if(type=="S"){s.p=(1-fb)*0.1;s.pt=100;s.t=(1-
fb)*0.0001;Lamb=0.00006;s.pb=fb*0.1;s.tb=fb*0.0001;s.b=0.00001;}
if(type=="M"){s.p=(1-fb)*10;s.pt=90;s.t=(1-
fb)*0.005;Lamb=0.003;s.pb=fb*10;s.tb=fb*0.005;s.b=0.00023;}
if(type=="F"){s.p=(1-fb)*100;s.pt=0;s.t=(1-fb)*0;Lamb=0.003;s.pb=fb*100;s.tb=fb*0;s.b=0.0002;}

#James (2007) parameters
if(type=="J"){s.p=(1-fb)*10;s.pt=100;s.t=(1-fb)*0.02;Lamb=0.003;s.pb=fb*10;s.tb=fb*0.02;s.b=0.0002;}

R[1:13,60]=s.p
R[15:27,60]=s.t
R[28:40,60]=s.b
R[55,60]=Lamb
for(i in 1:13){R[i,i+14]=s.pt}
for(i in 1:13){R[i,i+27]=s.pb}
for(i in 1:13){R[i+14,i+27]=s.tb}

h.days = h * 365.25  #Pu-239 half-life in days

R.dtpa=R
R.wo=R
R.wo[41:60,61:67]=0  #removes dtpa influence

Pu.atoms = matrix(c(0, 0, 0, 0, 0, 0,0,0,0,0), nrow = 1, byrow = TRUE)
colnames(Pu.atoms) = c("Time(d)", "Urine", "Faeces", "Tot.Body",
                       "Skeleton", "Liver","Blood","ST0","lung","ET")
Pu.atoms = Pu.atoms[-1, ]
organs=Pu.atoms
colnames(organs) = c("Time(d)", "Blood", "ST0", "ST1",
                     "Liver1", "Liver2","Trab.Surf","Cort.Surf","Systemic","Lungs+ET")
final= matrix(c(0, 0, 0, 0, 0, 0,0,0,0,0,0,0), nrow = 1, byrow = TRUE)
colnames(final) = c("Time(d)","Systemic","Lungs","LNth","Skeleton","Cortical","Trabecular","Liver",
    "Kidneys","Testes","ST1","ST2")
final=final[-1,]

N=(t/df)
```

```
kr=R[42,62] #ST1.ST1t initial transfer rate
l1=R[53,63] #liver1.liver1t initial transfer rate
l2=R[45,64] #liver2.liver2t initial transfer rate
ts=R[51,65] #TrabSurf.TrabBSt initial transfer rate
cs=R[48,66] #CortSurf.CortBSt initial transfer rate
for (i in 1:N) {
   R=R.wo

   for(j in 1:length(d)){
            if(df<1){
                     if(floor(i*df+1)==d[j]){ R = R.dtpa;}
                  }

   else {if(i==d[j]){ R=R.dtpa; }
         }
         }

   k = 1*df
   n = i*df

   last=decays(R,k,h.days)$summary[,2]
   last1=last
   last1[69:70]=0
   if(k>=1) last1=decays(R,k-1,h.days)$summary[,2]

   pu.1 = last[70] - last1[70] #incremental urine
   pu.2 = last[69] - last1[69] #incremental fecal
   pu.3 = sum(last[1:67]) #systemic burden
   pu.4 = sum(last[47:52]) #skeleton burden
   pu.5 = sum(last[45],last[53],last[63],last[64]) #liver burden includes DTPA
   pu.6 = sum(last[60],last[67]) #blood burden includes DTPA compartment
   pu.7 = sum(last[41],last[61]) #ST0 burden includes DTPA compartment
   pu.8 = sum(last[1:10],last[15:24],last[28:37]) #lung burden
   pu.9 = sum(last[11:14],last[25:27],last[38:40]) #ET Airway burden
   pu.new = matrix(c(n, pu.1, pu.2, pu.3, pu.4, pu.5,pu.6,pu.7,pu.8,pu.9), nrow = 1,
               byrow = T)
   Pu.atoms = rbind(Pu.atoms, pu.new)

   #setup matrix for tracking organ content
   o.1 = sum(last[60]) #blood burden
   o.2 = sum(last[41]) #ST0 burden
   o.3 = sum(last[42]) #ST1 burden
   o.4 = sum(last[53]) #liver 1 burden
   o.5 = sum(last[45]) #liver 2 burden
   o.6 = sum(last[51]) #Trab Surface burden
   o.7 = sum(last[48]) #Cort Surface burden
   o.8 = sum(last[41:67]) #Systemic burden without lungs
   o.9 = sum(last[1:40]) #Lung burden including ET Airways
   o.new = matrix(c(n, o.1, o.2, o.3, o.4, o.5,o.6,o.7,o.8,o.9), nrow = 1, byrow = T)
   organs = rbind(organs, o.new)

   #setup matrix for tracking organ content
   f.1 = sum(last[41:67]) #systemic without lungs
   f.2 = sum(last[1:9],last[15:23],last[28:36]) #Lungs, larynx, trachea
   f.3 = sum(last[10],last[24],last[37]) #LNth thoracic lymph nodes
   f.4 = sum(last[47:52]) #Skeleton
   f.5 = sum(last[47:49]) #Cortical
   f.6 = sum(last[50:52]) #Trabecular
   f.7 = sum(last[45],last[53]) #Liver
   f.8 = sum(last[44]) #Kidneys
   f.9 = sum(last[46]) #Testes
   f.10 = sum(last[42]) #ST1
```

```
    f.11 = sum(last[43]) #ST2

    f.new = matrix(c(n, f.1, f.2, f.3, f.4, f.5,f.6,f.7,f.8,f.9,f.10,f.11), nrow = 1, byrow = T)
    final = rbind(final, f.new)

  #Update R matrix diagonal amounts based on last run
    for(j in 1:length(last)){R.dtpa[j,j]=last[j];R.wo[j,j]=last[j];}

  }
  Pu.atoms
  structure(list(Pu.atoms = Pu.atoms,organs=organs,final=final))
}
```

Pu.wound

This function can be used to construct IRF tables for various wound types. This function was used for verification against IAEA Safety Report Series No. 37 (2004) tables for intakes by injection and ingestion. The wound type can be specified for weak, moderate, strong, avid, colloid, 123 (i.e., IDEAS case 123 optimization), injection (inj= "TRUE"), and ingestion (ing= "TRUE"). Time is specified as 38 to represent the total logarithmic time periods in the IRF table. The rate matrix is specified for a ^{239}Pu wound model that includes the ICRP 67 systemic model with the NCRP 156 wound model without specifying DTPA compartments.

Example:

To obtain an IRF table for an injection:
> Pu.wound(R=R.Pu,inj="TRUE")

To obtain an IRF table for a strong-retention wound:
> Pu.wound(R=R.Pu,type="strong")

Function:

```
Pu.wound= function (inj = "FALSE", ing = "FALSE",R=R,type="strong",t=38)
{
   #adjust R for wound type
   if(type=="weak"){R[1:3,1:3]=matrix(c(1,20,0,2.8,0,0.25,0.08,0,0),nrow=3,byrow=TRUE);R[1,24]=45;}
   if(type=="moderate"){R[1:3,1:3]=matrix(c(1,30,0,0.4,0,0.065,0.02,0,0),nrow=3,byrow=TRUE);R[1,24]=45;}
   if(type=="strong"){R[1:3,1:3]=matrix(c(1,0.6,0,0.024,0,0.01,0.0012,0,0),nrow=3,byrow=TRUE);R[1,24]=0.67;}
   if(type=="avid"){R[1:3,1:3]=matrix(c(1,30,0,0.03,0,10,0.005,0,0),nrow=3,byrow=TRUE);R[1,24]=7;}
   if(type=="colloid"){R[1:4,1:4]=0;R[2,2]=1;R[1,24]=0.5; R[1,2]=2.5;R[2,1]=0.025;R[2,3]=0.05; R[2,4]=0.002;
      R[3,1]=0.0015;R[3,4]=0.0004;R[4,24]=0.03;}
   if(type=="123"){R[1:3,1:3]=matrix(c(0.5,0.094,0,0.026,0.5,0.01,0.0012,0,0),nrow=3,byrow=TRUE);R[1,24]=0.241;}

   h.days = 24065 * 365.25
   if (inj == "TRUE") {
      R[1:4, 1:4] = 0
      R[24, 24] = 1
   }
   if (ing == "TRUE") {
      R[1:4, 1:4] = 0
      R[18, 18] = 1
   }


   #set compartment location for urine, feces, blood, liver and skeleton
   ku=dim(R)[1]
```

```
   kf=ku-1

   for(kk in 1:ku){
      if(colnames(R)[kk]=="Blood"){kb1=kk;}
      if(colnames(R)[kk]=="Liver2"){kl1=kk;
                              for(kk2 in (kl1:ku)){
                                 if(colnames(R)[kk2]=="Liver1")kl2=kk2}}
      if(colnames(R)[kk]=="CortVol" || colnames(R)[kk]=="Cort.Vol"){ks1=kk;ks2=ks1+5;}
   }


Pu.atoms = matrix(c(0, 0, 0, 0, 0, 0,0,0), nrow = 1, byrow = T)
colnames(Pu.atoms) = c("Time(d)", "Urine", "Faeces", "Tot.Body",
                       "Skeleton", "Liver","Blood","Wound")
Pu.atoms = Pu.atoms[-1, ]

for (i in 1:t) {
   if (i <= 10) k = i
   if (i > 10 && i <= 19) k = (i - 9) * 10
   if (i > 19 && i <= 28) k = (i - 18) * 100
   if (i > 28 && i <= 37) k = (i - 27) * 1000
   if (i == 38) k = (i - 36) * 10000

   last=decays(R,k,h.days)$summary[,2]
   pu.1 = last[ku] - decays(R,k - 1, h.days)$summary[ku, 2] #incremental urine
   pu.2 = last[kf] - decays(R,k - 1, h.days)$summary[kf, 2] #incremental feces
   pu.3 = sum(last[1:(kf-1)]) #whole body quantity
   pu.4 = sum(last[ks1:ks2])  #total skeleton quantity
   pu.5 = sum(last[kl1],last[kl2]) #,last[27]) #liver quantity
   pu.6 = sum(last[kb1]) #blood quantity
   pu.7 = sum(decays(R,k,h.days)$summary[1:4,2]) #wound quantity
   pu.new = matrix(c(k, pu.1, pu.2, pu.3, pu.4, pu.5,pu.6,pu.7), nrow = 1, byrow = T)
   Pu.atoms = rbind(Pu.atoms, pu.new)
}
Pu.atoms
structure(list(Pu.atoms = Pu.atoms))
}
```

Appendix 2: Model Verification with the R Programming Language

^{239}Pu Injection:

The model assumed that an intravenous injection of ^{239}Pu into the blood compartment. Comparison with the IAEA Safety Report Series No. 37 (2004) results indicated almost an identical comparison with only a minor exception that was possibly due to rounding. For example, the total body on day 10,000 indicated 0.6649 where the IAEA result was 0.67.

```
> Pu.wound(R=R.Pu,inj="TRUE")
$Pu.atoms
      Time(d)        Urine       Faeces  Tot.Body  Skeleton     Liver        Blood Wound
 [1,]       1 8.185227e-03 1.605829e-03 0.9902089 0.2164938 0.1300206 0.4391491664     0
 [2,]       2 4.485451e-03 4.297964e-03 0.9814254 0.3201987 0.1922862 0.2336856166     0
 [3,]       3 2.599661e-03 4.189040e-03 0.9746366 0.3792890 0.2277496 0.1428322308     0
 [4,]       4 1.709280e-03 3.132688e-03 0.9697946 0.4168643 0.2502875 0.0942088546     0
 [5,]       5 1.206981e-03 2.166317e-03 0.9664212 0.4421222 0.2654254 0.0643911263     0
 [6,]       6 8.889915e-04 1.477696e-03 0.9640544 0.4595283 0.2758464 0.0446973120     0
 [7,]       7 6.753552e-04 1.016790e-03 0.9623622 0.4716517 0.2830938 0.0312340072     0
 [8,]       8 5.278387e-04 7.099782e-04 0.9611243 0.4801343 0.2881545 0.0218930416     0
 [9,]       9 4.246874e-04 5.033741e-04 0.9601962 0.4860822 0.2916927 0.0153725008     0
[10,]      10 3.520805e-04 3.623790e-04 0.9594816 0.4902580 0.2941668 0.0108095380     0
[11,]      20 1.745124e-04 4.956529e-05 0.9562001 0.4999516 0.2996782 0.0004394042     0
[12,]      30 1.554994e-04 4.023419e-05 0.9541491 0.5004187 0.2997071 0.0001586594     0
[13,]      40 1.428121e-04 3.950961e-05 0.9522672 0.5005760 0.2996062 0.0001659840     0
[14,]      50 1.318542e-04 3.903309e-05 0.9505073 0.5006828 0.2995266 0.0001804234     0
[15,]      60 1.222920e-04 3.856542e-05 0.9488540 0.5007499 0.2994707 0.0001940046     0
[16,]      70 1.139403e-04 3.810022e-05 0.9472941 0.5007806 0.2994364 0.0002065775     0
[17,]      80 1.066412e-04 3.763772e-05 0.9458164 0.5007781 0.2994221 0.0002182104     0
[18,]      90 1.002573e-04 3.717832e-05 0.9444112 0.5007450 0.2994259 0.0002289727     0
[19,]     100 9.466935e-05 3.672236e-05 0.9430700 0.5006838 0.2994464 0.0002389286     0
[20,]     200 6.521447e-05 3.240608e-05 0.9319332 0.4989645 0.3002916 0.0003052684     0
[21,]     300 5.581751e-05 2.861747e-05 0.9229090 0.4961502 0.3017274 0.0003350455     0
[22,]     400 5.144920e-05 2.537519e-05 0.9148662 0.4929651 0.3033005 0.0003476158     0
[23,]     500 4.843670e-05 2.263466e-05 0.9074769 0.4897228 0.3048147 0.0003519702     0
[24,]     600 4.588969e-05 2.033164e-05 0.9006134 0.4865518 0.3061908 0.0003523175     0
[25,]     700 4.359046e-05 1.840053e-05 0.8942024 0.4834984 0.3074018 0.0003506530     0
[26,]     800 4.148015e-05 1.678150e-05 0.8881884 0.4805735 0.3084437 0.0003479429     0
[27,]     900 3.953612e-05 1.542259e-05 0.8825254 0.4777737 0.3093223 0.0003446703     0
[28,]    1000 3.774372e-05 1.427976e-05 0.8771737 0.4750904 0.3100469 0.0003410884     0
[29,]    2000 2.582404e-05 9.042949e-06 0.8350693 0.4529655 0.3108548 0.0003037607     0
[30,]    3000 2.007676e-05 7.563915e-06 0.8041875 0.4366241 0.3043337 0.0002735986     0
[31,]    4000 1.699568e-05 6.812967e-06 0.7785742 0.4241799 0.2941031 0.0002506291     0
[32,]    5000 1.513507e-05 6.287610e-06 0.7559797 0.4144270 0.2820944 0.0002326653     0
[33,]    6000 1.387582e-05 5.876091e-06 0.7353772 0.4064319 0.2694243 0.0002181423     0
[34,]    7000 1.294065e-05 5.538233e-06 0.7162305 0.3995105 0.2567514 0.0002060599     0
[35,]    8000 1.219777e-05 5.252797e-06 0.6982268 0.3931914 0.2444588 0.0001957666     0
[36,]    9000 1.157967e-05 5.006342e-06 0.6811659 0.3871658 0.2327579 0.0001868224     0
[37,]   10000 1.104872e-05 4.789741e-06 0.6649093 0.3812411 0.2217529 0.0001789213     0
[38,]   20000 7.818644e-06 3.419911e-06 0.5319935 0.3184667 0.1468636 0.0001282817     0
```

IAEA Safety Report Series No. 37 (2004) ^{239}Pu injection retention fraction table
Radionuclide: ^{239}Pu
Intake: Injection
f1: 0.00050

Time(d)	Urine	Faeces	Tot.Body	Skeleton	Liver
1	8.2E-03	1.6E-03	9.9E-01	2.2E-01	1.3E-01
2	4.5E-03	4.3E-03	9.8E-01	3.2E-01	1.9E-01
3	2.6E-03	4.2E-03	9.7E-01	3.8E-01	2.3E-01
4	1.7E-03	3.1E-03	9.7E-01	4.2E-01	2.5E-01
5	1.2E-03	2.2E-03	9.7E-01	4.4E-01	2.7E-01
6	8.9E-04	1.5E-03	9.6E-01	4.6E-01	2.8E-01
7	6.7E-04	1.0E-03	9.6E-01	4.7E-01	2.8E-01
8	5.3E-04	7.1E-04	9.6E-01	4.8E-01	2.9E-01
9	4.2E-04	5.0E-04	9.6E-01	4.9E-01	2.9E-01
10	3.5E-04	3.6E-04	9.6E-01	4.9E-01	2.9E-01
20	1.7E-04	5.0E-05	9.6E-01	5.0E-01	3.0E-01
30	1.6E-04	4.0E-05	9.5E-01	5.0E-01	3.0E-01
40	1.4E-04	3.9E-05	9.5E-01	5.0E-01	3.0E-01
50	1.3E-04	3.9E-05	9.5E-01	5.0E-01	3.0E-01
60	1.2E-04	3.9E-05	9.5E-01	5.0E-01	3.0E-01
70	1.1E-04	3.8E-05	9.5E-01	5.0E-01	3.0E-01
80	1.1E-04	3.8E-05	9.5E-01	5.0E-01	3.0E-01
90	1.0E-04	3.7E-05	9.4E-01	5.0E-01	3.0E-01
100	9.5E-05	3.7E-05	9.4E-01	5.0E-01	3.0E-01
200	6.5E-05	3.2E-05	9.3E-01	5.0E-01	3.0E-01
300	5.6E-05	2.9E-05	9.2E-01	5.0E-01	3.0E-01
400	5.1E-05	2.5E-05	9.1E-01	4.9E-01	3.0E-01
500	4.8E-05	2.3E-05	9.1E-01	4.9E-01	3.0E-01
600	4.6E-05	2.0E-05	9.0E-01	4.9E-01	3.1E-01
700	4.4E-05	1.8E-05	8.9E-01	4.8E-01	3.1E-01
800	4.1E-05	1.7E-05	8.9E-01	4.8E-01	3.1E-01
900	3.9E-05	1.5E-05	8.8E-01	4.8E-01	3.1E-01
1000	3.8E-05	1.4E-05	8.8E-01	4.8E-01	3.1E-01
2000	2.6E-05	9.0E-06	8.4E-01	4.5E-01	3.1E-01
3000	2.0E-05	7.6E-06	8.0E-01	4.4E-01	3.0E-01
4000	1.7E-05	6.8E-06	7.8E-01	4.2E-01	2.9E-01
5000	1.5E-05	6.3E-06	7.6E-01	4.1E-01	2.8E-01
6000	1.4E-05	5.9E-06	7.4E-01	4.1E-01	2.7E-01
7000	1.3E-05	5.5E-06	7.2E-01	4.0E-01	2.6E-01
8000	1.2E-05	5.2E-06	7.0E-01	3.9E-01	2.4E-01
9000	1.2E-05	5.0E-06	6.8E-01	3.9E-01	2.3E-01
10000	1.1E-05	4.8E-06	6.7E-01	3.8E-01	2.2E-01
20000	7.8E-06	3.4E-06	5.3E-01	3.2E-01	1.5E-01

^{239}Pu Ingestion:

The model assumed all of the activity was placed in the stomach compartment. Comparison with the IAEA Safety Report Series No. 37 (2004) results were consistent and appeared to be identical by inspection, with the exception of the IAEA results being rounded.

```
> Pu.wound(R=R.Pu,ing="TRUE")
$Pu.atoms
      Time(d)        Urine       Faeces     Tot.Body     Skeleton        Liver        Blood Wound
 [1,]       1 3.365021e-06 2.822620e-01 0.7177345835 9.128315e-05 5.482308e-05 2.576524e-04     0
 [2,]       2 2.587914e-06 3.888870e-01 0.3288449288 1.512834e-04 9.085056e-05 1.324571e-04     0
 [3,]       3 1.446556e-06 1.968833e-01 0.1319601784 1.843289e-04 1.106852e-04 7.883856e-05     0
 [4,]       4 9.288953e-07 8.134303e-02 0.0506162082 2.049233e-04 1.230396e-04 5.130853e-05     0
 [5,]       5 6.474691e-07 3.139831e-02 0.0192172501 2.186354e-04 1.312593e-04 3.485967e-05     0
 [6,]       6 4.730687e-07 1.179470e-02 0.0074220766 2.280459e-04 1.368947e-04 2.413607e-05     0
 [7,]       7 3.570987e-07 4.379539e-03 0.0030421801 2.345889e-04 1.408076e-04 1.684730e-05     0
 [8,]       8 2.773910e-07 1.617977e-03 0.0014239255 2.391634e-04 1.435380e-04 1.180253e-05     0
 [9,]       9 2.217762e-07 5.964501e-04 0.0008272536 2.423698e-04 1.454468e-04 8.284475e-06     0
[10,]      10 1.826779e-07 2.196981e-04 0.0006073728 2.446203e-04 1.467815e-04 5.823579e-06     0
[11,]      20 8.756060e-08 3.510680e-08 0.0004778900 2.498376e-04 1.497592e-04 2.314914e-07     0
[12,]      30 7.785635e-08 2.012270e-08 0.0004768565 2.500822e-04 1.497797e-04 7.946478e-08     0
[13,]      40 7.149278e-08 1.975012e-08 0.0004759146 2.501616e-04 1.497292e-04 8.280140e-08     0
[14,]      50 6.600084e-08 1.951167e-08 0.0004750339 2.502154e-04 1.496892e-04 9.001971e-08     0
[15,]      60 6.120858e-08 1.927793e-08 0.0004742066 2.502493e-04 1.496610e-04 9.681763e-08     0
[16,]      70 5.702306e-08 1.904542e-08 0.0004734261 2.502650e-04 1.496437e-04 1.031111e-07     0
[17,]      80 5.336509e-08 1.881426e-08 0.0004726869 2.502641e-04 1.496363e-04 1.089341e-07     0
[18,]      90 5.016587e-08 1.858463e-08 0.0004719839 2.502478e-04 1.496380e-04 1.143213e-07     0
[19,]     100 4.736553e-08 1.835673e-08 0.0004713130 2.502175e-04 1.496481e-04 1.193048e-07     0
[20,]     200 3.260663e-08 1.619917e-08 0.0004657439 2.493601e-04 1.500694e-04 1.525125e-07     0
[21,]     300 2.790086e-08 1.430524e-08 0.0004612327 2.479543e-04 1.507867e-04 1.674192e-07     0
[22,]     400 2.571532e-08 1.268436e-08 0.0004572125 2.463627e-04 1.515728e-04 1.737132e-07     0
[23,]     500 2.420908e-08 1.131429e-08 0.0004535191 2.447424e-04 1.523297e-04 1.758952e-07     0
[24,]     600 2.293588e-08 1.016293e-08 0.0004500886 2.431575e-04 1.530175e-04 1.760716e-07     0
[25,]     700 2.178663e-08 9.197506e-09 0.0004468842 2.416315e-04 1.536229e-04 1.752412e-07     0
[26,]     800 2.073182e-08 8.388100e-09 0.0004438783 2.401696e-04 1.541438e-04 1.738877e-07     0
[27,]     900 1.976012e-08 7.708738e-09 0.0004410479 2.387703e-04 1.545830e-04 1.722526e-07     0
[28,]    1000 1.886422e-08 7.137403e-09 0.0004383731 2.374292e-04 1.549453e-04 1.704628e-07     0
[29,]    2000 1.290640e-08 4.519460e-09 0.0004173296 2.263715e-04 1.553501e-04 1.518080e-07     0
[30,]    3000 1.003378e-08 3.780167e-09 0.0004018957 2.182044e-04 1.520917e-04 1.367337e-07     0
[31,]    4000 8.493833e-09 3.404844e-09 0.0003890950 2.119851e-04 1.469792e-04 1.252540e-07     0
[32,]    5000 7.563907e-09 3.142282e-09 0.0003778032 2.071108e-04 1.409780e-04 1.162762e-07     0
[33,]    6000 6.934554e-09 2.936616e-09 0.0003675069 2.031151e-04 1.346461e-04 1.090180e-07     0
[34,]    7000 6.467177e-09 2.767765e-09 0.0003579382 1.996561e-04 1.283128e-04 1.029796e-07     0
[35,]    8000 6.095908e-09 2.625113e-09 0.0003489407 1.964981e-04 1.221696e-04 9.783535e-08     0
[36,]    9000 5.786998e-09 2.501944e-09 0.0003404145 1.934868e-04 1.163220e-04 9.336541e-08     0
[37,]   10000 5.521653e-09 2.393694e-09 0.0003322902 1.905259e-04 1.108222e-04 8.941674e-08     0
[38,]   20000 3.907392e-09 1.709111e-09 0.0002658650 1.591544e-04 7.339562e-05 6.410919e-08     0
```

IAEA Safety Report Series No. 37 (2004) ^{239}Pu ingestion retention fraction table
Radionuclide: ^{239}Pu
Intake: Ingestion
f1: 0.00050

Time(d)	Urine	Faeces	Tot.Body	Skeleton	Liver
1	3.4E-06	2.8E-01	7.2E-01	9.1E-05	5.5E-05
2	2.6E-06	3.9E-01	3.3E-01	1.5E-04	9.1E-05
3	1.4E-06	2.0E-01	1.3E-01	1.8E-04	1.1E-04
4	9.3E-07	8.1E-02	5.1E-02	2.1E-04	1.2E-04
5	6.5E-07	3.1E-02	1.9E-02	2.2E-04	1.3E-04
6	4.7E-07	1.2E-02	7.4E-03	2.3E-04	1.4E-04
7	3.6E-07	4.4E-03	3.0E-03	2.3E-04	1.4E-04
8	2.8E-07	1.6E-03	1.4E-03	2.4E-04	1.4E-04
9	2.2E-07	6.0E-04	8.3E-04	2.4E-04	1.5E-04
10	1.8E-07	2.2E-04	6.1E-04	2.4E-04	1.5E-04
20	8.7E-08	3.5E-08	4.8E-04	2.5E-04	1.5E-04
30	7.8E-08	2.0E-08	4.8E-04	2.5E-04	1.5E-04
40	7.1E-08	2.0E-08	4.8E-04	2.5E-04	1.5E-04
50	6.6E-08	2.0E-08	4.8E-04	2.5E-04	1.5E-04
60	6.1E-08	1.9E-08	4.7E-04	2.5E-04	1.5E-04
70	5.7E-08	1.9E-08	4.7E-04	2.5E-04	1.5E-04
80	5.3E-08	1.9E-08	4.7E-04	2.5E-04	1.5E-04
90	5.0E-08	1.9E-08	4.7E-04	2.5E-04	1.5E-04
100	4.7E-08	1.8E-08	4.7E-04	2.5E-04	1.5E-04
200	3.3E-08	1.6E-08	4.7E-04	2.5E-04	1.5E-04
300	2.8E-08	1.4E-08	4.6E-04	2.5E-04	1.5E-04
400	2.6E-08	1.3E-08	4.6E-04	2.5E-04	1.5E-04
500	2.4E-08	1.1E-08	4.5E-04	2.5E-04	1.5E-04
600	2.3E-08	1.0E-08	4.5E-04	2.4E-04	1.5E-04
700	2.2E-08	9.2E-09	4.5E-04	2.4E-04	1.5E-04
800	2.1E-08	8.4E-09	4.4E-04	2.4E-04	1.5E-04
900	2.0E-08	7.7E-09	4.4E-04	2.4E-04	1.5E-04
1000	1.9E-08	7.1E-09	4.4E-04	2.4E-04	1.5E-04
2000	1.3E-08	4.5E-09	4.2E-04	2.3E-04	1.6E-04
3000	1.0E-08	3.8E-09	4.0E-04	2.2E-04	1.5E-04
4000	8.5E-09	3.4E-09	3.9E-04	2.1E-04	1.5E-04
5000	7.6E-09	3.1E-09	3.8E-04	2.1E-04	1.4E-04
6000	6.9E-09	2.9E-09	3.7E-04	2.0E-04	1.3E-04
7000	6.5E-09	2.8E-09	3.6E-04	2.0E-04	1.3E-04
8000	6.1E-09	2.6E-09	3.5E-04	2.0E-04	1.2E-04
9000	5.8E-09	2.5E-09	3.4E-04	1.9E-04	1.2E-04
10000	5.5E-09	2.4E-09	3.3E-04	1.9E-04	1.1E-04
20000	3.9E-09	1.7E-09	2.7E-04	1.6E-04	7.3E-05

^{239}Pu Inhalation:

The lung model assumed an absorption Type S and 5-μm AMAD particle size. Comparison with the IAEA Safety Report Series No. 37 (2004) results indicated almost an identical comparison with a few exceptions that were possibly due to rounding. For example, the total body on day 4 indicated 0.09048 where the IAEA result was 0.091, and the fecal result on day 8000 indicated 1.348 where the IAEA result indicated 1.4.

```
> Pu.lung2(R.lung)
$Pu.atoms
      Time(d)        Urine       Faeces    Tot.Body         Lung     Skeleton        Liver        Blood
 [1,]       1 2.349495e-06 1.143834e-01 0.492593248 0.0640823491 6.226993e-05 3.739775e-05 1.308410e-04
 [2,]       2 1.359557e-06 1.635710e-01 0.249955893 0.0625084161 9.388072e-05 5.637754e-05 7.352845e-05
 [3,]       3 8.362509e-07 8.427063e-02 0.136598025 0.0617518251 1.130954e-04 6.791016e-05 4.842500e-05
 [4,]       4 5.921156e-07 3.541919e-02 0.090477951 0.0611184245 1.263878e-04 7.588463e-05 3.509227e-05
 [5,]       5 4.557056e-07 1.409563e-02 0.072445440 0.0605140208 1.363080e-04 8.183293e-05 2.693604e-05
 [6,]       6 3.698098e-07 5.678073e-03 0.065318866 0.0599255532 1.440788e-04 8.648978e-05 2.153659e-05
 [7,]       7 3.122356e-07 2.477792e-03 0.062308021 0.0593509485 1.503975e-04 9.027411e-05 1.782296e-05
 [8,]       8 2.725088e-07 1.275966e-03 0.060835795 0.0587896284 1.557077e-04 9.345245e-05 1.522166e-05
 [9,]       9 2.447274e-07 8.227810e-04 0.059940667 0.0582412247 1.603077e-04 9.620405e-05 1.338089e-05
[10,]      10 2.251623e-07 6.474355e-04 0.059266478 0.0577054054 1.644032e-04 9.865247e-05 1.206826e-05
[11,]      20 1.771209e-07 4.385799e-04 0.054318158 0.0529730863 1.953152e-04 1.171030e-04 8.517061e-06
[12,]      30 1.720332e-07 3.500319e-04 0.050436114 0.0491960261 2.215270e-04 1.327326e-04 7.833500e-06
[13,]      40 1.689030e-07 2.812270e-04 0.047326702 0.0461608082 2.458778e-04 1.472503e-04 7.349576e-06
[14,]      50 1.664202e-07 2.276110e-04 0.044818566 0.0437032989 2.687822e-04 1.609076e-04 6.962747e-06
[15,]      60 1.644406e-07 1.857121e-04 0.042779678 0.0416969622 2.905118e-04 1.738696e-04 6.650010e-06
[16,]      70 1.628752e-07 1.528746e-04 0.041108049 0.0400440081 3.112771e-04 1.862643e-04 6.395202e-06
[17,]      80 1.616531e-07 1.270622e-04 0.039724706 0.0386686736 3.312434e-04 1.981920e-04 6.185857e-06
[18,]      90 1.607170e-07 1.067100e-04 0.038568339 0.0375121129 3.505406e-04 2.097317e-04 6.012296e-06
[19,]     100 1.600202e-07 9.061228e-05 0.037591233 0.0365285043 3.692709e-04 2.209454e-04 5.866986e-06
[20,]     200 1.601872e-07 3.302978e-05 0.032379627 0.0311088257 5.372225e-04 3.223112e-04 5.130924e-06
[21,]     300 1.646375e-07 2.435601e-05 0.029599725 0.0280751596 6.842064e-04 4.125926e-04 4.773013e-06
[22,]     400 1.690601e-07 2.121993e-05 0.027319613 0.0255595285 8.162650e-04 4.952212e-04 4.487502e-06
[23,]     500 1.725382e-07 1.897506e-05 0.025297161 0.0233240691 9.354161e-04 5.711807e-04 4.235968e-06
[24,]     600 1.749798e-07 1.703558e-05 0.023481974 0.0213167258 1.043069e-03 6.411066e-04 4.010628e-06
[25,]     700 1.764875e-07 1.530634e-05 0.021849581 0.0195108955 1.140434e-03 7.055396e-04 3.807970e-06
[26,]     800 1.771969e-07 1.375717e-05 0.020380735 0.0178853512 1.228585e-03 7.649641e-04 3.625382e-06
[27,]     900 1.772370e-07 1.236830e-05 0.019058537 0.0164214191 1.308479e-03 8.198178e-04 3.460645e-06
[28,]    1000 1.767225e-07 1.112296e-05 0.017867881 0.0151024136 1.380970e-03 8.704974e-04 3.311816e-06
[29,]    2000 1.572715e-07 3.940410e-06 0.010808693 0.0072508108 1.832356e-03 1.212393e-03 2.402674e-06
[30,]    3000 1.352535e-07 1.505097e-06 0.008154229 0.0042555138 2.030852e-03 1.380625e-03 2.018409e-06
[31,]    4000 1.193167e-07 6.604944e-07 0.007016270 0.0029465937 2.136110e-03 1.466211e-03 1.820579e-06
[32,]    5000 1.084579e-07 3.522510e-07 0.006420364 0.0022556523 2.202537e-03 1.506753e-03 1.694614e-06
[33,]    6000 1.007453e-07 2.278156e-07 0.006034010 0.0018163538 2.249144e-03 1.519738e-03 1.599914e-06
[34,]    7000 9.485520e-08 1.687564e-07 0.005740750 0.0014981138 2.282914e-03 1.514570e-03 1.521304e-06
[35,]    8000 9.004119e-08 1.348181e-07 0.005497458 0.0012504852 2.306735e-03 1.497018e-03 1.452627e-06
[36,]    9000 8.590818e-08 1.119399e-07 0.005286373 0.0010510369 2.322112e-03 1.470968e-03 1.391055e-06
[37,]   10000 8.224601e-08 9.491280e-08 0.005098878 0.0008877435 2.330070e-03 1.439185e-03 1.335063e-06
[38,]   20000 5.807037e-08 3.188663e-08 0.003870195 0.0002006368 2.154356e-03 1.068090e-03 9.519341e-07
```

IAEA Safety Report Series No. 37 (2004) ^{239}Pu ingestion retention fraction table
Radionuclide: ^{239}Pu
Intake: Inhalation Type S
Aerosol size: 5.0-μm AMAD
f1: 0.00001

Time(d)	Urine	Faeces	Tot.Body	Lungs	Skeleton	Liver
1	2.3E-06	1.1E-01	4.9E-01	6.4E-02	6.2E-05	3.7E-05
2	1.4E-06	1.6E-01	2.5E-01	6.3E-02	9.4E-05	5.6E-05
3	8.3E-07	8.4E-02	1.4E-01	6.2E-02	1.1E-04	6.8E-05
4	5.9E-07	3.5E-02	9.1E-02	6.1E-02	1.3E-04	7.6E-05
5	4.5E-07	1.4E-02	7.3E-02	6.1E-02	1.4E-04	8.2E-05
6	3.7E-07	5.7E-03	6.6E-02	6.0E-02	1.4E-04	8.6E-05
7	3.1E-07	2.5E-03	6.2E-02	6.0E-02	1.5E-04	9.0E-05
8	2.7E-07	1.3E-03	6.1E-02	5.9E-02	1.6E-04	9.3E-05
9	2.4E-07	8.2E-04	6.0E-02	5.8E-02	1.6E-04	9.6E-05
10	2.3E-07	6.5E-04	5.9E-02	5.8E-02	1.6E-04	9.9E-05
20	1.8E-07	4.4E-04	5.4E-02	5.3E-02	2.0E-04	1.2E-04
30	1.7E-07	3.5E-04	5.1E-02	4.9E-02	2.2E-04	1.3E-04
40	1.7E-07	2.8E-04	4.7E-02	4.6E-02	2.5E-04	1.5E-04
50	1.7E-07	2.3E-04	4.5E-02	4.4E-02	2.7E-04	1.6E-04
60	1.6E-07	1.9E-04	4.3E-02	4.2E-02	2.9E-04	1.7E-04
70	1.6E-07	1.5E-04	4.1E-02	4.0E-02	3.1E-04	1.9E-04
80	1.6E-07	1.3E-04	4.0E-02	3.9E-02	3.3E-04	2.0E-04
90	1.6E-07	1.1E-04	3.9E-02	3.8E-02	3.5E-04	2.1E-04
100	1.6E-07	9.1E-05	3.8E-02	3.7E-02	3.7E-04	2.2E-04
200	1.6E-07	3.3E-05	3.2E-02	3.1E-02	5.4E-04	3.2E-04
300	1.6E-07	2.4E-05	3.0E-02	2.8E-02	6.9E-04	4.1E-04
400	1.7E-07	2.1E-05	2.7E-02	2.6E-02	8.2E-04	5.0E-04
500	1.7E-07	1.9E-05	2.5E-02	2.3E-02	9.4E-04	5.7E-04
600	1.8E-07	1.7E-05	2.4E-02	2.1E-02	1.0E-03	6.4E-04
700	1.8E-07	1.5E-05	2.2E-02	2.0E-02	1.1E-03	7.1E-04
800	1.8E-07	1.4E-05	2.0E-02	1.8E-02	1.2E-03	7.7E-04
900	1.8E-07	1.2E-05	1.9E-02	1.6E-02	1.3E-03	8.2E-04
1000	1.8E-07	1.1E-05	1.8E-02	1.5E-02	1.4E-03	8.7E-04
2000	1.6E-07	4.0E-06	1.1E-02	7.3E-03	1.8E-03	1.2E-03
3000	1.4E-07	1.5E-06	8.2E-03	4.3E-03	2.0E-03	1.4E-03
4000	1.2E-07	6.6E-07	7.0E-03	3.0E-03	2.1E-03	1.5E-03
5000	1.1E-07	3.5E-07	6.4E-03	2.3E-03	2.2E-03	1.5E-03
6000	1.0E-07	2.3E-07	6.1E-03	1.8E-03	2.3E-03	1.5E-03
7000	9.5E-08	1.7E-07	5.8E-03	1.5E-03	2.3E-03	1.5E-03
8000	9.0E-08	1.4E-07	5.5E-03	1.3E-03	2.3E-03	1.5E-03
9000	8.6E-08	1.1E-07	5.3E-03	1.1E-03	2.3E-03	1.5E-03
10000	8.2E-08	9.5E-08	5.1E-03	8.9E-04	2.3E-03	1.4E-03
20000	5.8E-08	3.2E-08	3.9E-03	2.0E-04	2.2E-03	1.1E-03

Appendix 3: Human Data

Langham Human Data

The following tables provide the excretion data collected in percent of injected dose:

Table 35: Pu(IV) content of blood samples in percent of injected dose with respect to total blood volume.

Days	Hp-1	Hp-2	Hp-3	Hp-4	Hp-5	Hp-6	Hp-7	Hp-8	Hp-9	Hp-10	Hp-12
1/6	46.02		28.32	83.31	31.51	36.70	32.57	37.64	40.83	51.57	5.31
1	21.83	19.35			6.23	10.97	16.40	14.51	12.39	24.66	
2		8.38	11.56								
3		10.03		16.64	1.16	2.94	6.97	4.94	6.22	20.06	
4			4.22								
5					0.66						
6	3.33	4.25	2.17	6.14		1.00	2.96	2.07	3.91	4.91	
8		2.32	1.42								
9				4.6							
10	1.42				0.39	0.38	1.13	1.37	2.21	1.72	
13			0.61	2.34							
15					0.11	0.26	0.66	0.71	1.42	1.02	
17			0.51	1.45							
22		0.70			0.18	0.25					
23			0.25	0.72							
29							0.37				
30										0.36	
31											0.51
36									0.42		
42								0.17			
46											0.45

Table 36: Pu(IV) content of urine samples in percent of injected dose.

Day	Hp-l	Hp-2	Hp-3	Hp-4	Hp-5	Hp-6	Hp-7	Hp-8	Hp·9	Hp-10	Hp-12	Chi-I	Chi-II	Chi-III	Cal-I
I	0.181	0.472	0.569	0.44	0.296		0.217	0.377	0.16	0.414	0.101	0.857	2.531*	0.152	0.48
2	0.146	0.294	0.289	0.236	0.166	0.216	0.212	0.232	0.085	0.33	0.103	0.182	0.153	0.167	0.15
3	0.114	0.174	0.112	0.221	0.077	0.127	0.137	0.128	0.069	0.218	0.088	0.063	0.184	0.067	0.12
4	0.094	0.123	0.107	0.132	0.052	0.111	0.096	0.14	0.066	0.17	0.078	0.077	0.133	0.033	0.031
5	0.069	0.116	0.078	0.116	0.03	0.076	0.069	0.083	0.047	0.089	0.068	0.026	0.032	0.042	0.037
6	0.066	0.061	0.043	.119*	0.02	0.057	0.059	0.078	0.052	0.06	0.044	0.0256	0.029	0.042	
7	0.062	0.062	0.043	0.077	0.033	0.044	0.045	0.066	0.05	0.079	0.069	0.0234	0.024	0.024	
8	0.055	0.048	0.049	0.081	0.026	0.043	0.037	0.057	0.032	0.065	0.08	0.0227	0.023	0.025	0.016
9	0.051	0.046	0.022	.095*	0.027	0.032	0.033	0.047	0.032	0.051	0.043		0.027	0.019	0.069
10	0.045	0.038	0.027	.081*	0.022	0.031	0.023	0.05	0.035	0.044	0.038	.0082*	0.034	0.03	0.026
11	0.04	0.048	0.027	.075*	0.021		0.018	0.044	0.026	0.041	0.038	0.0097	0.047	0.019	0.036
12	0.038	0.039	0.015	.072*	0.026	0.024	0.019	0.023	0.03	0.038	0.027	0.0095	0.047	0.014	0.029
13	0.034	0.045	0.02	.067*	0.023	0.023	0.019	0.037	0.027	0.029	0.03	0.0236	0.018	0.034	
14	0.035	0.036	0.02	.058*	0.018	0.02	0.013	0.035	0.03	0.029	0.039	0.007	0.034	0.009	
15	0.034	0.039	0.028	0.05	0.015	0.022	0.012	0.035	0.03	0.025	0.029	0.0059	0.026	0.016	0.013
16	0.026	0.024	0.024	0.033	0.02	0.017	0.012	0.036	.049*	0.021	0.023	0.0109	0.012	0.004	0.016
17	0.027	0.027	0.021	0.032	0.02	0.013	0.011	0.032	0.038	0.023	0.029		0.028		0.0056
18	0.026	0.02	0.017	0.037	0.02	0.015	0.011	0.029	0.027	0.021	0.026		0.026		0.01
19	0.025	0.019	0.018	0.032	0.018	0.015	0.01	0.031	0.029	0.017	0.029	0.0022	0.015		0.006
20	0.017	0.021	0.012	0.025	0.021	0.013	0.008	0.032	0.029	0.018	0.032	0.0093	0.038		0.0048
21	0.017	0.017	0.019	0.029	0.02	0.012	0.01	0.029	0.032	0.022	0.025	0.0076	0.032		0.0017
22	0.016	0.015	0.014	0.035	0.018	0.012	0.013	0.021	0.032	0.016	0.025	0.0145	0.027		0.005
23	0.025	0.018	0.014	0.014			0.008	0.021	0.032	0.019	0.039	0.0151	0.029		0.0091
24	0.021	0.014					0.008	0.025	0.032	0.016	0.023	0.0128	0.02		0.0076
25	0.013	0.014		0.011			0.008	0.023	0.029	0.016	0.021	0.0128	.148*		0.011
26		0.017		0.011			0.007	0.022	0.032	0.016	0.023	0.0175	0.024		0.0022
27		0.008		0.008			0.008	0.028	0.032	0.014	0.017	0.0151	.043*		0.0044
28		0.009					0.008	0.023	0.024	0.013	0.024	0.0197	0.034		0.0074
29		0.009					0.008	0.019	0.025	0.014	0.023	0.0138	0.022		0.0043

Table 36 Continued.

Day	Hp-l	Hp-2	Hp-3	Hp-4	Hp-5	Hp-6	Hp-7	Hp-8	Hp·9	Hp-10	Hp-12	Chi-I	Chi-II	Chi-III	Cal-I
30		0.008					0.006	0.021	0.023	0.014	0.021	0.0151	0.024		0.0069
31		0.007					0.005	0.017	0.025		0.021	0.01	0.027		0.0077
32		0.007					0.007	0.016	0.024		0.012	0.01	0.02		0.0063
33		0.009					0.006	0.015	0.022		.037*	0.017	0.011		0.0073
34		0.009					0.006	0.015	0.02		0.02	0.0139	0.008		0.0084
35							0.006		0.022		0.026	0.0127	0.009		0.0069
36							0.006	0.015	0.022		0.018	0.0165	0.015		0.0079
37							0.006	0.011			.023*	0.0111	0.011		0.0063
38								0.016			0.018	0.0174	0.009		0.0085
39								0.012			0.021	0.0112	0.009		0.0064
40								0.017			0.019	0.0072	0.009		0.0072
41								0.019			0.013	0.0092	0.011		0.008
42								0.014			0.013	0.0127			0.0081
43								0.016			0.015	0.0095	0.017		0.0076
44								0.014			0.015	0.0031			0.0055
45								0.013			0.017	0.013	0.018		0.0063
46								0.015				0.012			0.0073
47								0.014			0.015		0.02		0.0059
48								0.014			0.017	0.0064			0.0059
49								0.018			0.015	0.0063			0.0063
50								0.014				0.0054	0.018		0.0078
51								0.013				0.007			0.0082
52											0.035	0.0073			0.0098
53								0.013			0.019	0.0023			0.0074
54								0.013			0.043				0.0077
55								0.015			0.043*	0.0073	0.014		0.0096
56								0.013			0.036	0.003			0.0064
57								0.012			0.018	0.0075			0.005
58								0.013			0.036	0.0094			0.0058
59								0.012				0.011			0.0098
60								0.011				0.0063	0.022		0.0067
61								0.012				0.0068			0.0066
62								0.01				0.0092			0.0058
63								0.009				0.0094			0.0077
64								0.012				0.0071			0.0042
65								0.011				0.0099	0.024		0.0042
66												0.014			0.0047
67												0.014			0.0064
68												0.011			0.0068
69												0.011			0.007
70												0.014			0.01
71												0.0096			0.0072
72												0.0089	0.014		0.0092
73												0.0083			0.0069
74												0.01			0.0079
75												0.013			0.0051
76												0.0081			0.0041
77												0.0043			0.0065
78												0.014			0.0074
79												0.0052			0.0066
80												0.0046	0.024		0.0048
81												0.0042			0.0055
82												0.002	0.018		0.008
83												0.0041			0.0068
84												0.0029			0.0022
85												0.007			
86												0.0046			0.01
87												0.0076			0.0079
88												0.0086			0.0037
89												0.0049			0.0071
90												0.0032	0.017		0.0077
91												0.0075			0.0088
92												0.014			0.0071
93												0.006			0.006
94															0.0071
95												0.0093	0.017		0.0052
96												0.011	0.015		0.0042

Table 36 Continued.

Day	Hp-l	Hp-2	Hp-3	Hp-4	Hp-5	Hp-6	Hp-7	Hp-8	Hp·9	Hp-10	Hp-12	Chi-I	Chi-II	Chi-III	Cal-I
97												0.0083			0.0057
98												0.012	0.013		0.0053
99												0.006			0.007
100												0.0096			0.0061
101												0.005			0.0052
102												0.009	0.008		0.004
103												0.006			0.007
104												0.0086			0.0051
105												0.019			0.0058
106												0.0075			0.0046
107												0.0098			0.006
108												0.0063	0.009		0.0052
109															0.0044
110												0.0056			0.0015
111												0.0085			0.0042
112												0.015			0.0051
113												0.0095	0.007		0.0058
114												0.011			0.0029
115												0.0145	0.009		0.0053
116															0.0047
117												0.0069			0.0023
118												0.0035			0.0039
119												0.0066			0.0036
120												0.0051	0.007		0.0025
121												0.0041			0.0047
122															0.0039
123												0.0115			0.0014
124												0.0086			0.0039
125												0.0106	0.009		0.0036
126												0.0037			0.0032
127												0.008	0.011		0.004
128												0.0073			0.0019
129												0.0052			0.0024
130												0.0054			0.0014
131												0.0075			0.0011
132												0.0055	0.008		0.0038
133												0.0088			0.0037
134												0.0091			0.0027
135												0.011	0.007		0.0029
136												0.0056			0.0026
137												0.0075			0.0032
138												0.0073	0.009		0.001
525						0.002									
1610						0.0011									
1645			0.0008												

*results not included in Langham et al. (1980) revised mean due to Chauvenet Criterion.

Table 37: Pu(IV) content of fecal samples in percent of injected dose.

Day	Hp-1	Hp-2	Hp-3	Hp-4	Hp-5	Hp-6	Hp-7	Hp-8	Hp-9	Hp-10	Hp-12	Chi-I
1	.052*	0.204	.018*	0.134	.004*	0.085	0.147	0.178	0.333	0.087	0.37	0.25
2	0.221	0.204	0.157	0.274	0.311	0.085	0.12	0.266	0.389	0.087	0.37	0.465
3	0.241	0.204	0.157	0.274	0.311	0.179	0.087	0.21	0.389	0.087	0.297	0.294
4	0.05	0.317	0.095	0.306	0.185	0.179	0.08	0.08	0.131	0.11	0.297	0.38
5	0.105	0.317	0.099	0.306	0.11	0.179	0.055	0.08	0.131	0.11	0.183	0.223
6	0.046		0.07	0.126	0.11	0.179	0.055	0.08	0.131	0.11	0.183	0.116
7	0.021		0.07	0.126	0.11	0.037	0.055	0.08	0.131	0.11	0.02	0.083
8	0.021	0.12	0.07	0.126	0.064	0.037	0.055	0.07	0.131	0.034	0.02	0.112
9	0.021	0.12	0.07	0.126	0.051	0.037	0.032	0.07	0.131	0.034	0.02	
10	0.021	0.084	0.027	0.117	0.051	0.037	0.032	0.07	0.131	0.034	0.02	0.021
11	0.046	0.084	0.027	0.117	0.052	0.023	0.032	0.07	0.118	0.034	0.02	
12	0.046	0.084	0.027	0.117	0.052	0.023	0.032	0.045	0.118	0.034	0.02	0.083
13	0.046	0.084	0.027	0.117	0.032	0.023	0.023	0.045	0.118	0.034	0.02	0.045
14	0.046	0.062	0.023	0.085	0.032	0.023	0.023	0.045	.118*	0.022	0.02	0.044
15	0.035	0.062	0.023	0.085	0.032	0.015	0.023	0.045	.118*	0.022	0.023	0.042
16	0.035	0.062	0.023	0.04	0.017	0.015	0.023	0.032	.414*	0.022	0.023	0.034

Table 37 Continued.

Day	Hp-1	Hp-2	Hp-3	Hp-4	Hp-5	Hp-6	Hp-7	Hp-8	Hp-9	Hp-10	Hp-12	Chi-I
17	0.035	0.062	0.023	0.04	0.017	0.015	0.016	0.032	.157*	0.022	0.023	
18	0.035	0.055	0.016	0.04	0.017	0.015	0.016	0.025	.157*	0.022	0.023	0.031
19	0.015	0.055	0.016	0.028	0.017	0.015	0.016	0.025	0.055	0.012	0.053	0.027
20	0.015	0.055	0.016	0.028	0.02	0.015	0.016	0.025	0.055	0.012	0.053	0.019
21	0.015	0.055	0.016	0.028	0.02	0.01	0.008	0.025	0.055	0.012	0.053	0.019
22	0.015	0.022	0.006	0.028	0.02	0.01	0.008	0.045	0.055	0.012	0.053	0.018
23	0.017	0.022	0.006	0.026			0.008	0.045	0.052	0.012	0.026	0.01
24	0.017	0.022					0.008	0.009	.052*	0.012	0.026	0.023
25		0.022					0.011	0.009	.052*	0.006	0.026	0.013
26		0.021					0.011	0.009	.052*	0.006	0.026	0.023
27		0.021					0.011	0.009	.043*	0.006	0.016	0.0083
28							0.011	0.009	.043*	0.006	0.016	0.0069
29								0.009	0.043	0.006	0.016	0.0158
30								0.018	0.043	0.006	0.016	0.0063
31								0.018	0.035		0.016	0.0074
32								0.018	0.035		0.016	0.0062
33								0.018	0.035		0.016	0.0079
34								0.018	0.035		0.016	0.0079
35								0.018	0.035		0.022	0.0054
36								0.018			0.022	0.0054
37								0.028			0.022	0.005
38								0.028			0.022	0.0042
39								0.011				0.0047
40								0.011				0.0066
41								0.011				0.0064
42								0.011				0.0053
43								0.011			0.008	0.0047
44								0.011			0.008	0.0092
45								0.014			0.008	0.0042
46								0.014			0.008	0.0033
47								0.014				0.0028
48								0.008				0.0054
49								0.008				0.0047
50								0.008				0.004
51								0.008				
52								0.01				
53								0.01				
54								0.01				0.0038
55								0.01				
56								0.01				
57								0.007				
58								0.007				0.0043
59								0.007				
60								0.007				
61								0.008				
62								0.008				0.0048
63								0.008				
64								0.008				
68												0.0063
70												0.0045
74												0.005
78												0.0033
79				0.006			0.005					
80				0.006			0.005					
81				0.006			0.005					
82				0.006			0.005					0.0042
83							0.006					
84							0.006					
85							0.006					
86												0.005
90												0.0042
94												0.004
98												0.005
100												0.0056
102												0.0038
106												0.0043
108												0.0038

Table 37 Continued.

Day	Hp-1	Hp-2	Hp-3	Hp-4	Hp-5	Hp-6	Hp-7	Hp-8	Hp-9	Hp-10	Hp-12	Chi-I
112												0.0021
116												0.0029
120												0.0032
126												0.003
130												0.0037
136												0.0034
138												0.0025

*results not included in Langham et al. (1980) revised mean due to Chauvenet Criterion.

UK Data I

The following tables provide the results collected in percent of injected dose:

Table 38: Blood content of Pu(IV) in % injection (Talbot et al. 1997).

Time	A	B	C	D	E	F	G	H	I	J	K	L
4m			75.49	67.22								
5m	83.24											
28m	76.00											
30m		71.00		64.00		77.00		96.00	80.00		91.00	79.00
31m			66.00		75.00		90.00			82.00		
33m												
42m		69.92										
59m	74.79											
1h		67.40		61.24				92.05	80.00			76.92
62m					72.09					72.93		
65m						71.62	81.32				86.34	
66m			56.51									
73m		66.31										
2h	68.16	59.11	49.27	58.94	69.19	64.62	75.38	82.85	74.77	71.42	81.27	71.93
6h	61.52	50.46	28.25	46.04	56.80	45.82	58.02	63.56	60.13	48.75	61.37	61.54
1d	33.90	23.86	11.57	25.60	34.42	19.01	31.61	31.65	33.52	21.09	31.36	35.67
2d	19.42		5.47	14.87								
3d	13.27	11.35	2.58	9.12	12.38	4.85	16.31	10.48	14.69	7.52	13.08	17.21
4d											10.29	
5d	8.99	6.60	1.54	4.56	6.16	2.32	10.74	5.44	9.10	3.89	8.04	10.52
7d	5.19	4.00	1.31	2.81	3.26	1.24	8.31	3.38	5.54	2.23	5.46	7.28
14d	2.96	2.34	0.41	0.87	0.76	0.43	4.52	1.45	2.30	0.91	1.82	2.20
15d			0.32	0.78					2.14	0.83		
21d	1.69	0.68			0.47	0.19	2.83	0.83	1.15	0.49	1.14	1.12
22d					0.42							
31d											0.76	
106d											0.04	

Table 39: Urine content of Pu(IV) in % injection (Talbot et al. 1993, 1997).

Days	A	B	C	D	E	F	G	H	I	J	K	L
1	0.286	0.283	1.095	0.894	1.333	1.423	1.290	1.427	1.094	1.210	1.102	1.317
2	0.253	0.201	0.187	0.386	0.3087	0.2202	0.269	0.214	0.22	0.236	0.235	0.38
3	0.225	0.173	0.1273	0.282	0.1936	0.1224	0.209	0.158	0.17	0.143	0.064	0.27
4	0.12	0.096	0.0768	0.1794	0.138	0.0833	0.144		0.132	0.134	0.095	0.211
5	0.113	0.098	0.0578	0.1322	0.1063	0.0557	0.161		0.101	0.122	0.097	0.15
6	0.086	0.077	0.0464	0.0985	0.0878	0.0437	0.121	0.074	0.096	0.11	0.064	0.146
7	0.078	0.071	0.0385	0.0896	0.0665	0.0354	0.114	0.038	0.085	0.094	0.055	0.101
8	0.056	0.063	0.0461	0.0799	0.0663	0.0297	0.09		0.068	0.069	0.064	0.099
9	0.058	0.06	0.0268	0.0705	0.0486	0.0276		0.042	0.062	0.061	0.057	0.095
10	0.05	0.036	0.0296	0.0572	0.0428	0.023	0.081		0.051	0.062	0.035	0.089
11	0.042	0.049	0.0268	0.0455	0.0377	0.0224	0.076	0.036	0.054	0.058		0.073
12	0.042	0.044	0.0256	0.0468	0.032	0.0153			0.046	0.046	0.03	0.066
13	0.04	0.039	0.0217	0.0448	0.0332	0.0131	0.075	0.029	0.047	0.039		0.059
14	0.032	0.034	0.0193	0.0378	0.0201	0.0273	0.069	0.029	0.049	0.049		0.061
15	0.022	0.021	0.0188	0.0387	0.0271	0.0172	0.066	0.024	0.047	0.043	0.034	0.053
16	0.022	0.027	0.0208	0.0347	0.0272	0.0167		0.024	0.04	0.039	0.021	0.044
17	0.027	0.029	0.0196	0.0329	0.0237	0.0155	0.065		0.044	0.036	0.024	0.047
18	0.041	0.032	0.0163	0.0332	0.0209	0.0154	0.064	0.026	0.04	0.04	0.019	0.037
19	0.025	0.031	0.0133	0.0272	0.0167	0.0141	0.063	0.035	0.045	0.033	0.022	0.044
20	0.019	0.019	0.015	0.0217	0.0237	0.0152	0.061		0.04	0.03	0.025	0.032
21	0.016	0.019	0.0141	0.0214	0.0188	0.0146	0.058	0.017	0.036	0.038	0.031	0.036
22	0.009					0.014			0.039	0.037	0.027	
23	0.025									0.033		
38						0.0084						
39						0.0085				0.0198		
40						0.007				0.018		
41					0.0128	0.009		0.0084		0.0197		
42					0.0124	0.0084		0.0161		0.0195		
43			0.0073	0.0113	0.0113	0.0075		0.0162	0.0218			0.0184
44			0.0075	0.0098					0.0192			0.0191
45			0.0066	0.0106					0.0185			0.0176
46							0.0338					0.016
47							0.0325					
48							0.0345					
49							0.0311					
50											0.0202	
51											0.0137	
52											0.0102	
53											0.0104	
72						0.0067						
73						0.0058						
74						0.0068						
75						0.0061						
76						0.0061						
77						0.0063						
78			0.0047									
79			0.0061	0.0074								
80			0.0053	0.0066								
81			0.0039	0.0064								
82								0.0089				
83								0.0105		0.0092		0.0073
84							0.0167	0.0094		0.0098		0.0091
85					0.0094		0.0156			0.0073		0.0113
86					0.0105		0.0174	0.0113	0.0141	0.0081		0.0121
87					0.0086		0.0139		0.012			
88									0.0134			
89									0.0113			
90											0.0142	
91											0.0073	
92											0.011	
93											0.0149	
94											0.0187	
95											0.012	

Table 40: Fecal content of Pu(IV) in % injection (Talbot et al. 1993, 1997).

Day	A	B	C	D	E	F	G	H	I	J	K	L
1	0.0010	0.2820	0.0598	0.1020	0.0228	0.1915	0.2582	0.1791	0.0480		0.0198	0.0102
2	0.1160	0.2810	0.1706	0.2680	0.2018	0.2469	0.3422	0.1635	0.3210	0.9666	0.7038	0.0414
3	0.2160	0.3660	0.2957	0.2690	0.1248	0.1494	0.5260	0.2842	0.1520			0.2293
4	0.2100	0.2440	0.0829	0.0743	0.4382	0.0873	0.0933	0.2840	0.3436	0.6318	0.2628	0.2982
5	0.2440	0.2300	0.0575	0.1582	0.1911	0.0643	0.3520	0.1389	0.4214	0.2591		0.3307
6	0.3310	0.1230	0.0409	0.0688	0.2594	0.0579	0.2222	0.1167	0.2445	0.3310		0.1872
7	0.3720	0.1450	0.0557	0.0842	0.1530	0.0483	0.1843	0.0626	0.4016	0.5313	0.4130	0.1857
8	0.1290	0.1300	0.0228	0.0651	0.1541	0.0347	0.2096	0.0734	0.3469	0.0947		0.1054
9	0.0150	0.1100	0.0362	0.0601	0.0400	0.0347	0.1249	0.0502	0.1885	0.0447	0.1077	0.0757
10	0.0600	0.0390	0.0296	0.0708	0.0233	0.0315	0.1280	0.0751	0.0822	0.1311		0.1237
11	0.0770	0.0390	0.0269	0.0325	0.0648		0.1938	0.0406	0.2452	0.0754		0.0910
12	0.1220	0.1400	0.0168	0.0664	0.0605	0.0590	0.0792	0.0521		0.0806		0.1006
13	0.1110	0.1190	0.0383	0.0348	0.0514	0.0240	0.0725	0.0608			0.0961	0.0693
14	0.0590	0.0760	0.0120	0.0263	0.0252	0.0270	0.1384	0.0336		0.0857		0.0888
15	0.0550	0.0560	0.0181	0.0364	0.0288	0.0214	0.2187	0.0687	0.2379	0.1698	0.1355	0.0536
16	0.0570	0.0280	0.0089	0.0161	0.0143	0.0191	0.1131	0.0238	0.1837			0.0185
17	0.0320	0.0660	0.0228	0.0259	0.0384	0.0142	0.0400	0.0328	0.0861	0.0488	0.0735	0.0840
18	0.0480	0.0400	0.0108	0.0262	0.0258	0.0130	0.1082	0.0289	0.1286	0.1326		0.0943
19	0.0430	0.0500	0.0033	0.0170		0.0133	0.1351	0.0271	0.1768			0.0371
20	0.0310	0.0240	0.0121	0.0117	0.0156	0.0138	0.0399	0.0270	0.2069	0.0542		0.0380
21	0.0420	0.0250	0.0075	0.0170	0.0072	0.0092	0.0577	0.0102		0.0153	0.0741	0.0481
22	0.0190	0.0170				0.0107			0.0488	0.0229		
23		0.0240								0.0834		
36						0.0037						
37						0.0048						
38						0.0032						
39						0.0021						
40										0.0100		
41						0.0048		0.0059		0.0343		
42			0.0043		0.0051	0.0037		0.0095	0.0097	0.0209		
43			0.0042	0.0057	0.0054	0.0031		0.0091	0.0078			0.0295
44			0.0035	0.0042		0.0016		0.0045	0.0073			0.0144
45			0.0027	0.0044		0.0046			0.0043			0.0313
46							0.0200					0.0105
47							0.0195					
48							0.0199					
49							0.0169					
50											0.0161	
72						0.0037						
73						0.0019						
75						0.0046						
76						0.0023						
77			0.0022									
78			0.0008			0.0032						
79			0.0011	0.0041								
80			0.0012	0.0030								
81			0.0016	0.0028								
83								0.0069				0.0130
84							0.0214	0.0065		0.0147		0.0086
85							0.0132	0.0071				0.0073
86					0.0035		0.0158		0.0112	0.0136		0.0123
87							0.0114		0.0165			
90											0.0063	
91											0.0068	
92											0.0064	
93											0.0100	

Table 41: Liver retention of Pu(IV) in % of injection (Newton et al. 1998).

Days	A	B	C	D	E	F	G	H	I	J	K	L
0.01	5			5	9	10	15	8	12	10	10	14
0.02		7										
0.03							13					
0.05			3	11				12	16			
0.06	8				13		12			12	12	17
0.07		6			8							
0.16		11										
0.23							21					20
0.24										31	18	
0.26		15		12	14	27		27				
0.27									26			
0.3	12											
1	27	27		33	27	50	35	43	43	47	36	33
3	37	40		56	50	64	52	63	60	62	50	45
4											52	
5	43	43		65	58	68			65	64		52
7	48	49			62	71	62	65	70	70	55	54
8				86								
10				85	64	69						
14	50	54			65	76	58	75			59	60
15				77					73	74		
18					66							
21	52	53					63	78	77	68	60	64
23				94								
30						75						
31											58	68
32									77	76		
35					71							
36	51											
43		65										
44								78		73	58	62
48						76						
49		52			69		62					
51									77			
53				82								
71					70							
76		61										
77									81			
78	53									76		
79				88								
84		60										
86			87					83				
87						77	59					
99					70							
106											65	
109												68
120		66		81								
136			86		70							
151							64					
153				78								
154									76			
155										77		
161								90				
164		67										
172												68
177			86			76					65	
189					71							
220				87								
221									75			
224										76		
228							60	94				
230						81						
240			84		66							
253												67
261											64	
275			88	83								
289								95				

Table 41 Continued.

Days	A	B	C	D	E	F	G	H	I	J	K	L
297							62					
307										84		
312									74			
311			86									
338				85		80						
366			86		64							
393						82						
437					66							

UK Data II

The urinary excretion is provided in the following table:

Table 42: Urine content of Pu(IV) in % injection (Ham and Harrison 2000).

Day	1	2	3	4	5	Day	1	2	3	4	5
1	0.8835	1.3706	1.1712	1.4411	1.9405	174	0.0058				
2	0.3157	0.2760	0.2695	0.2532	0.3432	193			0.0079		
3	0.1389	0.2287	0.2404	0.1395	0.1662	205	0.0051				
4	0.1351	0.1731	0.1610	0.0953	0.1851	216		0.0085			
5	0.0948	0.1275	0.1134	0.0820	0.0831	254	0.0046				
6	0.0825	0.0881	0.0978	0.0718	0.1275	263		0.0094	0.0067		
7	0.1069	0.1013	0.0924	0.0529	0.0897	290				0.0143	
8	0.0591	0.0676	0.0809		0.0869	294					0.0033
9		0.0653	0.0713		0.0737	325	0.0047				
10	0.0460					378		0.0066			
11		0.0293				382			0.0064		
14		0.0384			0.0348	470					0.0061
16	0.0258					471				0.0121	
19		0.0322				483		0.0081			
20	0.0187				0.0192	484			0.0053		
23					0.0163	521	0.0041				
27		0.0265				648		0.0073			
28	0.0176					651			0.0053		
30					0.0187	664	0.0034				
40		0.0184				853	0.0024				
45	0.0105					1111			0.0044		
68		0.0163				1119			0.0050		
71					0.0117	1139		0.0050			
75			0.0088			1155	0.0026				
78	0.0069					1583			0.0038		
84				0.0055		1584		0.0043			
105			0.0142			1798		0.0038			
109		0.0133				1801			0.0044		
122	0.0066					1943	0.0050				
146	0.0061					1970		0.0062			
157			0.0094			2197	0.0026				
160		0.0106									

Compiled Average Human Data

Table 43: Average blood content based on fraction of injection quantity.

Days	Average	Days	Average	Days	Average	Days	Average
0.002778	0.713581	2	0.119408	23	0.00485	900*	0.000742
0.003472	0.832381	3	0.100899	29	0.0037	1000*	0.000708
0.019444	0.76	4	0.072526	30	0.0036	2000*	0.000487
0.020833	0.797143	5	0.060415	31	0.006359	3000*	0.000388
0.021528	0.7825	6	0.034156	36	0.0042	4000*	0.000334
0.029167	0.699188	7	0.041667	42	0.0017	5000*	0.0003
0.040972	0.747937	8	0.0187	46	0.0045	6000*	0.000277
0.041667	0.755218	9	0.046	106	0.000423	7000*	0.000259
0.043056	0.725119	10	0.012314	200*	0.001089	8000*	0.000245
0.045139	0.797598	13	0.01475	300*	0.001031	9000*	0.000233
0.045833	0.565068	14	0.017473	400*	0.000974	10000*	0.000224
0.050694	0.663147	15	0.008254	500*	0.000919	20000*	0.000167
0.083333	0.689078	17	0.0098	600*	0.000869		
0.25	0.535232	21	0.0106	700*	0.000823		
1	0.2298	22	0.003872	800*	0.000781		

*Augmented data from the Leggett 2005 model prediction.

Table 44: Average urine content based on fraction of injection quantity.

Days	Average	Days	Average	Days	Average	Days	Average
1	0.008092	45	0.000131	89	7.77E-05	133	6.25E-05
2	0.002353	46	0.000168	90	1.05E-04	134	5.90E-05
3	0.001547	47	0.000175	91	7.87E-05	135	6.97E-05
4	0.001162	48	0.000156	92	1.07E-04	136	4.10E-05
5	0.000862	49	0.000153	93	8.97E-05	137	5.35E-05
6	0.000718	50	0.000131	94	1.29E-04	138	5.77E-05
7	0.000649	51	0.000105	95	1.09E-04	146	6.10E-05
8	0.000562	52	0.000156	96	1.01E-04	157	9.40E-05
9	0.000488	53	0.000104	97	7.00E-05	160	1.06E-04
10	0.000418	54	0.000212	98	1.01E-04	174	5.80E-05
11	0.000386	55	0.000115	99	6.50E-05	193	7.90E-05
12	0.000322	56	0.000146	100	7.85E-05	205	5.10E-05
13	0.000335	57	0.000106	101	5.10E-05	216	8.50E-05
14	0.000318	58	0.000161	102	7.00E-05	254	4.60E-05
15	0.000293	59	0.000109	103	6.50E-05	263	8.05E-05
16	0.000239	60	0.000115	104	6.85E-05	290	1.43E-04
17	0.000279	61	8.47E-05	105	1.30E-04	294	3.30E-05
18	0.000268	62	8.33E-05	106	6.05E-05	325	4.70E-05
19	0.000247	63	8.70E-05	107	7.90E-05	378	6.60E-05
20	0.000229	64	7.77E-05	108	6.83E-05	382	6.40E-05
21	0.000228	65	1.23E-04	109	8.85E-05	470	6.10E-05
22	0.000205	66	9.35E-05	110	3.55E-05	471	1.21E-04
23	0.000212	67	1.02E-04	111	6.35E-05	483	8.10E-05
24	0.000179	68	1.14E-04	112	1.01E-04	484	5.30E-05
25	0.000159	69	9.00E-05	113	7.43E-05	521	4.10E-05
26	0.000172	70	1.20E-04	114	6.95E-05	525	7.30E-05
27	0.000161	71	9.50E-05	115	9.60E-05	651	5.30E-05
28	0.00018	72	9.70E-05	116	4.70E-05	664	3.40E-05
29	0.000153	73	7.00E-05	117	4.60E-05	853	2.40E-05
30	0.000158	74	8.23E-05	118	3.70E-05	1111	4.40E-05
31	0.00015	75	8.25E-05	119	5.10E-05	1119	5.00E-05
32	0.000128	76	6.10E-05	120	4.87E-05	1139	5.00E-05
33	0.000125	77	5.70E-05	121	4.40E-05	1155	2.60E-05
34	0.000125	78	8.25E-05	122	5.25E-05	1583	3.80E-05
35	0.000138	79	6.33E-05	123	6.45E-05	1584	4.30E-05
36	0.000143	80	9.06E-05	124	6.25E-05	1610	2.00E-05
37	9.08E-05	81	5.00E-05	125	7.73E-05	1645	9.50E-06
38	0.000129	82	9.23E-05	126	3.45E-05	1798	3.80E-05
39	0.000126	83	7.58E-05	127	7.67E-05	1801	4.40E-05
40	0.000129	84	7.94E-05	128	4.60E-05	1943	5.00E-05
41	0.000122	85	1.01E-04	129	3.80E-05	1970	6.20E-05
42	0.00013	86	1.10E-04	130	3.40E-05	2197	2.60E-05
43	0.000132	87	1.00E-04	131	4.30E-05	9934	2.52E-05
44	0.000117	88	8.57E-05	132	5.77E-05	10008	1.41E-05

Table 45: Average fecal content based on fraction of injected quantity.

Days	Average	Days	Average	Days	Average	Days	Average
1	0.001481	27	0.000119	53	1.00E-04	84	1.14E-04
2	0.002822	28	9.78E-05	54	6.90E-05	85	8.40E-05
3	0.002428	29	0.00018	55	1.00E-04	86	1.02E-04
4	0.002192	30	0.000179	56	1.00E-04	87	1.40E-04
5	0.001889	31	0.000191	57	7.00E-05	90	5.25E-05
6	0.001449	32	0.000188	58	5.65E-05	91	6.80E-05
7	0.001513	33	0.000192	59	7.00E-05	92	6.40E-05
8	0.000968	34	0.000192	60	7.00E-05	93	1.00E-04
9	0.000696	35	0.000201	61	8.00E-05	94	4.00E-05
10	0.000626	36	0.000123	62	6.40E-05	98	5.00E-05
11	0.000719	37	0.00015	63	8.00E-05	100	5.60E-05
12	0.000663	38	0.000144	64	8.00E-05	102	3.80E-05
13	0.000587	39	5.93E-05	68	6.30E-05	106	4.30E-05
14	0.000475	40	9.20E-05	70	4.50E-05	108	3.80E-05
15	0.000655	41	1.25E-04	72	3.70E-05	112	2.10E-05
16	0.000385	42	8.69E-05	73	1.90E-05	116	2.90E-05
17	0.000386	43	8.85E-05	74	5.00E-05	120	3.20E-05
18	0.000432	44	7.08E-05	75	4.60E-05	126	3.00E-05
19	0.000398	45	9.19E-05	76	2.30E-05	130	3.70E-05
20	0.000349	46	1.12E-04	77	2.20E-05	136	3.40E-05
21	0.000274	47	1.21E-04	78	2.43E-05	138	2.50E-05
22	0.000241	48	1.11E-04	79	4.05E-05	9934	1.05E-05
23	0.000276	49	9.87E-05	80	3.80E-05	10008	5.33E-06
24	0.000167	50	9.37E-05	81	3.85E-05		
25	0.000145	51	8.00E-05	82	5.07E-05		
26	0.00016	52	1.00E-04	83	8.63E-05		

Table 46: Average liver content based on fraction of injected quantity.

Days	Average	Days	Average	Days	Average	Days	Average
1	0.36	49	0.61	161	0.9	366	0.75
3	0.53	51	0.77	164	0.67	393	0.82
4	0.52	53	0.82	172	0.68	437	0.66
5	0.57	71	0.7	177	0.76	500*	0.47
7	0.61	76	0.61	189	0.71	600*	0.45
8	0.86	77	0.81	220	0.87	700*	0.44
10	0.73	78	0.65	221	0.75	800*	0.43
14	0.62	79	0.88	224	0.76	900*	0.41
15	0.75	84	0.6	228	0.77	1000*	0.4
18	0.66	86	0.85	230	0.81	2000*	0.34
21	0.64	87	0.68	240	0.75	3000*	0.32
23	0.94	99	0.7	253	0.67	4000*	0.31
30	0.75	106	0.65	261	0.64	5000*	0.3
31	0.63	109	0.68	275	0.86	6000*	0.29
32	0.77	120	0.74	289	0.95	7000*	0.28
35	0.71	136	0.78	297	0.62	8000*	0.28
36	0.51	151	0.64	307	0.84	9000*	0.27
43	0.65	153	0.78	312	0.74	10000*	0.26
44	0.68	154	0.76	311	0.86	20000*	0.2
48	0.76	155	0.77	338	0.83		

*Augmented data from the Leggett 2005 model model prediction.

IDEAS Case 123

Table 47: IDEAS Case 123 wound and *in vitro* results, with chelation(c) treatment (Hurtgen et al. 2007).

Urine Excretion Days	Urine Bq/d	Chelation[a]	Fecal Bq/d	Blood Serum Bq/L	Wound Bq
0	130.61				
1	146.52			3,182.00	
2	82.51		45.14	3,761.67	
3	12,580.00	c		2,312.50	
4	5,291.00	c	291.56	352.73	
5	3,885.00	c	643.80	317.58	
6	3,059.90	c	203.13	125.06	
7	2,797.20	c	777.00	106.81	
8	584.60		3,492.80		
9	525.40		1,302.40	145.53	
10	2,967.40	c		115.81	
11	721.50		251.23	37.37	
12	407.00				
13	395.90		160.21	87.69	
14	349.65		240.50		
15	325.60		44.77		
16	274.91		142.82	111.74	
17	319.31		167.61	94.35	
18			105.08		
19	146.52				
20	206.83				
21	194.25				
22	202.76		210.53		
23	102.86		89.54	79.55	
24	113.22				
25	89.91		90.28		
26	96.20		85.10		
27	1,783.40	c	52.54	93.49	
28	1,520.70	c	58.83	23.06	
29	1,135.90	c	136.90	16.65	
30	1,295.00	c	33.45		
31	754.80		66.97	21.95	
32	332.26		60.31		
33	250.49		77.33		
34	325.97				
35	259.00				
56				67.46	
61					77,700
90		c		47.24	
91				24.30	
92		c		33.63	62,530
93				29.29	
94		c		22.78	
95				30.65	
120	18.50	c		46.37	
121				29.60	
122				41.19	
123				41.56	
124		c		31.27	
127				33.30	
128		c		35.83	55,500
130				33.79	
133		c		36.75	
134				19.36	
135				22.20	
136				33.55	
140				37.00	
154					55,130
187				55.38	
194					53,280
210	20.35				

Table 47 Continued.

Urine Excretion Days	Urine Bq/d	Chelation[a]	Fecal Bq/d	Blood Serum Bq/L	Wound Bq
231					42,550
256					38,850
262				45.14	
282					34,891
294				34.78	
311					34,558
324				31.82	
342					31,672
361				27.13	
378					27,898
420	6.29				
432				22.69	
438					27,824
462				18.38	
471					30,303
493				17.02	
508					31,709
555					31,783

[a] DTPA was listed in the records without describing whether it was due to Ca-DTPA or Zn-DTPA.

USTUR Case 0269

The Urine and fecal excretion were obtained for 20 years post intake with the results (^{239}Pu) obtained from the USTUR and provided in the following table:

Table 48: USTUR 0269 excretion data and days chelation was administered.

Day	Urine (Bq)	Fecal (Bq)	CaEDTA (x's)	Oral CaEDTA (g)	CaDTPA (g)	Day	Urine (Bq)	Fecal (Bq)	CaEDTA (x's)	Oral CaEDTA (g)	CaDTPA (g)
0.2	1.7067					658	0.1183				
0.3	1.3200					722	0.1567				
0.5	1.8467		1			756	0.1267				
1	48.6667	5000.0	2			756	0.0004				
2	72.1667	4833.3	2			779	0.1703				
3	111.3		2			809	0.3450				
4	59.75	2333.3	2			812	0.2103				
5	14.66	500.0	1			813	0.2613				
6	2.121					814	0.2613				
7	3.406	15.75				815	0.1940				
8	3.4833	1.750				817	0.2080				
9	3.0133	2.767				819	0.1557				
11	1.9067	2.250				820	0.2133				
12	1.4567	8.817	2			821	0.1593				
13	23.9767	6.967	2			822	0.1957				
14	27.1267		2			823	0.2007				
15	27.5400	6.350	2			824	0.1727				
16	19.1167	2.317	2			825	0.1393				
17	20.0000	0.918				833	0.1837				
18	4.8500	0.593				834	0.2140				
19	4.3667	1.188				835	0.2327				
20	3.3333	1.612				836	0.2273				
21	2.6000	0.510	2			837	0.1613				
22	15.5167	0.633	2			837	0.2893				
23	29.8333	1.397	2			837	0.2060				
24	16.7333		2			840	0.1933				
25	26.5000		1			841	0.2167				
26	15.7000					842	0.1500				
27	3.8333					843	0.1733				
28	3.6500					844	0.1533				
29	2.6167		2			845	0.2667				
30	14.3567		2			846	0.0933				
31	11.0167		2			847	0.1867				
32	29.5000		2			848	0.2900				
33	16.0667		1			849	0.1600				
34	23.1667		1			850	0.1467				
35	24.0000		2			851	0.1733				
36	23.1667		2			852	0.1533				
37	20.6333		2			853	0.1667				
38	22.7333		2			854	0.2667				
39	25.9333					855	0.2433				
40	6.1533					856	0.2150				
41	3.5267					865	0.2133				
42	2.8067					868					0.2x2
43	1.4133					869	8.533				0.4x2
44	2.7833					870	10.433				0.6x2
45	1.7867			2		871	12.050				0.8x2
46	2.3333	0.857		2		872	14.817				
47	2.5833	4.000		2		873	12.933				
48	2.6967			2		874	7.7167				0.8x2
49	2.9500	3.767		2		875	16.800				
50	3.6667			2		876	7.7500				
51	4.6333	3.817				877	10.050				
52	2.5533					878	6.4500				
53	1.1933					879	4.8500				
54	1.3550	2.000				900	0.2150				
55	1.6133	1.650				901	0.1850				
56	1.8000					930					0.8x2
57	0.6933					931	11.915				
58	2.0833		2	2		932	7.9500				
59	12.1167		2	2		933	5.3183				0.8x2
60	15.2667	1.800	2			934	2.5117				
61	13.3000		2			935	9.1300				

Table 48 Continued.

Day	Urine (Bq)	Fecal (Bq)	CaEDTA (x's)	Oral CaEDTA (g)	CaDTPA (g)	Day	Urine (Bq)	Fecal (Bq)	CaEDTA (x's)	Oral CaEDTA (g)	CaDTPA (g)
62	12.6667		2			936	7.2817				
63	13.7833	2.165	2	2		937	6.5817				0.8x2
64	13.5833	0.745	2	2		938	11.016				
65	22.3000	1.257				939	7.3000				
66	15.1167					940	5.7833				0.8x2
71	1.8667	3.418				941	13.033				
72	1.8833					942	6.916				
73	2.0167					943	5.197				
74	1.8333					944	5.277				0.8x2
75	1.6833					945	10.667				
76	1.5833					946	6.767				0.8x2
77	0.3500	0.475	2			947	10.515				
78	2.1500	1.717	2			948	6.6217				0.8x2
79	19.2500	0.337	2			949	11.127				
80	14.8833		2			950	8.3467				
81	6.5000		2			951	4.8483				0.8x2
82	9.6500		2			952	12.101				
83	9.4833		2			953	7.9383				1x2
84	9.0667		2			954	6.9550				
85	9.3833					955	7.3117				1x2
86	7.0167					956	9.6833				
87	2.1200					957	9.5683				
88	1.4500					958	5.8167				1x2
89	0.9333					959	11.760				
91	1.2700					960	6.5517				1x2
92	2.0000					961	10.337				
93	1.2100					962	6.3367				1x2
94	0.1567	0.187				963	8.1450				
95	1.4633	0.472				964	8.7600				
96	0.8767					965	4.8517				
97	0.4567			8		966	4.6967				
98	0.4867	1.640		8		967	3.9483				
99	1.1267			8		968	3.2850				
100	1.5133			8		969	0.1917				
101	1.6283			8		970	2.1400				
102	1.9333					971	2.0383				
103	1.6183					972	1.4883				
104	1.4967		1			989	0.2567				
105	0.9933		2			1030	1.6933				1
106	6.6333		2			1037					1
107	8.8667		2			1046					1
108	8.0667		2			1050					1
109	8.5667					1051	8.2633				
110	7.8333					1053					1
111	1.8267		2			1054	7.2700				
112	1.1467		2			1067	0.3350				
113	7.7467		2			1073	0.7400				
114	8.5933					1978					1
115	4.1667					1080	3.0367				
116	5.3833					1081					1
117	4.6500					1985					1
118	0.9800					1087	3.9267				
119	1.3050					1088					1
120	4.4500					1092					1
121	5.6500					1094	2.2633				
122	7.3000					1094.5	0.0767				
123	3.0250					1101	0.3267	0.015			
124	5.9500					1103	0.4767	0.002			
125	1.7500					1115	0.2850	0.004			
126	1.6033					1122	0.1573	0.002			
127	1.0400					1123		0.010			
128	1.0733					1124					
129	1.0883					1125		1.905			
130	0.9167					1127					1
131	1.0133	0.278				1129	2.7883				
132	1.1500					1130		0.046			1
133	0.8833					1134					1
134	0.7950					1136	3.2333	0.757			
135	0.7900					1137		1.522			1
136	0.6467					1141					1
137	0.9050					1143	5.4333				
138	0.5433	0.088				1144					1
139	0.4483		2			1150	1.4883				
140	0.6600		2			1164	0.2550				
141	6.6500		2			1169		1.552			1

Table 48 Continued.

Day	Urine (Bq)	Fecal (Bq)	CaEDTA (x's)	Oral CaEDTA (g)	CaDTPA (g)	Day	Urine (Bq)	Fecal (Bq)	CaEDTA (x's)	Oral CaEDTA (g)	CaDTPA (g)
142	10.6000		2			1171	5.9883				
143	9.6167		2			1172		0.049			1
144	9.4500					1176					1
145	4.9000					1179					1
146	2.0167		2			1183					1
147	0.9717		1			1186					1
148	7.8833		2			1199	0.4200				
149	11.7583		2			1206	0.2233				
150	14.5333		2			1211					1
151	13.4500					1213	2.0817				
152	13.9667					1214		0.263			1
153	2.9000					1218					1
154	1.9833					1220	5.0783				
155	1.5783					1221		0.197			1
156	0.9950					1225		0.462			1
157	0.9500					1226		0.827			
158	0.7733					1227	5.3800	0.083			
159	0.7500					1228					1
160	0.5933		2			1232					1
161	0.9500		2			1234	1.2450				1
162	5.2333		2			1241	0.4317				
163	8.7000		2			1241.5	0.3467				
164	8.6833		2			1247	0.0833	1.552			
165	10.8167					1247.5	0.1700				
166	10.6333					1255	0.0833				
167	1.7833					1262	0.0833	0.002			
168	1.8500					1262.5	0.0833				
169	1.3000					1269	0.0802	0.027			
170	0.8733					1276	0.1122	0.053			
171	0.7750					1283	0.0673				
172	0.7317					1290	0.1067				
173	0.8800					1297	0.2217				
176	0.7383		2			1304	0.2217				
177	6.6000		2			1311	0.1900	0.067			
178	8.1667		2			1318	0.2367	0.032			
179	8.6167		2			1323		0.082			
180	6.0833					1324		0.017			
181	2.7333					1325		0.005			
182	1.7000					1326		0.002			
183	1.0383					1330		0.098		1	
184	0.9500					1332	1.2583	0.002			
185	0.9683					1333	1.0383	1.063			
186	0.9850					1334	1.3400	0.194			
187	0.8233					1335	1.0725	0.061			
188	1.0100					1336	0.6318	0.039			
189	0.7417					1337	0.5117	0.012			
190	0.5550					1338	0.4517	0.013			
191	0.8633					1339	0.3950	0.067			
192	0.5450					1342	0.2247	0.050			
193	0.6283					1349	0.1928				
194	0.6100					1356	0.2210				
195	1.2033					1481	0.1222				
196	0.3467					1527	0.0417				
197	0.4967		2			1555	0.1033	0.008			
198	0.6417					1591	0.1017	0.027			
199	0.5450					1631	0.1478	0.001			
200	0.7650	0.487				1632	0.1145	0.006			
201	0.6967					1633	0.1310	0.006			
202	0.6633					1634	0.1007	0.017			
203	0.7750					1635	0.0960				
204	0.7117					1637					1
205	0.6483	0.060				1638	6.1500	0.842			
206	0.6083					1639	2.7667	0.168			1
207	0.7433					1640	6.7333	0.348			
208	0.7733	0.138				1641	5.9167				1
209	0.6400					1642	4.0467	0.019			
210	0.7300					1654	0.6667	0.016			
211	0.5300					1673	0.0605	0.026			
212	0.4317					1674	0.1245	0.032			
213	0.3767					1675	0.1538	0.041			
214	0.4583					1676	0.1465				
215	0.4083					1677	0.1318				
216	0.6150					1682	0.0978				
217	0.4550					1709	0.0873				
218	0.5217		1			1730	0.1098				

Table 48 Continued.

Day	Urine (Bq)	Fecal (Bq)	CaEDTA (x's)	Oral CaEDTA (g)	CaDTPA (g)	Day	Urine (Bq)	Fecal (Bq)	CaEDTA (x's)	Oral CaEDTA (g)	CaDTPA (g)
219	0.4883					1752	0.0603				
220	2.4450					1856	0.0802				
222	0.2017					1891	0.0128				
225	0.2417					1957	0.0553				
231	0.3833					2031	0.0535				
238	0.1500					2081	0.0585				
245	0.5667					2273	0.0315				
259	0.4417					2410	0.0612				
566	0.4483					2446	0.0837				
273	0.4400					3019	0.0477				
277	0.5233					3245	0.0333				
284	0.5533					3567	0.0170				
301	0.5083					3922	0.0467				
305	0.5100					4286	0.0583				
312	0.4167					4649	0.0350				
319	0.3900					5007	0.0600				
329	0.4000					5377	0.0517	0.001			
340	0.5733					5769	0.0058	0.002			
350	0.5117					6085	0.0107	0.002			
350.5	0.4467					6086	0.0038				
380	0.3400					6087	0.0060				
497	0.4533					6105	0.0017				
506	0.1717					6483	0.0028				
568	0.1247					6840	0.0280				
569	0.2848					7212	0.0122				
609	0.1583					7563	0.0023				
630	0.1167										

Note: ZrCi treatments were administered on days 76 and 93. Daily Decholin treatments were administered from days 5959 to 5963.

Appendix 4: Rate Matrices

The following rate matrices were used in this research. They are shown in tabular form and can be used to construct rate matrices with compartment, row and column designation for compartment 1 (Comp 1) to compartment 2 (Comp 2) paths defined with appropriate transfer rate.

ICRP 67 Rate Matrix for intravenous injection (R.67)

Table 49: Rate matrix specified for R.67 with intravenous injection into the blood compartment.

Comp 1	Comp 2	Transfer Rate	row	col	Comp 1	Comp 2	Transfer Rate	row	col
ST0	Blood	0.693	1	20	GI.SI	GI.ULI	6	15	16
ST1	Bladder	0.000475	2	19	GI.SI	Blood	6.00E-05	15	20
ST1	Blood	0.000475	2	20	GI.ULI	GI.LLI	1.8	16	17
ST2	Blood	1.90E-05	3	20	GI.LLI	Faeces	1	17	21
Kidneys.other	Blood	0.00139	4	20	Kidneys.Urine	Bladder	0.01386	18	19
Liver2	Blood	0.000211	5	20	Bladder	Urine	12	19	22
Testes	Blood	0.00019	6	20	Blood	ST0	0.2773	20	1
CortVol	CortMarrow	8.21E-05	7	9	Blood	ST1	0.0806	20	2
CortSurf	CortVol	4.11E-05	8	7	Blood	ST2	0.0129	20	3
CortSurf	CortMarrow	8.21E-05	8	9	Blood	Kidneys..other.	0.00323	20	4
CortMarrow	Blood	0.0076	9	20	Blood	Testes	0.00023	20	6
TrabVol	TrabMarrow	0.000493	10	12	Blood	CortSurf	0.1294	20	8
TrabSurf	TrabVol	0.000247	11	10	Blood	TrabSurf	0.1941	20	11
TrabSurf	TrabMarrow	0.000493	11	12	Blood	Liver1	0.1941	20	13
TrabMarrow	Blood	0.0076	12	20	Blood	GI.ULI	0.0129	20	16
Liver1	Liver2	0.00177	13	5	Blood	Kidneys.Urine	0.00647	20	18
Liver1	GI.SI	0.000133	13	15	Blood	Bladder	0.0129	20	19
GI.ST	GI.SI	24	14	15	Blood	Blood	1	20	20

ICRP 67 Rate Matrix with NCRP 156 Wound (R.Pu)

Table 50: Rate matrix specified for R.Pu with strong-retention default wound parameters.

Comp 1	Comp 2	Transfer Rate	row	col	Comp 1	Comp 2	Transfer Rate	row	col
Soluble	Soluble	1	1	1	Trab.Marrow	Blood	0.0076	16	24
Soluble	CIS	0.6	1	2	Liver1	Liver2	0.00177	17	9
Soluble	Blood	0.67	1	24	Liver1	GI.SI	0.000133	17	19
CIS	Soluble	0.024	2	1	GI.ST	GI.SI	24	18	19
CIS	PABS	0.01	2	3	GI.SI	GI.ULI	6	19	20
CIS	LN	2.00E-05	2	4	GI.SI	Blood	6.00E-05	19	24
PABS	Soluble	0.0012	3	1	GI.ULI	GI.LLI	1.8	20	21
PABS	LN	2.00E-05	3	4	GI.LLI	Faeces	1	21	25
ST0	Blood	0.693	5	24	Kidneys.Urine	Bladder	0.01386	22	23
ST1	Bladder	0.000475	6	23	Bladder	Urine	12	23	26
ST1	Blood	0.000475	6	24	Blood	ST0	0.2773	24	5
ST2	Blood	1.90E-05	7	24	Blood	ST1	0.0806	24	6
Kidneys.other	Blood	0.00139	8	24	Blood	ST2	0.0129	24	7
Liver2	Blood	0.000211	9	24	Blood	Kidneys.other	0.00323	24	8
Testes	Blood	0.00019	10	24	Blood	Testes	0.00023	24	10
Cort.Vol	Cort.Marrow	8.21E-05	11	13	Blood	Cort.Surf	0.1294	24	12
Cort.Surf	Cort.Vol	4.11E-05	12	11	Blood	Trab.Surf	0.1941	24	15
Cort.Surf	Cort.Marrow	8.21E-05	12	13	Blood	Liver1	0.1941	24	17
Cort.Marrow	Blood	0.0076	13	24	Blood	GI.ULI	0.0129	24	20
Trab.Vol	Trab.Marrow	0.000493	14	16	Blood	Kidneys.Urine	0.00647	24	22
Trab.Surf	Trab.Vol	0.000247	15	14	Blood	Bladder	0.0129	24	23
Trab.Surf	Trab.Marrow	0.000493	15	16					

Modified ICRP 67 Rate Matrix with NCRP 156 Wound (R.67mod)

Table 51: Rate matrix specified for R.67mod using strong-retention default wound parameters.

Comp 1	Comp 2	Transfer Rate	row	col	Comp 1	Comp 2	Transfer Rate	row	col
Soluble	Soluble	1	1	1	Liver1	Blood	0.0405	17	24
Soluble	CIS	0.6	1	2	GI.ST	GI.SI	24	18	19
Soluble	Blood	0.67	1	24	GI.SI	GI.ULI	6	19	20
CIS	Soluble	0.024	2	1	GI.SI	Blood	6.00E-05	19	24
CIS	PABS	0.01	2	3	GI.ULI	GI.LLI	1.8	20	21
CIS	LN	2.00E-05	2	4	GI.LLI	Faeces	1	21	25
PABS	Soluble	0.0012	3	1	Kidneys.Urine	Bladder	0.0018	22	23
PABS	LN	2.00E-05	3	4	Bladder	Urine	12	23	26
ST0	Blood	0.342	5	24	Blood	ST0	0.153	24	5
ST1	Blood	0.000475	6	24	Blood	ST1	0.04	24	6
ST2	Blood	1.00E-05	7	24	Blood	ST2	0.006	24	7
Kidneys.other	Blood	0.000127	8	24	Blood	Kidneys.other	0.000139	24	8
Liver2	Blood	0.000356	9	24	Blood	Liver2	0.2587	24	9
Testes	Blood	0.00038	10	24	Blood	Testes	0.00027	24	10
CortVol	CortMarrow	8.21E-05	11	13	Blood	CortVol	0.0035	24	11
CortSurf	CortVol	2.05E-05	12	11	Blood	CortSurf	0.0672	24	12
CortSurf	CortMarrow	8.21E-05	12	13	Blood	TrabVol	0.0106	24	14
CortMarrow	Blood	0.0076	13	24	Blood	TrabSurf	0.0955	24	15
TrabVol	TrabMarrow	0.000493	14	16	Blood	Liver1	0.2457	24	17
TrabSurf	TrabVol	0.000123	15	14	Blood	GI.ULI	0.0092	24	20
TrabSurf	TrabMarrow	0.000493	15	16	Blood	Kidneys.Urine	0.0215	24	22
TrabMarrow	Blood	0.0076	16	24	Blood	Bladder	0.0125	24	23
Liver1	GI.SI	0.000833	17	19					

Leggett 2005 model with NCRP 156 Wound (R.Leg)

Table 52: Rate matrix specified for R.Leg with injection simulated as 70% to blood compartment and 30% to ST0.

Comp 1	Comp 2	Transfer Rate	row	col	Comp 1	Comp 2	Transfer Rate	row	col
Soluble	CIS	0.6	1	2	Liver2	Blood2	0.000127	18	26
Soluble	Blood	0.67[1]	1	25	GI.ST	GI.SI	24	19	20
CIS	Soluble	0.024	2	1	GI.SI	GI.ULI	6	20	21
CIS	PABS	0.01	2	3	GI.SI	Blood	6.00E-05	20	25
CIS	LN	2.00E-05	2	4	GI.ULI	GI.LLI	1.8	21	22
PABS	Soluble	0.0012	3	1	GI.LLI	Faeces	1	22	27
PABS	LN	2.00E-05	3	4	Kidneys.Urine	Bladder	0.017329	23	24
ST0	ST0	0.3	5	5	Bladder	Urine	12	24	28
ST0	Blood	0.099	5	25	Blood	ST1	0.018511	25	6
ST1	Blood2	0.001386	6	26	Blood	ST2	0.0231	25	7
ST2	Blood2	0.0001266	7	26	Blood	Kidneys.other.	0.000385	25	8
Kidneys.other.	Blood2	0.0001266	8	26	Blood	Testes	0.00027	25	9
Testes	Blood2	0.00038	9	26	Blood	CortVol	0.00462	25	10
CortVol	CortMarrow	8.21E-05	10	12	Blood	CortSurf	0.08778	25	11
CortSurf	CortVol	2.05E-05	11	10	Blood	TrabVol	0.01386	25	13
CortSurf	CortMarrow	8.21E-05	11	12	Blood	TrabSurf	0.12474	25	14
CortMarrow	Blood2	0.0076	12	26	Blood	Liver0	0.462	25	16
TrabVol	TrabMarrow	0.000493	13	15	Blood	GI.ULI	0.01155	25	21
TrabSurf	TrabVol	0.000123	14	13	Blood	Kidneys.Urine	0.0077	25	23
TrabSurf	TrabMarrow	0.000493	14	15	Blood	Bladder	0.0154	25	24
TrabMarrow	Blood2	0.0076	15	26	Blood	Blood	0.7	25	25
Liver0	Liver1	0.045286	16	17	Blood2	ST0	28.95	26	5
Liver0	GI.SI	0.000924	16	20	Blood2	Bladder	3.5	26	24
Liver1	Liver2	0.00038	17	18	Blood2	Blood	67.55	26	25
Liver1	Blood2	0.00152	17	26					

[1] Although not depicted in this rate matrix, the soluble compartment was assumed to be divided with 70% going to the Blood1 compartment and 30% going to the ST0 compartment. This research did not include wound coupling with the Leggett 2005 model.

Pu-DTPA optimized for IDEAS Case 123 with original ICRP 67 model (R.123)

Table 53: Rate matrix specified for R.123 using optimized wound parameters for IDEAS Case 123.

Comp 1	Comp 2	Transfer Rate	row	col	Comp 1	Comp 2	Transfer Rate	row	col
Soluble	Soluble	0.5	1	1	Liver1	Liver1t	2.2	17	27
Soluble	CIS	0.094	1	2	GI.ST	GI.SI	24	18	19
Soluble	Blood	0.241	1	24	GI.SI	GI.ULI	6	19	20
CIS	Soluble	0.026	2	1	GI.SI	Blood	6.00E-05	19	24
CIS	CIS	0.5	2	2	GI.ULI	GI.LLI	1.8	20	21
CIS	PABS	0.01	2	3	GI.LLI	Faeces	1	21	29
CIS	LN	2.00E-05	2	4	Kidneys.Urine	Bladder	0.0139	22	23
PABS	Soluble	0.0012	3	1	Bladder	Urine	12	23	30
PABS	LN	2.00E-05	3	4	Blood	ST0	0.277	24	5
ST0	Blood	0.693	5	24	Blood	ST1	0.0806	24	6
ST0	ST0t	3.65	5	25	Blood	ST2	0.0129	24	7
ST1	Bladder	0.000475	6	23	Blood	Kidneys.other	0.00323	24	8
ST1	Blood	0.000475	6	24	Blood	Testes	0.00023	24	10
ST1	ST1t	1.93	6	26	Blood	CortSurf	0.129	24	12
ST2	Blood	1.90E-05	7	24	Blood	TrabSurf	0.194	24	15
Kidneys.other	Blood	0.00139	8	24	Blood	Liver1	0.194	24	17
Liver2	Blood	0.000211	9	24	Blood	GI.ULI	0.0129	24	20
Testes	Blood	0.00019	10	24	Blood	Kidneys.Urine	0.00647	24	22
CortVol	CortMarrow	8.21E-05	11	13	Blood	Bladder	0.0129	24	23
CortSurf	CortVol	4.11E-05	12	11	Blood	Bloodt	1.38	24	28
CortSurf	CortMarrow	8.21E-05	12	13	ST0t	Bloodt	300	25	28
CortMarrow	Blood	0.0076	13	24	ST1t	Bloodt	0.12	26	28
TrabVol	TrabMarrow	0.000493	14	16	Liver1t	GI.SI	0.067	27	19
TrabSurf	TrabVol	0.000247	15	14	Liver1t	Bloodt	0.067	27	28
TrabSurf	TrabMarrow	0.000493	15	16	Bloodt	GI.ULI	4	28	20
TrabMarrow	Blood	0.0076	16	24	Bloodt	Bladder	45.7	28	23
Liver1	Liver2	0.00177	17	9	Bloodt	ST0t	145	28	25
Liver1	GI.SI	0.000133	17	19					

Pu-DTPA optimized for IDEAS Case 123 with modified ICRP 67 model (R.123mod)

Table 54: Rate matrix specified for R.123mod using optimized wound parameters for IDEAS Case 123.

Comp 1	Comp 2	Transfer Rate	row	col	Comp 1	Comp 2	Transfer Rate	row	col
Soluble	Soluble	0.5	1	1	GI.SI	GI.ULI	6	19	20
Soluble	CIS	0.094	1	2	GI.SI	Blood	6.00E-05	19	24
Soluble	Blood	0.241	1	24	GI.ULI	GI.LLI	1.8	20	21
CIS	Soluble	0.026	2	1	GI.LLI	Faeces	1	21	29
CIS	CIS	0.5	2	2	Kidneys.Urine	Bladder	0.0018	22	23
CIS	PABS	0.01	2	3	Bladder	Urine	12	23	30
CIS	LN	2.00E-05	2	4	Blood	ST0	0.153	24	5
PABS	Soluble	0.0012	3	1	Blood	ST1	0.04	24	6
PABS	LN	2.00E-05	3	4	Blood	ST2	0.006	24	7
ST0	Blood	0.342	5	24	Blood	Kidneys.other	0.000139	24	8
ST0	ST0t	3.65	5	25	Blood	Liver2	0.2587	24	9
ST1	Blood	0.00095	6	24	Blood	Testes	0.0002695	24	10
ST1	ST1t	1.925	6	26	Blood	CortVol	0.0035	24	11
ST2	Blood	1.9E-05	7	24	Blood	CortSurf	0.0672	24	12
Kidneys.other	Blood	0.000127	8	24	Blood	TrabVol	0.0106	24	14
Liver2	Blood	0.000356	9	24	Blood	TrabSurf	0.0955	24	15
Testes	Blood	0.00038	10	24	Blood	Liver1	0.2457	24	17
CortVol	CortMarrow	8.21E-05	11	13	Blood	GI.ULI	0.0092	24	20
CortSurf	CortVol	2.05E-05	12	11	Blood	Kidneys.Urine	0.0215	24	22
CortSurf	CortMarrow	8.21E-05	12	13	Blood	Bladder	0.0125	24	23
CortMarrow	Blood	0.0076	13	24	Blood	Bloodt	1.378	24	28
TrabVol	TrabMarrow	0.000493	14	16	ST0t	Bloodt	300	25	28
TrabSurf	TrabVol	0.000123	15	14	ST1t	Bloodt	0.12	26	28
TrabSurf	TrabMarrow	0.000493	15	16	Liver1t	GI.SI	0.067	27	19
TrabMarrow	Blood	0.0076	16	24	Liver1t	Bloodt	0.067	27	28
Liver1	GI.SI	0.000833	17	19	Bloodt	GI.ULI	4	28	20
Liver1	Blood	0.0405	17	24	Bloodt	Bladder	45.7	28	23
Liver1	Liver1t	2.2	17	27	Bloodt	ST0t	145	28	25
GI.ST	GI.SI	24	18	19					

Pu-DTPA with Modified ICRP 67 and NCRP 156 wound (R.67DTPA.0v1)

Table 55: Rate matrix specified for R.67DTPA.0v1 using strong-retention default wound parameters.

Comp 1	Comp 2	Transfer Rate	row	col	Comp 1	Comp 2	Transfer Rate	row	col
Soluble	Soluble	1	1	1	GI.SI	GI.ULI	6	19	20
Soluble	CIS	0.6	1	2	GI.SI	Blood	6.00E-05	19	24
Soluble	Blood	0.67	1	24	GI.ULI	GI.LLI	1.8	20	21
CIS	Soluble	0.024	2	1	GI.LLI	Faeces	1	21	29
CIS	PABS	0.01	2	3	Kidneys.Urine	Bladder	0.0018	22	23
CIS	LN	2.00E-05	2	4	Bladder	Urine	12	23	30
PABS	Soluble	0.0012	3	1	Blood	ST0	0.153	24	5
PABS	LN	2.00E-05	3	4	Blood	ST1	0.04	24	6
ST0	Blood	0.342	5	24	Blood	ST2	0.006	24	7
ST0	ST0t	3.65	5	25	Blood	Kidneys.other	0.000462	24	8
ST1	Blood	0.00095	6	24	Blood	Liver2	0.2587	24	9
ST1	ST1t	1.925	6	26	Blood	Testes	0.00023	24	10
ST2	Blood	1.00E-05	7	24	Blood	CortVol	0.0035	24	11
Kidneys.other	Blood	0.000127	8	24	Blood	CortSurf	0.0672	24	12
Liver2	Blood	0.000356	9	24	Blood	TrabVol	0.0106	24	14
Testes	Blood	0.00038	10	24	Blood	TrabSurf	0.0955	24	15
CortVol	CortMarrow	8.21E-05	11	13	Blood	Liver1	0.2457	24	17
CortSurf	CortVol	2.05E-05	12	11	Blood	GI.ULI	0.0092	24	20
CortSurf	CortMarrow	8.21E-05	12	13	Blood	Kidneys.Urine	0.0215	24	22
CortMarrow	Blood	0.0076	13	24	Blood	Bladder	0.0125	24	23
TrabVol	TrabMarrow	0.000493	14	16	Blood	Bloodt	1.378	24	28
TrabSurf	TrabVol	0.000123	15	14	ST0t	Bloodt	300	25	28
TrabSurf	TrabMarrow	0.000493	15	16	ST1t	Bloodt	0.12	26	28
TrabMarrow	Blood	0.0076	16	24	Liver1t	GI.SI	0.067	27	19
Liver1	GI.SI	0.000833	17	19	Liver1t	Bloodt	0.067	27	28
Liver1	Blood	0.0405	17	24	Bloodt	GI.ULI	4	28	20
Liver1	Liver1t	2.2	17	27	Bloodt	Bladder	45.7	28	23
GI.ST	GI.SI	24	18	19	Bloodt	ST0t	145	28	25

Modified ICRP 67 systemic model and NCRP 156 wound (R.67Mod24)

Table 56: Rate matrix specified for R.67Mod24 using strong-retention default wound parameters.

Comp 1	Comp 2	Transfer Rate	row	col	Comp 1	Comp 2	Transfer Rate	row	col
Soluble	CIS	0.6	1	2	GI.ST	GI.SI	24	18	19
Soluble	Blood	0.67	1	24	GI.SI	GI.ULI	6	19	20
CIS	Soluble	0.024	2	1	GI.SI	Blood	6.00E-05	19	24
CIS	PABS	0.01	2	3	GI.ULI	GI.LLI	1.8	20	21
CIS	LN	2.00E-05	2	4	GI.LLI	Faeces	1	21	25
PABS	Soluble	0.0012	3	1	Kidneys.Urine	Bladder	0.0018	22	23
PABS	LN	2.00E-05	3	4	Bladder	Urine	12	23	26
ST0	Blood	0.342	5	24	Blood	ST0	0.153	24	5
ST1	Blood	0.00095	6	24	Blood	ST1	0.04	24	6
ST2	Blood	1.9E-05	7	24	Blood	ST2	0.006	24	7
Kidneys.other	Blood	0.000127	8	24	Blood	Kidneys.other	0.000139	24	8
Liver2	Blood	0.000356	9	24	Blood	Liver2	0.2587	24	9
Testes	Blood	0.00038	10	24	Blood	Testes	0.0002695	24	10
CortVol	CortMarrow	8.21E-05	11	13	Blood	CortVol	0.0035	24	11
CortSurf	CortVol	2.05E-05	12	11	Blood	CortSurf	0.0672	24	12
CortSurf	CortMarrow	8.21E-05	12	13	Blood	TrabVol	0.0106	24	14
CortMarrow	Blood	0.0076	13	24	Blood	TrabSurf	0.0955	24	15
TrabVol	TrabMarrow	0.000493	14	16	Blood	Liver1	0.2457	24	17
TrabSurf	TrabVol	0.000123	15	14	Blood	GI.ULI	0.0092	24	20
TrabSurf	TrabMarrow	0.000493	15	16	Blood	Kidneys.Urine	0.0215	24	22
TrabMarrow	Blood	0.0076	16	24	Blood	Bladder	0.0125	24	23
Liver1	GI.SI	0.000833	17	19	Blood	Blood	1	24	24
Liver1	Blood	0.0405	17	24					

ICRP 66 lung model coupled with the ICRP 67 systemic model (R.lung)

Table 57: Rate matrix specified for R.lung used for verification of model performance against ICRP 66 lung model.

Comp 1	Comp 2	Transfer Rate	row	col	Comp 1	Comp 2	Transfer Rate	row	col
AI1	AI1	0.0159	1	1	bb2t	Blood	1.00E-04	19	47
AI1	bb1	0.02	1	4	bbseqt	LNTHt	0.01	20	24
AI1	AI1t	100	1	15	bbseqt	Blood	1.00E-04	20	47
AI1	Blood	0.1	1	47	BB1t	ET2t	10	21	25
AI2	AI2	0.0318	2	2	BB1t	Blood	1.00E-04	21	47
AI2	bb1	0.001	2	4	BB2t	ET2t	0.03	22	25
AI2	AI2t	100	2	16	BB2t	Blood	1.00E-04	22	47
AI2	Blood	0.1	2	47	BBseqt	LNTHt	0.01	23	24
AI3	AI3	0.0053	3	3	BBseqt	Blood	1.00E-04	23	47
AI3	bb1	1.00E-04	3	4	LNTHt	Blood	1.00E-04	24	47
AI3	LNTH	2.00E-05	3	10	ET2t	GI.ST	100	25	41
AI3	AI3t	100	3	17	ET2t	Blood	1.00E-04	25	47
AI3	Blood	0.1	3	47	ETseqt	LNETt	0.001	26	27
bb1	bb1	0.006523	4	4	ETseqt	Blood	1.00E-04	26	47
bb1	BB1	2	4	7	LNETt	Blood	1.00E-04	27	47
bb1	bb1t	100	4	18	ST0	Blood	0.693	28	47
bb1	Blood	0.1	4	47	ST0	ST0t[1]	3.65	28	48
bb2	bb2	0.0044	5	5	ST1	Bladder	0.000475	29	46
bb2	BB1	0.03	5	7	ST1	Blood	0.000475	29	47
bb2	bb2t	100	5	19	ST1	ST1t[1]	1.93	29	49
bb2	Blood	0.1	5	47	ST2	Blood	1.90E-05	30	47
bbseq	bbseq	7.70E-05	6	6	Kidneys.other	Blood	0.00139	31	47
bbseq	LNTH	0.01	6	10	Liver2	Blood	0.000211	32	47
bbseq	bbseqt	100	6	20	Testes	Blood	0.00019	33	47
bbseq	Blood	0.1	6	47	Cort.Vol	Cort.Marrow	8.21E-05	34	36
BB1	BB1	0.011868	7	7	Cort.Surf	Cort.Vol	4.11E-05	35	34
BB1	ET2	10	7	11	Cort.Surf	Cort.Marrow	8.21E-05	35	36
BB1	BB1t	100	7	21	Cort.Marrow	Blood	0.0076	36	47
BB1	Blood	0.1	7	47	Trab.Vol	Trab.Marrow	0.000493	37	39
BB2	BB2	0.005907	8	8	Trab.Surf	Trab.Vol	0.000247	38	37
BB2	ET2	0.03	8	11	Trab.Surf	Trab.Marrow	0.000493	38	39
BB2	BB2t	100	8	22	Trab.Marrow	Blood	0.0076	39	47
BB2	Blood	0.1	8	47	Liver1	Liver2	0.00177	40	32
BBseq	BBseq	0.000125	9	9	Liver1	GI.SI	0.000133	40	42
BBseq	LNTH	0.01	9	10	Liver1	Liver1t[1]	2.2	40	50
BBseq	BBseqt	100	9	23	GI.ST	GI.SI	24	41	42
BBseq	Blood	0.1	9	47	GI.SI	GI.ULI	6	42	43
LNTH	LNTHt	100	10	24	GI.SI	Blood	6.00E-05	42	47
LNTH	Blood	0.1	10	47	GI.ULI	GI.LLI	1.8	43	44
ET2	ET2	0.3998	11	11	GI.LLI	Faeces	1	44	53
ET2	ET2t	100	11	25	Kidneys.Urine	Bladder	0.0139	45	46
ET2	GI.ST	100	11	41	Bladder	Urine	12	46	54
ET2	Blood	0.1	11	47	Blood	ST0	0.277	47	28
ETseq	ETseq	2.00E-04	12	12	Blood	ST1	0.0806	47	29
ETseq	LNET	0.001	12	13	Blood	ST2	0.0129	47	30
ETseq	ETseqt	100	12	26	Blood	Kidneys.other	0.00323	47	31
ETseq	Blood	0.1	12	47	Blood	Testes	0.00023	47	33
LNET	LNETt	100	13	27	Blood	Cort.Surf	0.129	47	35

Table 57 Continued.

Comp 1	Comp 2	Transfer Rate	row	col	Comp 1	Comp 2	Transfer Rate	row	col
LNET	Blood	0.1	13	47	Blood	Trab.Surf	0.194	47	38
ET1	ET1	0.34	14	14	Blood	Liver1	0.194	47	40
ET1	Envir	1	14	52	Blood	GI.ULI	0.0129	47	43
AI1t	bb1t	0.02	15	18	Blood	Kidneys.Urine	0.00647	47	45
AI1t	Blood	1.00E-04	15	47	Blood	Bladder	0.0129	47	46
AI2t	bb1t	0.001	16	18	Blood	Bloodt[1]	1.38	47	51
AI2t	Blood	1.00E-04	16	47	ST0t	Bloodt	300	48	51
AI3t	bb1t	1.00E-04	17	18	ST1t	Bloodt	0.12	49	51
AI3t	LNTHt	2.00E-05	17	24	Liver1t	GI.SI	0.067	50	42
AI3t	Blood	1.00E-04	17	47	Liver1t	Bloodt	0.067	50	51
bb1t	BB1t	2	18	21	Bloodt	GI.ULI	4	51	43
bb1t	Blood	1.00E-04	18	47	Bloodt	Bladder	45.7	51	46
bb2t	BB1t	0.03	19	21	Bloodt	ST0t	145	51	48

[1] The DTPA transitional compartments were set to 0 when validation was performed against the IAEA Safety Report Series No. 37 (2004).

Pu-DTPA with original ICRP 67 and ICRP 66 lung model (R.LungPu.orig67b)

Table 58: Rate matrix specified for R.LungPu.orig67b.[1]

Comp 1	Comp 2	Transfer Rate	row	col	Comp 1	Comp 2	Transfer Rate	row	col
AI1	AI1	0.0159	1	1	bbseqt	bbseqb	1.00E-05	20	33
AI1	bb1	0.02	1	4	bbseqt	Blood	9.00E-05	20	60
AI1	AI1t	100	1	15	BB1t	ET2t	10	21	25
AI1	AI1b	0.01	1	28	BB1t	BB1b	1.00E-05	21	34
AI1	Blood	0.09	1	60	BB1t	Blood	9.00E-05	21	60
AI2	AI2	0.0318	2	2	BB2t	ET2t	0.03	22	25
AI2	bb1	0.001	2	4	BB2t	BB2b	1.00E-05	22	35
AI2	AI2t	100	2	16	BB2t	Blood	9.00E-05	22	60
AI2	AI2b	0.01	2	29	BBseqt	LNTHt	0.01	23	24
AI2	Blood	0.09	2	60	BBseqt	BBseqb	1.00E-05	23	36
AI3	AI3	0.0053	3	3	BBseqt	Blood	9.00E-05	23	60
AI3	bb1	1.00E-04	3	4	LNTHt	LNTHb	1.00E-05	24	37
AI3	LNTH	2.00E-05	3	10	LNTHt	Blood	9.00E-05	24	60
AI3	AI3t	100	3	17	ET2t	ET2b	1.00E-05	25	38
AI3	AI3b	0.01	3	30	ET2t	GI.ST	100	25	54
AI3	Blood	0.09	3	60	ET2t	Blood	9.00E-05	25	60
bb1	bb1	0.006523	4	4	ETseqt	LNETt	0.001	26	27
bb1	BB1	2	4	7	ETseqt	ETseqb	1.00E-05	26	39
bb1	bb1t	100	4	18	ETseqt	Blood	9.00E-05	26	60
bb1	bb1b	0.01	4	31	LNETt	LNETb	1.00E-05	27	40
bb1	Blood	0.09	4	60	LNETt	Blood	9.00E-05	27	60
bb2	bb2	0.0044	5	5	AI1b	Blood	2.00E-04	28	60
bb2	BB1	0.03	5	7	AI2b	Blood	2.00E-04	29	60
bb2	bb2t	100	5	19	AI3b	Blood	2.00E-04	30	60
bb2	bb2b	0.01	5	32	bb1b	Blood	2.00E-04	31	60
bb2	Blood	0.09	5	60	bb2b	Blood	2.00E-04	32	60
bbseq	bbseq	7.70E-05	6	6	bbseqb	Blood	2.00E-04	33	60
bbseq	LNTH	0.01	6	10	BB1b	Blood	2.00E-04	34	60
bbseq	bbseqt	100	6	20	BB2b	Blood	2.00E-04	35	60
bbseq	bbseqb	0.01	6	33	BBseqb	Blood	2.00E-04	36	60
bbseq	Blood	0.09	6	60	LNTHb	Blood	2.00E-04	37	60
BB1	BB1	0.0118677	7	7	ET2b	GI.ST	100	38	54
BB1	ET2	10	7	11	ET2b	Blood	2.00E-04	38	60
BB1	BB1t	100	7	21	ETseqb	Blood	2.00E-04	39	60
BB1	BB1b	0.01	7	34	LNETb	Blood	2.00E-04	40	60
BB1	Blood	0.09	7	60	ST0	Blood	0.693	41	60
BB2	BB2	0.005907	8	8	ST0	ST0t	3.65	41	61
BB2	ET2	0.03	8	11	ST1	Bladder	0.000475	42	59
BB2	BB2t	100	8	22	ST1	Blood	0.000475	42	60
BB2	BB2b	0.01	8	35	ST1	ST1t	1.93	42	62
BB2	Blood	0.09	8	60	ST2	Blood	1.90E-05	43	60
BBseq	BBseq	0.0001253	9	9	Kidneys..other.	Blood	0.00139	44	60
BBseq	LNTH	0.01	9	10	Liver2	Blood	0.000211	45	60
BBseq	BBseqt	100	9	23	Testes	Blood	0.00019	46	60
BBseq	BBseqb	0.01	9	36	Cort.Vol	Cort.Marrow	8.21E-05	47	49
BBseq	Blood	0.09	9	60	Cort.Surf	Cort.Vol	4.11E-05	48	47
LNTH	LNTHt	100	10	24	Cort.Surf	Cort.Marrow	8.21E-05	48	49
LNTH	LNTHb	0.01	10	37	Cort.Marrow	Blood	0.0076	49	60

Table 58 Continued.

Comp 1	Comp 2	Transfer Rate	row	col	Comp 1	Comp 2	Transfer Rate	row	col
LNTH	Blood	0.09	10	60	Trab.Vol	Trab.Marrow	0.000493	50	52
ET2	ET2	0.3998	11	11	Trab.Surf	Trab.Vol	0.000247	51	50
ET2	ET2t	100	11	25	Trab.Surf	Trab.Marrow	0.000493	51	52
ET2	ET2b	0.01	11	38	Trab.Marrow	Blood	0.0076	52	60
ET2	GI.ST	100	11	54	Liver1	Liver2	0.00177	53	45
ET2	Blood	0.09	11	60	Liver1	GI.SI	0.000133	53	55
ETseq	ETseq	2.00E-04	12	12	Liver1	Liver1t	2.2	53	63
ETseq	LNET	0.001	12	13	GI.ST	GI.SI	24	54	55
ETseq	ETseqt	100	12	26	GI.SI	GI.ULI	6	55	56
ETseq	ETseqb	0.01	12	39	GI.SI	Blood	6.00E-05	55	60
ETseq	Blood	0.09	12	60	GI.ULI	GI.LLI	1.8	56	57
LNET	LNETt	100	13	27	GI.LLI	Faeces	1	57	69
LNET	LNETb	0.01	13	40	Kidneys.Urine	Bladder	0.0139	58	59
LNET	Blood	0.09	13	60	Bladder	Urine	12	59	70
ET1	ET1	0.34	14	14	Blood	ST0	0.277	60	41
ET1	Envir	1	14	68	Blood	ST1	0.0806	60	42
AI1t	bb1t	0.02	15	18	Blood	ST2	0.0129	60	43
AI1t	AI1b	1.00E-05	15	28	Blood	Kidneys..other.	0.00323	60	44
AI1t	Blood	9.00E-05	15	60	Blood	Testes	0.00023	60	46
AI2t	bb1t	0.001	16	18	Blood	Cort.Surf	0.129	60	48
AI2t	AI2b	1.00E-05	16	29	Blood	Trab.Surf	0.194	60	51
AI2t	Blood	9.00E-05	16	60	Blood	Liver1	0.194	60	53
AI3t	bb1t	1.00E-04	17	18	Blood	GI.ULI	0.0129	60	56
AI3t	LNTHt	2.00E-05	17	24	Blood	Kidneys.Urine	0.00647	60	58
AI3t	AI3b	1.00E-05	17	30	Blood	Bladder	0.0129	60	59
AI3t	Blood	9.00E-05	17	60	Blood	Bloodt	1.38	60	67
bb1t	BB1t	2	18	21	ST0t	Bloodt	300	61	67
bb1t	bb1b	1.00E-05	18	31	ST1t	Bloodt	0.12	62	67
bb1t	Blood	9.00E-05	18	60	Liver1t	GI.SI	0.067	63	55
bb2t	BB1t	0.03	19	21	Liver1t	Bloodt	0.067	63	67
bb2t	bb2b	1.00E-05	19	32	Bloodt	GI.ULI	4	67	56
bb2t	Blood	9.00E-05	19	60	Bloodt	Bladder	45.7	67	59
bbseqt	LNTHt	0.01	20	24	Bloodt	ST0t	145	67	61

[1] The rate matrix omitted fields 64 to 66 which were used in investigating other chelation compartment possibilities. Since the functions required a 70 dimension square matrix, it is suggested to put in dummy variables for defining compartments 64 to 66 without specifying transfer rates. This rate matrix defaulted to a Type S with a 5-µm particle size and was modified based on specifications with the R function (e.g., MLE.lung). Values for the bound compartment transfer rates were provided by the function (e.g., Pu.Lung3C).

Pu-DTPA with modified ICRP 67 and ICRP 66 lung model (R.LungPu.origbv1):

Table 59: Rate matrix specified for R.LungPu.origbv1.[1]

Comp 1	Comp 2	Transfer Rate	row	col	Comp 1	Comp 2	Transfer Rate	row	col
AI1	AI1	0.0159	1	1	bbseqt	Blood	9.00E-05	20	60
AI1	bb1	0.02	1	4	BB1t	ET2t	10	21	25
AI1	AI1t	100	1	15	BB1t	BB1b	1.00E-05	21	34
AI1	AI1b	0.01	1	28	BB1t	Blood	9.00E-05	21	60
AI1	Blood	0.09	1	60	BB2t	ET2t	0.03	22	25
AI2	AI2	0.0318	2	2	BB2t	BB2b	1.00E-05	22	35
AI2	bb1	0.001	2	4	BB2t	Blood	9.00E-05	22	60
AI2	AI2t	100	2	16	BBseqt	LNTHt	0.01	23	24
AI2	AI2b	0.01	2	29	BBseqt	BBseqb	1.00E-05	23	36
AI2	Blood	0.09	2	60	BBseqt	Blood	9.00E-05	23	60
AI3	AI3	0.0053	3	3	LNTHt	LNTHb	1.00E-05	24	37
AI3	bb1	1.00E-04	3	4	LNTHt	Blood	9.00E-09	24	60
AI3	LNTH	2.00E-05	3	10	ET2t	ET2b	1.00E-05	25	38
AI3	AI3t	100	3	17	ET2t	GI.ST	100	25	54
AI3	AI3b	0.01	3	30	ET2t	Blood	9.00E-05	25	60
AI3	Blood	0.09	3	60	ETseqt	LNETt	0.001	26	27
bb1	bb1	0.006523	4	4	ETseqt	ETseqb	1.00E-05	26	39
bb1	BB1	2	4	7	ETseqt	Blood	9.00E-05	26	60
bb1	bb1t	100	4	18	LNETt	LNETb	1.00E-05	27	40
bb1	bb1b	0.01	4	31	LNETt	Blood	9.00E-05	27	60
bb1	Blood	0.09	4	60	AI1b	Blood	2.00E-04	28	60
bb2	bb2	0.0044	5	5	AI2b	Blood	2.00E-04	29	60
bb2	BB1	0.03	5	7	AI3b	Blood	2.00E-04	30	60
bb2	bb2t	100	5	19	bb1b	Blood	2.00E-04	31	60
bb2	bb2b	0.01	5	32	bb2b	Blood	2.00E-04	32	60
bb2	Blood	0.09	5	60	bbseqb	Blood	2.00E-04	33	60
bbseq	bbseq	7.70E-05	6	6	BB1b	Blood	2.00E-04	34	60
bbseq	LNTH	0.01	6	10	BB2b	Blood	2.00E-04	35	60
bbseq	bbseqt	100	6	20	BBseqb	Blood	2.00E-04	36	60
bbseq	bbseqb	0.01	6	33	LNTHb	Blood	2.00E-04	37	60
bbseq	Blood	0.09	6	60	ET2b	GI.ST	100	38	54
BB1	BB1	0.0118677	7	7	ET2b	Blood	2.00E-04	38	60
BB1	ET2	10	7	11	ETseqb	Blood	2.00E-04	39	60
BB1	BB1t	100	7	21	LNETb	Blood	2.00E-04	40	60
BB1	BB1b	0.01	7	34	ST0	Blood	0.342	41	60
BB1	Blood	0.09	7	60	ST0	ST0t	3.65	41	61
BB2	BB2	0.005907	8	8	ST1	Blood	0.00095	42	60
BB2	ET2	0.03	8	11	ST1	ST1t	1.93	42	62
BB2	BB2t	100	8	22	ST2	Blood	1.9E-05	43	60
BB2	BB2b	0.01	8	35	Kidneys..other.	Blood	0.000127	44	60
BB2	Blood	0.09	8	60	Liver2	Blood	0.000356	45	60
BBseq	BBseq	0.0001253	9	9	Testes	Blood	0.00038	46	60
BBseq	LNTH	0.01	9	10	Cort.Vol	Cort.Marrow	8.21E-05	47	49
BBseq	BBseqt	100	9	23	Cort.Surf	Cort.Vol	2.05E-05	48	47
BBseq	BBseqb	0.01	9	36	Cort.Surf	Cort.Marrow	8.21E-05	48	49
BBseq	Blood	0.09	9	60	Cort.Marrow	Blood	0.0076	49	60
LNTH	LNTHt	100	10	24	Trab.Vol	Trab.Marrow	0.000493	50	52
LNTH	LNTHb	0.01	10	37	Trab.Surf	Trab.Vol	0.000123	51	50
LNTH	Blood	0.09	10	60	Trab.Surf	Trab.Marrow	0.000493	51	52
ET2	ET2	0.3998	11	11	Trab.Marrow	Blood	0.0076	52	60
ET2	ET2t	100	11	25	Liver1	GI.SI	0.000833	53	55
ET2	ET2b	0.01	11	38	Liver1	Blood	0.0405	53	60
ET2	GI.ST	100	11	54	Liver1	Liver1t	2.2	53	63

Table 59 Continued.

Comp 1	Comp 2	Transfer Rate	row	col	Comp 1	Comp 2	Transfer Rate	row	col
ET2	Blood	0.09	11	60	GI.ST	GI.SI	24	54	55
ETseq	ETseq	2.00E-04	12	12	GI.SI	GI.ULI	6	55	56
ETseq	LNET	0.001	12	13	GI.SI	Blood	6.00E-05	55	60
ETseq	ETseqt	100	12	26	GI.ULI	GI.LLI	1.8	56	57
ETseq	ETseqb	0.01	12	39	GI.LLI	Faeces	1	57	69
ETseq	Blood	0.09	12	60	Kidneys.Urine	Bladder	0.0018	58	59
LNET	LNETt	100	13	27	Bladder	Urine	12	59	70
LNET	LNETb	0.01	13	40	Blood	ST0	0.153	60	41
LNET	Blood	0.09	13	60	Blood	ST1	0.04	60	42
ET1	ET1	0.34	14	14	Blood	ST2	0.006	60	43
ET1	Envir	1	14	68	Blood	Kidneys..other.	0.000139	60	44
AI1t	bb1t	0.02	15	18	Blood	Liver2	0.2587	60	45
AI1t	AI1b	1.00E-05	15	28	Blood	Testes	0.0002695	60	46
AI1t	Blood	9.00E-05	15	60	Blood	Cort.Vol	0.0035	60	47
AI2t	bb1t	0.001	16	18	Blood	Cort.Surf	0.0672	60	48
AI2t	AI2b	1.00E-05	16	29	Blood	Trab.Vol	0.0106	60	50
AI2t	Blood	9.00E-05	16	60	Blood	Trab.Surf	0.0955	60	51
AI3t	bb1t	1.00E-04	17	18	Blood	Liver1	0.2457	60	53
AI3t	LNTHt	2.00E-05	17	24	Blood	GI.ULI	0.0092	60	56
AI3t	AI3b	1.00E-05	17	30	Blood	Kidneys.Urine	0.0215	60	58
AI3t	Blood	9.00E-05	17	60	Blood	Bladder	0.0125	60	59
bb1t	BB1t	2	18	21	Blood	Bloodt	1.38	60	67
bb1t	bb1b	1.00E-05	18	31	ST0t	Bloodt	300	61	67
bb1t	Blood	9.00E-05	18	60	ST1t	Bloodt	0.12	62	67
bb2t	BB1t	0.03	19	21	Liver1t	GI.SI	0.067	63	55
bb2t	bb2b	1.00E-05	19	32	Liver1t	Bloodt	0.067	63	67
bb2t	Blood	9.00E-05	19	60	Bloodt	GI.ULI	4	67	56
bbseqt	LNTHt	0.01	20	24	Bloodt	Bladder	45.7	67	59
bbseqt	bbseqb	1.00E-05	20	33	Bloodt	ST0t	145	67	61

[1]The rate matrix omitted fields 64 to 66 which were used in investigating other chelation compartment possibilities. Since the functions required a 70 dimension square matrix, it is suggested to put in dummy variables for defining compartments 64 to 66 without specifying transfer rates. This rate matrix defaulted to a Type S with a 5-µm particle size and was modified based on specifications with the R function (e.g., MLE.lung). Values for the bound compartment transfer rates were provided by the function (e.g., Pu.Lung3C).

Appendix 5: Intake Retention Fraction Tables

Intake retention fraction tables were constructed for the ICRP 67 and Leggett 2005 biokinetic models that were used in this research.

ICRP 67 Plutonium IRF (ICRP67.IRF)

Table 60: IRF table constructed from ICRP 67 systemic model for intravenous injection.

Time(d)	Urine	Faeces	Tot.Body	Skeleton	Liver	Blood
1	8.18E-03	1.61E-03	0.9902121	0.2167521	0.1300415	0.438813327
2	4.48E-03	4.30E-03	0.981435	0.3205147	0.1922776	0.233402381
3	2.60E-03	4.19E-03	0.9746529	0.3796182	0.2277123	0.142628671
4	1.71E-03	3.13E-03	0.9698167	0.4171959	0.2502284	0.094063733
5	1.20E-03	2.16E-03	0.966448	0.4424528	0.2653501	0.064286014
6	8.87E-04	1.48E-03	0.9640849	0.4598567	0.2757589	0.044620207
7	6.74E-04	1.02E-03	0.9623956	0.4719774	0.2829973	0.031177087
8	5.27E-04	7.09E-04	0.96116	0.4804574	0.288051	0.021850936
9	4.24E-04	5.03E-04	0.9602337	0.4864027	0.2915841	0.015341357
10	3.51E-04	3.62E-04	0.9595207	0.4905763	0.2940543	0.010786522
20	1.74E-04	4.95E-05	0.9562468	0.5002621	0.2995551	0.00043818
30	1.55E-04	4.02E-05	0.9542002	0.500729	0.2995836	0.000158357
40	1.43E-04	3.95E-05	0.9523218	0.5008866	0.2994826	0.000165701
50	1.32E-04	3.90E-05	0.950565	0.5009938	0.2994031	0.000180126
60	1.22E-04	3.86E-05	0.9489141	0.5010613	0.2993471	0.000193693
70	1.14E-04	3.81E-05	0.9473563	0.5010925	0.2993129	0.000206253
80	1.07E-04	3.76E-05	0.9458804	0.5010904	0.2992985	0.000217874
90	1.00E-04	3.72E-05	0.9444768	0.5010578	0.2993023	0.000228625
100	9.46E-05	3.67E-05	0.9431369	0.5009971	0.2993227	0.000238571
200	6.52E-05	3.24E-05	0.9320103	0.4992842	0.3001672	0.000304846
300	5.58E-05	2.86E-05	0.9229964	0.4964775	0.3016021	0.000334597
400	5.14E-05	2.54E-05	0.9149653	0.4933005	0.3031742	0.00034716
500	4.84E-05	2.26E-05	0.907588	0.4900665	0.3046877	0.000351516
600	4.58E-05	2.03E-05	0.9007367	0.4869039	0.3060631	0.000351868
700	4.35E-05	1.84E-05	0.8943376	0.4838588	0.3072736	0.00035021
800	4.14E-05	1.68E-05	0.8883353	0.4809423	0.3083153	0.000347507
900	3.95E-05	1.54E-05	0.8826837	0.4781507	0.3091937	0.000344243
1000	3.77E-05	1.43E-05	0.8773432	0.4754756	0.3099183	0.000340669
2000	2.58E-05	9.04E-06	0.835342	0.4534271	0.3107331	0.000303416
3000	2.01E-05	7.56E-06	0.804551	0.4371519	0.3042265	0.000273313
4000	1.70E-05	6.81E-06	0.7790202	0.4247654	0.2940143	0.000250391
5000	1.51E-05	6.29E-06	0.7565021	0.4150634	0.2820259	0.000232468
6000	1.39E-05	5.87E-06	0.7359708	0.4071138	0.2693766	0.000217981
7000	1.29E-05	5.54E-06	0.7168908	0.4002335	0.2567247	0.00020593
8000	1.22E-05	5.25E-06	0.6989499	0.3939519	0.2444525	0.000195665
9000	1.16E-05	5.01E-06	0.6819481	0.3879605	0.2327714	0.000186747
10000	1.10E-05	4.79E-06	0.6657472	0.3820673	0.2217854	0.00017887
20000	7.83E-06	3.42E-06	0.5332404	0.3194993	0.1470395	0.000128396

Leggett 2005 Model Plutonium IRF (Legg05.IRF)

Table 61: IRF table constructed from the Leggett 2005 model for intravenous injection.

Days	Urine	Faeces	Tot.Body	Skeleton	Liver	Blood
1	7.26E-03	1.05E-03	0.991689	0.115376	0.230632	0.34374
2	4.16E-03	2.96E-03	0.984565	0.173114	0.345829	0.176938
3	2.26E-03	3.02E-03	0.979288	0.203758	0.406753	0.098041
4	1.36E-03	2.33E-03	0.975599	0.221493	0.441805	0.060008
5	9.16E-04	1.68E-03	0.973005	0.232919	0.464205	0.041039
6	6.94E-04	1.23E-03	0.971085	0.241125	0.480139	0.031029
7	5.73E-04	9.50E-04	0.969562	0.24757	0.492529	0.025283
8	5.02E-04	7.86E-04	0.968273	0.252956	0.50278	0.021619
9	4.55E-04	6.86E-04	0.967132	0.25763	0.51159	0.019014
10	4.20E-04	6.22E-04	0.96609	0.261774	0.519325	0.016988
20	2.49E-04	3.60E-04	0.958422	0.286776	0.563098	0.006628
30	1.81E-04	2.27E-04	0.953545	0.297031	0.576576	0.003
40	1.49E-04	1.48E-04	0.95013	0.302007	0.579103	0.001722
50	1.30E-04	1.00E-04	0.947552	0.305118	0.577732	0.001291
60	1.18E-04	7.10E-05	0.945489	0.307583	0.575037	0.001158
70	1.08E-04	5.31E-05	0.943758	0.309826	0.57194	0.001124
80	1.01E-04	4.19E-05	0.942252	0.311987	0.568764	0.001121
90	9.38E-05	3.50E-05	0.940905	0.314106	0.565615	0.001124
100	8.81E-05	3.07E-05	0.939674	0.316191	0.562523	0.001126
200	6.07E-05	2.27E-05	0.93011	0.33506	0.534501	0.001089
300	5.34E-05	2.14E-05	0.92226	0.350693	0.510419	0.001031
400	4.97E-05	2.02E-05	0.915036	0.363872	0.489342	0.000974
500	4.68E-05	1.91E-05	0.908249	0.375101	0.470735	0.000919
600	4.42E-05	1.80E-05	0.901844	0.384706	0.454229	0.000869
700	4.18E-05	1.71E-05	0.895787	0.392917	0.439547	0.000823
800	3.97E-05	1.62E-05	0.890045	0.399918	0.426463	0.000781
900	3.77E-05	1.54E-05	0.884592	0.405856	0.414789	0.000742
1000	3.59E-05	1.47E-05	0.879402	0.410858	0.404363	0.000708
2000	2.47E-05	1.01E-05	0.837768	0.428387	0.344305	0.000487
3000	1.97E-05	8.01E-06	0.806891	0.420248	0.321651	0.000388
4000	1.69E-05	6.90E-06	0.781254	0.406826	0.309946	0.000334
5000	1.52E-05	6.20E-06	0.75865	0.393854	0.301179	0.0003
6000	1.40E-05	5.71E-06	0.73806	0.382553	0.293046	0.000277
7000	1.31E-05	5.34E-06	0.718939	0.37286	0.284981	0.000259
8000	1.24E-05	5.05E-06	0.700949	0.364423	0.276924	0.000245
9000	1.18E-05	4.81E-06	0.683867	0.356898	0.268936	0.000233
10000	1.13E-05	4.62E-06	0.667537	0.350008	0.261091	0.000224
20000	8.48E-06	3.46E-06	0.530225	0.291838	0.195983	0.000167

Modified ICRP 67 Plutonium IRF

Table 62: IRF table constructed from the modified ICRP 67 systemic model for intravenous injection (R.67Mod24).

Days	Urine	Faeces	Tot.Body	Skeleton	Liver	Blood
1	7.79E-03	1.14E-03	0.9910711	0.1165008	0.3285561	0.412566923
2	3.83E-03	3.01E-03	0.9842265	0.1666806	0.4636361	0.189888027
3	1.88E-03	2.85E-03	0.9794978	0.1913252	0.5241819	0.10185835
4	1.09E-03	2.05E-03	0.9763522	0.2055816	0.5544228	0.06436755
5	7.46E-04	1.39E-03	0.9742119	0.2152038	0.5712012	0.046474569
6	5.72E-04	9.81E-04	0.9726586	0.222474	0.5812265	0.036648035
7	4.72E-04	7.42E-04	0.971444	0.2283683	0.5873869	0.030477419
8	4.07E-04	6.04E-04	0.9704324	0.233354	0.5910762	0.026191476
9	3.61E-04	5.21E-04	0.9695507	0.2376873	0.5930641	0.023017549
10	3.26E-04	4.66E-04	0.9687586	0.2415276	0.5938312	0.020576093
20	2.00E-04	2.79E-04	0.9629923	0.2672278	0.5772359	0.011191517
30	1.65E-04	2.08E-04	0.9588373	0.2840659	0.5559742	0.008290455
40	1.42E-04	1.59E-04	0.9555226	0.2967587	0.5391949	0.00638365
50	1.25E-04	1.22E-04	0.9528201	0.3064806	0.5263683	0.004961383
60	1.12E-04	9.43E-05	0.9505813	0.3139564	0.5165787	0.003887462
70	1.02E-04	7.33E-05	0.9486955	0.3197244	0.509097	0.003075977
80	9.41E-05	5.74E-05	0.9470788	0.3241922	0.5033676	0.00246305
90	8.80E-05	4.53E-05	0.9456677	0.3276689	0.4989693	0.002000383
100	8.32E-05	3.62E-05	0.9444141	0.3303891	0.4955828	0.001651407
200	6.36E-05	1.01E-05	0.9355871	0.3402849	0.4844002	0.000658642
300	5.61E-05	8.72E-06	0.9287223	0.3425335	0.482486	0.000614393
400	5.03E-05	8.71E-06	0.9225404	0.3437157	0.4813496	0.000615762
500	4.55E-05	8.69E-06	0.9168887	0.3445397	0.4802717	0.000613951
600	4.14E-05	8.63E-06	0.9116892	0.34519	0.4791267	0.000609326
700	3.79E-05	8.55E-06	0.9068757	0.3457448	0.4778759	0.00060347
800	3.49E-05	8.46E-06	0.9023913	0.346242	0.4765089	0.000597193
900	3.24E-05	8.37E-06	0.8981872	0.3467005	0.4750269	0.000590861
1000	3.03E-05	8.28E-06	0.8942222	0.3471307	0.4734361	0.000584636
2000	2.03E-05	7.54E-06	0.8622147	0.3506434	0.4532601	0.000532194
3000	1.75E-05	6.98E-06	0.8362809	0.3535136	0.4293224	0.000492689
4000	1.61E-05	6.52E-06	0.8127894	0.3559577	0.4048595	0.000460674
5000	1.51E-05	6.14E-06	0.7908936	0.3578356	0.3813202	0.000433519
6000	1.42E-05	5.80E-06	0.7702861	0.3589909	0.3593151	0.000409866
7000	1.35E-05	5.51E-06	0.750791	0.3593348	0.3390515	0.000388935
8000	1.28E-05	5.24E-06	0.7322795	0.3588477	0.3205404	0.000370221
9000	1.22E-05	5.00E-06	0.7146482	0.3575606	0.3036982	0.000353367
10000	1.17E-05	4.79E-06	0.6978104	0.3555348	0.288399	0.000338101
20000	8.20E-06	3.38E-06	0.5606711	0.3111202	0.1922975	0.00023865

Appendix 6: Example Rate Matrix

Example rate matrix was for the Pu-DTPA model coupled with the modified ICRP 67 systemic model proposed in this research. Example was provided to illustrate how the rate matrix was constructed with NCRP 156 wound model integration and Pu-DTPA compartments specified for chelation days. [Note: set transitional pathways (i.e, ST0 to ST0t, ST1 to ST1t, Liver1 to Liver1t, and Blood to Bloodt) to zero on days chelation was not administered.]

Compartments	Soluble	CIS	PABS	LN	ST0	ST1	ST2	Kidneys-other	Liver2	Testes	CortVol	CortSurf	CortMarrow	TrabVol	TrabSurf	TrabMarrow	Liver1	GI-ST	GI-SI	GI-ULI	GI-LLI	Kidneys-Urine	Bladder	Blood	ST0t	ST1t	Liver1t	Bloodt	Faeces	Urine
Soluble	1	0.6																						0.67						
CIS	0.024	0	0.01	0.00002																										
PABS	0.0012		0	0.00002																										
LN				0																										
ST0																								0.342	3.65					
ST1																								0.000475		1.925				
ST2																								0.00001						
Kidneys-other																								0.000127						
Liver2																								0.000356						
Testes																								0.00038						
CortVol													0.0000821																	
CortSurf											0.0000205		0.0000821																	
CortMarrow																0.000493								0.0076						
TrabVol														0.000123		0.000493														
TrabSurf																								0.0076						
TrabMarrow																														
Liver1																			8.33E-04					0.0405			2.2			
GI-ST																			24											
GI-SI																				6				0.00006						
GI-ULI																					1.8									
GI-LLI																													1	
Kidneys-Urine																							0.0018							
Bladder																														12
Blood					0.153	0.04	6.00E-03	0.000139	0.2587	0.00027	0.0035	0.0672		0.0106	0.0955		0.2457			0.0092		0.0215	0.0125	0				1.378			
ST0t																												300			
ST1t																												0.12			
Liver1t																			0.067									0.067			
Bloodt																				4			45.7		145						
Faeces																															
Urine																															

Appendix 7: Copyright Permissions

Wolters Kluwer
Health

Lippincott Williams & Wilkins
Two Commerce Square
2001 Market Street
Philadelphia PA 19103

215 521 8607 tel
www.LWW.com

January 20, 2014

Mr. Kevin Konzen
Idaho State University
4605 E 185 N
Rigby, ID 83442
kkonzen@aol.com

Dear Kevin:

We are pleased to grant permission for the reproduction of the following:

Re: Ross: Histology: A Text and Atlas, 6e (9780781772006)
Spec. Matl: Thesis/Dissertation
Material Used: Figure 18.11
Perm. Request No: 140108-001995

There is no fee for this request. Permission is granted for print and electronic usage (CD-ROM and/or internet usage). This permission is a one-time, non-exclusive grant for English language use as described in your request. Permission is valid only if the requested material is original to Lippincott Williams & Wilkins. Permission is granted under the condition that a credit line is prominently placed and includes: the author(s), title of book, editor, copyright holder, and year of publication. Any additional use of this material including promotional or commercial use in either print, digital or mobile device format is prohibited without the permission of the publisher. Please contact the Wolters Kluwer Health/Lippincott Williams & Wilkins Book Permissions group at permissions@lww.com. The requestor agrees to secure written permission from the author (for book material only).

If these terms are acceptable, please sign below and return this license to:

Permissions Department
Wolters Kluwer Health/Lippincott Williams & Wilkins
Two Commerce Square
2001 Market Street
Philadelphia, PA 19103

Permission becomes effective upon our receipt of the signed license with payment made via check, if applicable, to us. Please retain a copy of this license for your files.

Requestor: Kevin Konzen Date: 1/26/14

RE: Permission for use of Fig. 18.11 in Histology: A text and atlas (2011)

Pawlina, Wojciech, M.D., M.D.

Dear Kevin,

Please feel free to use this illustration in your work. Good luck with the defending your dissertation.

My best,

Wojciech Pawlina, MD

From: kevink3737@aol.com [kevink3737@aol.com]
Sent: Saturday, August 02, 2014 8:20 AM
To: Pawlina, Wojciech, M.D.
Subject: Permission for use of Fig. 18.11 in Histology: A text and atlas (2011)

Dr. Wojciech,

I am in need of the author's permission for use of Fig 18.11 in Histology: A Text and Atlas (2011). I had obtained permission from Wolters Kluwer Health/Lippi Wilkins (attached) that also required obtaining permission from the author.

The figure is a schematic diagram of a plate of hepatocytes interposed between hepatic sinusoids.

This figure will appear in my PhD dissertation titled, "Development of a Plutonium-DTPA biokinetic model with suggested modification to the plutonium system currently under review.

The figure is important in illustrating the distinction between the hepatocytes and Kupffer cells in development of the liver compartments in the biokinetic mode

I also wanted to say that I found your book very enlightening and was referenced heavily within my dissertation.

Thank You,
Kevin Konzen

OXFORD UNIVERSITY PRESS LICENSE TERMS AND CONDITIONS

Aug 02, 2014

This is a License Agreement between Kevin Konzen ("You") and Oxford University Press ("Oxford University Press") provided by Copyright Clearance Center ("CCC"). The license consists of your order details, the terms and conditions provided by Oxford University Press, and the payment terms and conditions.

All payments must be made in full to CCC. For payment instructions, please see information listed at the bottom of this form.

License Number	3423911226173
License date	Jul 07, 2014
Licensed content publisher	Oxford University Press
Licensed content publication	Radiation Protection Dosimetry
Licensed content title	Ustur whole body case 0269: demonstrating effectiveness of i.v. Ca-DTPA for Pu:
Licensed content author	A. C. James, L. B. Sasser, D. B. Stuit, S. E. Glover, E. H. Carbaugh
Licensed content date	11/01/2007
Type of Use	Thesis/Dissertation
Institution name	None
Title of your work	Development of a Plutonium-DTPA biokinetic model with suggested modification to the plutonium systemic model
Publisher of your work	n/a
Expected publication date	Sep 2014
Permissions cost	0.00 USD
Value added tax	0.00 USD
Total	0.00 USD
Total	0.00 USD
Terms and Conditions	

STANDARD TERMS AND CONDITIONS FOR REPRODUCTION OF MATERIAL FROM AN OXFORD UNIVERSITY PRESS JOURNAL

1. Use of the material is restricted to the type of use specified in your order details.

2. This permission covers the use of the material in the English language in the following territory: world. If you have requested additional permission to translate this material, the terms and conditions of this reuse will be set out in clause 12.

3. This permission is limited to the particular use authorized in (1) above and does not allow you to sanction its use elsewhere in any other format other than specified above, nor does it apply to quotations, images, artistic works etc that have been reproduced from other sources which may be part of the material to be used.

4. No alteration, omission or addition is made to the material without our written consent. Permission must be re-cleared with Oxford University Press if/when you decide to reprint.

5. The following credit line appears wherever the material is used: author, title, journal, year, volume, issue number, pagination, by permission of Oxford University Press or the sponsoring society if the journal is a society journal. Where a journal is being published on behalf of a learned society, the details of that society must be included in the credit line.

6. For the reproduction of a full article from an Oxford University Press journal for whatever purpose, the corresponding author of the material concerned should be informed of the proposed use. Contact details for the corresponding authors of all Oxford University Press journal contact can be found alongside either the abstract or full text of the article concerned, accessible from www.oxfordjournals.org Should there be a problem clearing these rights, please contact journals.permissions@oup.com

7. If the credit line or acknowledgement in our publication indicates that any of the figures, images or photos was reproduced, drawn or modified from an earlier source it will be necessary for you to clear this permission with the original publisher as well. If this permission has not been obtained, please note that this material cannot be included in your publication/photocopies.

8. While you may exercise the rights licensed immediately upon issuance of the license at the end of the licensing process for the transaction, provided that you have disclosed complete and accurate details of your proposed use, no license is finally effective unless and until full payment is received from you (either by Oxford University Press or by Copyright Clearance Center (CCC)) as provided in CCC's Billing and Payment terms and conditions. If full payment is not received on a timely basis, then any license preliminarily granted shall be deemed automatically revoked and shall be void as if never granted. Further, in the event that you breach any of these terms and conditions or any of CCC's Billing and Payment terms and conditions, the license is automatically revoked and shall be void as if never granted. Use of materials as described in a revoked license, as well as any use of the materials beyond the scope of an unrevoked license, may constitute copyright infringement and Oxford University Press reserves the right to take any and all action to protect its copyright in the materials.

9. This license is personal to you and may not be sublicensed, assigned or transferred by you to any other person without Oxford University Press's written permission.

10. Oxford University Press reserves all rights not specifically granted in the combination of (i) the license details provided by you and accepted in the course of this licensing transaction, (ii) these terms and conditions and (iii) CCC's Billing and Payment terms and conditions.

11. You hereby indemnify and agree to hold harmless Oxford University Press and CCC, and their

respective officers, directors, employs and agents, from and against any and all claims arising out of your use of the licensed material other than as specifically authorized pursuant to this license.

12. Other Terms and Conditions: Permission is granted for the reuse of the requested material in your academic thesis/dissertation. However, please note that any further use or distribution will require additional permission. Inclusion under a Creative Commons license or any other open-access license allowing onward reuse is prohibited.

v1.4

You will be invoiced within 48 hours of this transaction date. You may pay your invoice by credit card upon receipt of the invoice for this transaction. Please follow instructions provided at that time.
To pay for this transaction now; please remit a copy of this document along with your payment. Payment should be in the form of a check or money order referencing your account number and this invoice number RLNK501345761.
Make payments to "COPYRIGHT CLEARANCE CENTER" and send to:

Copyright Clearance Center
Dept 001
P.O. Box 843006
Boston, MA 02284-3006
Please disregard electronic and mailed copies if you remit payment in advance.
Questions? customercare@copyright.com or +1-855-239-3415 (toll free in the US) or +1-978-646-2777.

Gratis licenses (referencing $0 in the Total field) are free. Please retain this printable license for your reference. No payment is required.

WOLTERS KLUWER HEALTH LICENSE TERMS AND CONDITIONS

Aug 02, 2014

This is a License Agreement between Kevin Konzen ("You") and Wolters Kluwer Health ("Wolters Kluwer Health") provided by Copyright Clearance Center ("CCC"). The license consists of your order details, the terms and conditions provided by Wolters Kluwer Health, and the payment terms and conditions.

All payments must be made in full to CCC. For payment instructions, please see information listed at the bottom of this form.

License Number	3418440344226
License date	Jun 29, 2014
Licensed content publisher	Wolters Kluwer Health
Licensed content publication	Health Physics: The Radiation Safety Journal
Licensed content title	THE CONRAD APPROACH TO BIOKINETIC MODELING OF DTPA DECORPORATION THERAPY
Licensed content author	Bastian Breustedt, Eric Blanchardon, Philippe Bérard, et al
Licensed content date	Jan 1, 2010
Volume Number	99
Issue Number	4
Type of Use	Dissertation/Thesis
Requestor type	Individual
Portion	Figures/table/illustration
Number of figures/tables/illustrations	1
Figures/tables/illustrations used	Figure 2
Author of this Wolters Kluwer article	No
Title of your thesis / dissertation	Development of a Plutonium-DTPA biokinetic model with suggested modification to the plutonium systemic model
Expected completion date	Sep 2014
Estimated size(pages)	280
Billing Type	Invoice
Billing address	4605 E 185 N RIGBY, ID 83442 United States
Total	0.00 USD

Terms and Conditions

Terms and Conditions

1. A credit line will be prominently placed and include: for books - the author(s), title of book, editor, copyright holder, year of publication; For journals - the author(s), title of article, title of journal, volume number, issue number and inclusive pages.
2. The requestor warrants that the material shall not be used in any manner which may be considered derogatory to the title, content, or authors of the material, or to Wolters Kluwer.
3. Permission is granted for a one time use only within 12 months from the date of this invoice. Rights herein do not apply to future reproductions, editions, revisions, or other derivative works. Once the 12-month term has expired, permission to renew must be submitted in writing.
4. Permission granted is non-exclusive, and is valid throughout the world in the English language and the languages specified in your original request.
5. Wolters Kluwer cannot supply the requestor with the original artwork or a "clean copy."
6. The requestor agrees to secure written permission from the author (for book material only).
7. Permission is valid if the borrowed material is original to a Wolters Kluwer imprint (Lippincott-Raven Publishers, Williams & Wilkins, Lea & Febiger, Harwal, Igaku-Shoin, Rapid Science, Little Brown & Company, Harper & Row Medical, American Journal of Nursing Co, and Urban & Schwarzenberg - English Language).
8. If you opt not to use the material requested above, please notify Rightslink within 90 days of the original invoice date.
9. Please note that articles in the ahead-of-print stage of publication can be cited and the content may be re-used by including the date of access and the unique DOI number. Any final changes in manuscripts will be made at the time of print publication and will be reflected in the final electronic version of the issue.?Disclaimer: Articles appearing in the Published Ahead-of-Print section have been peer-reviewed and accepted for publication in the relevant journal and posted online before print publication. Articles appearing as publish ahead-of-print may contain statements, opinions, and information that have errors in facts, figures, or interpretation. Accordingly, Lippincott Williams & Wilkins, the editors and authors and their respective employees are not responsible or liable for the use of any such inaccurate or misleading data, opinion or information contained in the articles in this section.
10. 1This permission does not apply to images that are credited to publications other than Wolters Kluwer journals. For images credited to non-Wolters Kluwer journal publications, you will need to obtain permission from the journal referenced in the figure or table legend or credit line before making any use of the image(s) or table(s).
11. In case of **Disease Colon Rectum, Plastic Reconstructive Surgery, The Green Journal, Critical Care Medicine, Pediatric Critical Care Medicine, the American Heart Publications, the American Academy of Neurology** the following guideline applies: no drug brand/trade name or logo can be included in the same page as the material re-used
12. When requesting a permission to translate a full text article, Wolters Kluwer/Lippincott Williams & Wilkins requests to receive the pdf of the translated document
13. "Adaptations of single figures do not require Wolters Kluwer **further** approval if the permission has been granted previously. However, the adaptation should be credited as follows:?Adapted with permission from Lippincott Williams and Wilkins/Wolters Kluwer Health: [JOURNAL NAME] (reference citation), copyright (year of publication)" **Please note that modification of text within figures or full-text articles is strictly forbidden.**
14. The following statement needs to be added when reprinting the material in Open Access journals only: 'promotional and commercial use of the material in print, digital or mobile device format is prohibited without the permission from the publisher Lippincott Williams & Wilkins. Please contact journalpermissions@lww.com for further information".
15. Other Terms and Conditions:

v1.8

You will be invoiced within 48 hours of this transaction date. You may pay your invoice by credit card upon receipt of the invoice for this transaction. Please follow instructions

provided at that time.
To pay for this transaction now; please remit a copy of this document along with your payment. Payment should be in the form of a check or money order referencing your account number and this invoice number RLNK501339496.
Make payments to "COPYRIGHT CLEARANCE CENTER" and send to:

Copyright Clearance Center
Dept 001
P.O. Box 843006
Boston, MA 02284-3006
Please disregard electronic and mailed copies if you remit payment in advance.
Questions? customercare@copyright.com or +1-855-239-3415 (toll free in the US) or +1-978-646-2777.

Gratis licenses (referencing $0 in the Total field) are free. Please retain this printable license for your reference. No payment is required.

ELSEVIER LICENSE
TERMS AND CONDITIONS

Dec 02, 2013

This is a License Agreement between Kevin Konzen ("You") and Elsevier ("Elsevier") provided by Copyright Clearance Center ("CCC"). The license consists of your order details, the terms and conditions provided by Elsevier, and the payment terms and conditions.

All payments must be made in full to CCC. For payment instructions, please see information listed at the bottom of this form.

Supplier	Elsevier Limited The Boulevard,Langford Lane Kidlington,Oxford,OX5 1GB,UK
Registered Company Number	1982084
Customer name	Kevin Konzen
Customer address	4605 E 185 N RIGBY, ID 83442
License number	3281090322731
License date	Dec 02, 2013
Licensed content publisher	Elsevier
Licensed content publication	Archives of Biochemistry and Biophysics
Licensed content title	Osteoclast–osteoblast communication
Licensed content author	Koichi Matsuo,Naoko Irie
Licensed content date	15 May 2008
Licensed content volume number	473
Licensed content issue number	2
Number of pages	9
Start Page	201
End Page	209
Type of Use	reuse in a thesis/dissertation
Portion	figures/tables/illustrations
Number of figures/tables/illustrations	1
Format	both print and electronic
Are you the author of this Elsevier article?	No
Will you be translating?	No

Order reference number	OsteoblastFig4
Title of your thesis/dissertation	The influence of chelation therapy on the biokinetics of incorporated plutonium.
Expected completion date	Jan 2015
Estimated size (number of pages)	200
Elsevier VAT number	GB 494 6272 12
Permissions price	0.00 USD
VAT/Local Sales Tax	0.00 USD / 0.00 GBP
Total	0.00 USD

Terms and Conditions

INTRODUCTION

1. The publisher for this copyrighted material is Elsevier. By clicking "accept" in connection with completing this licensing transaction, you agree that the following terms and conditions apply to this transaction (along with the Billing and Payment terms and conditions established by Copyright Clearance Center, Inc. ("CCC"), at the time that you opened your Rightslink account and that are available at any time at http://myaccount.copyright.com).

GENERAL TERMS

2. Elsevier hereby grants you permission to reproduce the aforementioned material subject to the terms and conditions indicated.

3. Acknowledgement: If any part of the material to be used (for example, figures) has appeared in our publication with credit or acknowledgement to another source, permission must also be sought from that source. If such permission is not obtained then that material may not be included in your publication/copies. Suitable acknowledgement to the source must be made, either as a footnote or in a reference list at the end of your publication, as follows:

"Reprinted from Publication title, Vol /edition number, Author(s), Title of article / title of chapter, Pages No., Copyright (Year), with permission from Elsevier [OR APPLICABLE SOCIETY COPYRIGHT OWNER]." Also Lancet special credit - "Reprinted from The Lancet, Vol. number, Author(s), Title of article, Pages No., Copyright (Year), with permission from Elsevier."

4. Reproduction of this material is confined to the purpose and/or media for which permission is hereby given.

5. Altering/Modifying Material: Not Permitted. However figures and illustrations may be altered/adapted minimally to serve your work. Any other abbreviations, additions, deletions and/or any other alterations shall be made only with prior written authorization of Elsevier Ltd. (Please contact Elsevier at permissions@elsevier.com)

6. If the permission fee for the requested use of our material is waived in this instance, please be advised that your future requests for Elsevier materials may attract a fee.

7. Reservation of Rights: Publisher reserves all rights not specifically granted in the combination of (i) the license details provided by you and accepted in the course of this licensing transaction, (ii) these terms and conditions and (iii) CCC's Billing and Payment terms and conditions.

8. License Contingent Upon Payment: While you may exercise the rights licensed immediately upon issuance of the license at the end of the licensing process for the transaction, provided that you have disclosed complete and accurate details of your proposed use, no license is finally effective unless and until full payment is received from you (either by publisher or by CCC) as provided in CCC's Billing and Payment terms and conditions. If full payment is not received on a timely basis, then any license preliminarily granted shall be deemed automatically revoked and shall be void as if never granted. Further, in the event that you breach any of these terms and conditions or any of CCC's Billing and Payment terms and conditions, the license is automatically revoked and shall be void as if never granted. Use of materials as described in a revoked license, as well as any use of the materials beyond the scope of an unrevoked license, may constitute copyright infringement and publisher reserves the right to take any and all action to protect its copyright in the materials.

9. Warranties: Publisher makes no representations or warranties with respect to the licensed material.

10. Indemnity: You hereby indemnify and agree to hold harmless publisher and CCC, and their respective officers, directors, employees and agents, from and against any and all claims arising out of your use of the licensed material other than as specifically authorized pursuant to this license.

11. No Transfer of License: This license is personal to you and may not be sublicensed, assigned, or transferred by you to any other person without publisher's written permission.

12. No Amendment Except in Writing: This license may not be amended except in a writing signed by both parties (or, in the case of publisher, by CCC on publisher's behalf).

13. Objection to Contrary Terms: Publisher hereby objects to any terms contained in any purchase order, acknowledgment, check endorsement or other writing prepared by you, which terms are inconsistent with these terms and conditions or CCC's Billing and Payment terms and conditions. These terms and conditions, together with CCC's Billing and Payment terms and conditions (which are incorporated herein), comprise the entire agreement between you and publisher (and CCC) concerning this licensing transaction. In the event of any conflict between your obligations established by these terms and conditions and those established by CCC's Billing and Payment terms and conditions, these terms and conditions shall control.

14. Revocation: Elsevier or Copyright Clearance Center may deny the permissions described in this License at their sole discretion, for any reason or no reason, with a full refund payable to you. Notice of such denial will be made using the contact information provided by you. Failure to receive such notice will not alter or invalidate the denial. In no event will Elsevier or Copyright Clearance Center be responsible or liable for any costs, expenses or damage incurred by you as a result of a denial of your permission request, other than a refund of the amount(s) paid by you to Elsevier and/or Copyright Clearance Center for denied permissions.

LIMITED LICENSE

The following terms and conditions apply only to specific license types:

15. **Translation**: This permission is granted for non-exclusive world **English** rights only unless your license was granted for translation rights. If you licensed translation rights you may only translate this content into the languages you requested. A professional translator must perform all translations and reproduce the content word for word preserving the integrity of the article. If this license is to re-use 1 or 2 figures then permission is granted for non-exclusive world rights in all languages.

16. **Website**: The following terms and conditions apply to electronic reserve and author websites:
Electronic reserve: If licensed material is to be posted to website, the web site is to be password-protected and made available only to bona fide students registered on a relevant course if:
This license was made in connection with a course,
This permission is granted for 1 year only. You may obtain a license for future website posting,
All content posted to the web site must maintain the copyright information line on the bottom of each image,
A hyper-text must be included to the Homepage of the journal from which you are licensing at http://www.sciencedirect.com/science/journal/xxxxx or the Elsevier homepage for books at http://www.elsevier.com , and
Central Storage: This license does not include permission for a scanned version of the material to be stored in a central repository such as that provided by Heron/XanEdu.

17. **Author website** for journals with the following additional clauses:

All content posted to the web site must maintain the copyright information line on the bottom of each image, and the permission granted is limited to the personal version of your paper. You are not allowed to download and post the published electronic version of your article (whether PDF or HTML, proof or final version), nor may you scan the printed edition to create an electronic version.
A hyper-text must be included to the Homepage of the journal from which you are licensing at http://www.sciencedirect.com/science/journal/xxxxx . As part of our normal production process, you will receive an e-mail notice when your article appears on Elsevier's online service ScienceDirect (www.sciencedirect.com). That e-mail will include the article's Digital Object Identifier (DOI). This number provides the electronic link to the published article and should be included in the posting of your personal version. We ask that you wait until you receive this e-mail and have the DOI to do any posting.

Central Storage: This license does not include permission for a scanned version of the material to be stored in a central repository such as that provided by Heron/XanEdu.

18. **Author website** for books with the following additional clauses:
Authors are permitted to place a brief summary of their work online only.
A hyper-text must be included to the Elsevier homepage at http://www.elsevier.com . All content posted to the web site must maintain the copyright information line on the bottom of each image.
You are not allowed to download and post the published electronic version of your chapter, nor may you scan the printed edition to create an electronic version.

Central Storage: This license does not include permission for a scanned version of the material to be stored in a central repository such as that provided by Heron/XanEdu.

19. **Website** (regular and for author): A hyper-text must be included to the Homepage of the journal from which you are licensing at http://www.sciencedirect.com/science/journal/xxxxx. or for books to the Elsevier homepage at http://www.elsevier.com

20. **Thesis/Dissertation**: If your license is for use in a thesis/dissertation your thesis may be submitted to your institution in either print or electronic form. Should your thesis be published commercially, please reapply for permission. These requirements include permission for the Library and Archives of Canada to supply single copies, on demand, of the complete thesis and include permission for UMI to supply single copies, on demand, of the complete thesis. Should your thesis be published commercially, please reapply for permission.

21. **Other Conditions**:

v1.6

If you would like to pay for this license now, please remit this license along with your payment made payable to "COPYRIGHT CLEARANCE CENTER" otherwise you will be invoiced within 48 hours of the license date. Payment should be in the form of a check or money order referencing your account number and this invoice number RLNK501172634. Once you receive your invoice for this order, you may pay your invoice by credit card. Please follow instructions provided at that time.

Make Payment To:
Copyright Clearance Center
Dept 001
P.O. Box 843006
Boston, MA 02284-3006

For suggestions or comments regarding this order, contact RightsLink Customer Support: customercare@copyright.com or +1-877-622-5543 (toll free in the US) or +1-978-646-2777.

Gratis licenses (referencing $0 in the Total field) are free. Please retain this printable license for your reference. No payment is required.